CARBONACEOUS NANOMATERIALS AND COMPOSITES: GREEN TECHNIQUES FOR ORGANIC SYNTHESIS

A Thesis submitted to the University of North Bengal

For the Award of
Doctor of Philosophy
in
Chemistry

By

Prasun Choudhury

Guide

Prof. Basudeb Basu

Department of Chemistry
University of North Bengal
November-2020

Dedicated

to

My Parents

DECLARATION

I declare that the thesis entitled "**CARBONACEOUS NANOMATERIALS AND COMPOSITES: GREEN TECHNIQUES FOR ORGANIC SYNTHESIS**" has been prepared by me under the under the guidance of Dr. Basudeb Basu, Professor of Chemistry, University of North Bengal. No part of this thesis has formed the basis for the award of any degree or fellowship previously.

Prasun Choudhury

Prasun Choudhury
Department of Chemistry
University of North Bengal
Darjeeling-734013
West Bengal
India

Date: 25.11.2020

UNIVERSITY OF NORTH BENGAL

Accredited by NAAC with Grade A

DEPARTMENT OF CHEMISTRY

P.O. NORTH BENGAL UNIVERSITY, Raja Rammohunpur, Dist. Darjeeling, West Bengal, India, PIN - 734013.
PHONE : (0353) 2776 381, Fax: (0353) 2699 001

Ref. No..... *Dated* 24. 11. 20 20

CERTIFICATE

I certify that Mr. **PRASUN CHOUDHURY** has prepared the thesis entitled **CARBONACEOUS NANOMATERIALS AND COMPOSITES: GREEN TECHNIQUES FOR ORGANIC SYNTHESIS**, for the award of Ph.D. degree of the University of North Bengal, under my guidance. He has carried out the work at the Department of Chemistry, University of North Bengal. No part of this thesis has formed the basis for the award of any degree or fellowship previously.

24.11.2020

Professor (Dr.) B. Basu, Ph.D., FAScT (Retired)
Department of Chemistry
University of North Bengal
Darjeeling 734013, India

Professor (Retd.)
Department of Chemistry
University of North Bengal
Darjeeling - 734013, India

Visiting Professor, Raiganj University (Presently)
Uttar Dinajpur 733134, India
Mobile: +91 9434428477
Email: basudeb.basu@gmail.com
Email: basu_nbu@hotmail.com

URKUND

Urkund Analysis Result

Analysed Document:	Prasun Choudhury_Chemistry.pdf (D84737546)
Submitted:	11/11/2020 7:58:00 AM
Submitted By:	nbuplg@nbu.ac.in
Significance:	8 %

Sources included in the report:

https://www.researchgate.net/publication/273473000_A_comparative_study_of_the_catalytic_activity_of_nanosized_oxides_in_the_one-pot_synthesis_of_highly_substituted_dihydropyridines
https://lirias.kuleuven.be/retrieve/475237
https://iris.uniroma1.it/retrieve/handle/11573/917801/327726/Tesi%20di%20dottorato%20Iazzetti%20Antonia%20car.pdf

Instances where selected sources appear:

34

24.11.2020

Professor (Retd.)
Department of Chemistry
University of North Bengal
Darjeeling - 734013, India

Prasun Choudhury
25.11.2020

ACKNOWLEDGEMENT

This is a great pleasure for me to thank all those people, without whom I would not have been able to complete the entire journey of my Ph.D.

First of all, I would like to express my sincere gratitude towards my honourable supervisor Dr. Basudeb Basu (Retired Professor, Department of Chemistry, University of North Bengal) for allowing me to work under his guidance. His expertise and constant motivation was invaluable in carrying out the research work.

I would also like to thank Dr. Pranab Ghosh (Professor, Department of Chemistry, University of North Bengal) for helping me every single time. I would always remember his kind words, encouragement and support not only during my research period, but also during the M. Sc. days.

I am thankful to the Dr. Sajal Das, Associate Pofessor, Department of Chemistry, University of North Bengal for his cooperation throughout the entire period of my research work.

I express my sincere gratitude to the Head, Department of Chemistry, University of North Bengal and all the faculty members and non-teaching staff of this department.

I would also like to acknowledge Dr. Goutam De, Chief Scientist & Head, Nano-Structured Materials Division, CSIR-CGCRI, Kolkata, for allowing me to visit his laboratory and carry out characterization of our catalysts.

It gives me immense pleasure to thank all my labmates for their support and cooperation during the entire journey of my Ph.D. I am thankful to Kinkar sir, Sujit sir, Debasish da, Babli di, Samir da and Sankar da for their continuous help and support.

I express my special thanks to Suchandra, Bijeta and Rabindra whose help and support have been always with me during my research period.

I would also like to thank Prasanjit da, Gyan da, Puja di, Goutam, Aminul, Arindam, Ashim and all other scholars with whom I have worked or shared ideas during this time.

Thanks are also due to Shreyasi Chattopadhyay, CSIR-CGCRI, Kolkata for her help in characterizing our catalysts.

I convey my special thanks to Amit and Mihir for their valuable contribution in my research work.

My special thanks are extended to the M. Sc. students who have worked with me during my research period.

I would also express my thanks to Dr. Mayukh Deb, Micro-Analyst, Department of Chemistry, University of North Bengal for carrying out NMR analysis.

I would like to thank UGC, New Delhi for my Junior Research Fellowship and Senior Research Fellowship and DST-SERB, Govt. of India, for infrastructural facilities.

The journey would remain incomplete if I fail to express my gratitude to Lab No. 103, Department of Chemistry, University of North Bengal, where I have carried out my entire research work.

All that I have achieved till now would have been impossible without my parents, Mr. Pranab Choudhury and Mrs. Sampa Choudhury. Their endless support, love, patience, encouragement and sacrifices have brought me here today. Without their blessings I could never be the person that I am today.

Finally, despite my best efforts some unintentional errors might have crept in. Suggestions and critisims will be thankfully accepted.

I thank you all for making this journey memorable.

Prasun Choudhury
25.11.2020

Prasun Choudhury

ABSTRACT

The present thesis entitled "**CARBONACEOUS NANOMATERIALS AND COMPOSITES: GREEN TECHNIQUES FOR ORGANIC SYNTHESIS**" mainly focuses on the design and catalytic applications of graphene-based nanomaterials in organic synthesis. The development of graphene-based materials like graphene oxide (GO), reduced graphene oxide (rGO), CNTs, etc., has been an emerging area of research. Graphene and functionalized graphenes possesses unique structural properties which led to their wide application in frontier areas of chemistry and material science. In this thesis I have focused on the preparation and catalytic applications of functionalized graphenes and metal supported graphene-based nanocomposites. The thesis is divided into two chapters and those chapters are further subdivided into different sections as outlined below.

Chapter I has been divided into four parts. **Section A** presents a brief review on carbonaceous nanomaterials. The origin and advancement in the field of carbonaceous nanomaterials like graphene, fullerenes, CNTs, etc., have been highlighted. The two main routes for the functionalization of graphene have been briefly discussed. Different approaches for the synthesis of graphene oxide via oxidative chemical exfoliation have been elucidated. Special emphasis has been given on the use of graphene oxide as a carbocatalyst in organic synthesis.

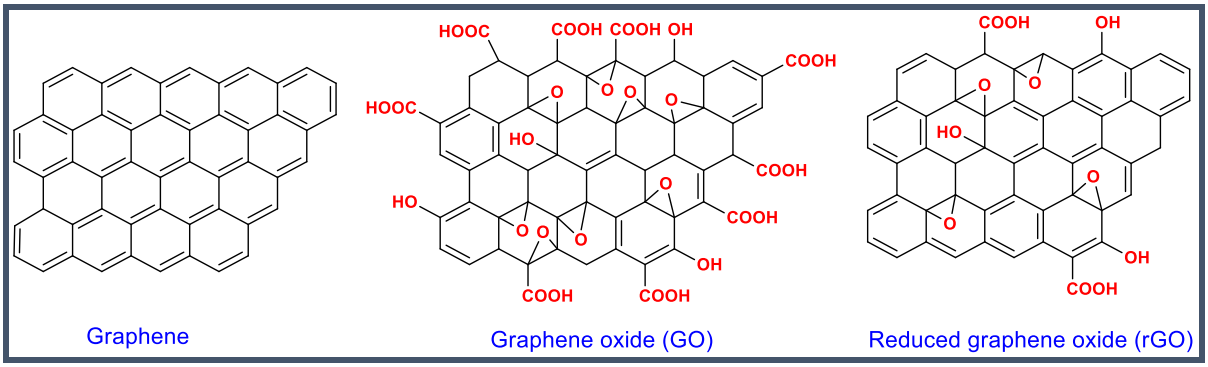

Graphene oxide catalyzed cross dehydrogenative coupling (CDC) between aromatic compounds and thiols have been presented in **Section B**. GO in combination with NaI has been used as the catalytic system for the regiospecific C–H sulfenylation of 1*H*-indole, 2-naphthol, resorcinol and 2-naphthylamines. A green strategy devoid of any transition metal and strong oxidants has been developed. Moreover, the use of thiols in place of other sulfenylation reagent makes the overall protocol atom-economic and environmentally benign. The heterogeneous nature of GO facilitates its easy reusability without any significant loss in its catalytic activity.

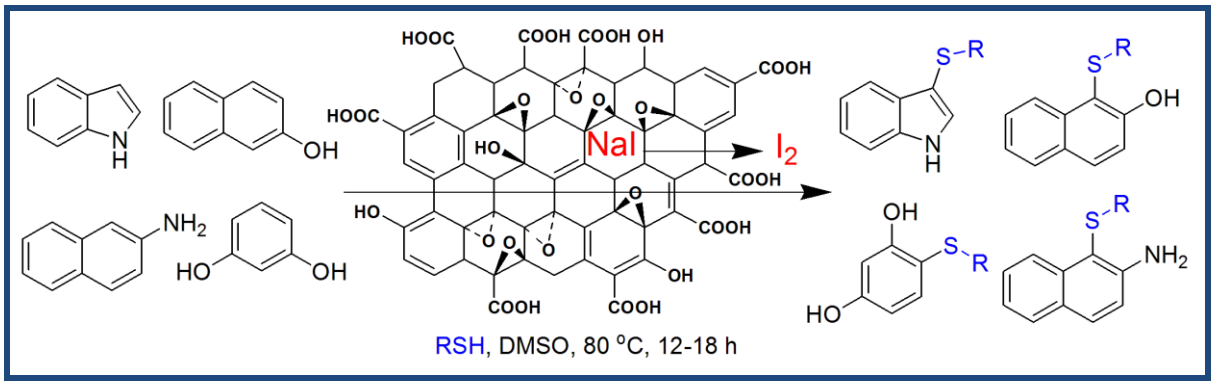

In **Section C** amine functionalized graphene oxide nanosheets (AFGONs) has been prepared by using a facile amine coupling reaction between GO and (3-aminopropyl)triethoxysilane. The nanocomposite has been used as a bifunctional catalyst for the selective formation of functionalized 1,4-dihydropyridines (1,4-DHPs), acridinediones and polyhydroquinolines. It has been presumed that a cooperative effect between the acidic and basic functionalities present in AFGONs might have exerted high catalytic efficiency as well as prevented over oxidation of the pyridine derivatives. A plausible mechanism has been proposed on the basis of control experiments. The reactions can be scaled up conveniently and the catalyst could be recycled for five consecutive runs without loss in its activity.

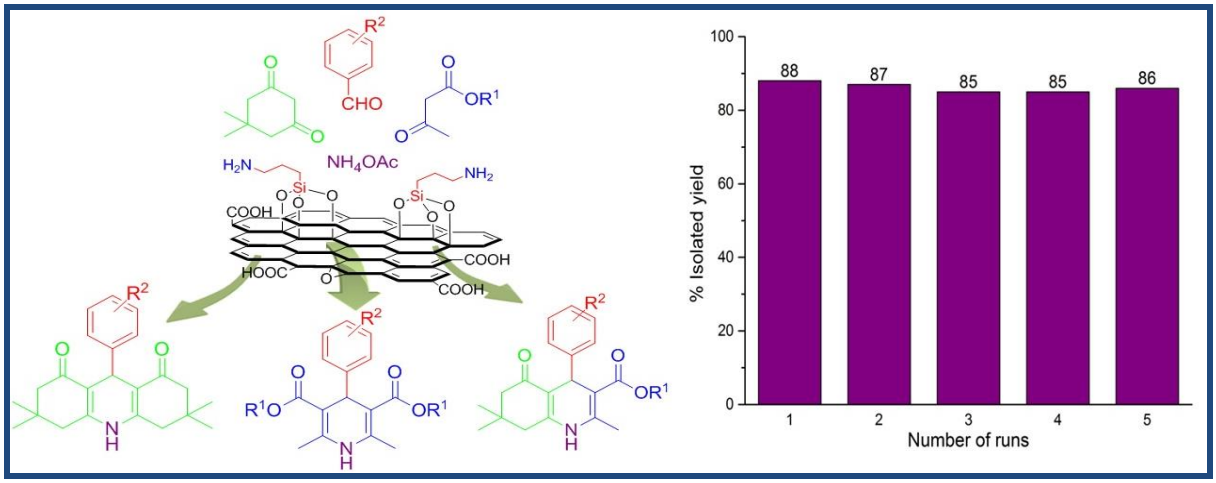

In **Section D** graphene oxide has been used as a carbocatalyst in Stadler-Ziegler reaction under continuous flow mode. The flow reactor is a relatively newer technology and constitutes a new paradigm for molecular assembly. In this section a sustainable continuous-flow protocol for the conversion of aryl amines to unsymmetrical thioethers has been described. This reaction undergoes through a two-step process involving graphene oxide catalyzed diazotization followed by sulfenylation with aryl/alkyl thiols. The GO catalytic bed has been found to be recyclable for ten consecutive runs without significant loss in its performance.

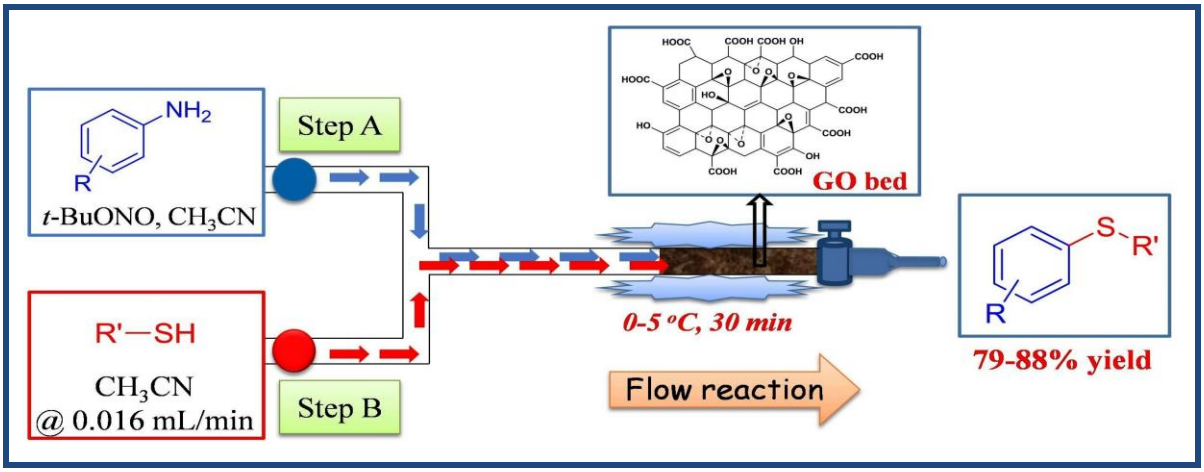

Chapter II has been divided into three sections. **Section A** presents a brief overview about the design and development of transition metal decorated graphene-based nanocomposites. The most common supports for anchorage of metal/metal oxide NPs include polymer blended graphene, graphene-zeolite and graphene-silica. Further applications of these nanocomposites as catalyst in synthetic organic chemistry has also been illustrated.

The synthesis and characterization of a new ternary nanocomposite (Ni–rGO–zeolite) based on reduced graphene oxide, zeolite Y and nickel NPs has been presented in **Section B**. The nanocomposite has been found to be an excellent catalyst for the regioselective synthesis of 1,2,3-triazoles in aqueous media. This is the first example of a heterogeneous nickel catalyzed alkyne azide cycloaddition (NiAAC). Moreover, the nanocomposite catalyst could be reused for four runs without loss in its activity.

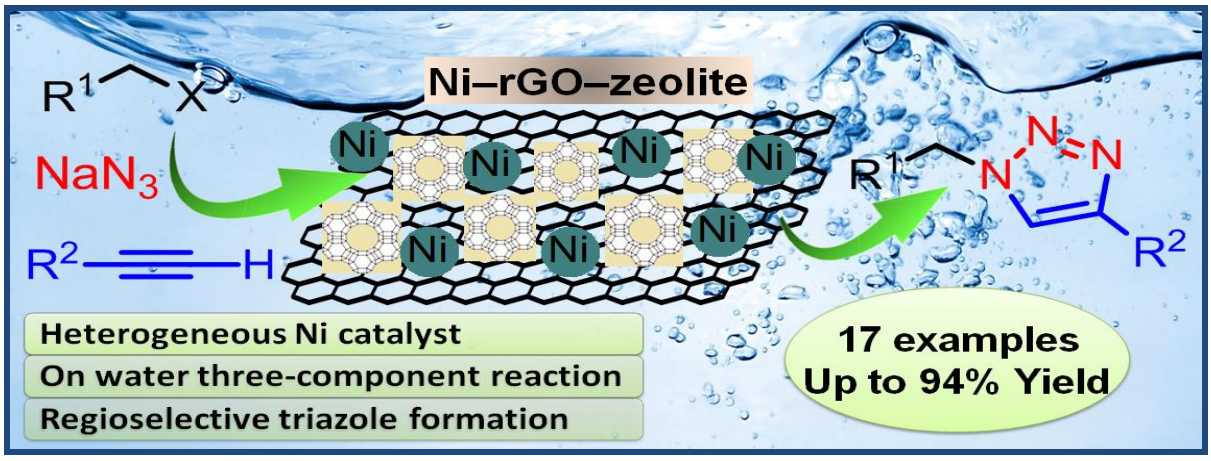

Section C represents the synthesis of another ternary nanocomposite material (Cu@GO–SiO_2) from graphene oxide, silica and copper NPs. The spectroscopic and microscopic characterization of the nanocomposite revealed the presence of copper species in different oxidation states. This resulted in the exceptional catalytic activity of this nanocomposite towards different cross-coupling reactions like C–S, C–C, C–O and C–N.

PREFACE

In order to meet the ever increasing demand for new catalytic systems, researchers around the globe have focussed on the development of graphene-based materials as catalysts. It is widely accepted that the modern chemical industry requires alternative and environment friendly catalytic processes. This trend towards 'green chemistry' necessitates an entire shift from traditional concepts of process efficiency that largely focuses on chemical yield, to the one that assigns economic value to eliminating waste at the source and avoids use of toxic and / or hazardous substances. Fortunately, the rapid growth and improved understanding of nanoscience and nanotechnology has paved the way for better atom efficiency. Novel approaches based on nanomaterials can revolutionize the technology used in modern heterogeneous catalysis. This research work has been primarily focused on the synthesis of graphene-based nanomaterials and their catalytic application towards different organic transformations.

Chapter I, Section A provides a brief review on carbonaceous nanomaterials, their origin and classification. In **Section B** graphene oxide has been used as a carbocatalyst for the regiospecific C–H sulfenylation of 1*H*-indole, 2-naphthol, resorcinol and 2-naphthylamines. In **Section C** amine functionalized graphene oxide nanosheets (AFGONs) has been prepared and used as a bifunctional catalyst for the selective formation of functionalized 1,4-dihydropyridines (DHPs), acridinediones and polyhydroquinolines. In **Section D** graphene oxide has been used as a carbocatalyst in the Stadler-Ziegler reaction for the synthesis of thioethers under continuous flow mode. **Chapter II** has been divided into three sections. **Section A** presents a brief overview about the design and development of transition metal decorated graphene-based nanocomposites. In **Section B** a new ternary nanocomposite (Ni–rGO–zeolite) has been prepared and used for the regioselective synthesis of 1,2,3-triazoles in aqueous media. The last section i.e., **Section C** represents the synthesis of another ternary nanocomposite (Cu@GO–SiO_2) and its application towards C–S, C–C, C–O and C–N cross-coupling reactions.

TABLE OF CONTENTS

CHAPTER I
Section B

CHAPTER I
Section C

CHAPTER I
Section D

CHAPTER II
Section A

CHAPTER II
Section B

CHAPTER II
Section C

LIST OF TABLES

LIST OF SCHEMES

LIST OF FIGURES

LIST OF APPENDICES

APPENDIX A:

List of Research Publications

APPENDIX B:

Oral and Poster Presentations

APPENDIX A

List of Publications (Related to Thesis Work)

1. "Sustainable and Site-Selective C–H Sulfenylation of Aromatic Compounds with Thiol using Catalytic Graphene Oxide and NaI", **Prasun Choudhury**, Babli Roy and Basudeb Basu*, *Asian J. Org. Chem*. 2017, **6**, 1569-1574.
2. "Amine-functionalized graphene oxide nanosheets (AFGONs): an efficient bifunctional catalyst for selective formation of 1,4-dihydropyridines, acridinediones and polyhydroquinolines", **Prasun Choudhury**, Pranab Ghosh and Basudeb Basu*, *Mol. Div*. 2020, **24**, 283-294.
3. "Graphene oxide-catalyzed two-step continuous-flow conversion of aryl amine to unsymmetrical thioether", **Prasun Choudhury** and Basudeb Basu*, *J. Flow Chem*. 2020, **10**, 389-396.
4. "Ni–rGO–zeolite Nanocomposite: An Efficient Heterogeneous Catalyst for One–Pot Synthesis of Triazoles in Water", **Prasun Choudhury**, Shreyasi Chattopadhyay, Goutam De*, Basudeb Basu* (Communicated).
5. "Cu@GO-SiO_2 Nanocomposite: An efficient Catalyst for C–S, C–C, C–O and C–N coupling reactions", **Prasun Choudhury**, Kinkar Biswas and Basudeb Basu* (Manuscript under preparation).

Book Chapters (Not Related to Thesis Work)

1. "Graphene oxide nanosheets as sustainable carbocatalysts: Synthesis of medicinally important heterocycles", **Prasun Choudhury** and Basudeb Basu*, in *Sustainable and Green Approaches in Medicinal Chemistry*, ed. B. K.Banik, Elsevier, pp. 47-74.
2. "Advances on Greener Processes for Triazole Synthesis via Azide-Alkyne Cycloaddition Reactions", **Prasun Choudhury** and Basudeb Basu*, in *Advanced Synthetic Techniques*, ed. G. Brahmachari, Elsevier, Vol. 1 (Communicated).
3. "Sustainable synthesis of benzimidazoles, quinoxalines and their congeners", **Prasun Choudhury** and Basudeb Basu*, in *Green Catalytic Systems and Solvents*, ed. G. Brahmachari, Elsevier, Vol. 2 (Communicated).

APPENDIX B

Oral Presentation

1. Regiospecific C–H Sulfenylation of Aromatic Compounds with Thiol using Catalytic Graphene Oxide and NaI, **Prasun Choudhury** and Basudeb Basu*, National Seminar on "Frontiers in Chemistry 2017-18", Organized by Department of Chemistry, University of North Bengal, Darjeeling, India.

Poster Presentation

1. Amine Functionalized Graphene Oxide Nanosheets (AFGONs): An efficient Bifunctional Catalyst for Multicomponent Reactions at Ambient Temperature, **Prasun Choudhury** and Basudeb Basu*, International Seminar on "Frontiers in Chemistry 2018", Organized by Department of Chemistry, University of North Bengal, Darjeeling, India.

ABBREVIATIONS

AAC	Azide alkyne cycloaddition
AFGONs	Amine functionalized graphene oxide nanosheets
API	Active pharmaceutical ingredients
APTES	3-(Aminopropyl)triethoxysilane
Br	broad
°C	Degree Celsius
CDC	Cross dehydrogenative coupling
CFL	Compact fluorescent lamp
CMG	Chemically modified graphene
CNT	Carbon nanotube
CVD	Chemical vapour deposition
D	Dimensional
d	Doublet
dd	Doublet of doublet
DDQ	2,3-Dichloro-2,6-dicyanobenzoquinone
DHP	Dihydropyridine
DME	1,2-Dimethoxyethane
DMF	N,N-Dimethylformamide
DMSO	Dimethyl sulfoxide
EDS	Energy dispersive X-ray spectroscopy
eV	Electron volt
FT-IR	Fourier transform infrared spectroscopy
GO	Graphene oxide
h	hour
HPLC	High performance liquid chromatography
HRMS	High resolution mass spectrometry
Hz	Hertz
ICP-AES	Inductively coupled plasma atomic emission spectroscopy
IL	Ionic liquid
i-Pr	Isopropyl
LED	Light emitting diode

Lit.	Literature
m	Multiplet
MCR	Multi-component reaction
mg	Milligram
MHz	Mega hertz
min	minute
mL	millilitre
mmol	millimole
mol%	Mole percent
MOF	Metal organic framework
MW	Microwave
NAC	Nanoporous activated carbon
NHC	N-heterocyclic carbene
NMR	Nuclear magnetic resonance spectroscopy
NPs	Nanoparticles
PEG	Polyethylene glycol
ppm	Parts per million
PTC	Phase transfer catalyst
q	Quartet
rGO	Reduced graphene oxide
rpm	Revolution per minute
r.t.	Room temperature
s	Singlet
SAED	Selected area electron diffraction patterns
SDS	Sodium dodecyl sulfate
SEM	Scanning electron microscopy
SET	Single electron transfer
t	Triplet
t-Bu	*Tert*-butyl
t-BuONO	*Tert*–butylnitrite
TBHP	*Tert*-butylhydroperoxide
TBAB	Tetrabutylammonium bromide
TBAI	Tetrabutylammonium iodide

TEM	Transmission electron microscopy
TEOS	Tetraethylorthosilicate
THF	Tetrahydrofuran
TLC	Thin layer chromatography
TMS	Tetramethylsilane
TON	Turnover number
Ts	Tosyl
XPS	X-ray photoelectron spectroscopy
XRD	X-ray diffraction
VACE	Value added chemical entities

Chapter I

Section A

Carbonaceous Nanomaterials

I.A.1 Carbonaceous nanomaterials

Carbonaceous nanomaterials are a group of amorphous solids consisting of micro crystallites with a graphite lattice. They differ from pristine graphite on the part that they have a random imperfect structures, varied pore sizes and possesses various surface functional groups over a broad range.[1] Commonly known carbonaceous nanomaterials include activated carbons, graphenes, carbon molecular sieves and carbon fibers. Recently, graphene fiber has been incorporated into this group.[2] These materials are classified into four different categories: fullerenes, graphene-based materials, carbon nanotubes (CNTs) and nanoporous activated carbon (NAC). Graphene-based nanomaterials are further subdivided into pure graphene, graphene oxide (GO), reduced graphene oxide (rGO) and chemically modified graphenes (CMGs) or graphene nanocomposites.

Fullerene is an allotrope of carbon with an enclosed cage like structure bearing fused rings of five to seven atoms. The carbon atoms are connected by single and double bonds and the molecule may be spherical, ellipsoid, tube or other shapes.[3] The most common being C_{60} named after buckminsterfullerene, also called buckyballs for its resemblance with standard soccer balls (Figure I.A.1). The C_{60} packs 12 pentagons and 20 hexagons, and all carbon atoms are arranged at the 60 vertices of a truncated icosahedron.[3] The structure is highly symmetrical having 32 faces. The presence of fullerenes has been predicted for long time, but it has been accidentally synthesized by Harold Kroto and co-workers in 1985.[4]

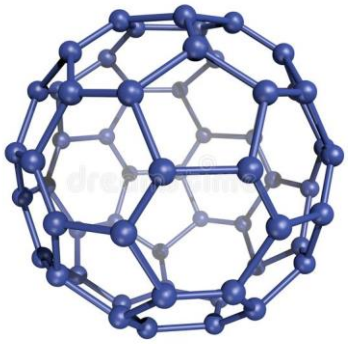

Figure I.A.1 Model of a C_{60} buckyball.

Graphene is an infinite two-dimensional (2D) carbon monolayer made entirely of sp^2 carbon atoms arrayed in a honeycomb fashion (Figure I.A.2).[5,6] This single-atom-thick sheet can be considered as the elementary building block for other allotropes of carbon like fullerenes and carbon nanotubes. The material has been theorized since decades but has been isolated and characterized only after 2004 by Andre Geim and Konstantin Novoselov.[7] It has remarkable

physical and chemical properties with immense potential for diverse applications. For example, it is the thinnest, lightest and strongest material known to man. Furthermore, it is the best conductor of heat and electricity at room temperature and also absorbs light uniformly across the visible and near infrared region of the spectrum. The surface area of graphene could reach up to 2630 m^2g^{-1}, which is much higher than many known materials.[8] Owing to the high surface area of this nanomaterial it exhibits exorbitantly high catalytic activity.[9]

The oxidised form of graphene is known as graphene oxide (GO). It is a two-dimensional graphene sheet with bountiful oxygenated functional groups on their basal plane and peripheral edges (Figure I.A.2).[10] During the fabrication process of GO, the π-conjugated arrangement is broken thereby making the material highly water dispersible. Moreover, it is the primary precursor for the synthesis of various graphene-based nanomaterials.

The reduced graphene oxide (rGO) can be considered in between graphene and graphene oxide, as it contains fewer functional groups as compared to GO (Figure I.A.2).[11] It is prepared from GO by chemical, thermal or electrochemical techniques. The graphene like properties of rGO makes it a suitable candidate for the fabrication of sensors, optoelectronic devices and in the preparation of composite materials.[11]

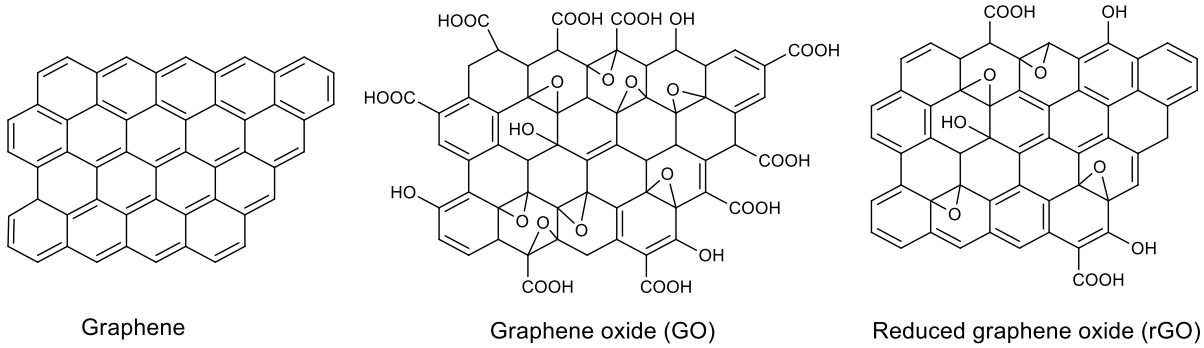

Figure I.A.2 Structure of monolayer graphene, graphene oxide and reduced graphene oxide.

Graphene nanocomposites refers to the intertwining of graphenes with other materials like polymers, metal oxide or metal nanoparticles, metal organic frameworks (MOFs) and other porous materials like silica, zeolites, etc.[12,13] Graphene nanocomposites show superior chemical and physical properties as compared to conventional composite materials. These nanocomposites also exhibit multifarious properties by combining the characteristics of individual components.

Carbon nanotubes (CNTs), also called buckytubes, are cylindrical molecules that consist of rolled-up sheets of single layer carbon atoms (graphene).[14] They can be divided into single-

walled CNTs (SWCNTs) with diameter of less than 1 nm, or multi-walled CNTs (MWCNTs) with diameter more than 100 nm (Figure I.A.3). The SWCNTs are made up of single layer carbon atoms, while MWCNTs consists of several multilateral graphene sheets that are rolled upon itself in concentric tubes.[15] Just like graphene, the carbon atoms in CNTs are sp^2 bonded with each other. There are various methods for the synthesis of CNTs, which include chemical vapor deposition (CVD), the arc-discharge method, flame synthesis method and other modified methods.[16] Owing to their unique structures; CNTs exhibit exceptional properties such as high electrical conductivity. Moreover, their large specific area, rich hollow and layered structure renders remarkable applications in diverse fields.

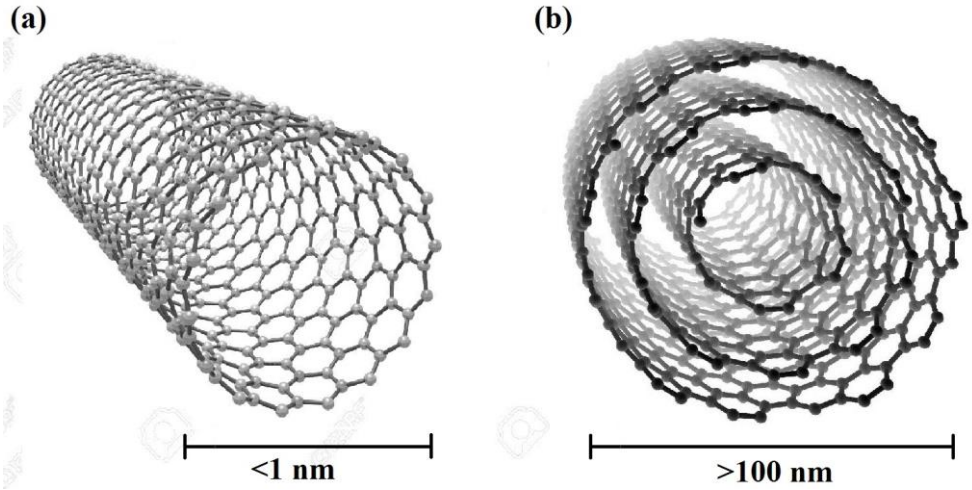

Figure I.A.3 Molecular representations of (a) SWCNT and (b) MWCNT.

Among the various carbonaceous nanomaterials, our studies has been primarily focussed on the synthesis and catalytic applications of graphene-based nanomaterials (GO and CMGs).

I.A.2 The wonder material graphene: A breakthrough invention in nanoscience

Ever since the isolation of graphene by Andre Geim and Konstantin Novoselov, the perception of how we see the nano world has changed entirely. In 2004, they isolated graphene by repetitive peeling of graphite layers using a scotch tape.[7] Although, this 'scotch tape' method undeniably gives a single layer of carbons, the method has been less useful for practical purposes due to very low yield. The synthesis of graphene has been based on two different methods, the 'top-down' approach and the 'bottom-up' approach. While the 'top-down' approach involves the separation of stacked layers of graphite to yield single layer graphene sheets, the 'bottom-up' approach comprises of the synthesis of graphene form alternative carbon sources (Figure I.A.4). In spite of the different routes to synthesize

graphene, its large scale production in an affordable manner still continues to be a considerable challenge.

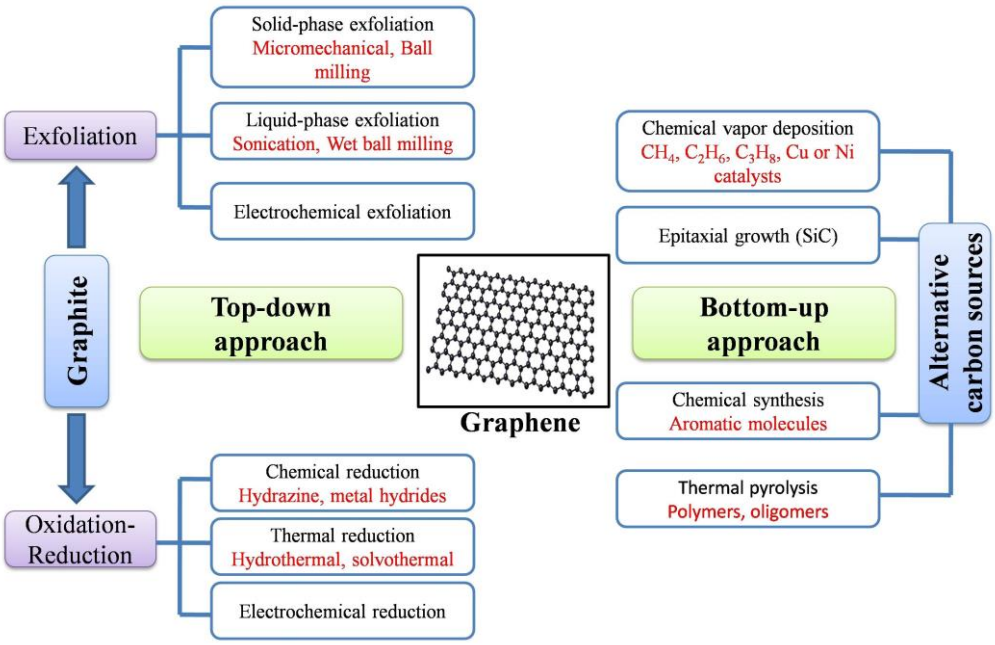

Figure I.A.4 Schematic illustration for the synthesis of graphene by 'top-down' and 'bottom-up' approaches.

I.A.2.1 Functionalization of graphenes

The two main ways for functionalization graphenes have been based on covalent and non-covalent methods (Figure I.A.5). Covalent functionalization of graphenes has been achieved by direct attachment of organic functionalities either to pristine graphene or to graphene oxide (GO). Graphene oxide itself can be considered as functionalized graphene along with its reduced form, the reduced graphene oxide (rGO). On the other hand, non-covalent functionalization of graphenes takes place through π-π interaction between the graphene surface and other moieties (Figure I.A.5). Another route for the functionalization of graphene involves the deposition of metal and metal oxide nanoparticles (NPs) on the surface of graphene sheets. The type of interaction between graphene and the nanoparticles can either be covalent or non-covalent, depending on the method of preparation of the composite material and the nature of the nanoparticles involved. For instance, palladium has a higher affinity towards graphene due to the partial covalent nature of binding between them.[17] The immobilization of metal and metal oxide NPs on graphene and functionalized graphenes have been dealt in detail in Chapter 2, Section A.

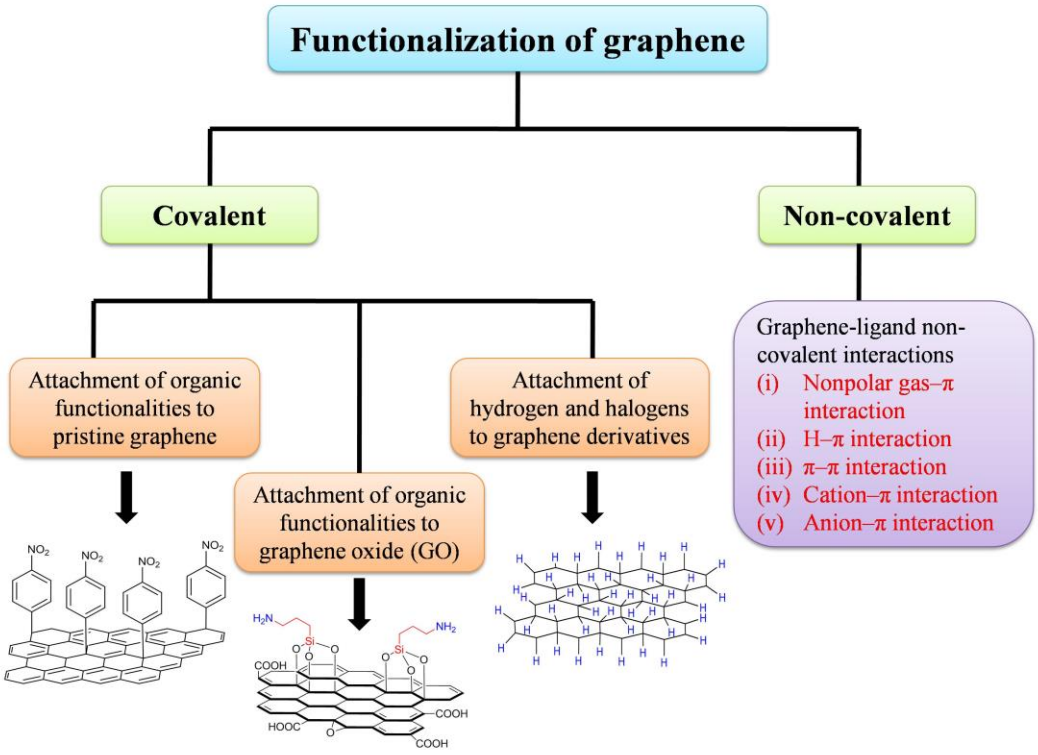

Figure I.A.5 Different routes for the functionalization of graphene.

I.A.2.2 Covalent functionalization of graphene

The covalent functionalization of graphenes has been done by three different routes, one involving the formation of covalent bonds between free radicals or dienophiles and C=C bonds of pristine graphene. The second route and by far the most explored one involve graphene oxide (GO) as the starting material (Scheme I.A.1). In this case, the formation of covalent bond occurs between different functional groups and oxygenated functional groups of GO. Moreover, GO can be transformed into reduced graphene oxide (rGO) which can then be further functionalized. The third one involves direct attachment of hydrogen and halogens to graphene derivatives leading to the formation of 'graphane' and fluorographene (graphene fluoride).

Tour and co-workers,[18] have decorated graphene with nitrophenyls via heating diazonium salt to produce highly reactive free radical, which subsequently reacts with sp^2 carbon atoms of graphene (Scheme I.A.2). This covalent functionalization of graphene results in decrease in the conductivity of graphene in a controlled manner, due to disruption of the π network. Moreover, it has been found that this covalent attachment of nitrophenyls leads to the introduction of a band gap.[19] Thus functionalization of graphene in this way could make them potentially useful for fabrication of semiconducting nanomaterials.

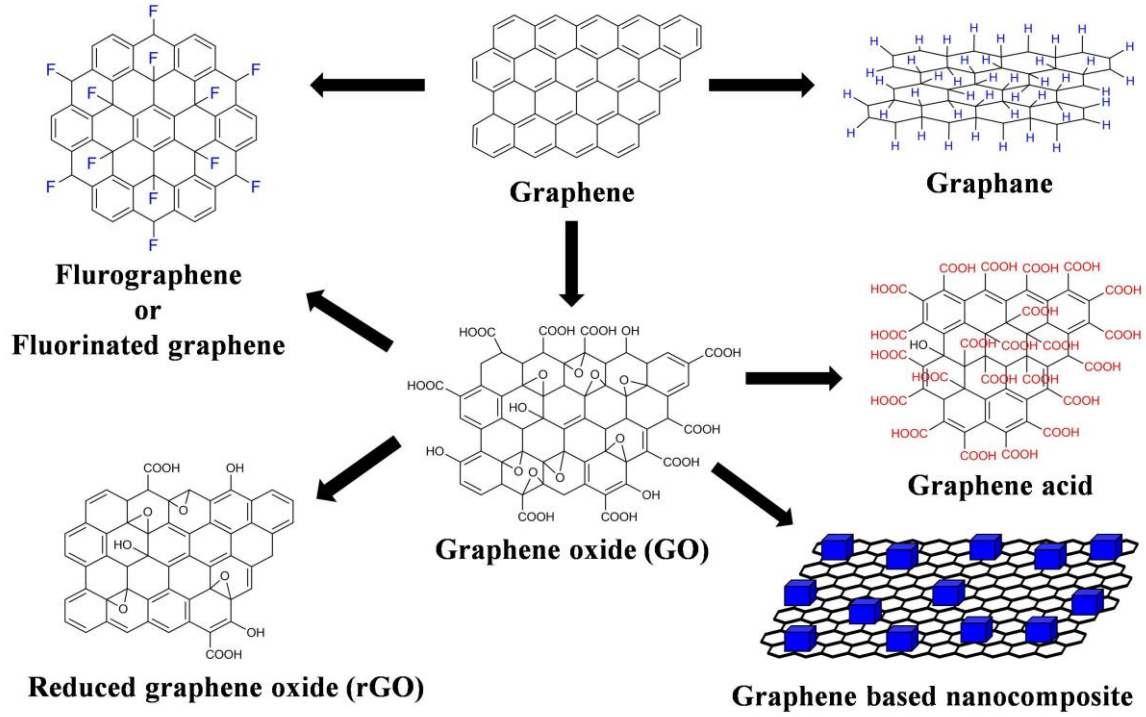

Scheme I.A.1 Schematic representation for the functionalization of graphene.

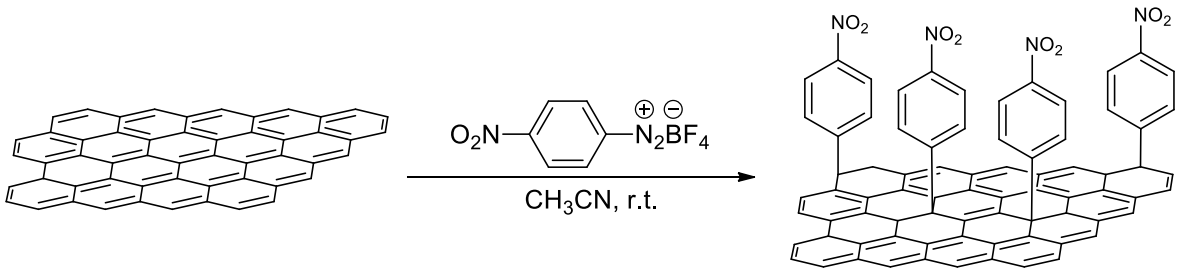

Scheme I.A.2 Covalent attachment of nitrophenyls with graphene.

The reaction of graphenes with dienophiles is another common route for the covalent functionalization. Azomethine ylide has been utilized as the prevalent dienophile for this purpose. For instance, graphene sheets have been decorated with dihydroxyphenyl groups through attachment with pyrrolidine rings (Scheme I.A.3). The attachment takes place via a 1,3-dipolar cycloaddition of azomethine ylide. The introduction of hydroxyl groups into graphene increases its dispersibility in polar solvents.[20]

Owing to the rich chemistry of hydroxyl, carbonyl, epoxy and carboxyl functional groups, GO has been selected as the primary precursor for the synthesis of various functionalized graphenes through covalent attachment. For instance, GO functionalized with $–CH_2OH$ terminated regioregular poly(3-hexylthiophene) (P_3HT) has been accomplished through the

formation of ester linkage with the carboxyl groups of GO (Scheme I.A.4). The presence of abundant –OH groups in the material facilitated its solubility in common organic solvents. The investigators designed a photovoltaic device by further combining this composite material (P_3HT/GO) with C_{60}. This combination resulted in a 200% increase in the power conversion efficiency in comparison to P_3HT/C_{60} system. This exceptional increase has been due to the extended electron delocalization that took place after the covalent attachment of P_3HT with GO.[21]

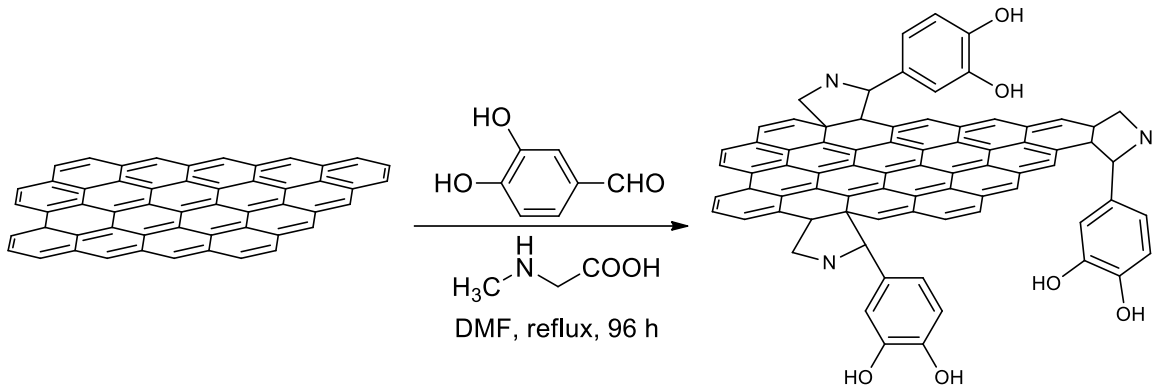

Scheme I.A.3 Functionalization of graphene via 1,3-dipolar cycloaddition of azomethine ylide.

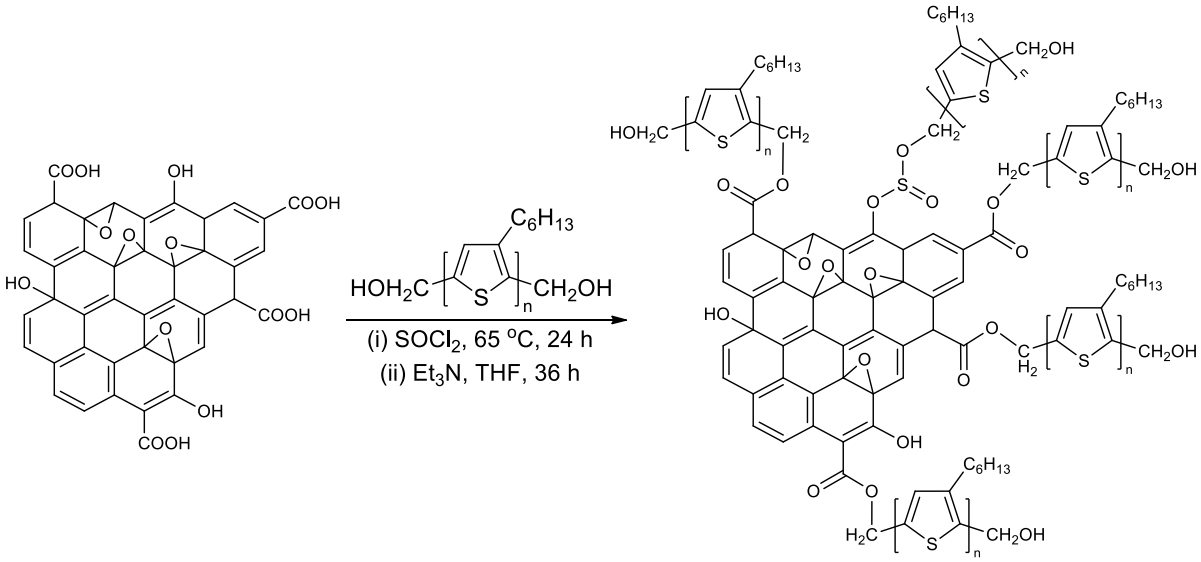

Scheme I.A.4 Synthesis of P_3HT grafted graphene.

In another approach a hybrid material has been prepared by covalent attachment between graphene oxide and pyrrolidine ring anchored C_{60} fullerene.[22] The pyrrolidine ring of C_{60} formed an amide linkage with the carboxyl groups present of the surface of GO (Scheme I.A.5). Such GO–C_{60} hybrid materials could find application in the fabrication of optoelectronic devices due to their excellent optical and electronic properties.

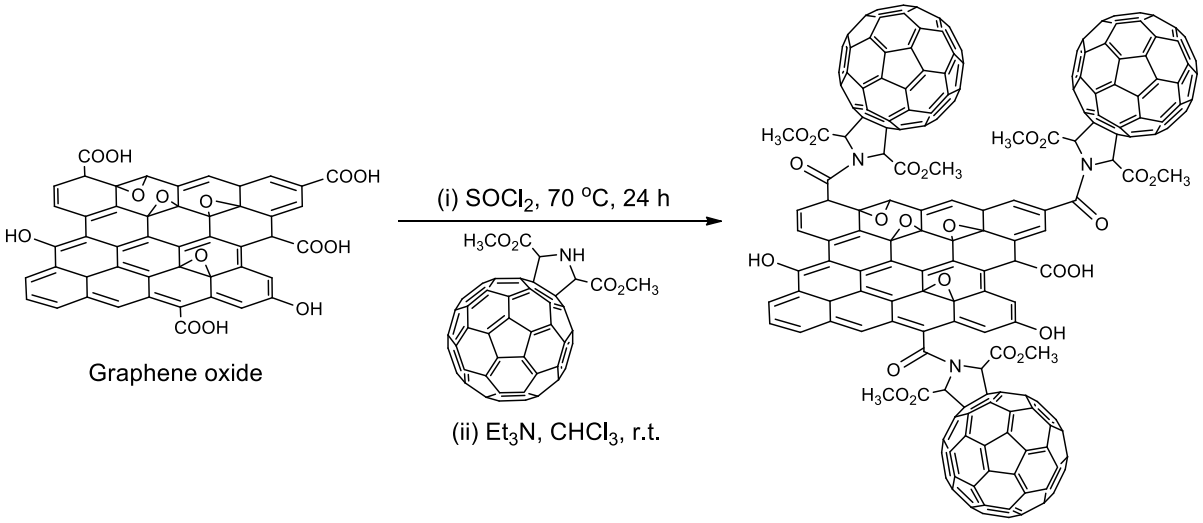

Scheme I.A.5 Formation of GO–C_{60} hybrid material form graphene oxide.

I.A.2.3 Graphene oxide (GO)

Graphene oxide (GO), the oxidised form of graphene has been primarily used as precursor for bulk scale production of graphene based materials. Although the name suggests similarity with graphene, GO exhibits widely different properties form pristine graphene. This is due to the disruption of the conjugated π network of graphene during its chemical treatment. Whereas pristine graphene is composed of sp^2 carbons spread endlessly, GO is highly functionalized with diverse oxygenated functional groups like hydroxyl, epoxy, carboxyl, etc.[10] The hydroxyl and epoxide groups lie on the basal plane and the carboxyl groups are located at the peripheral edges of GO sheets (Scheme I.A.6). Thus graphene oxide can be considered as a single layer of graphite sheet with a variety of different hydrophilic oxygenated functional groups.

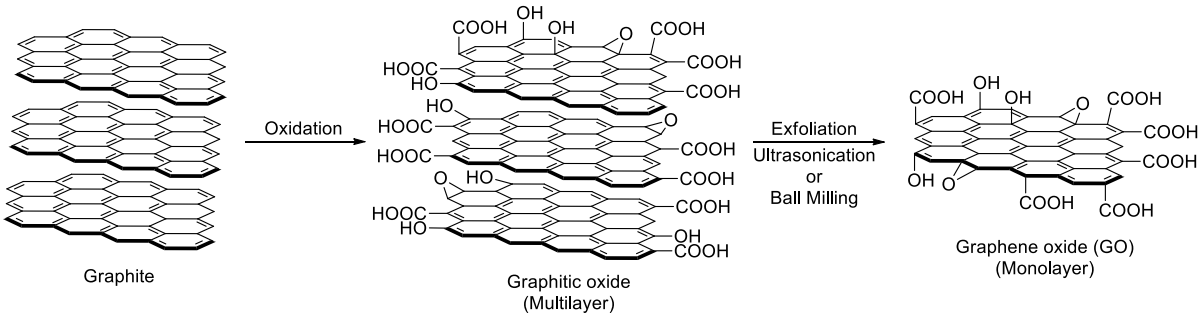

Scheme I.A.6 Schematic representation for the synthesis of graphene oxide (GO).

Owing to the presence of carboxyl and hydroxyl groups, graphene oxide has been found to be slightly acidic in nature (pH 4.5 at 0.1 mg mL^{-1}).[23] Furthermore, in solution graphene oxide shows three different pK_a values of 4.3, 6.6 and 9.0 corresponding to carboxyl, phenolic and

hydroxyl groups respectively.[24,25] The presence of ionisable groups has been reflected in their high dispersibility in aqueous medium. However, the solubility of GO in aqueous medium decreases with the decrease in the pH value of the dispersion because the repulsive force between GO sheets gets weakened due to the protonation of carboxyl and phenolic groups. Moreover, exfoliated graphene oxide also forms stable colloidal dispersions in water due to the electrostatic repulsion between the GO sheets resulted after ionisation of the carboxyl and phenolic groups.

I.A.2.4 Milestones in the synthesis of graphene oxide

The synthesis of multilayer graphene oxide can be classified into three different categories based on the type of chemical oxidising agents used. They are the chlorate method, the permanganate method and the third method comprising of novel oxidants like chromate,[26] ferrate,[27] benzoyl peroxide,[28] etc.

I.A.2.4a Chlorate methods

The first synthesis of multilayered graphene oxide dates back to 1859, when Benjamin Brodie heated lamellar graphite in presence of strong oxidising agents.[29] The main objective was to unravel the chemical structure of this material. In his experiment, Brodie treated graphite with a mixture of potassium chlorate ($KClO_3$) and fuming nitric acid (HNO_3) at 60 °C for 3-4 days. At that time $KClO_3$ was commonly used as a source of molecular oxygen and nitric acid was known to react strongly with aromatic carbons. The product obtained after repeated oxidative treatments was found to be acidic in nature, which led Brodie to coin the term ‘graphic acid’ for this new material.

In 1898 L. Staudenmaier,[30] modified the Brodie’s method by adding potassium chlorate in small portion during the course of the reaction. Moreover, sulfuric acid (H_2SO_4) was also added in small amounts in order to increase the acidity of the mixture and shortening the overall reaction time. The main objective behind the use of H_2SO_4 was to reduce the amount of fuming nitric acid, thereby evading large emission of toxic gases (NO_2, N_2O_4) and making the process comparatively safer. The material thus obtained in this was found to posses similar properties to that of Brodie’s graphic acid.

Forty years later, Hofmann,[31] attempted to develop an even safer alternative method by using $KClO_3$ and non-fuming nitric acid. Although the material formed in this way possessed similar properties, the level of oxidation was found to be lower.

I.A.2.4b Permanganate methods

Almost one hundred years after the initial discovery of Brodie, Hummers and Offeman,[32] developed the fastest, safest and most convenient method for the synthesis of graphene oxide. Their method of oxidative chemical exfoliation consisted of potassium permanganate along with sulfuric acid and a small amount of sodium nitrate. The level of oxidation was similar to that of Brodie's method; however, the absence of $KClO_3$ prevented the release of explosive ClO_2 gas. Although the release of ClO_2 gas could be eliminated, the formation of other toxic gases (NO_2, N_2O_4) could not be avoided. Moreover, the GO synthesized by Hummers' method contains traces of sulfur and nitrogen presumably as covalently bonded sulphates and nitrates. Nevertheless, Hummers' method remains as a fundamental process for producing large quantities of graphite oxide even today.

Recently, an improved method for the preparation of graphene oxide has been developed. Tour and co-workers,[33] ameliorated Hummers' method by replacing sodium nitrate with phosphoric acid for the oxidative chemical exfoliation of graphite. The GO produced through this method has a higher yield, more uniform structure and a higher level of oxidation. Hence, this method has been regarded as the fourth principal method for the preparation of GO.

I.A.2.4c Other methods

Apart from the chlorate and permanganate method, several modern ways to oxidise graphite have evolved. For instance, potassium chromate has been used as oxidant either using Jones conditions,[27] or in combination with HNO_3 or $HClO_4$.[34] Moreover, potassium ferrate has also been used to oxidise graphite in presence of sulfuric acid at room temperature,[27] or with hydrogen peroxide in aqueous media at 50 °C.[35] Other routes for the preparation of graphene oxide include benzoyl peroxide,[28] and acid-free oxidation in presence of oxone.[36] The key routes for the oxidative exfoliation of graphite towards the synthesis of GO are listed in Table I.A.1.

Table I.A.1 Prevalent strategies for the synthesis of GO

Classification	Method	Conditions	Year
Chlorate	Brodie	$KClO_3$, fuming HNO_3, 60 °C, 3-4 d	1859
	Staudenmaier	$KClO_3$, HNO_3 + H_2SO_4, 60 °C, 1-2 d	1898
	Hofmann	$KClO_3$, HNO_3 (non-fuming)	1937
Permanganate	Hummers	$KMnO_4$ + $NaNO_3$, H_2SO_4, 35 °C, 2 h	1958
	Tour	$KMnO_4$, H_2SO_4 + H_3PO_4, 50 °C, 12 h	2010

	Mechanochemical	$KMnO_4$, ball mill, 500 rpm, 3 h	2013
	Microwave assisted	$KMnO_4$, H_2SO_4, 250 W, 150 s	2014
	Room temperature	$KMnO_4$, H_2SO_4, 10-25 °C, 4-8 h	2019
Chromate	Jones	H_2CrO_4, H_2SO_4	1978
	Cr(VI)	K_2CrO_4, $HClO_3$, HNO_3, 50 °C, 24 h	2012
Ferrate	Room temperature	K_2FeO_4, H_2SO_4, r.t., 1 h	2015
	Fe(VI)	K_2FeO_4 + H_2O_2, H_2O, 50 °C, ~ 4 h	2016
Peroxide	Organic process	$C_{14}H_{10}O_4$, 110 °C, 10 min	2009
Oxone	Acid-free	$KHSO_5$, DMF, heat	2015

Besides these methods there are several other procedures which employ combination of different reagents, co-oxidants and physical promoters. Furthermore, the electrochemical approaches are also used for large scale production of high quality graphene oxide. These methods are considered more environmentally benign than chemical methods in terms of low waste generation.[37,38] A careful optimization of the amount of water and the temperature of the reaction leads to the formation of either hydroxyl- and epoxide-rich GO sheets or more carbonyl-rich domains.[39]

I.A.2.5 Structure of graphene oxide

Among the various known models for the structure of graphene oxide, the model that accounts for most of the experimental observations has been proposed by Lerf-Klinowski in the late 1990s.[40-43] After a series of analytical studies using ^{1}H, ^{13}C solid state NMR and FT-IR, Lerf-Klinowski concluded that GO contains two different regions. Those are aliphatic regions with six-membered rings and aromatic regions with non-oxidized benzene rings. The actual distribution of oxygenated functional groups on GO is not fully understood due to its non-stoichiometric composition. Nevertheless, several different models for the structure of GO have been suggested by different groups which are presented in Figure I.A.6.

Owing to the presence of different oxygenated functionalities in GO, it has been frequently used as catalyst in diverse organic reactions. Few examples of graphene oxide as a carbocatalyst in organic transformations are presented below.

In 2010 C. W. Bielawaski,[44] was the first to demonstrate the oxidative property of GO in synthetic organic transformation. They employed GO (200 wt%) for the oxidation of alcohols

to carbonyl compounds and hydration of alkynes to corresponding ketones, thus establishing the propensity of GO towards oxidation reaction (Scheme I.A.7).

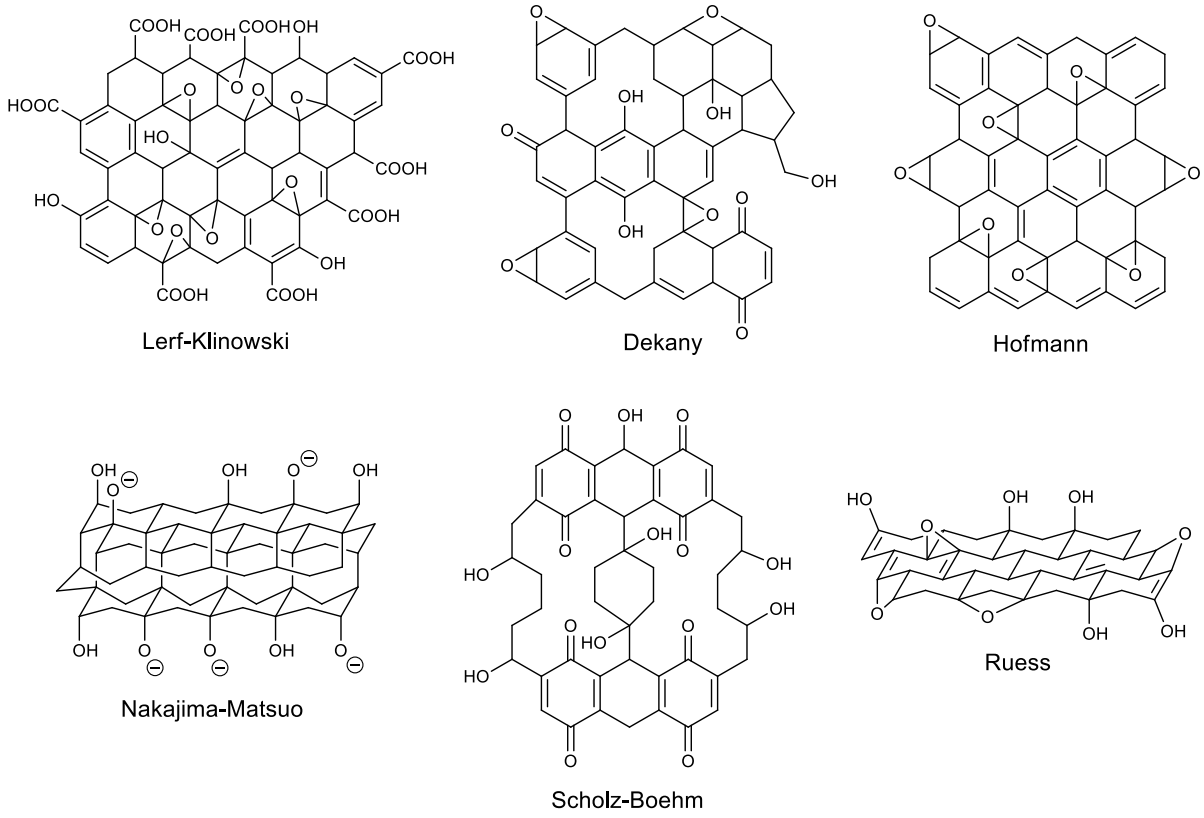

Figure I.A.6 Different structural models of GO.

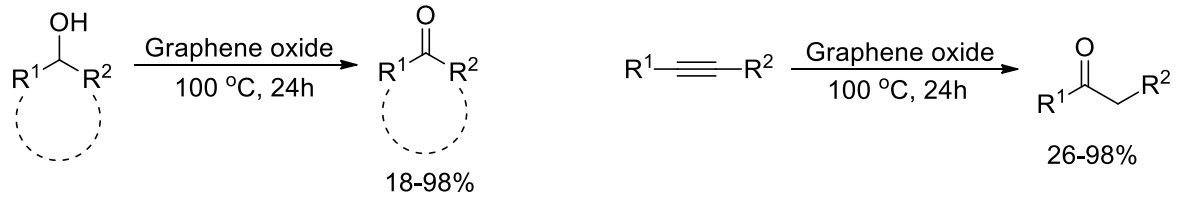

Scheme I.A.7 Graphene oxide mediated oxidation and hydration reactions.

The same group reported graphene oxide as an effective oxidant for the C–H oxidation of various olefins, methyl benzenes and diarylmethanes.[45] Moreover, the catalyst was also used successfully for dehydrogenation of aromatic hydrocarbons. The advantage of the protocol was that no additional co-oxidants or transition metal catalysts were required (Scheme I.A.8). Bielawaski and co-workers,[46] accomplished the oxidation of thiols and sulfides to disulfides and sulfoxides using graphene oxide. The heterogeneous nature of the catalyst led to easy isolation and purification of the final products (Scheme I.A.9).

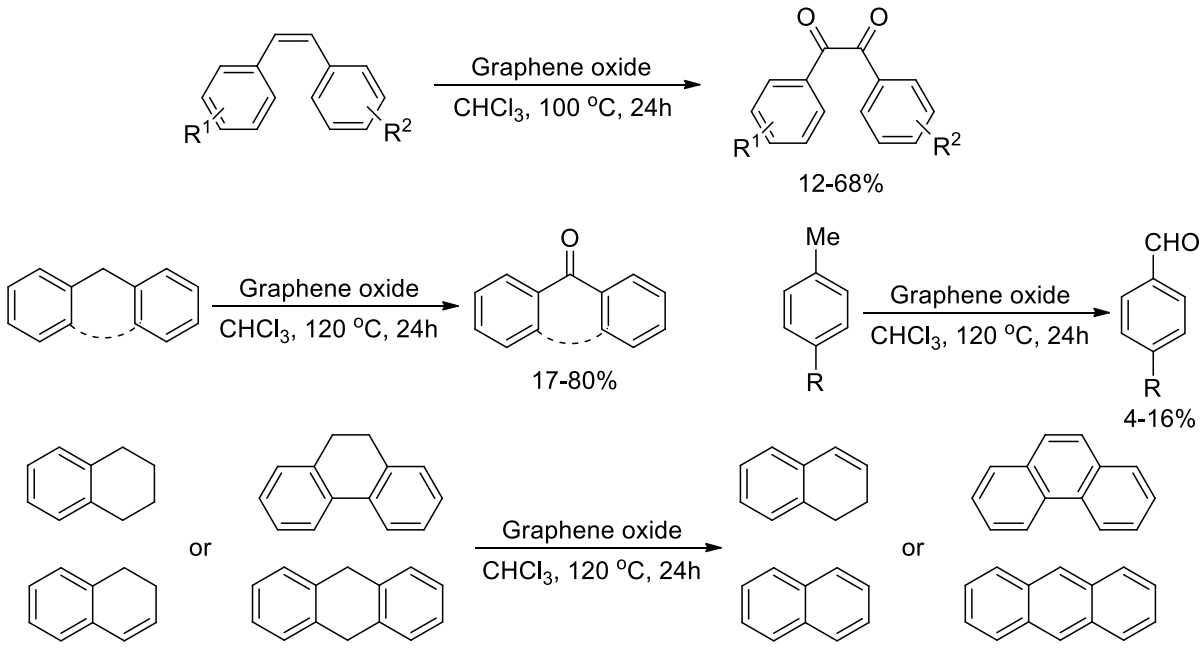

Scheme I.A.8 GO mediated oxidation and dehydrogenation reactions.

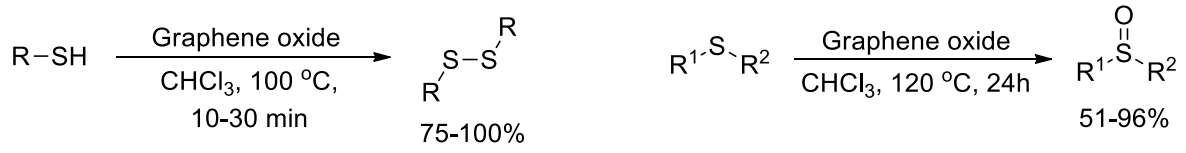

Scheme I.A.9 Oxidation of thiols and sulfides in presence of GO.

Apart from oxidation reactions, GO nanosheets have been successfully employed as catalyst in the synthesis of diversely functionalized heterocyclic compounds like 2-pyrrolidinones, furanones and 2-oxo dihydropyrroles (Scheme I.A.10).[47]

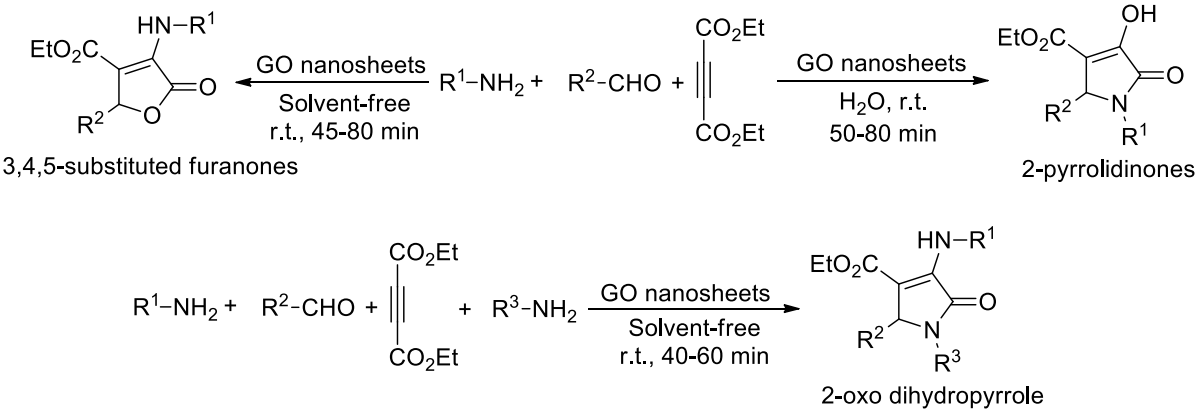

Scheme I.A.10 GO nanosheets catalyzed synthesis of heterocyclic compounds.

The acidic nature of GO has been utilized in the thioacetalization of aldehyde under solvent-free conditions.[48] A range of symmetrical as well as unsymmetrical thioacetals have been synthesized using catalytic amount of GO (Scheme I.A.11).

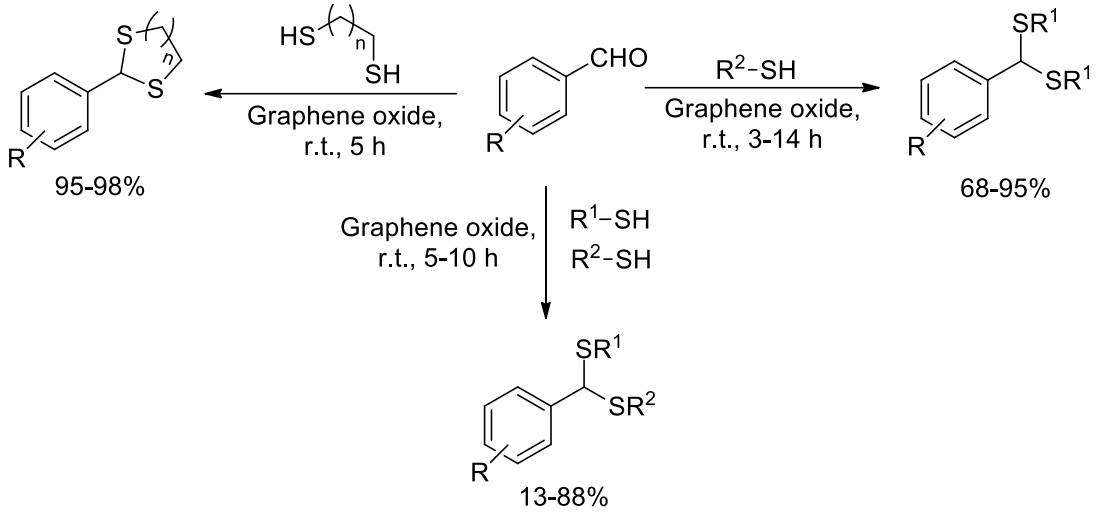

Scheme I.A.11 GO catalyzed thioacetalization of aldehydes.

I.A.2.6 Reduced graphene oxide (rGO)

The reduced form of graphene oxide generated by reductive exfoliation treatment of GO has been regarded as reduced graphene oxide (rGO). This material has mechanical and optoelectronic properties very close to that of pristine graphene.[11] Reduced graphene oxide possesses graphene-like basal plane with specific zones containing oxidized chemical entities. The graphene-like properties makes this material a suitable candidate for myriads of application and fabrication of optoelectronic and energy storage devices.[49] Reduced graphene oxide can be easily prepared in large quantities form GO by thermal,[50] electrochemical,[51,52] microwave- and photo-assisted methods.[53,54] During the reduction process of GO, the removal of epoxy and hydroxyl groups are more facile than that of carboxyl groups. The carbon-oxygen ratio determines the level of reduction that has been achieved. Henceforth, it is noteworthy to mention that the quality and property of rGO depends on the method by which it has been prepared. Chemical reduction of GO has been generally performed by using hydrazine hydrate and other hydrazine derivatives.[55] Other commonly used reducing agents include sodium borohydride,[56] sodium borohydride in combination with sulfuric acid,[57] hydroiodic acid,[58] etc. Apart from these reagents, some organic reducing agents like ascorbic acid,[59] amino acids and various leaf extracts have been employed for the synthesis of rGO.[60] Since, most of the oxidising and acidic functionalities are lost during the reduction process, rGO have been seldom used as catalyst. However, rGO is used for immobilization of

metal NPs or in the preparation of diverse nanocomposite materials, which subsequently exhibits exceptional catalytic property.[61]

I.A.2.7 Other graphene derivatives

Apart from graphene oxide (GO), reduced graphene oxide (rGO) and chemically modified graphenes (CMGs), there are few other graphene derivatives that have emerging in the recent years. These include graphane (fully hydrogenated graphene), graphol (hydroxyl form), thiographene, graphene acid, halogenated graphene, graphene fibers, etc. Sofo and co-workers,[62] theoretically predicted the existence of graphane and fluorinated graphane. The material could be synthesized by exposing graphene to cold hydrogen plasma.[63,64] The characterization of graphane indicated conversion of sp^2 domains into sp^3 without the loss of hexagonal symmetry. Owing to the complete loss of conjugation in graphane, it behaves as an insulator.

Fluorographene or graphene fluoride has been synthesized by the treatment of XeF_2 on graphene at room temperature.[65] During fluorination the sp^2 carbon atoms reorganize to sp^3 carbon in fluorographene, which changes its structure and optical properties. Fluorographene behaves as an insulator and shows anisotropic negative magnetoresistance.[66]

Graphene fiber is a new generation of macroscopically assembled carbonaceous fiber comprising of individual units graphene and its derivatives.[67] Graphene fibers have been prepared by wet spinning of graphene oxide liquid crystals followed by reduction.[68] The material is expected to possess extreme mechanical and transport properties which could find application in textiles, electronic devices, photodetectors, supercapacitors and batteries.

I.A.2.8 Non-covalent functionalization of graphene

Graphene sheets are hydrophobic in nature and forms multilayer due to π-π stacking. To avoid this π-π stacking, non-covalent functionalization of graphene is essential. Non-covalent functionalization is an attractive method since it allows attachment of different functional groups to graphene without disturbing the π-electronic network.[69] The type of contact through which graphenes could be non-covalently functionalized includes nonpolar gas-π interaction, H-π interaction, π-π interaction, cation-π interaction and anion-π interaction.

I.A.3 References

References are given in BIBLIOGRAPHY under Chapter I, Section A.

Chapter I

Section B

Graphene Oxide (GO) Promoted Direct C–H Sulfenylation of Aromatic Compounds

I.B.1 Introduction

Cross-dehydrogenative coupling (CDC) has emerged as a breakthrough synthetic strategy for the formation of C–C bonds.[1] It involves direct coupling of two different C–H bonds under oxidative conditions, hence the name cross-dehydrogenative coupling. The C–H bonds could be part of sp^3-C, sp^2-C and sp-C, for either of the partners (Scheme I.B.1). For example, Glaser coupling which is a coupling between two C(sp)–H bonds has been documented long before the concept of CDC has emerged.[2] Apart from C–C bond formation, C–X bonds are also generated via cross-dehydrogenative coupling between C–H and X–H (X = N, O, S, P, etc) bonds. This technique has been pioneered by Chao-Jun Li and co-workers in 2004 while working with the synthesis of propargylamines.[3] They successfully constructed C–C bond via C(sp^3)–H and C(sp)–H bond activation.

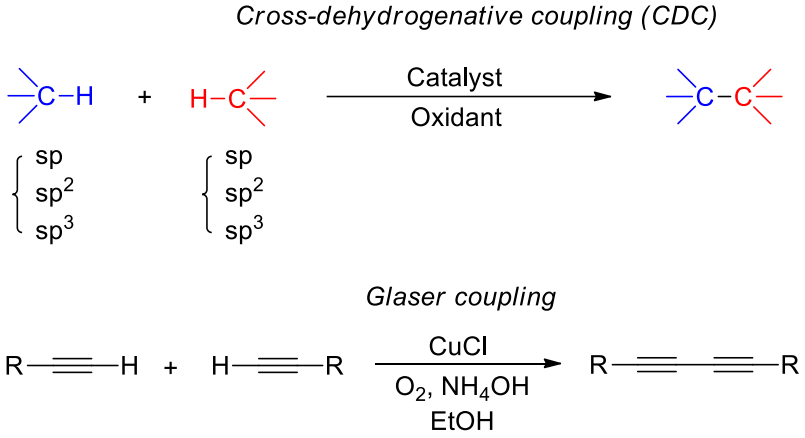

Scheme I.B.1 Cross-dehydrogenative coupling (CDC).

The classical method for the formation of C–C bond has been based on the nucleophile-electrophile approach. However, such transformation requires pre-functionalization of either of the reacting species. The methodology took a huge leap after the development of transition-metal catalyzed cross-coupling reactions[4] and metathesis reactions.[5] Although transition-metal catalyzed cross-coupling reactions sufficed the gaps to a great extent, the problem of pre-functionalization of the starting materials remained as a challenge. For instance, the presence of a leaving group is essential for one of the coupling partners. Besides, the use of expensive metal catalysts, harsh reaction conditions and lack of atom-economy are others limitations of transition-metal catalyzed coupling reactions. Hence, CDC has become an elegant strategy for direct access to C–C or C–X bonds.[6,7] Since the formation of C–C bond via CDC occurs at the expense of two C–H bonds, it is also known as dual C–H activation. In such transformation there is a loss of hydrogen, which is thermodynamically

unfavourable, hence an oxidant is used which acts as sink for excess electrons and make the overall process feasible.[8] Commonly used oxidants are hydrogen peroxide, *tert*-butylhydroperoxide (TBHP),[9-11] di-*tert*-butyl peroxide (DTBP),[12] molecular oxygen (O_2),[13,14] molecular iodine (I_2),[15] hypervalent iodine,[16,17] 2,3-dichloro-2,6-dicyanobenzoquinone (DDQ),[18] potassium perdisulfate ($K_2S_2O_8$).[19]

Ever since the origin of CDC, several different research groups have focussed their attention towards the development of this novel synthetic methodology.[20] Although transition-metal catalyzed CDC is well known; metal-free protocols are also gaining popularity due to environmental considerations. In this context, molecular iodine (I_2) has been recognized as an inexpensive and benign catalyst for CDC.[15] Numerous catalytic systems have been developed for the formation of C–C,[13,17,21,22] C–N,[23] C–O,[23,24] C–S,[14,25] and C–Se,[26,27] bonds via CDC. Furthermore, enantioselective CDC is also possible and has been reported for the alkynylation of tetrahydroisoquinolines.[28,29] Moreover, tetrahydroisoquinolines have also been alkynylated under mechanochemical conditions using ball milling technique in presence of DDQ as oxidant (Scheme I.B.2).[30]

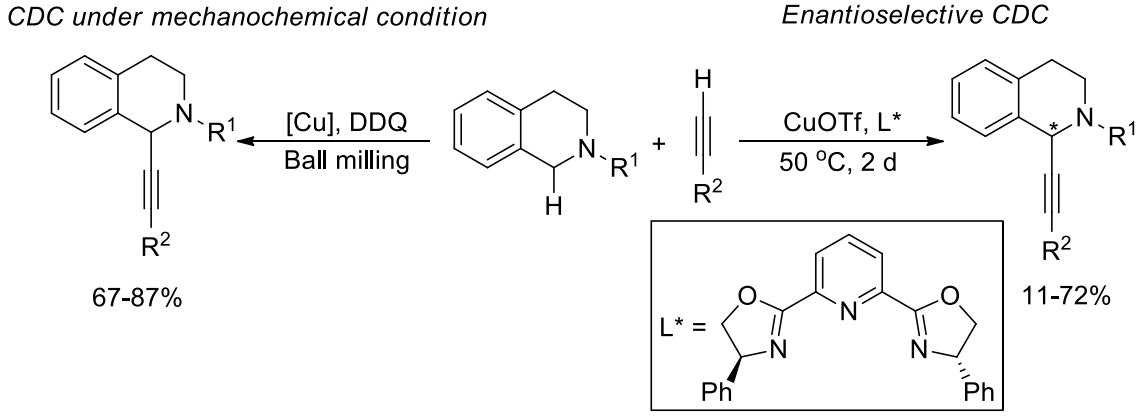

Scheme I.B.2 Cross-dehydrogenative coupling between C(sp^3)–H and C(sp)–H bond.

Organosulfur compounds are endowed with a wide range of potential biological activities.[31] The synthesis of heterocyclic scaffolds bearing sulfur unit has been the topic of immense research. For instance, functionalized indoles are prevalent in myriads of natural products possessing medicinal properties.[32-34] Among the various indole derivatives, 3-sulfenylindoles have received enormous attention because of their potential uses in the treatment of cancer,[35] heart diseases,[35] allergies,[36] HIV,[37] obesity, Alzheimer's disease,[35] and bacterial infections.[38] Moreover, indolylarylsulfones acts as HIV-1 non-nucleoside reverse transcriptase inhibitors.[39] The 3-sylfenylindoles are also found to be effective against tubulin polymerization,[40] and COX-2 inhibition.[41] Furthermore, aryl sulphides are essential building

blocks for several active pharmaceutical ingredients (APIs).[35] Few representative bioactive molecules with sulfur functionalized indole skeleton are shown in Figure I.B.1.

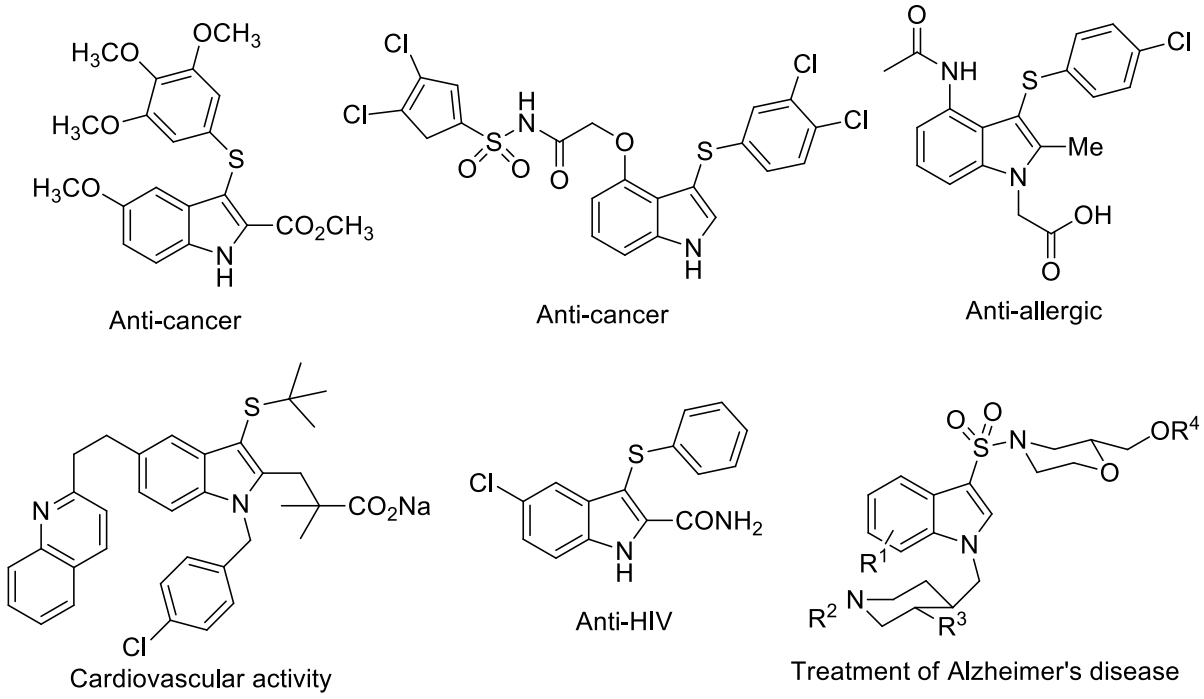

Figure I.B.1 Bioactive sulfur functionalized indoles.

Owing to their prevalence in numerous bioactive molecules, natural products and APIs the synthesis of 3-sulfenylindoles has attracted widespread attention. The two most common ways for the synthesis of 3-sulfenylindoles are: (a) the direct sulfenylation of indole ring and (b) the cyclization reactions of 2-alkynylanilines,[42,43] or N,N-dialkyl-2-iodoanilines (Scheme I.B.3).[44,45] The direct sulfenylation of indole ring has been carried out using diverse sulfenylating reagents like thiols,[46-51] disulfides,[52,53] sulfenyl halides,[54] sulfinates,[37,55] sulfonyl hydrazides,[56] sulfonyl chlorides[57,58] and N-thioimides.[59,60] In addition, the sulfenylation of indoles has been accomplished by using elemental sulfur as the sulfenylating reagent, avoiding the use of any organic sulfenylating reagents.[60]

Carbonaceous nanomaterials like graphenes and chemically modified graphenes (CMGs) have been used as catalyst for synthetic organic transformations since the first seminal paper by Bielawaski in 2010.[61] Ever since the concepts of green chemistry became customary in organic synthesis, the use of carbon based heterogeneous nanomaterials has become more popular.[62] Apart from its versatile catalytic activity, such catalysts can be re-used for several catalytic cycles without its activity getting diminished.

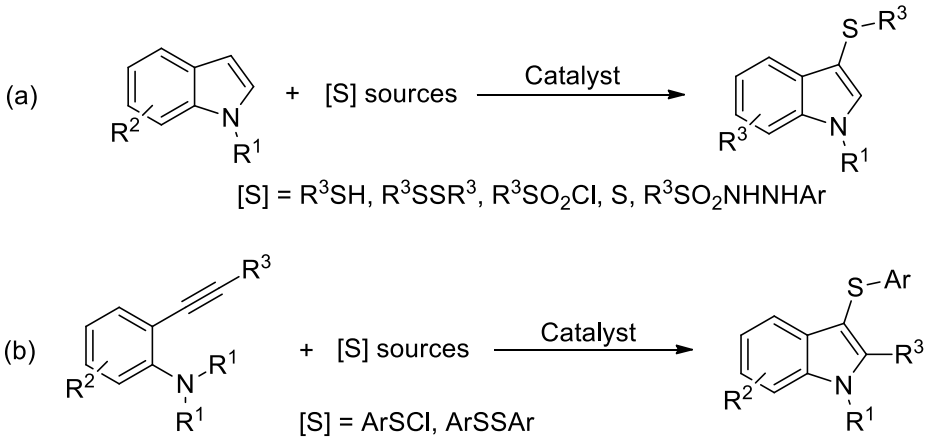

Scheme I.B.3 Common strategies for the synthesis of 3-sulfenylindoles.

I.B.2 Background and objectives

The fascinating biological profile of sulfenylated indoles intrigued researchers to develop numerous synthetic methods for its synthesis. Among the various known protocols, transition metal catalyzed regioselective sulfenylation of indole has been reported with various metals like Cu, Fe, Mg, Ce, V, Ru, etc.[58,59,63-67] The direct C–H sulfenylation of aromatic compounds have been reported either using peroxides or transition metal catalysts in combination with DMSO as oxidant.[68-71] Considering the toxicity as well as expensive nature of various transition metal based catalysts, metal-free methods have been developed. The most common approach has been the use molecular iodine in the presence of various sulfenylating reagents like thiols, disulfides, etc. However, most of these conditions using thiols as the sulfenylating reagent, required the presence of *tert*-butyl hydroperoxide (TBHP),[46] hydrogen peroxide (H_2O_2),[47] or DMSO as oxidant.[48-51] Moreover, the use of sulfenylating reagents other than thiols generated by-products thereby lowering atom economy of the reaction.[52,53,56,57] Although, the use of thiols in the regioselective sulfenylation, appears to be atom-economic, the presence of strong oxidants could lead to unwanted side reactions.[46-51] In another report, bovine serum albumin has been used as catalyst in combination with iodine for the regioselective sulfenylation of aromatic C(sp^2)–H using thiol.[72] Furthermore, the reaction has also been successful in the absence of any metal catalysts or iodine but required a strong base like NaOH.[73,74] A few examples citing recent developments in catalytic systems towards sulfenylation are presented below.

Iodine catalyzed regioselective sulfenylation of have been reported by using sulfonyl hydrazides as the sulfenylation reagent (Scheme I.B.4). The investigators presumed that the –$NHNH_2$ group of sulfonyl hydrazide removes the two oxygen atoms of the sulfonyl group

and serves as an effective sulfenylating agent. The sulfenyl group has been introduced selectively at the 3 position 1*H*-indole. However, when the 3 position of 1*H*-indole has been occupied the sulfenylation took place at the 2 position.[56]

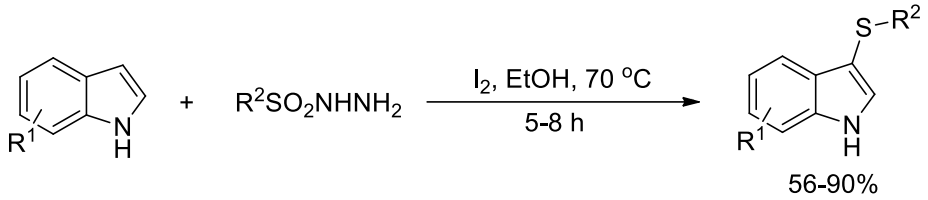

Scheme 1.B.4 Iodine catalyzed regioselective sulfenylation of 1*H*-indoles.

Microwave (MW) assisted synthesis of 3-sulfenyl and 3-selenylindoles have been achieved by using molecular iodine as catalyst.[53] The reaction took place in presence of DMSO as oxidant under MW irradiation (Scheme I.B.5). The authors suggested that iodine reacted with disulfide/diselenide and resulted in the formation of an electrophilic species RYI (Y = S/Se). The electrophilic species then reacted with indole leading to the formation of the desired product along with the concomitant release of HI.

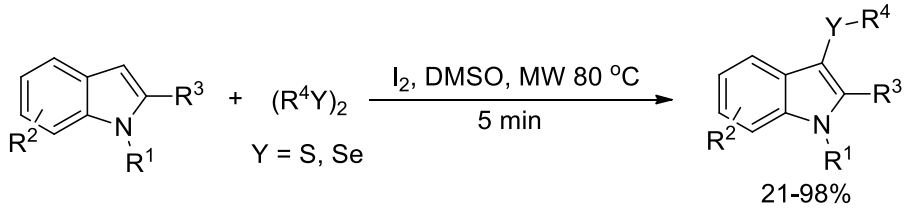

Scheme I.B.5 MW assisted and iodine catalyzed synthesis of 3-sulfenyl and 3-selenylindoles.

A facile method for the synthesis of 3-sulfenylindoles under mild conditions has been reported by using iodine as catalyst and TBHP as oxidant (Scheme I.B.6). A series of thiophenols and mercaptobenzoic acids have been used as the sulfenylation reagent furnishing the desired products in good to excellent yields. However, in the case of 3-substituted indoles, sulfenylation took place regioselectively at the 2 position. In addition 2,3-bis-sulfenylindoles has also been synthesized by following the same protocol. Moreover, the authors also carried out gram scale synthesis which afforded the desired product in 86% yield.[46]

An expedient synthesis of 3-sulfenylindoles has been reported by using cuprous chloride in presence of PPh_3 as reductant (Scheme I.B.7). The reaction conditions involve sulfonyl chloride as the sulfenylation reagent and the desired products have been obtained in 71-98%. Moreover, the investigators proposed a plausible mechanism.[58]

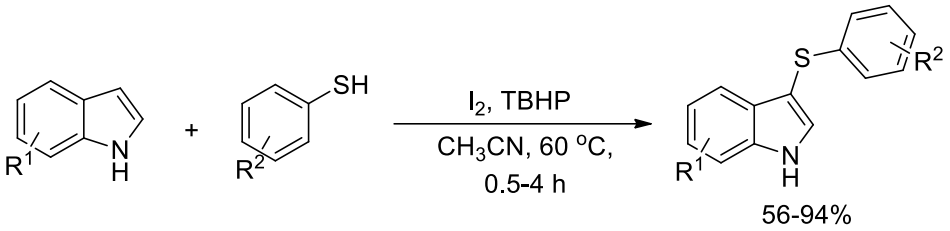

Scheme I.B.6 Molecular iodine catalyzed sulfenylation of indoles using thiophenols.

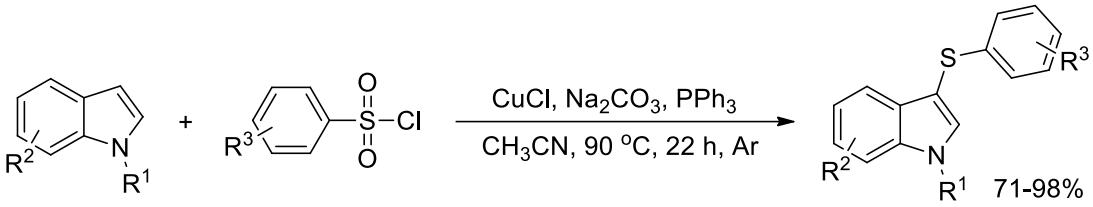

Scheme I.B.7 Copper catalyzed 3-sulfenylation of indoles.

Palladium catalyzed and ionic liquid mediated regioselective sulfenylation of indoles has been accomplished by using elemental sulfur as the sylfenylating reagent. The reaction conditions involve three-component strategy involving indoles, arylboronic acids and sulfur in the presence of copper iodide (Scheme I.B.8). Both 1*H*-indoles as well as N-substituted indoles reacted efficiently during the course of the reaction. Moreover, the protocol has been further extended towards the sulfenylation of 1*H*,1′*H*-2,2′-bisindole, pyrrole, furan, benzofuran and imidazo[1,2-*a*]pyridines. The investigators also suggested a plausible mechanism on the basis of some control experiments.[60]

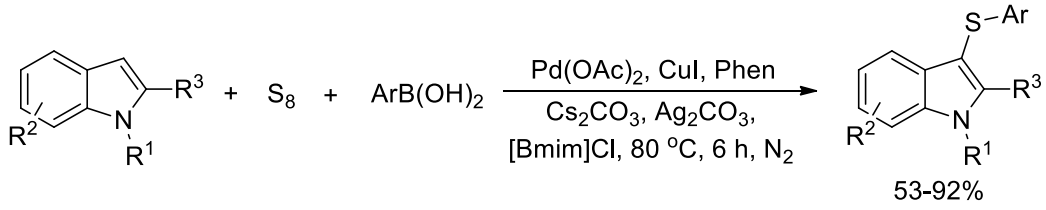

Scheme I.B.8 Palladium catalyzed regioslective sulfenylation of heteroarenes.

The regioselective sulfenylation of N-methylindoles has been developed under photoredox catalysis (Scheme I.B.9). The investigators have used $Ru(bpy)_3Cl_2$ as photoredox catalyst and arylsulfonyl chlorides as the sulfenylation reagent. The mechanism of the reaction involved a single electron transfer (SET) process generating radical intermediates.[63] A 23 W compact fluorescent lamp (CFL) has been used as the source of visible light.

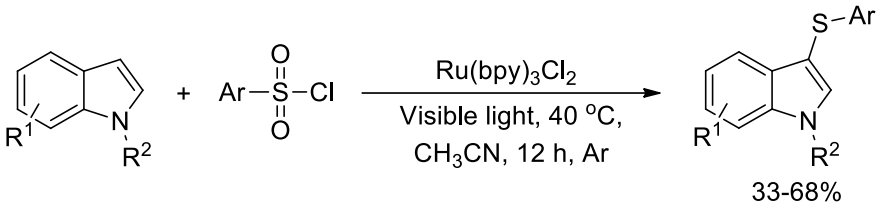

Scheme I.B.9 Visible light induced photocatalytic synthesis of 3-sulfenylindoles.

An efficient synthesis of 3-sulfenylindoles has been developed by using anhydrous $CeCl_3$ as catalyst.[59] N-(alkylthio) and N-(arylthio)phthalimides have been used as the sulfenylation reagent (Scheme I.B.10). The reaction conditions are facile and the desired products have been obtained in 80-95%.

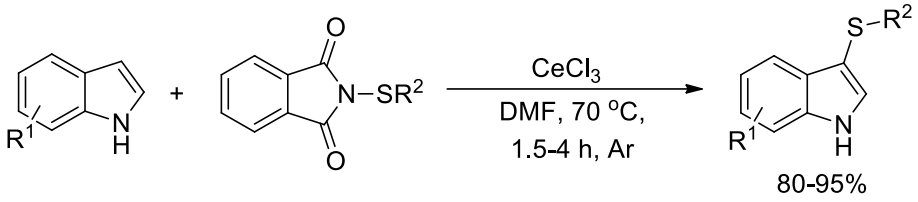

Scheme I.B.10 $CeCl_3$ catalyzed synthesis of 3-sulfenylindoles.

Potassium iodate (KIO_3) has been used as an oxidant for the metal-free chalcogenation of indoles and imidazopyridines (Scheme I.B.11). The authors carried out the synthesis using disulfides/diselenides and glycerol as a benign additive.[27] Moreover several control experiments have been performed to get insights into the mechanistic pathway for the reaction.

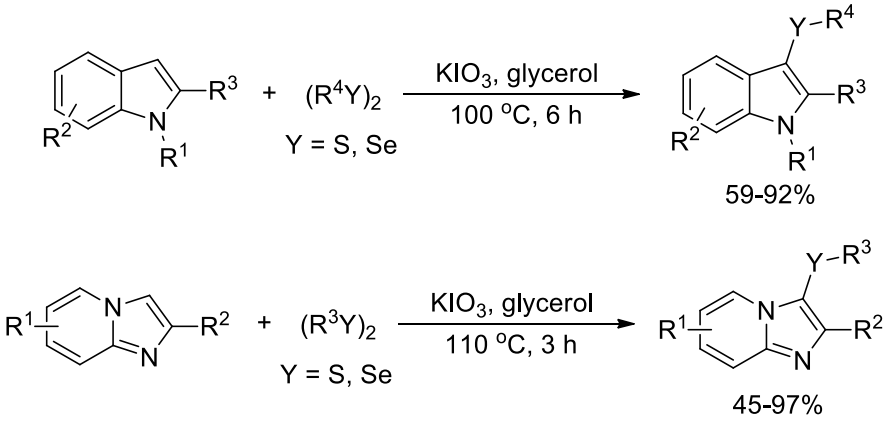

Scheme I.B.11 KIO_3 catalyzed chalcogenation of indoles and imidazopyridines.

A tetrabutylammonium iodide (TBAI) mediated and on-water sulfenylation of aromatic compounds has been developed.[25] Diverse aryl sulfides have been synthesized by using ethyl

arylsulfinates as the sulfenylation reagent (Scheme I.B.12). Moreover, bisthioethers of pyrroles through double sulfenylation has been carried out by employing the same protocol. The investigators also performed end product functionalization via Suzuki and Sonogashira coupling reaction.

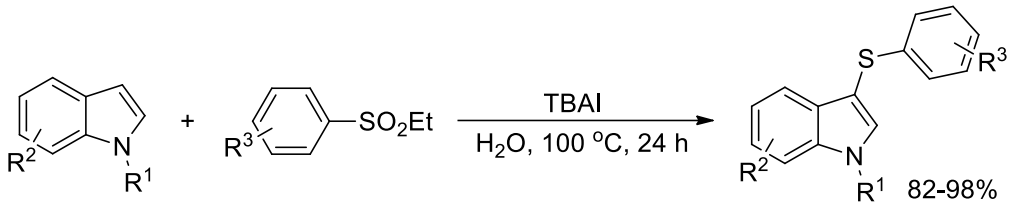

Scheme I.B.12 TBAI mediated and on-water sulfenylation of indoles.

In another report, Liu and co-workers,[75] have developed TBAI mediated synthesis of diverse 3-sulfenylindoles by using sulfinic acids as the sulfenylation reagent (Scheme I.B.13). The mechanism of the reaction involved the formation of disulfide intermediate along with in situ liberation of iodine from TBAI, in the presence of TsOH. A library of 3-sulfenylindoles has been synthesized in 70-99% yield.

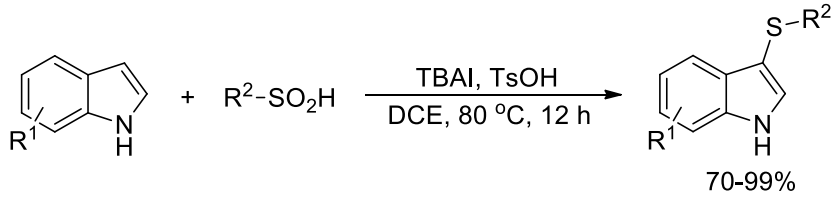

Scheme I.B.13 TBAI mediated synthesis of diverse 3-sulfenylindoles.

I.B.3 Present work: Results and discussions

Organic transformations that are greener and atom-economic have been of great interest recently. In this context, graphene oxide (GO) has emerged as an efficient cabocatalyst. GO could be obtained easily from graphite powder by oxidation and subsequent exfoliation.[76] Its mild acidic nature (pH 4.5 at 0.1 mg/ml),[77] and oxidising properties have been exploited in various organic transformations.[62] We have developed a new metal-free protocol for the regioselective sulfenylation of indole using thiols using catalytic graphene oxide (GO) and NaI as an additive (Scheme I.B.14).

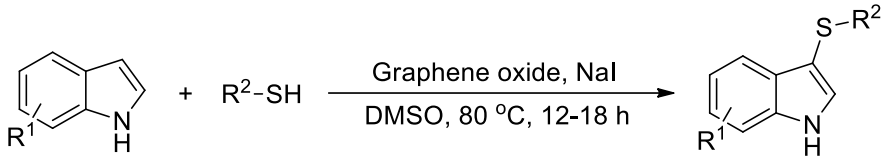

Scheme I.B.14 Graphene oxide catalyzed synthesis of 3-sulfenylindoles.

I.B.3.1 Optimization of reaction conditions

We began our preliminary investigations by using 1*H*-indole and 4-chlorothiophenol as model substrates for the reaction using GO and NaI under different conditions (Table I.B.1). Initially, we used GO (50 mg) and NaI (10 mol%) in toluene at 80 °C for 24 h. The reaction proceeded with isolation of the desired product **3a** in 68% yield (entry 1). The formation of the desired product 3-(4-chlorophenylthio)-1*H*-indole (**3a**) was confirmed by ^{1}H and ^{13}C NMR spectroscopy and by comparing its melting point with previously reported literature reports.[52] In the ^{13}C NMR spectrum, the peak at 102.4 ppm corresponds to C-3 of indole moiety which has been sulfenylated. After the confirmation of the desired product we continued further optimization of the reaction conditions. We then reduced the amount of GO to 25 mg which resulted in similar conversion (entry 2, 70%). While changing the solvent to polar aprotic (CH_3CN) or protic (MeOH) resulted in lower yield of the sulfenylated products (entries 4 and 5), the reaction in DMSO gave excellent conversion (entry 6, 97%). This was due to the oxidative nature of DMSO. There were reports suggesting the liberation of HI during the course of the reaction.[52] We assumed that the presence of DMSO along with GO oxidizes the HI back to I_2, which then continues the catalytic cycle. The absence of any of the components like GO, NaI or DMSO did exhibit considerable effect in the course of the reaction and in terms of yield of the product. For example, a neat mixture of reactants, GO and NaI afforded the product in lower yield (entry 7, 55%), while there was meagre conversion without using GO or NaI (entries 8 and 9). However, in the absence of GO and NaI, we did not observe any conversion (entry 10). Altering NaI with KI, KBr or NaCl lowered the yield of the product **3a** significantly (entries 11-13). Although the use of KI resulted in good yield of the desired product, its expensive nature prevented its further use in our catalytic system. The use of I_2 also afforded the desired product but in lower yield (entry 14, 64%). We presumed that that the freshly generated iodine via in situ oxidation of NaI was more active than commercially available molecular iodine. To check the viability of the catalytic system for industrial applications, we carried out gram scale synthesis of **3a** by employing the optimized reaction conditions. The reaction resulted in excellent conversion and the desired product **3a** was isolated in 94% yield (entry 15).

Table I.B.1 Optimization of reaction conditions[a]

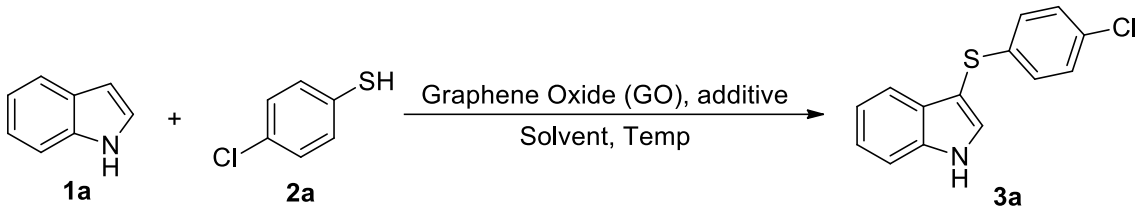

Entry	GO (mg)	Additive (10 mol%)	Solvent	Temp (°C) / time (h)	Yield (%)[b]
1	50	NaI	Toluene	80 / 24	68
2	25	NaI	Toluene	80 / 24	70
3	10	NaI	Toluene	100 / 24	43
4	25	NaI	CH_3CN	80 / 24	10
5	25	NaI	MeOH	80 / 24	12
6	**25**	**NaI**	**DMSO**	**80 / 12**	**97**
7	25	NaI	–	80 / 24	55
8	25	–	DMSO	80 / 24	Trace
9	–	NaI	DMSO	80 / 24	Trace
10	–	–	DMSO	80 / 24	–
11	25	KI	DMSO	80 / 12	72
12	25	KBr	DMSO	80 / 12	20
13	25	NaCl	DMSO	80 / 12	24
14	25	I_2	DMSO	80 / 12	64
15	60	NaI	DMSO	80 / 12	94[c]

[a]Reaction conditions: 1*H*-indole (1 mmol), 4-chlorothiophenol (1.5 mmol), additive (10 mol%), solvent (2 mL). [b]Isolated yield. [c]Reaction was performed in 10 mmol scale.

I.B.3.2 Synthesis of 3-sulfenylindoles

After optimization of the reaction conditions, various 1*H*-indoles and thiols were employed for the synthesis of 3-sulfenylindoles, as listed in Table I.B.2. Arylthiols containing chloro, methyl, amino group or 2-naphthylthiol worked efficiently leading to the exclusive formation of corresponding 3-sulfenylated products (**3a-d**). Further attempt with aliphatic thiols like cyclohexylthiol, *n*-pentylthiol or *n*-heptylthiol also worked fairly efficiently affording the desired products in 81-89% yields (**3e-g**). On the part of the indole moiety, we tried with an electron withdrawing group at C-6 position of indole and that too gave excellent conversions, exhibiting similar reactivity, selectivity and yield of products (**3h-j**). We then checked the presence of substituents in the N-containing five-membered ring of the indole moiety. Whereas 3-substituted indole underwent sulfenylation selectively at C-2 position (**3k**), the 2-substituted indole gave the corresponding 3-sulfenylated product in 95% yield (**3l**). Furthermore, heterocyclic thiols like 2-thiazoline-2-thiol and pyridine-2-thiol also worked efficiently furnishing the desired products in 81% and 89% yield respectively (**3m** and **3n**).

The formation of the desired products was confirmed by ^{1}H and ^{13}C NMR spectroscopy and by HRMS. For instance in case of **3b**, the ^{1}H NMR peak at δ 2.24 and 8.37 ppm corresponds to that of the CH_3 group of the thiol moiety and indole NH respectively. Similarly, the ^{13}C NMR peak at δ 20.9 ppm represents the CH_3 group of the thiol moiety. In case of **3f** the triplet centred at δ 2.68 ppm was due to the SCH_2 moiety of *n*-pentylthiol. The compound **3f** was subjected to ESI-HRMS analysis and the (*m/z*) for $C_{13}H_{17}NS$ $[M + H]^+$ was calculated at 220.1160 and found at 220.1156, which confirmed the formation of **3f**. The formation of **3h** was confirmed by the peak at 3.94 ppm due to the ester CH_3 group. Moreover, the doublet of doublet at δ 7.85 ppm (J = 1.5 and 8.4 Hz) was due to the H-5 of indole moiety. In case of ^{13}C NMR the peak at δ 137.9 ppm was due to the ester C=O group of indole.

Table I.B.2 Sulfenylation of indoles[a]

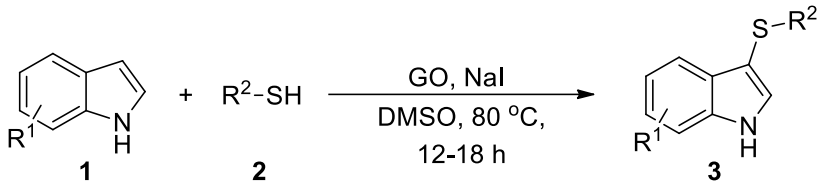

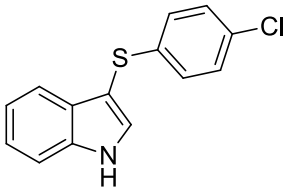

3a, 97%, 12 h

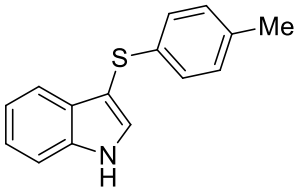

3b, 94, 12 h

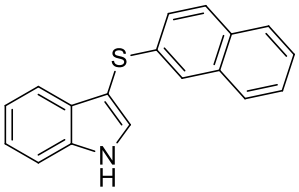

3c, 81%, 12 h

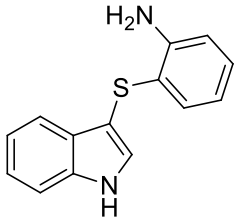

3d, 85%, 12 h

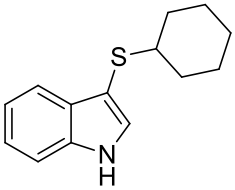

3e, 81%, 18 h

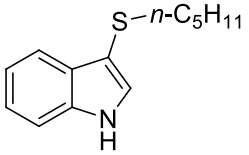

3f, 89%, 14 h

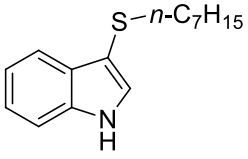

3g, 86%, 14 h

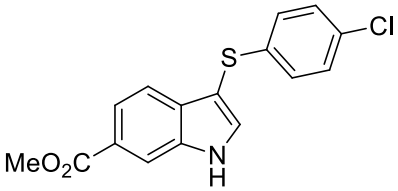

3h, 91%, 12 h

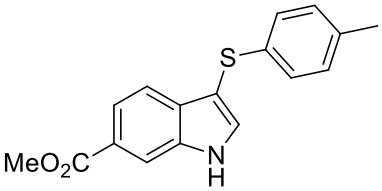

3i, 90%, 12 h

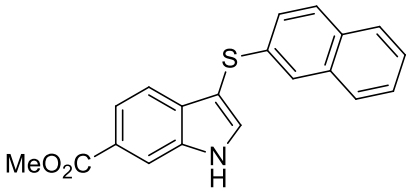

3j, 81%, 18 h

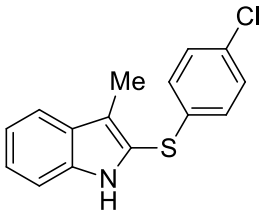

3k, 85%, 12 h

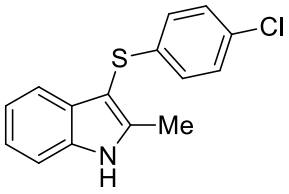

3l, 95%, 12 h

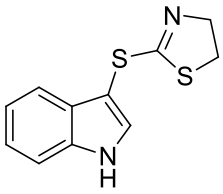

3m, 81%, 18 h

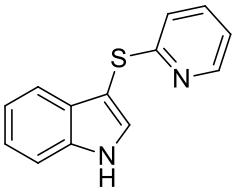

3n, 89%, 12 h

[a]Reaction conditions: **1** (1 mmol), **2** (1.5 mmol), NaI (10 mol%), GO (25 mg) and DMSO (2 mL) were stirred at 80 °C for 12-18 h.

I.B.3.3 Sulfenylation of 2-naphthol, resorcinol and 2-naphthylamine

We then extended the scope of the protocol towards the sulfenylation of other aromatic systems like 2-naphthol, resorcinol and 2-naphthylamine.[78,79] Gratifyingly, in all cases, the reaction worked successfully as well as selectively affording the desired sulfenylated products in good to excellent yields. The results are presented in Table I.B.3, I.B.4 and I.B.5. While 2-naphthol and 2-naphthylamine afforded exclusive formation of C-1 sulfenylated products, sulfenylation of resorcinol took place regioselectively at the C-4 position. Aromatic thiols with different substitutions and aliphatic thiols reacted in the same manner without any significant variations in terms of reactivity. The products were characterized by ^{1}H and ^{13}C NMR spectroscopy. In case of the compound **5e** the ^{1}H NMR peaks at δ 1.98 and 2.53 ppm were due to the two methyl groups of the thiol moiety. The same peaks appeared at δ 19.6 and 21.0 ppm in the ^{13}C NMR spectrum. The compound **7c** showed two triplets at δ 0.83 (J = 7.2 Hz) and 2.58 (J = 7.5 Hz) ppm due to the terminal CH_3 and SCH_2 moieties respectively of *n*-pentylthiol. In the ^{13}C NMR spectrum those peaks appeared at δ 13.9 and 37.1 ppm. In the ^{13}C NMR spectrum of **7d**, heteronuclear coupling between ^{13}C and ^{19}F was observed. The peak centred at δ 130.35 ppm showed J value of 189 Hz which was due to one-bond coupling between ^{13}C and ^{19}F. Similarly, the peaks at δ 116.46 (J = 87 Hz) and δ 128.80 (J = 30 Hz) ppm were respectively due to two-bond and three-bond coupling between ^{13}C and ^{19}F.

Table I.B.3 Sulfenylation of 2-naphthol[a]

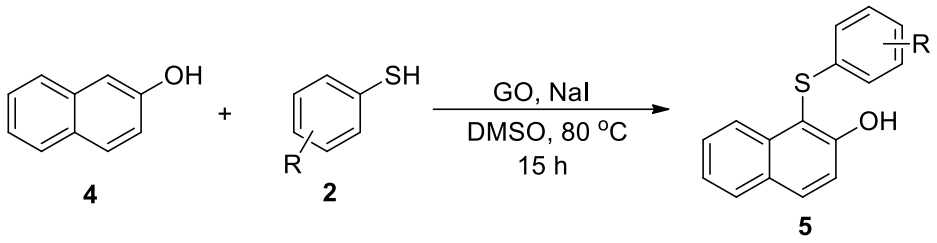

4 2 5

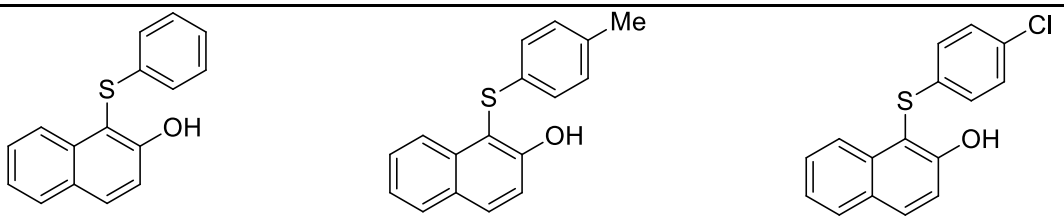

5a, 85% **5b**, 87% **5c**, 89%

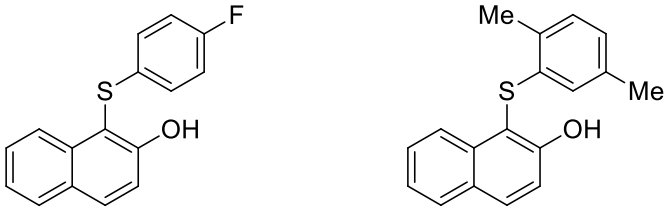

5d, 90% **5e**, 84%

[a]Reaction conditions: **4** (1 mmol), **2** (1.5 mmol), NaI (10 mol%), GO (25 mg) and DMSO (2 mL) were stirred at 80 °C for 15 h.

Table I.B.4 Sulfenylation of resorcinol[a]

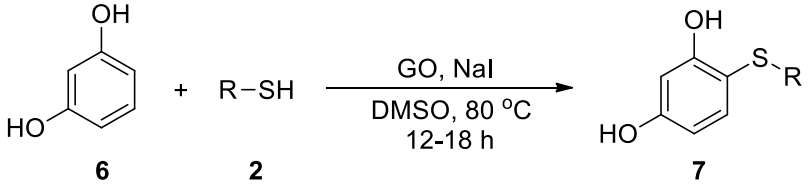

6 2 7

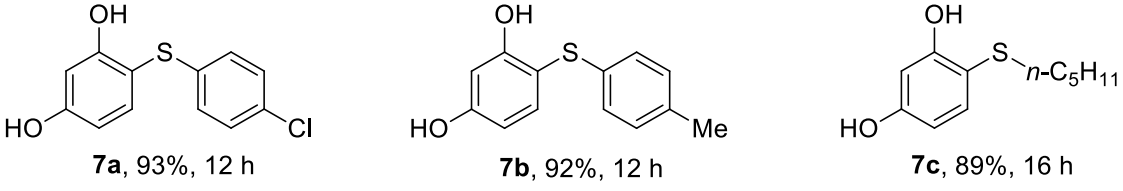

7a, 93%, 12 h **7b**, 92%, 12 h **7c**, 89%, 16 h

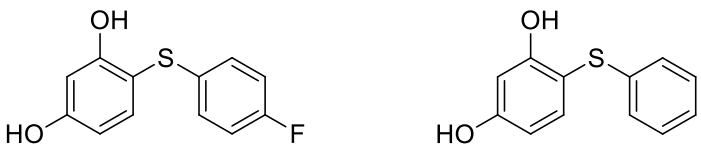

7d, 91%, 12 h **7e**, 84%, 18 h

[a]Reaction conditions: **6** (1 mmol), **2** (1.5 mmol), NaI (10 mol%), GO (25 mg) and DMSO (2 mL) were stirred at 80 °C for 12-18 h.

Table I.B.5 Sulfenylation of 2-naphthylamine[a]

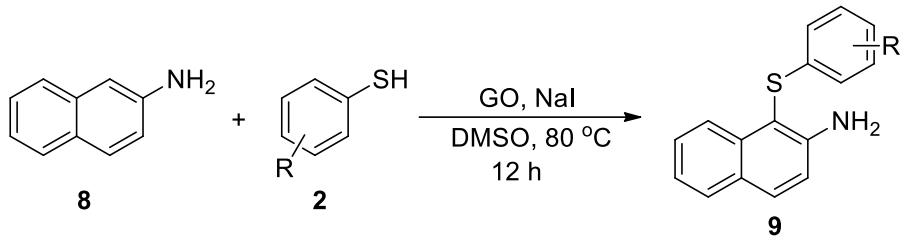

8 + **2** → **9**

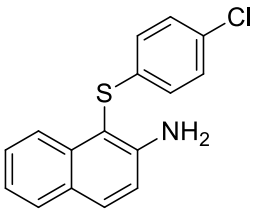 **9a**, 85%	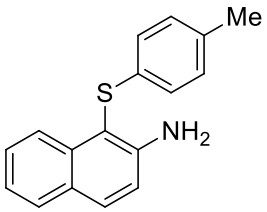 **9b**, 82%	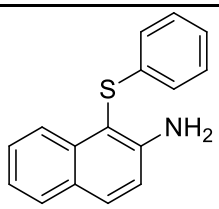 **9c**, 79%
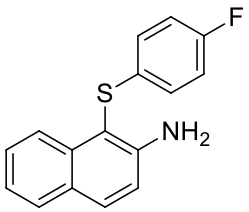 **9d**, 85%	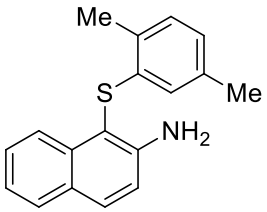 **9e**, 91%	

[a]Reaction conditions: **8** (1 mmol), **2** (1.5 mmol), NaI (10 mol%), GO (25 mg) and DMSO (2 mL) were stirred at 80 °C for 12 h.

I.B.3.4 Recyclability of graphene oxide

The reusability of the catalyst (GO) was evaluated in the sulfenylation of indole for the synthesis of **3a**. After the first run conducted in 2 mmol scale using GO (50 mg), the reaction mixture was partitioned between ethyl acetate and water and centrifuged at 5000 rpm. The supernatant was decanted and the process was repeated twice. The residual solid material was dried under vacuum to obtain free flowing GO powder. The recovery was however ~10% less than the used quantity. The recovered catalyst was then used for second run (1 mmol scale) using GO (25 mg) with almost equal efficiency. From the third run, there was a decreasing trend in its performance and after the fourth run, the isolated yield was significantly low (Figure I.B.2). The FT-IR spectrum of the recovered GO after first, second and fourth run was recorded (Figure I.B.3). The IR absorption after fourth run indicated partial loss of oxygenated functional groups which might be due to the repeated use of the recovered catalyst under the reaction condition.

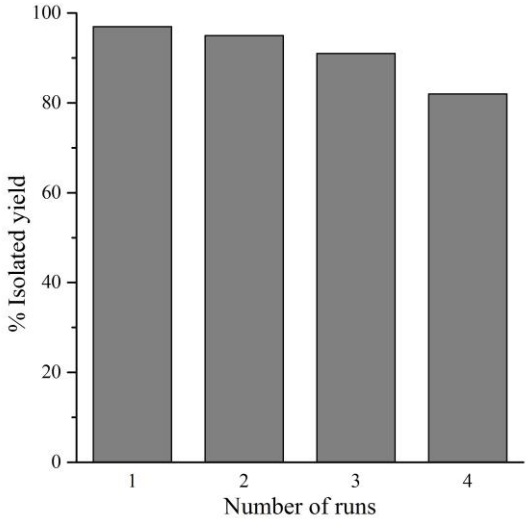

Figure I.B.2 Recyclability of GO for the sulfenylation of indole.

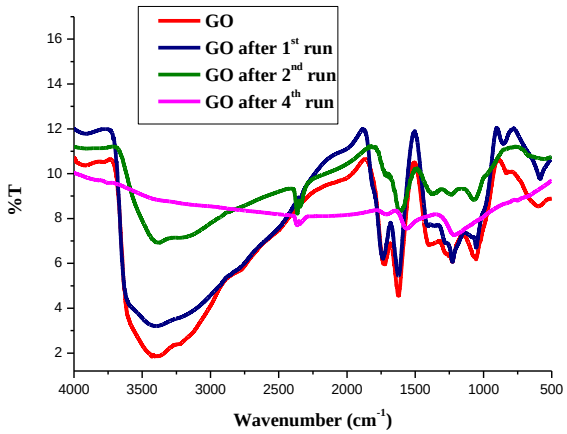

Figure I.B.3 FT-IR spectra of GO before and after first, second and fourth run.

The catalyst was then characterized by powder X-ray diffraction (XRD) for both fresh and recovered (after the first run) and found to be consistent with literature reports.[62,76] The XRD pattern of fresh GO was observed at 2θ = 9.5° and the recovered GO showed an additional peak at 2θ = 24.9° indicating partial reduction of GO (Figure I.B.4(a)). Thereafter, both the fresh as well as recovered catalyst were subjected to Raman analysis (Figure I.B.4(b)). The Raman spectra of GO clearly showed the D- and G-bands respectively at 1359 cm^{-1} and 1596 cm^{-1}. Similarly, the Raman spectra of recovered GO (after the first run) showed both the bands at 1360 cm^{-1} and 1591 cm^{-1}. Since the Raman spectra for both fresh and recovered catalyst were fairly similar, hence no conclusive information could be drawn. Furthermore, we quantified the amount of acidic functionalities on GO (both fresh and after the first run)

using pH titration (Figure I.B.5). The pH potentiometric acid-base titration of the fresh GO (50 mg) with 0.1 M NaOH aqueous solution using 50 mL of 0.5 M NaCl aqueous solution as back electrolyte was performed and calculated an approximate value of 1.68 mmol g^{-1} for the presence of carboxylic and hydroxyl groups.[77] In the case of using recovered GO (after the first run), the calculated value was 1.60 mmol g^{-1}. The results obtained thus confirmed that the acidic property of GO remained almost same even after the reaction.

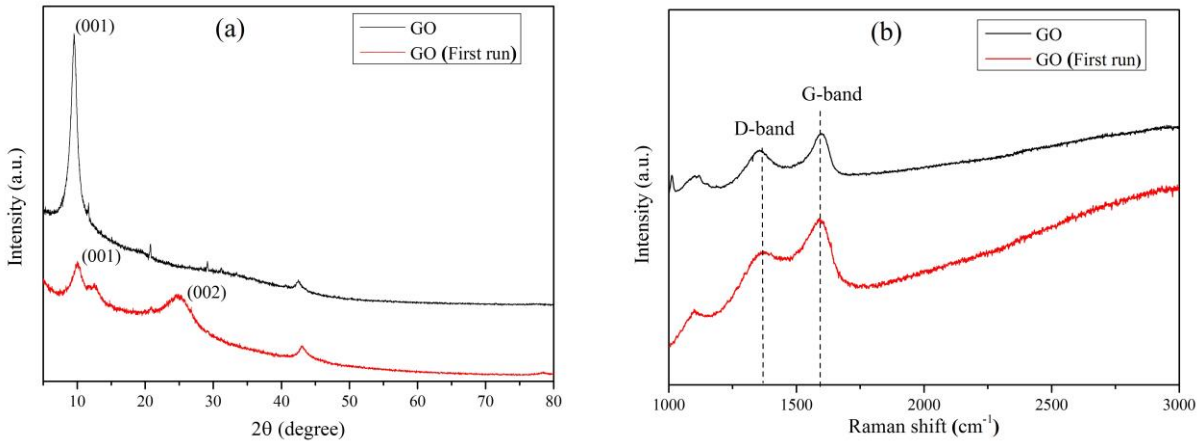

Figure I.B.4 (a) XRD patterns and (b) Raman spectra of GO fresh and after the first run.

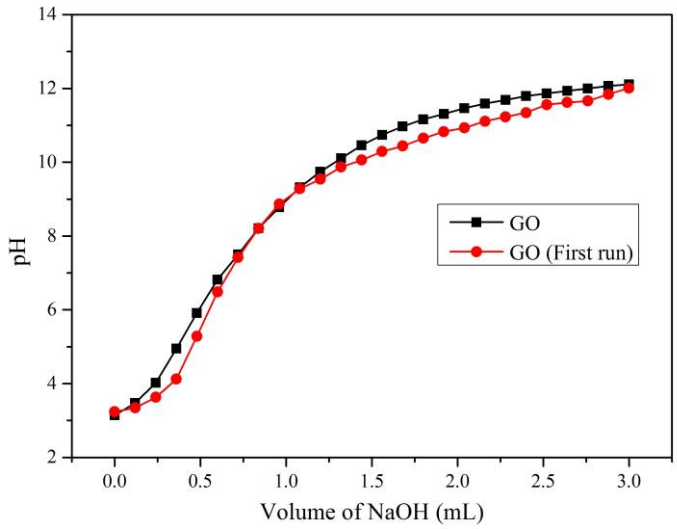

Figure I.B.5 The pH potentiometric titration curve of GO fresh and after the first run.

I.B.3.5 Plausible mechanism for the sulfenylation of indoles

Similar reactions with thiol mediated by molecular iodine (I_2) are believed to occur via disulfide formation, which subsequently produces an electrophilic species **10**.[52] We set up one reaction between 1*H*-indole and bis(4-chlorophenyl) disulfide which did not give the desired product (**3a**). This suggests that a strong oxidizing agent is essential for the reaction.

Moreover, GO catalyzed sulfenylation in the presence of molecular iodine (I_2) resulted in poor conversion (Table I.B.1, entry 14). Although we do not have clear explanation but we presumed that the freshly generated I_2 from the oxidation of NaI in the presence of GO could be more reactive towards thiol to form the electrophilic species **10**, which subsequently reacted with 1*H*-indole to form **11.** Finally, the intermediate 11 led to the formation of the desired product along with the liberation of HI. Thereafter HI underwent oxidation in the presence of GO in DMSO to form I_2 for the next catalytic cycle (Scheme I.B.15).

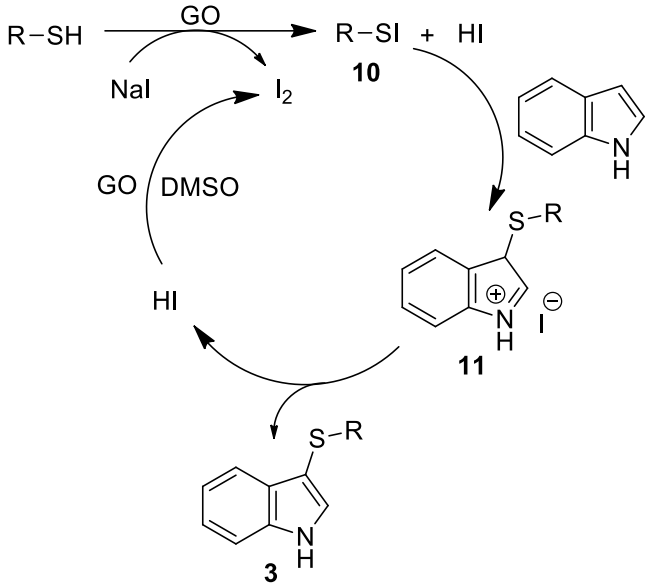

Scheme I.B.15 Proposed mechanism for the sulfenylation of 1*H*-indoles.

I.B.4 Conclusion

In summary, we have developed a metal-free, facile and atom-economic protocol for the site-selective C–H sulfenylation of various aromatic compounds using catalytic graphene oxide (GO). We believed that the freshly generated iodine in presence of GO could be highly reactive towards the formation of the electrophilic species that adds to indole to afford the desired thioethers. The reaction shows good tolerance towards several substituted aromatic systems. The present protocol is likely to attract the interest of synthetic chemists because of simple and greener aspects, devoid of strong oxidants, reusability of catalyst and broader applicability.

I.B.5 Experimental Section

I.B.5.1 General Information

All reagents were purchased from Sigma Aldrich and TCI, and used directly without further purification. The solvents were purchased from commercial suppliers and used after distillation. All the products were purified by column chromatography on 60-120 mesh silica gel (SRL, India). For TLC, Merck plates coated with silica gel 60, F_{254} were used. FT-IR spectra were recorded in FT-IR 8300 SHIMADZU spectrophotometer. The ^{1}H and ^{13}C NMR spectra were recorded at 300 MHz and 75 MHz respectively on Bruker AV 300 spectrometer in $CDCl_3$ and DMSO-d_6. Splitting patterns of protons were described as s (singlet), d (doublet), t (triplet), dd (doublet of doublet), m (multiplet) and br (broad). Chemical shifts (δ) were reported in parts per million (ppm) relative to TMS as internal standard. *J* values (coupling constant) were reported in Hz (Hertz). ^{13}C NMR spectra were recorded with complete proton decoupling ($CDCl_3$: δ 77.0 ppm and DMSO-d_6: 39.5 ppm). Centrifugation was done in REMI R-8C DX centrifuge at 5250 rpm. The X-ray diffraction studies were done using the Rigaku SmartLab (9 kW) diffractometer using CuKα radiation. Raman spectra were performed on ENSpectr R532 Raman microscope using 532 nm laser. The pH potentiometric titration was done by using Digital pH meter, Systronics, India.

I.B.5.2 Preparation of graphene oxide (GO)

Graphene oxide was prepared by following Tour's method.[76] In this method a 9:1 (v/v) mixture of H_2SO_4 / H_3PO_4 (180:20 mL) was added to a mixture of graphite powder (1.5 g) and $KMnO_4$ (9.0 g). The mixture was then stirred at 50 °C for 12 h. After cooling the mixture to room temperature, it was gradually poured into crushed ice (200 g), which was followed by the slow addition of H_2O_2 (30%, 1.5 mL). The solution was then centrifuged (5000 rpm) and the supernatant was discarded. The residual solid material was successively washed with deionised water (100 mL) and then with 30% HCl (100 mL). The solid material was then repeatedly washed with water and centrifuged. Finally, the solid brown material was collected and dried at 60 °C under vacuum to obtain solid graphene oxide.

I.B.5.3 General procedure for the sulfenylation of aromatic compounds

In a screw-capped sealed tube equipped with a magnetic stir bar, aromatic compounds (1 mmol), thiols (1.5 mmol), NaI (10 mol%) and GO (25 mg) were added to 2 mL of freshly distilled DMSO. The resulting reaction mixture was stirred at 80 °C for 12-18 h. After completion of the reaction (monitored by TLC), the reaction mixture was cooled to room temperature. The catalyst was then recovered through simple filtration. The reaction mixture was diluted with water and extracted by ethyl acetate (3 x 5 mL). Finally, the combined organic layer was dried over anhydrous Na_2SO_4 and concentrated. The residue was then further purified by column chromatography on silica gel using the light petroleum ether and

ethyl acetate as eluent to afford the desired products. All products were characterized by ^{1}H, ^{13}C NMR spectroscopy and compared with the reported melting points for known solid compounds.

I.B.5.4 Characterization data of compounds listed in Table I.B.2-I.B.5

3-(4-Chlorophenylthio)-1*H*-indole (3a)[52]

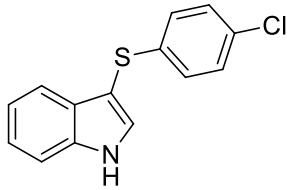

White solid; m.p.: 126–127 °C (Lit. m.p.: 127.5–128.3 °C); **^{1}H NMR ($CDCl_3$, 300 MHz):** δ 7.00–6.98 (m, 2H, ArH), 7.02–7.01 (m, 2H, ArH), 7.19–7.08 (m, 1H, ArH), 7.29–7.23 (m, 1H, ArH), 7.46–7.41 (m, 2H, ArH), 7.56 (d, *J* = 7.8 Hz, 1H, ArH), 8.41 (s, br, 1H, NH); **^{13}C NMR ($CDCl_3$, 75 MHz):** δ 102.4, 111.7, 119.5, 121.0, 123.2, 127.1, 128.7, 128.8, 130.5, 130.7, 136.5, 137.8.

3-(*p*-Tolylthio)-1*H*-indole (3b)[52]

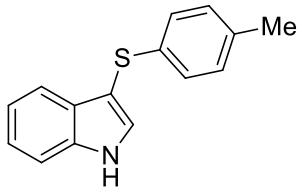

White solid; m.p.: 125–126 °C (Lit. m.p.: 125–126 °C); **^{1}H NMR ($CDCl_3$, 300 MHz):** δ 2.24 (s, 3H, CH_3), 7.03–6.95 (m, 4H, ArH), 7.28–7.12 (m, 2H, ArH), 7.45–7.40 (m, 2H, ArH), 7.61 (d, *J* = 7.2 Hz, 1H, ArH), 8.37 (s, br, 1H, NH); **^{13}C NMR ($CDCl_3$, 300 MHz):** δ 21.0, 103.3, 111.5, 119.7, 120.8, 123.0, 126.2, 129.1, 129.5, 130.5, 134.6, 135.4, 136.4.

3-(Naphthalen-2-ylthio)-1*H*-indole (3c)[56]

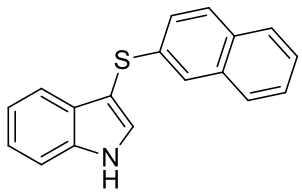

Off white solid; m.p.: 174–175 °C (Lit. m.p.: 141–143 °C); **^{1}H NMR ($CDCl_3$, 300 MHz):** δ 7.16–7.14 (m, 3H, ArH), 7.28–7.24 (m, 2H, ArH), 7.36–7.34 (m, 2H, ArH), 7.48–7.45 (m, 2H, ArH), 7.55–7.54 (m, 2H, ArH), 7.70–7.65 (m, 1H, ArH), 8.45 (s, br, 1H, NH); **^{13}C NMR ($CDCl_3$, 75 MHz):** δ 102.9, 111.6, 119.7, 120.9, 123.1, 123.5, 124.8, 125.0, 127.0, 127.6, 128.2, 130.6, 131.3, 133.7, 136.5, 136.7, 137.0, 139.9.

3-(2-Aminophenylthio)1*H*-indole (3d)[52]

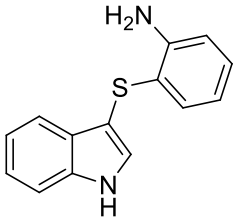

Brown solid; m.p.: 89–90 °C (Lit. m.p.: 93–95 °C); **^{1}H NMR ($CDCl_3$, 300 MHz):** δ 3.22 (d, *J* = 2.7, 2H, NH_2), 6.69–6.57 (m, 2H, ArH), 7.02–6.97 (m, 1H, ArH), 7.26–7.11 (m, 3H, ArH), 7.37–7.34 (m, 2H, ArH), 7.66 (d, *J* = 8.1 Hz, 1H, ArH), 8.36 (s, br, 1H, NH); **^{13}C NMR ($CDCl_3$, 75 MHz):** δ 111.5, 115.3, 119.0, 119.4, 120.6, 120.7, 122.8, 128.0, 128.7, 129.0, 132.0, 136.3, 145.6.

3-(Cyclohexylthio)-1*H*-indole (3e)[67]

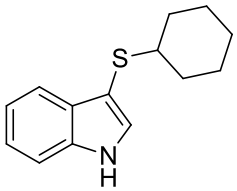

Light brown solid; m.p.: 96–97 °C (Lit. m.p.: 91–93.1 °C); **^{1}H NMR ($CDCl_3$, 300 MHz):** δ 1.42–1.16 (m, 5H, CH_2), 1.57–1.52 (m, 1H, CH_2), 1.65–1.61 (m, 1H, CH_2), 1.75–1.71 (m, 2H, CH_2), 1.96–1.92 (m, 2H, CH_2), 2.82–2.74 (m, 1H, CH), 7.26–7.17 (m, 2H, ArH), 7.30 (d, *J* = 2.4 Hz, 1H, ArH), 7.41–7.35 (m, 1H, ArH), 7.80–7.76 (m, 1H, ArH), 8.27 (s, br, 1H, NH); **^{13}C NMR ($CDCl_3$, 75 MHz):** δ 25.7, 26.2, 33.7, 47.5, 104.7, 111.3, 119.7, 120.4, 122.5, 130.2, 130.3, 136.2.

3-(Pentylthio)-1*H*-indole (3f)

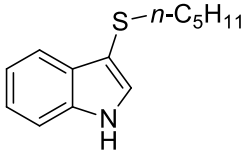

Colourless liquid; **^{1}H NMR ($CDCl_3$, 300 MHz):** δ 0.85 (t, *J* = 7.2 Hz, 3H, CH_3), 1.39–1.20 (m, 4H, CH_2), 1.65–1.49 (m, 2H, CH_2), 2.68 (t, *J* = 7.2 Hz, 2H, CH_2), 7.23–7.16 (m, 2H, ArH), 7.25–7.28 (m, 1H, ArH), 7.36–7.33 (m, 1H, ArH), 7.79–7.74 (m, 1H, ArH), 8.21 (s, br, 1H, NH); **^{13}C NMR ($CDCl_3$, 75 MHz):** δ 14.0, 22.3, 29.6, 30.7, 36.4, 106.2, 111.4, 119.4, 120.3, 122.6, 129.2, 129.5, 136.3; HRMS–ESI (*m/z*) calcd for $C_{13}H_{17}NS$ $[M + H]^+$ 220.1160 found 220.1156.

3-(Heptylthio)-1*H*-indole (3g)

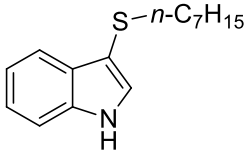

Colourless liquid; **^{1}H NMR (CDCl$_3$, 300 MHz):** δ 0.87–0.83 (m, 3H, CH_3), 1.30–1.23 (m, 7H, CH_2), 1.65–1.49 (m, 3H, CH_2), 2.68 (t, *J* = 7.2 Hz, 2H, CH_2), 7.23–7.17 (m, 3H, ArH), 7.36–7.32 (m, 1H, ArH), 7.79–7.77 (m, 1H, ArH), 8.19 (s, br, 1H, NH); **^{13}C NMR (CDCl$_3$, 75 MHz):** δ 14.1, 22.6, 28.5, 28.9, 30.0, 31.8, 36.4, 106.2, 11.5, 119.4, 120.4, 122.6, 129.2, 129.5, 136.3; HRMS–ESI (*m/z*) calcd for $C_{15}H_{21}NS$ $[M + H]^+$ 248.1473 found 248.1492.

Methyl 3-(4-chlorophenylthio)-1*H*-indole-6-carboxylate (3h)

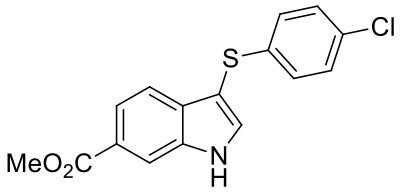

White solid; m.p.: 162–163 °C; **^{1}H NMR (CDCl$_3$, 300 MHz);** δ 3.94 (s, 3H, OCH_3), 7.13–6.98 (m, 4H, ArH), 7.64–7.57 (m, 2H, ArH), 7.85 (dd, *J* = 1.5, 8.4 Hz, 1H, ArH), 8.23 (s, 1H, ArH), 9.06 (s, br, 1H, NH); **^{13}C NMR (CDCl$_3$, 75 MHz):** δ 52.1, 103.1, 114.1, 119.1, 121.9, 124.9, 127.2, 128.8, 130.8, 132.5, 133.8, 135.9, 137.2, 167.9.

Methyl 3-(*p*-tolylthio)-1*H*-indole-6-carboxylate (3i)

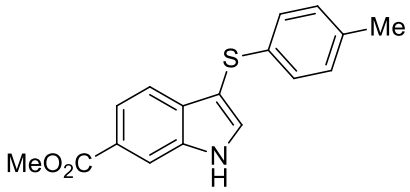

White solid; m.p.: 155–157 °C; **^{1}H NMR (CDCl$_3$, 300 MHz):** δ 2.24 (s, 3H, CH_3), 3.93 (s, 3H, OCH_3), 7.00–6.98 (m, 4H, ArH), 7.64–7.60 (m, 2H, ArH), 7.83 (dd, *J* = 1.5, 8.4 Hz, 1H, ArH), 8.20 (s, 1H, ArH), 8.91 (s, br, 1H, NH); **^{13}C NMR (CDCl$_3$, 75 MHz):** δ 20.8, 52.1, 104.3, 114.0, 119.4, 121.7, 124.7, 126.4, 129.6, 132.8, 133.5, 134.9, 135.0, 135.9, 168.0.

Methyl 3-(naphthalen-2-ylthio)-1*H*-indole-6-carboxylate (3j)

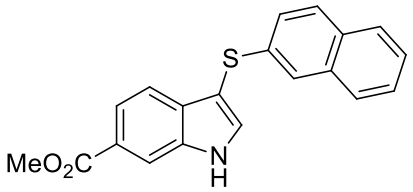

White solid; m.p.: 185–186 °C; **^{1}H NMR (DMSO-d$_6$, 300 MHz):** δ 3.91 (s, 3H, OCH_3), 7.27 (dd, *J* = 1.8, 8.7 Hz, 1H, ArH), 7.48–7.44 (m, 2H, ArH), 7.56–7.54 (m, 2H, ArH), 7.74–7.70

(m, 2H, ArH), 7.87–7.81 (m, 2H, ArH), 8.15 (d, *J* = 2.7 Hz, 1H, ArH), 8.22 (s, 1H, ArH); **^{13}C NMR (DMSO-d$_6$, 75 MHz):** δ 52.3, 100.7, 114.8, 118.7, 121.2, 123.5, 124.9, 125.8, 127.1, 127.2, 128.0, 128.9, 131.4, 132.8, 132.8, 133.7, 136.5, 136.6, 167.4.

2-(4-Chlorophenylthio)-3-methyl-1*H*-indole (3k)[80]

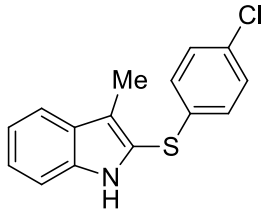

White solid; m.p.: 124–126 °C (Lit. m.p.: 126–127 °C); **^{1}H NMR (CDCl$_3$, 300 MHz):** δ 2.27–2.22 (s, 3H, CH_3), 6.84–6.81 (m, 2H, ArH), 7.05–7.02 (m, 3H, ArH), 7.15–7.06 (m, 2H, ArH), 7.50 (d, *J* = 8.1 Hz, 1H, ArH), 7.79 (s, br, 1H, NH); **^{13}C NMR (CDCl$_3$, 75 MHz):** δ 9.4, 111.0, 119.6, 119.8, 120.2, 120.9, 123.8, 127.7, 128.4, 129.2, 131.6, 135.8, 136.9.

3-(4-Chlorophenylthio)-2-methyl-1*H*-indole (3l)[81]

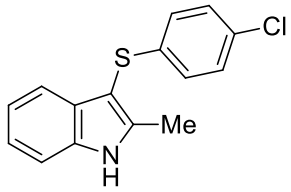

Light pink solid; m.p.: 97–99 °C (Lit. m.p.: 102–104 °C); **^{1}H NMR (CDCl$_3$, 300 MHz)**: δ 2.44–2.32 (m, 3H, CH_3), 6.95–6.94 (m, 2H, ArH), 7.20–7.06 (m, 4H, ArH), 7.28 (d, *J* = 7.8 Hz, 1H, ArH), 7.50 (d, *J* = 7.5 Hz, 1H, ArH), 8.15 (s, br, 1H, NH); **^{13}C NMR (CDCl$_3$, 75 MHz):** δ 12.1, 98.9, 110.8, 118.8, 120.9, 122.4, 126.8, 128.8, 130.0, 130.3, 135.5, 138.0, 141.3.

3-(4,5-Dihydrothiazol-2-ylthio)-1*H*-indole (3m)

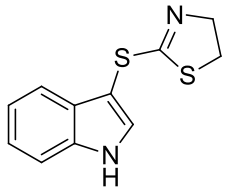

Off white solid; m.p.: 62 °C; **^{1}H NMR (CDCl$_3$, 300 MHz)**: δ 2.89 (t, *J* = 6.6 Hz, 2H, CH_2), 3.51 (t, *J* = 6.6 Hz, 2H, CH_2), 7.29–7.20 (m, 2H, ArH), 7.41–7.36 (m, 2H, ArH), 7.75–7.72 (m, 1H, ArH), 8.35 (s, br, 1H, NH); **^{13}C NMR (CDCl$_3$, 75 MHz):** δ 35.7, 44.5, 103.2, 111.7, 119.0, 120.9, 123.1, 129.1, 130.5, 131.7, 136.3.

3-(Pyridin-2-ylthio)-1*H*-indole (3n)[67]

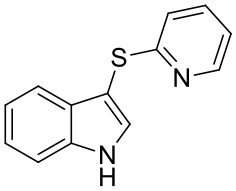

White solid; m.p.: 136 °C (Lit. m.p.: 137.2–138 °C); **^{1}H NMR (CDCl$_3$, 300 MHz):** δ 6.93–6.80 (m, 1H, ArH), 6.97–6.95 (m, 1H, ArH), 7.44–7.07 (m, 5H, ArH), 7.62 (d, *J* = 7.8 Hz, 1H, ArH), 8.40–8.38 (m, 1H, ArH), 9.52 (s, br, 1H, NH); **^{13}C NMR (CDCl$_3$, 75 MHz):** δ 100.6, 112.3, 119.6, 119.7, 120.4, 121.2, 123.3, 129.1, 131.9, 137.1, 149.2, 163.1.

1-(Phenylthio)naphthalen-2-ol (5a)[82]

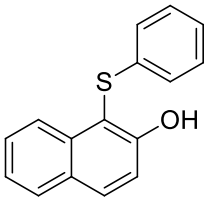

Off white solid; m.p.: 65–67 °C (Lit. m.p.: 66–67 °C); **^{1}H NMR (CDCl$_3$, 300 MHz):** δ 7.00–7.10 (m, 2H, ArH), 7.27–7.10 (m, 4H ArH), 7.39–7.31 (m, 2H, ArH), 7.51–7.45 (m, 1H, ArH), 7.80 (d, *J* = 8.1 Hz, 1H, ArH), 7.89 (dd, *J* = 3.6, 9 Hz, 1H, ArH), 8.21 (d, *J* = 7.8 Hz, 1H, ArH); **^{13}C NMR (CDCl$_3$, 75 MHz):** δ 108.0, 116.9, 123.9, 124.7, 125.9, 126.4, 128.0, 128.6, 129.2, 129.5, 132.8, 135.4, 135.4.

1-(*p*-Tolylthio)naphthalen-2-ol (5b)[82]

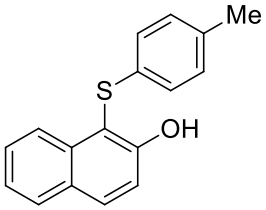

White solid; m.p.: 76–77 °C (Lit. m.p.: 78–79 °C); **^{1}H NMR (CDCl$_3$, 300 MHz):** δ 2.22 (s, 3H, CH_3), 6.99–6.91(m, 4H, ArH),7.50–7.21 (m, 4H, ArH), 7.87 (d, *J* = 8.7 Hz, 1H, ArH), 7.79 (d, *J* = 7.8 Hz, 1H, ArH) 8.22 (d, *J* = 8.4 Hz, 1H, ArH); **^{13}C NMR (CDCl$_3$, 75 MHz):** δ 20.8, 108.7, 116.8, 123.7, 124.7, 126.6, 127.8, 128.5, 129.4, 129.9, 131.7, 132.6, 135.4, 135.8, 156.8.

1-(4-Chlorophenylthio)naphthalen-2-ol (5c)[82]

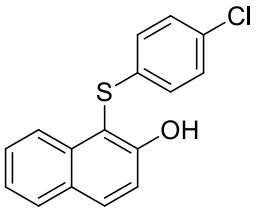

White solid; m.p.: 84–85 °C (Lit. m.p.: 84–85 °C); **^{1}H NMR ($CDCl_3$, 300 MHz):** δ 6.95–6.90 (m, 2H, ArH), 7.13–7.09 (m, 3H, ArH), 7.39–7.31 (m, 2H, ArH), 7.51–7.46 (m, 1H, ArH), 7.80 (d, *J* = 7.8 Hz, 1H, ArH), 7.89 (d, *J* = 9 Hz, 1H, ArH), 8.15 (d, *J* = 8.4 Hz, 1H, ArH); **^{13}C NMR ($CDCl_3$, 75 MHz):** δ 107.6, 116.9, 124.0, 124.4, 127.6, 128.1, 128.7, 129.3, 129.5, 131.9, 133.1, 133.9, 135.2, 157.0.

1-(4-Fluorophenylthio)naphthalen-2-ol (5d)[83]

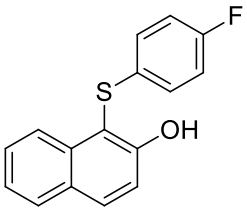

White solid; m.p.: 116–117 °C (Lit. m.p.: 116–119 °C); **^{1}H NMR ($CDCl_3$, 300 MHz):** δ 6.90–6.84 (m, 2H, ArH), 7.03–6.97 (m, 2H, ArH), 7.18 (s, 1H, ArH), 7.40–7.31 (m, 2H, ArH), 7.52–7.47 (m, 1H, ArH), 7.81 (d, *J* = 8.1 Hz, 1H, ArH), 7.90 (d, *J* = 8.7 Hz, 1H, ArH), 8.20 (d, *J* = 8.4 Hz, 1H, ArH); **^{13}C NMR ($CDCl_3$, 75 MHz)**: δ 108.4, 116.1, 116.4, 116.8, 123.9, 124.4, 128.0, 128.2, 128.3, 128.6, 129.5, 130.3, 132.9, 135.2, 156.8, 159.7, 163.0.

1-(2,5-Dimethylphenylthio)naphthalen-2-ol (5e)[84]

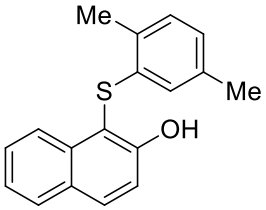

Yellow solid; m.p.: 57–58 °C (Lit. m.p.: 58–60 °C); **^{1}H NMR ($CDCl_3$, 300 MHz):** δ 1.98 (s, 3H, CH_3), 2.53 (s, 3H, CH_3), 6.20 (s, 1H, ArH), 6.82 (d, *J* = 7.5 Hz, 1H, ArH), 7.06 (d, *J* = 7.5 Hz, 2H, ArH), 7.48–7.33 (m, 3H, ArH), 7.82 (d, *J* = 8.1 Hz, 1H, ArH), 7.92 (d, *J* = 9.0 Hz, 1H, ArH), 8.14 (d, *J* = 8.4 Hz, 1H, ArH); **^{13}C NMR ($CDCl_3$, 75 MHz)**: δ 19.6, 21.0, 107.5, 116.8, 123.8, 124.7, 125.2, 126.4, 127.8, 128.5, 129.5, 130.2, 132.1, 132.7, 133.9, 135.5, 136.4, 157.1.

4-(4-Chlorophenylthio)benzene-1,3-diol (7a)[82]

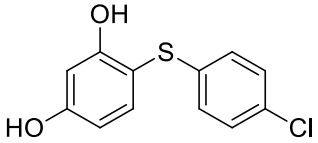

White solid; m.p.: 102–103 °C (Lit. m.p.: 99–100 °C); **^{1}H NMR ($CDCl_3$, 300 MHz):** δ 2.24 (s, br, 1H, OH), 6.09 (s, br, 1H, OH), 6.57–6.46 (m, 2H, ArH), 6.95 (d, *J* = 8.4

Hz, 2H, ArH), 7.17 (d, *J* = 8.1 Hz, 2H, ArH), 7.33 (d, *J* = 9 Hz, 1H, ArH); **^{13}C NMR ($CDCl_3$, 75 MHz):** δ 102.6, 106.8, 109.5, 127.5, 129.2, 131.8, 135.2, 138.2, 158.4, 159.6.

4-(*p*-Tolylthio)benzene-1,3-diol (7b)[82]

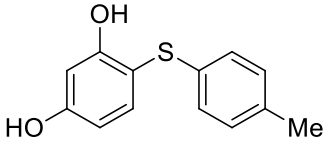

Pale brown solid; m.p.: 88–89 °C (Lit. m.p.: 77–78 °C); **^{1}H NMR ($CDCl_3$, 300 MHz):** δ 2.27 (s, 3H, CH_3), 5.72 (s, br, 1H, OH), 6.46 (dd, *J* = 3, 8.4 Hz, 1H, ArH), 6.61–6.55 (m, 2H, ArH), 7.05–6.95 (m, 4H, ArH), 7.38 (d, *J* = 8.4 Hz, 1H, ArH); **^{13}C NMR ($CDCl_3$, 75 MHz):** δ 20.9, 102.4, 108.0, 109.1, 126.7, 129.9, 133.0, 135.9, 138.0, 158.4, 159.2.

4-(Pentylthio)benzene-1,3-diol (7c)

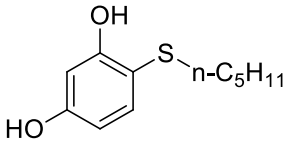

Pale yellow liquid; **^{1}H NMR ($CDCl_3$, 300 MHz):** δ 0.86 (t, *J* = 7.2 Hz, 3H, CH_3), 1.37–1.22 (m, 4H, CH_2), 1.67–1.47 (m, 2H, CH_2), 1.76–1.67 (m, 2H, CH_2), 2.26 (s, br, 1H, OH), 2.58 (t, *J* = 7.5 Hz, 2H, ArH), 6.21 (s, br, 1H, OH), 6.43–6.37 (m, 1H, ArH), 6.50 (d, *J* = 2.4 Hz, 1H, ArH), 6.96–6.88 (m, 1H, ArH), 7.32–7.26 (m, 1H, ArH); **^{13}C NMR ($CDCl_3$, 75 MHz)**: δ 13.9, 22.2, 29.2, 30.7, 37.8, 101.7, 108.5, 110.2, 137.2, 158.0, 158.4.

4-(4-Fluorophenylthio)benzene-1,3-diol (7d)

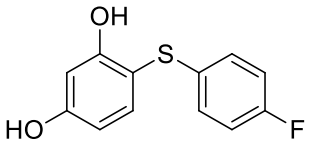

White solid; m.p.: 104–105 °C; **^{1}H NMR ($CDCl_3$, 300 MHz):** δ 6.47–6.43 (m, 2H, ArH), 6.70–6.55 (m, 5H, ArH), 6.87–6.78 (m, 4H, ArH), 7.78–7.77 (m, 1H, ArH); **^{13}C NMR ($CDCl_3$, 75 MHz):** δ 102.4, 109.7, 116.3, 116.6, 128.7, 128.8, 130.9, 144.9, 160.0, 160.6, 163.3.

4-(Phenylthio)benzene-1,3-diol (7e)[82]

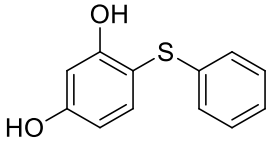

Brown solid; m.p.: 110–111 °C (Lit. m.p.: 111–112 °C); **^{1}H NMR ($CDCl_3$, 300 MHz)**: δ 1.90 (s, br, 1H, OH), 5.61 (s, br, 1H, OH), 6.60–6.45 (m, 3H, ArH), 7.25–7.02 (m, 5H,

ArH), 7.39 (d, *J* = 8.4 Hz, 1H); **^{13}C NMR ($CDCl_3$, 75 MHz)**: δ 102.4, 107.2, 109.2, 125.8, 126.1, 129.1, 136.6, 138.2, 158.5, 159.3.

1-(4-Chlorophenylthio)naphthalen-2-amine (9a)[84]

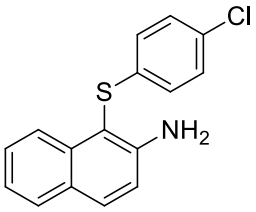

Deep brown solid; m.p.: 123–124 °C (Lit. m.p.: 123–125 °C); **^{1}H NMR ($CDCl_3$, 300 MHz):** δ 4.66 (s, br, 2H, NH_2), 6.95–6.86 (m, 2H, ArH), 7.00 (d, *J* = 9 Hz, 1H, ArH), 7.11–7.06 (m, 2H, ArH), 7.27–7.21 (m, 1H, ArH), 7.45–7.39 (m, 1H, ArH), 7.71 (t, *J* = 9 Hz, 2H, ArH), 8.20 (d, *J* = 8.4 Hz, 1H, ArH); **^{13}C NMR ($CDCl_3$, 75 MHz):** δ 104.1, 117.6, 122.7, 124.0, 127.1, 128.0, 128.4, 128.5, 129.1, 130.8, 132.1, 135.4, 136.4, 148.5.

1-(*p*-Tolylthio)naphthalen-2-amine (9b)[84]

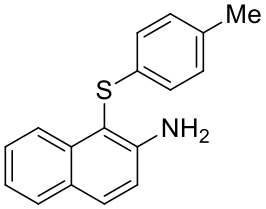

Deep brown solid; m.p.: 111–112 °C (Lit. m.p.: 113–115 °C); **^{1}H NMR ($CDCl_3$, 300 MHz):** δ 2.20 (s, 3H, CH_3), 4.43 (s, br, 2H, NH_2), 6.98–6.89 (m, 5H, ArH), 7.25–7.16 (m, 1H, ArH), 7.43–7.37 (m, 1H, ArH), 7.71–7.66 (m, 2H, ArH), 8.2 (d, *J* = 8.4 Hz, 1H, ArH); **^{13}C NMR ($CDCl_3$, 75 MHz):** δ 21.0, 105.2, 117.7, 122.6, 124.3, 126.1, 127.8, 128.4, 129.8, 131.7, 133.2, 134.9, 136.7, 148.4.

1-(Phenylthio)naphthalen-2-amine (9c)[84]

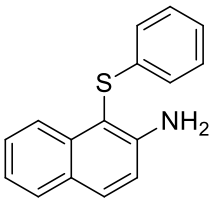

Deep brown solid; m.p.: 98–99 °C (Lit. m.p.: 99–101 °C); **^{1}H NMR ($CDCl_3$, 300 MHz):** δ 4.40 (s, br, 2H, NH_2), 7.03–6.87 (m, 4H, ArH), 7.05–7.04 (m, 1H, ArH), 7.15–7.09 (m, 1H, ArH), 7.26–7.17 (m, 1H, ArH), 7.46–7.37 (m, 1H, ArH), 7.73–7.67 (m, 2H, ArH), 8.26 (d, *J* = 8.1 Hz, 1H, ArH); **^{13}C NMR ($CDCl_3$, 75 MHz):** δ 104.5, 117.7, 122.7, 124.3, 125.1, 125.8, 127.9, 128.0, 128.4, 129.0, 132.0, 136.7, 137.0, 148.6.

1-(4-Fluorophenylthio)naphthalen-2-amine (9d)

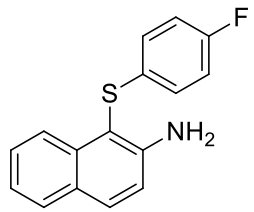

Brown solid; m.p.: 65–66 °C; **^{1}H NMR ($CDCl_3$, 300 MHz):** δ 4.66 (s, br, 2H, NH_2), 6.85–6.81 (m, 2H, ArH), 6.97–6.93 (m, 3H, ArH), 7.23 (t, *J* = 7 Hz, 1H, ArH), 7.41 (t, *J* = 7.5 Hz, 1H, ArH), 7.70–7.66 (m, 2H, ArH), 8.24 (d, *J* = 8.4, 1H, ArH); **^{13}C NMR ($CDCl_3$, 75 MHz):** δ 105.0, 116.0, 116.3, 117.8, 122.7, 124.1, 127.7, 127.8, 128.0, 128.5, 131.8, 131.9, 132.0, 136.6, 148.5, 159.4, 162.6.

1-(2,5-Dimethylphenylthio)naphthalen-2-amine (9e)[84]

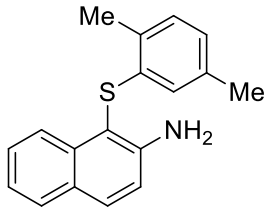

Light pink solid; m.p.: 60–61 °C (Lit. m.p.: 60–62 °C); **^{1}H NMR ($CDCl_3$, 300 MHz)**: δ 1.96 (s, 3H, CH_3), 2.49 (s, 3H, CH_3), 4.26 (s, br, 2H, NH_2), 6.25 (s, 1H, ArH), 6.76 (d, *J* = 7.5 Hz, 1H, ArH), 7.04–6.97 (m, 2H, ArH), 7.25–7.20 (m, 1H, ArH), 7.41–7.36 (m, 1H, ArH), 7.72–7.67 (m, 2H, ArH), 8.20 (d, *J* = 8.4 Hz, 1H, ArH); **^{13}C NMR ($CDCl_3$, 75 MHz)**: δ 19.5, 21.0, 104.0, 117.5, 122.4, 124.2, 124.5, 125.5, 127.6, 128.2, 128.4, 130.0, 131.5, 131.8, 135.0, 136.0, 136.7, 148.4.

I.B.5.5 Scanned copies of ^{1}H, ^{13}C NMR and HRMS spectra of 3-(pentylthio)-1*H*-indole (3f)

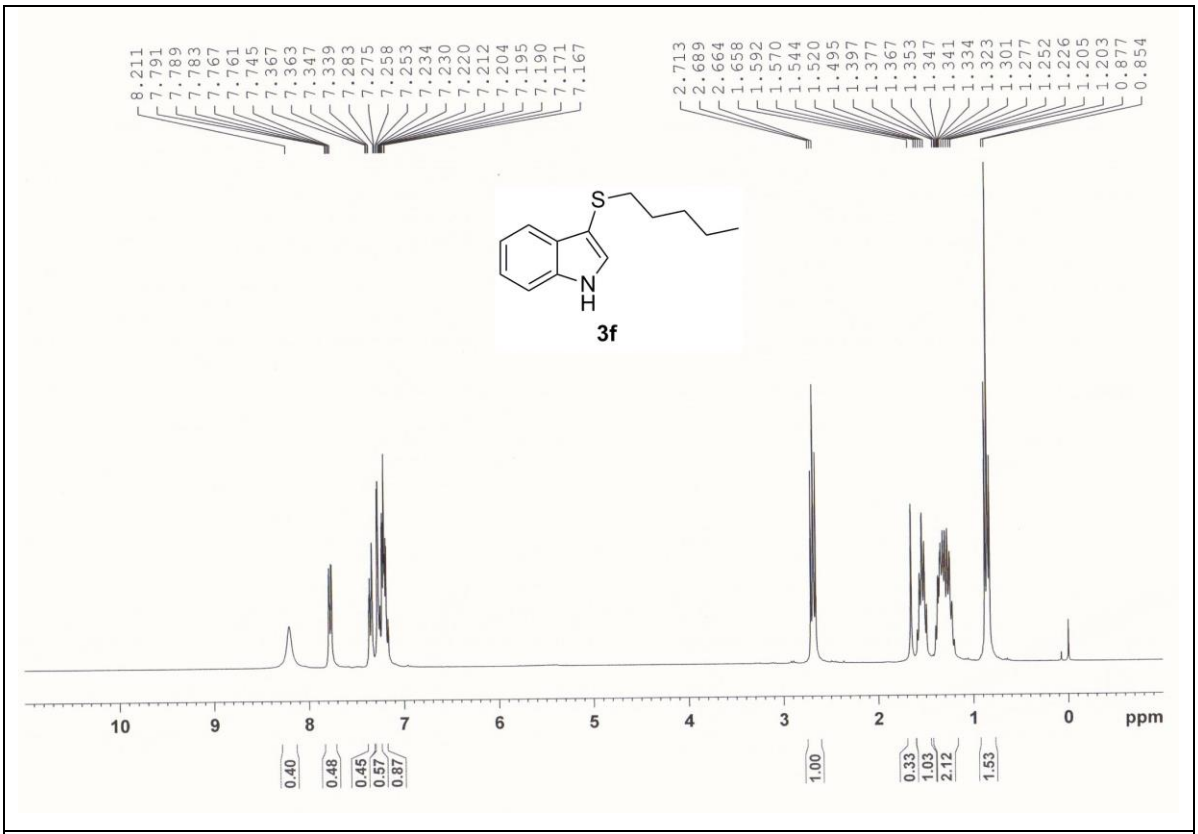

Figure I.B.6 Scanned copy of ^{1}H NMR spectrum of 3-(pentylthio)-1*H*-indole **(3f)**

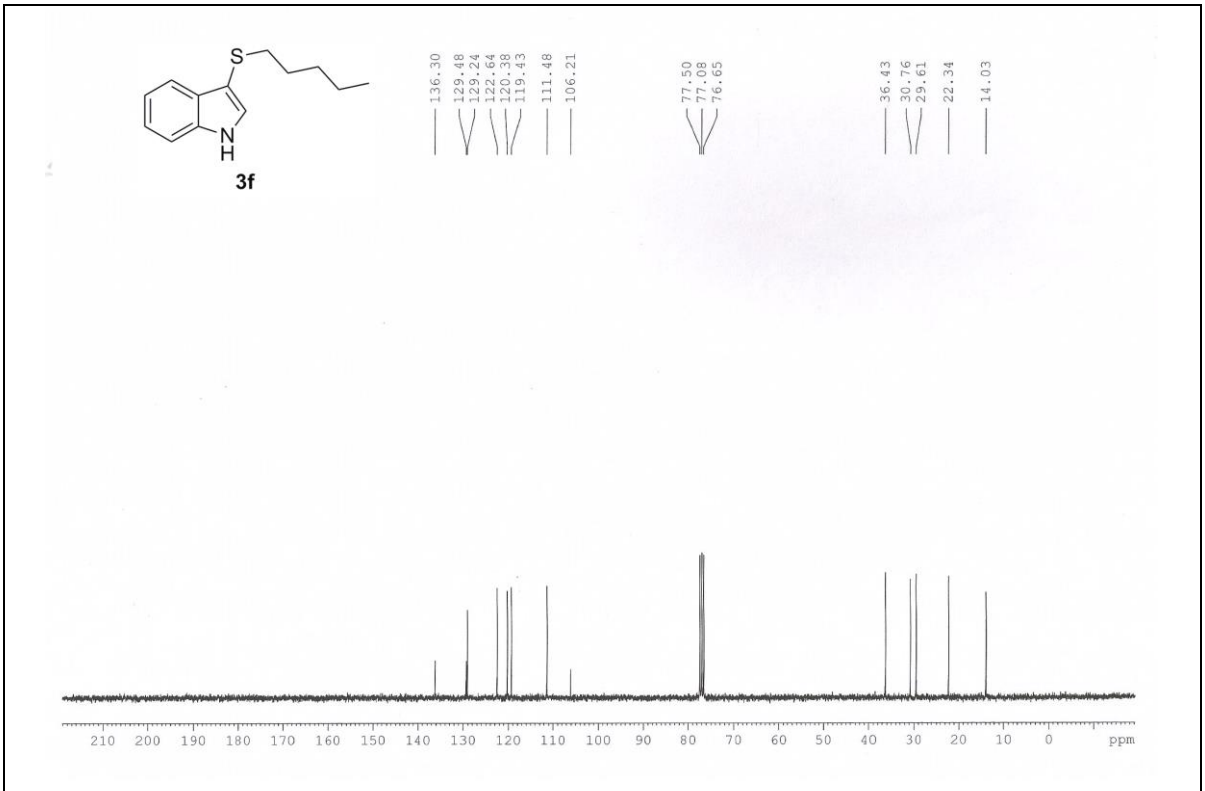

Figure I.B.7 Scanned copy of ^{13}C NMR spectrum of 3-(pentylthio)-1*H*-indole **(3f)**

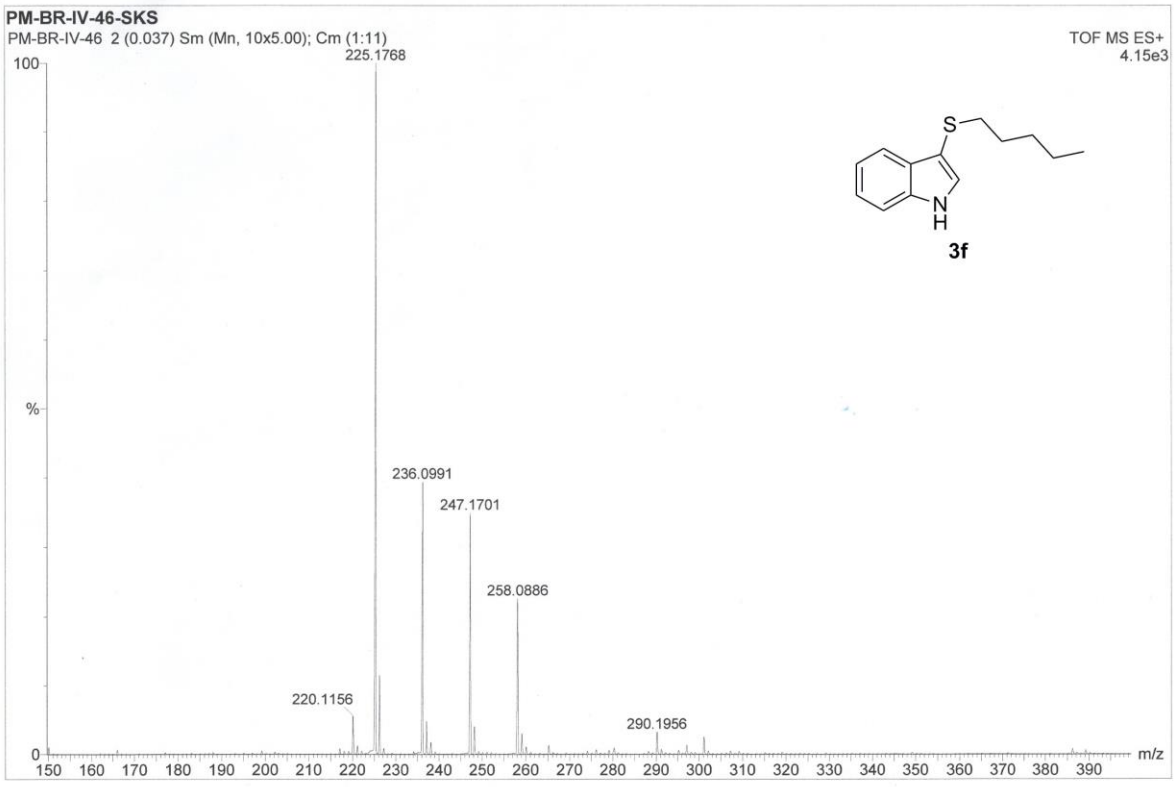

Figure I.B.8 Scanned copy of HRMS spectrum 3-(pentylthio)-1*H*-indole **(3f)**

I.B.6 References

References are given in BIBLIOGRAPHY under Chapter I, Section B.

Chapter I

Section C

Amine Functionalized Graphene Oxide Nanosheets (AFGONs): An Efficient Bifunctional Catalyst for the Synthesis of 1,4-Dihydropyridines

Chapter I

Section C

Amine Functionalized Graphene Oxide Nanosheets (AFGONs): An Efficient Bifunctional Catalyst for the Synthesis of 1,4-Dihydropyridines

I.C.1 Introduction

Among the various six membered nitrogen heterocycles, 1,4-dihydropyridines (1,4-DHPs) are well known for their widespread activity in the field of medicinal chemistry.[1] 1,4-DHPs are privileged pharmacophore for multifarious marketed drugs.[1] This structural scaffold has attracted much attention owing to its diverse pharmaceutical and biological profile. They have remarkable pharmacological efficiency and are used as bronchodilators, vasodilators, anti-hypertensive, anti-diabetic, anti-inflammatory, anti-HIV, anti-tuberculosis agents and acts as chemosensitizer in tumour therapy.[2-7] 1,4-DHPs like nifedipine, amlodipine and nitrendipine have been used as clinical drugs for calcium channel blockers in the treatment of cardiovascular diseases.[8-11] Besides, some 1,4-DHPs are also associated with therapeutic properties like non-competitive inhibition of topoisomerase I and HIV protease inhibition.[12-17] 1,4-Dihydropyridines also possess cerebral anti-ischemic properties, which could find application in the treatment of Alzheimer's disease.[18] Certain 1,4-DHPs due to their close resemblance with NADH coenzyme are considered as bio mimetic agents in biological redox processes.[19-21] 1,4-Dihydropyridines also acts important intermediates during the preparation of several alkaloids.[22] In the field of transfer hydrogenation 1,4-DHPs are often used as sacrificial hydrogen source for the reduction of organic compounds containing different functional groups like C=O, C=N, C=C, etc.[23] Few representative bioactive molecules possessing functionalized 1,4-dihydropyridine unit that are in clinical use are shown in Figure I.C.1.

The synthesis of 1,4-dihydropyridines has been first reported by Arthur Hantzsch in 1882.[24] This classical method involves one-pot three-component condensation between aldehyde, ethyl acetoacetate and ammonia, either in acetic acid or under refluxing ethanol (Scheme I.C.1). Although, this approach based on multicomponent reaction (MCR) has been followed even today, it has certain limitations like low yield of product, prolong reaction time and harsh reaction conditions.

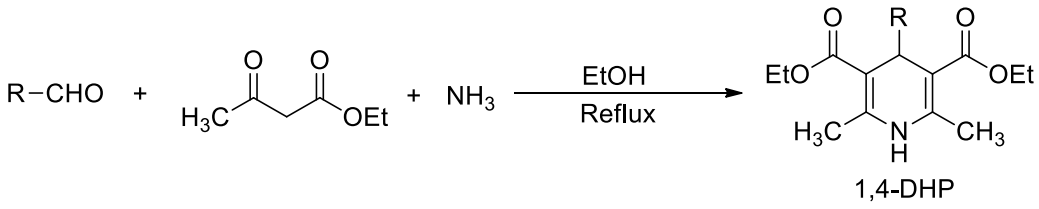

Scheme I.C.1 Classical three-component Hantzsch synthesis of 1,4-dihydropyridine.

I.C.1 Introduction

Among the various six membered nitrogen heterocycles, 1,4-dihydropyridines (1,4-DHPs) are well known for their widespread activity in the field of medicinal chemistry.[1] 1,4-DHPs are privileged pharmacophore for multifarious marketed drugs.[1] This structural scaffold has attracted much attention owing to its diverse pharmaceutical and biological profile. They have remarkable pharmacological efficiency and are used as bronchodilators, vasodilators, anti-hypertensive, anti-diabetic, anti-inflammatory, anti-HIV, anti-tuberculosis agents and acts as chemosensitizer in tumour therapy.[2-7] 1,4-DHPs like nifedipine, amlodipine and nitrendipine have been used as clinical drugs for calcium channel blockers in the treatment of cardiovascular diseases.[8-11] Besides, some 1,4-DHPs are also associated with therapeutic properties like non-competitive inhibition of topoisomerase I and HIV protease inhibition.[12-17] 1,4-Dihydropyridines also possess cerebral anti-ischemic properties, which could find application in the treatment of Alzheimer's disease.[18] Certain 1,4-DHPs due to their close resemblance with NADH coenzyme are considered as bio mimetic agents in biological redox processes.[19-21] 1,4-Dihydropyridines also acts important intermediates during the preparation of several alkaloids.[22] In the field of transfer hydrogenation 1,4-DHPs are often used as sacrificial hydrogen source for the reduction of organic compounds containing different functional groups like C=O, C=N, C=C, etc.[23] Few representative bioactive molecules possessing functionalized 1,4-dihydropyridine unit that are in clinical use are shown in Figure I.C.1.

The synthesis of 1,4-dihydropyridines has been first reported by Arthur Hantzsch in 1882.[24] This classical method involves one-pot three-component condensation between aldehyde, ethyl acetoacetate and ammonia, either in acetic acid or under refluxing ethanol (Scheme I.C.1). Although, this approach based on multicomponent reaction (MCR) has been followed even today, it has certain limitations like low yield of product, prolong reaction time and harsh reaction conditions.

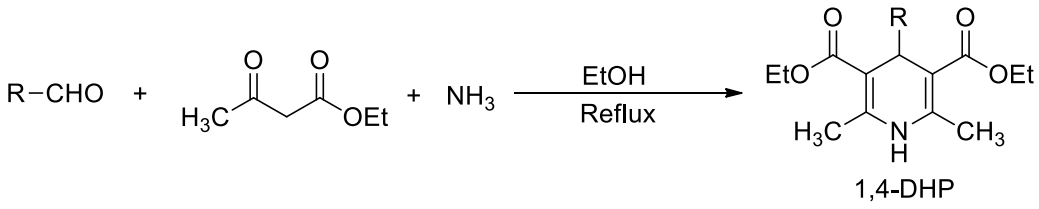

Scheme I.C.1 Classical three-component Hantzsch synthesis of 1,4-dihydropyridine.

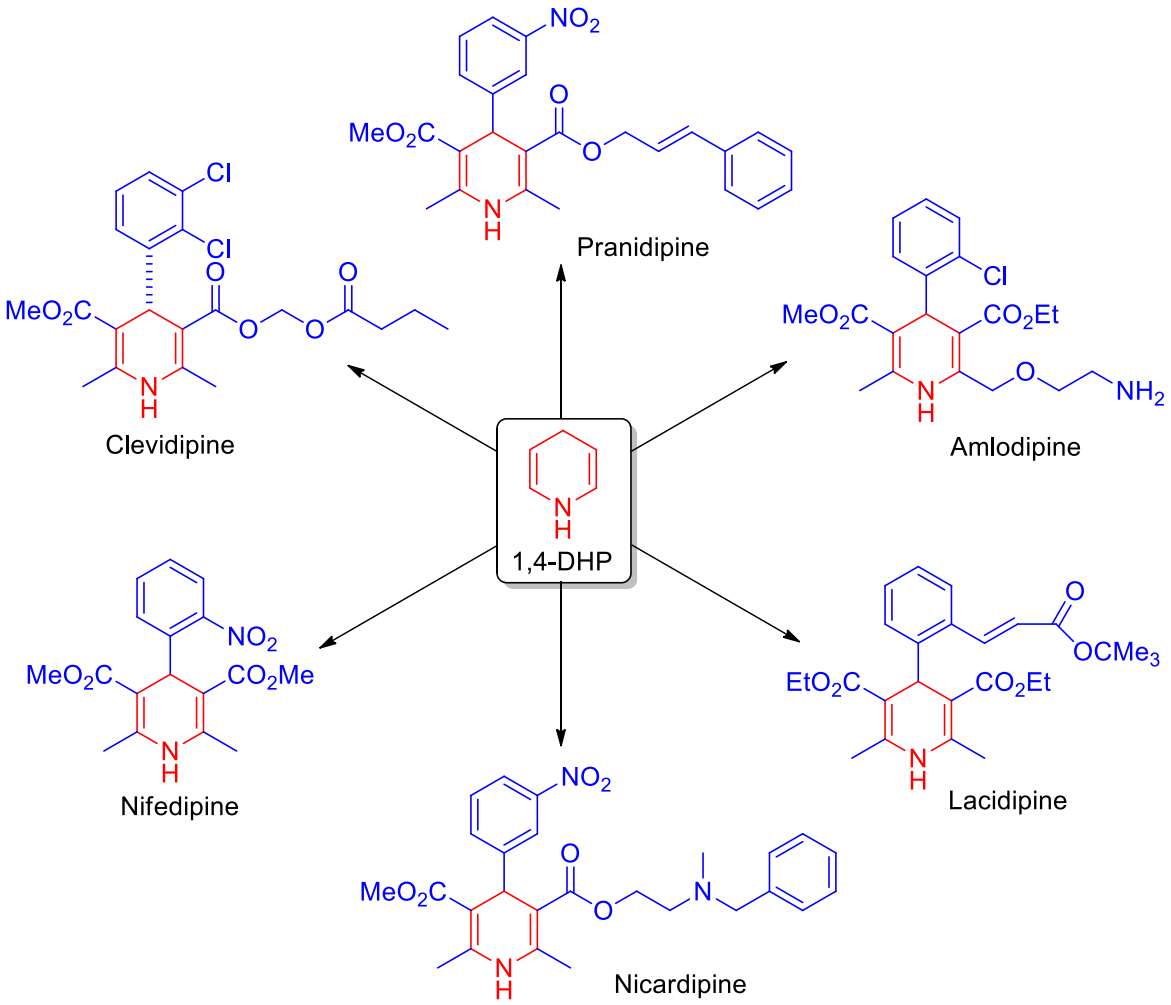

Figure I.C.1 Examples of clinical drugs bearing functionalized 1,4-dihydropyridine unit.

In the view of economical and environmental facets, organic synthesis that aims to maximize efficiency and minimize waste at source has been in demand recently. Although, myriads of new strategies have been developed, multicomponent reactions (MCRs) have emerged as an exceptional tool due to its remarkable synthetic efficiency, high atom economy, devoid of complex purification procedures, minimal waste generation and energy consumption.[25] MCRs can efficaciously enhance the reactivity of chemical processes and have been commonly used for the genesis of carbon-carbon and carbon-heteroatom bonds in a single step. Thus, MCRs allow direct and elegant access to library of complex structural diversity.

On the other hand, heterogeneous catalysts based on graphene and chemically modified graphenes (CMGs) have received prodigious attention owing to their potential for catalysis under benign conditions.[26] Moreover, functionalized graphenes possesses high surface area and diverse functionalities thereby facilitating catalytic performance.[27] Besides, such catalytic

systems could be easily re-used and provides a convenient and practical way to synthesize complex organic molecules.

I.C.2 Background and objectives

Owing to the limitations of the classical Hantzsch synthesis, innumerable strategies have been developed which attempts to improve the Hantzsch.[28] A wide range of homogeneous and heterogeneous catalysts have been employed for the synthesis of diverse 1,4-dihydropyridine derivatives.[29] Strong acids,[30,31] and silica based composites have been widely used as catalysts for the synthesis of 1,4-DHPs.[32,33] Apart from silica based composites various metal salts, metallic nanoparticles (NPs) and supported metal catalysts are also used as catalyst which often generates hazardous wastes thereby compromising environmental safety.[34-36] The use of magnetic nanocatalysts in Hantzsch synthesis renders easy removal of the catalyst after the reaction by using an external magnet.[37,38] Other commonly used catalytic systems for the synthesis of 1,4-DHPs include *p*-TSA,[39] montmorillonite clay,[40] sulfated polyborate,[41] zeolite,[42] chitosan NPs,[43] polyethylene glycol,[44] PPh_3,[45] ionic liquids (ILs),[46] heteropoly acids,[47] and organocatalysts.[48] Most of these procedures employ harsh reaction conditions, uses toxic solvents and requires tedious purification steps. The diverse strategies involved in the synthesis of 1,4-DHPs have been nicely presented in a review article by Wan and co-workers.[28] The following section represents few recent strategies involved in the synthesis of 1,4-DHPs.

Silica gel supported sodium bisulfate (SiO_2-$NaHSO_4$) has been prepared and used for the one-pot synthesis of 1,4-dihydropyridines at ambient temperature (Scheme I.C.2). Diverse 1,4-dihydropyridine derivatives were synthesized in good to excellent yields. The catalyst being heterogeneous in nature could be recycled and reused for further catalytic runs.[49]

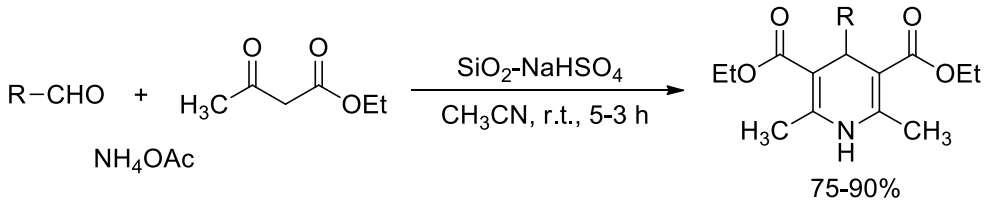

Scheme I.C.2 SiO_2-$NaHSO_4$ catalyzed synthesis of 1,4-dihydropyridines.

Kilbas and co-workers have prepared monodispersed Pd, Ru and Ni nanoparticles embedded on graphene oxide nanosheets by using double solvent reduction method under ultrasonication. The catalyst has been characterized by different spectroscopic techniques. The as-prepared nanocomposite (PdRuNi@GO) has been employed for the synthesis of 1,4-

dihydropyridines and hexahydroquinolines based on a multicomponent approach (Scheme I.C.3). The authors also suggested a plausible mechanism and checked recyclability of the catalyst for five cycles.[36]

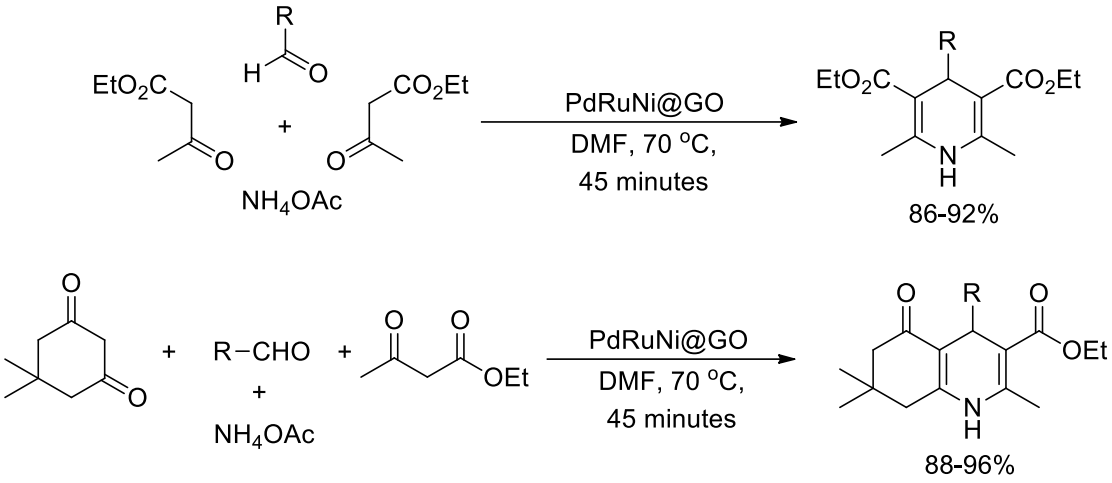

Scheme I.C.3 PdRuNi@GO catalyzed synthesis of 1,4-DHPs and hexahydroquinolines.

Zirconia supported sulfonic acid nanocomposite (n-ZrSA) has been prepared from nano zirconia by using chlorosulfonic acid. The material has been characterized in detail by spectroscopic techniques and used for four different multicomponent reactions. A wide range of hexahydroquinoline, 1,8-dioxo-decahydroacridine, polyhydroquinoline and 1,8-dioxo-octahydroxanthene derivatives were synthesized under solvent free conditions (Scheme I.C.4). The acidity strength of n-ZrSA has been determined by using Hammett acidity function and the acid capacities have been calculated by acid-base potentiometric titration.[30]

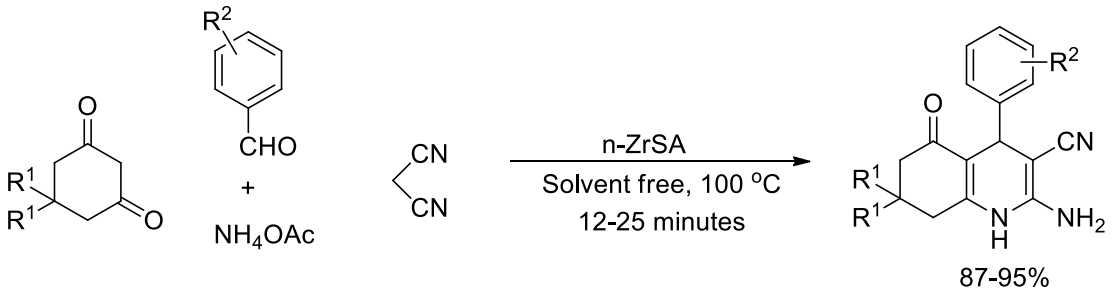

Scheme I.C.4 Zirconia sulfonic acid catalyzed synthesis of hexahydroquinolines.

An expedient synthesis of 1,4-dihydropyridines has been reported by using nano-Fe_2O_3 catalyst. The reaction conditions are facile and involve stirring of the reactants under solvent free conditions at 90 °C (Scheme I.C.5). The magnetic nature of the catalyst also facilitates easy recovery and recyclability. The investigators also proposed a mechanism where activation of the carbonyl group is facilitated by coordination with Fe^{3+} moiety.[38]

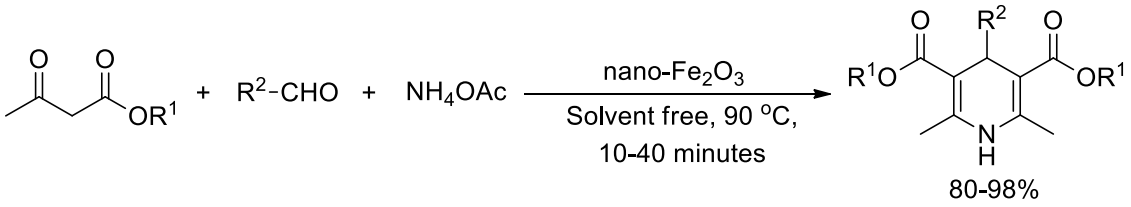

Scheme I.C.5 Three-component synthesis of 1,4-DHPs using nano-Fe_2O_3.

The synthesis of 1,4-DHPs has been accomplished by using sulfated polyborate as an efficient heterogeneous catalyst. The catalyst has been prepared from boric acid by dehydration followed by sulfonation using chlorosulfonic acid (Scheme I.C.6). The resulting material catalyzed the three-component reaction between β-ketoesters, aldehydes and ammonium carbonate under solvent free conditions.[41]

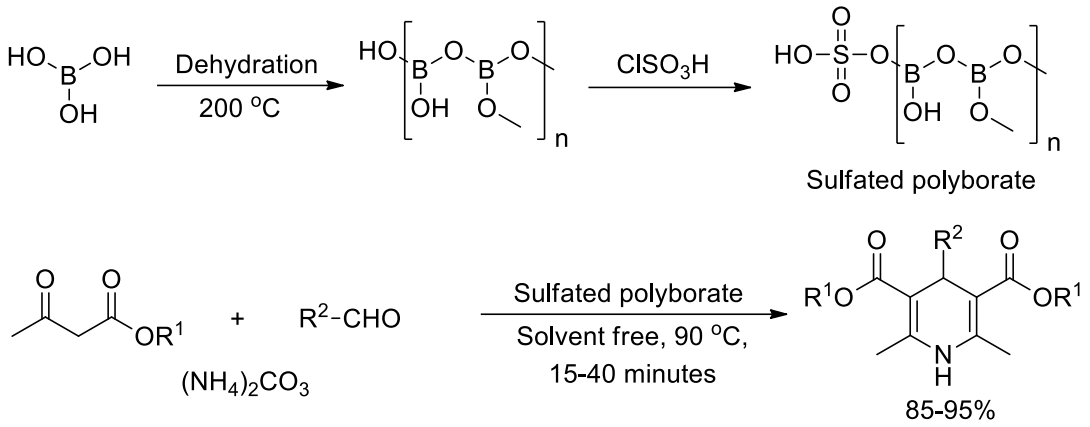

Scheme I.C.6 Synthesis of 1,4-DHPs using sulfated polyborate catalyst.

The synthesis of functionalized 1,8-dioxoacridines has been accomplished by using $Bi(NO_3)_3{\cdot}5H_2O$ at ambient temperature. A pseudo four-component reaction between 1,3-diketones, aldehydes and primary amines afforded the desired products in 63-99% yield (Scheme I.C.7). The authors proposed a plausible mechanism which initially involved Claisen-Schmidt condensation between 1,3-diketone and aldehyde catalyzed by Bi^{3+} ions.[34]

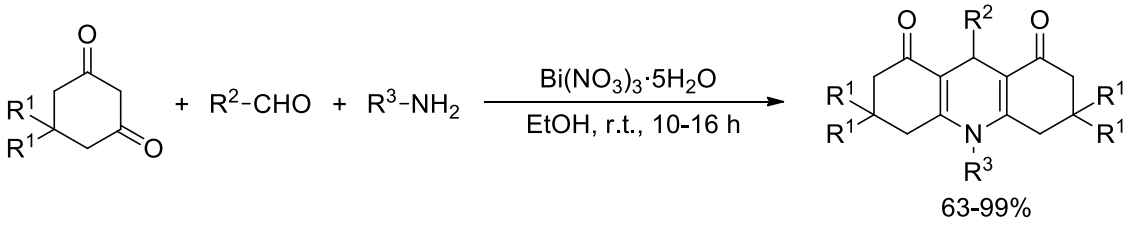

Scheme I.C.7 Bismuth nitrate catalyzed three-component synthesis of 1,8-dioxoacridines.

Ionic liquid catalyzed multicomponent synthesis of acridinediones has been reported by Zhu and co-workers.[46] A series of betainium based ionic liquid has been tested for their catalytic activity and betainium lactate [HBet][Lac] showed the highest activity (Scheme I.C.8). Moreover, the catalyst could be recycled for five runs without any loss in the yield of product. The investigators also proposed a plausible mechanism and showed the role of ionic liquid.

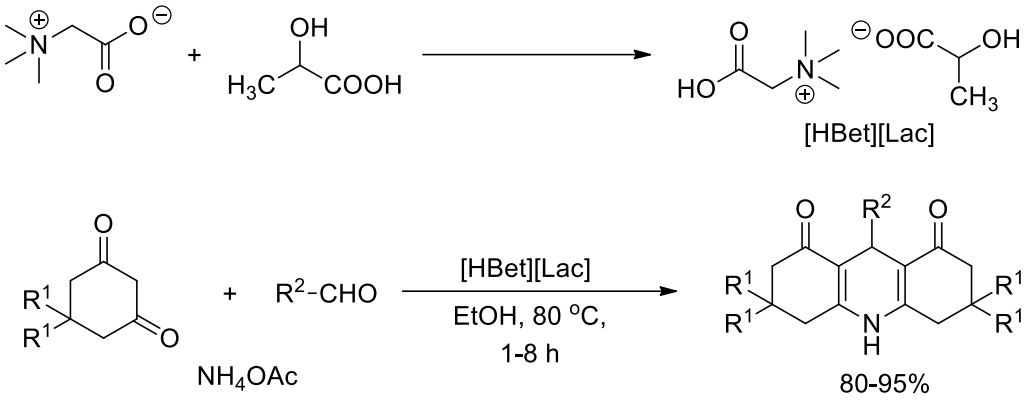

Scheme I.C.8 Betainium lactate catalyzed synthesis of acridinediones.

Silica functionalized sulfonic acid coated with ionic liquid has been prepared and characterized. Initially, activated silica and 3-mercaptopropyl (trimethoxy)silane were refluxed in toluene followed by oxidation of the resultant 3-mercaptopropylsilica. The silica functionalized sulfonic acid was then coated with ionic liquid [BMIM][PF_6]. The as-prepared catalyst (Silica-SO_3H-[BMIM][PF_6]) has been used for the solvent free synthesis of 1,4-dihydropyridines (Scheme I.C.9). The recyclability of the catalyst has been performed for seven cycles.[33]

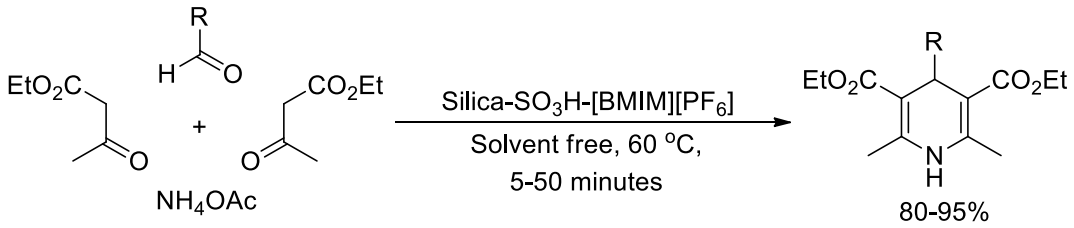

Scheme I.C.9 Silica-SO_3H-[BMIM][PF_6] catalyzed one-pot synthesis of 1,4-DHPs.

The synthesis of 1,4-dihydropyridines and N-substituted-1,4-dihydropyridines has been accomplished by using silica supported 12-tungstophosphoric acid catalyst (PW/SiO_2). The reaction conditions involve three-component condensation between aldehydes, β-ketoesters and ammonium acetate (or amines). The desired products were obtained in 55-98% at room temperature under solvent free conditions (Scheme I.C.10).[50]

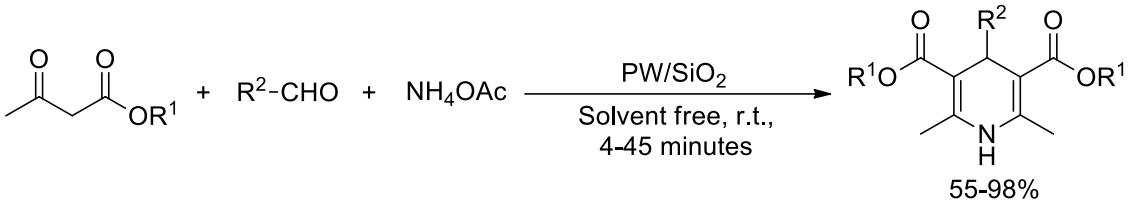

Scheme I.C.10 PW/SiO_2 catalyzed three-component synthesis of 1,4-DHPs.

Organocatalysts have been frequently used in the multicomponent synthesis of diverse heterocyclic compounds. Ultrasound assisted, *p*-TSA (*p*-toluenesulfonic acid) catalyzed synthesis of 1,4-DHPs has been achieved under aqueous micellar medium. The investigators have employed aqueous sodium dodecyl sulfate (SDS) in presence of *p*-TSA for the reaction and the corresponding products have been obtained in 90-97% yield (Scheme I.C.11). Moreover, the protocol has been further extended towards the synthesis of polyhydroquinolines.[39]

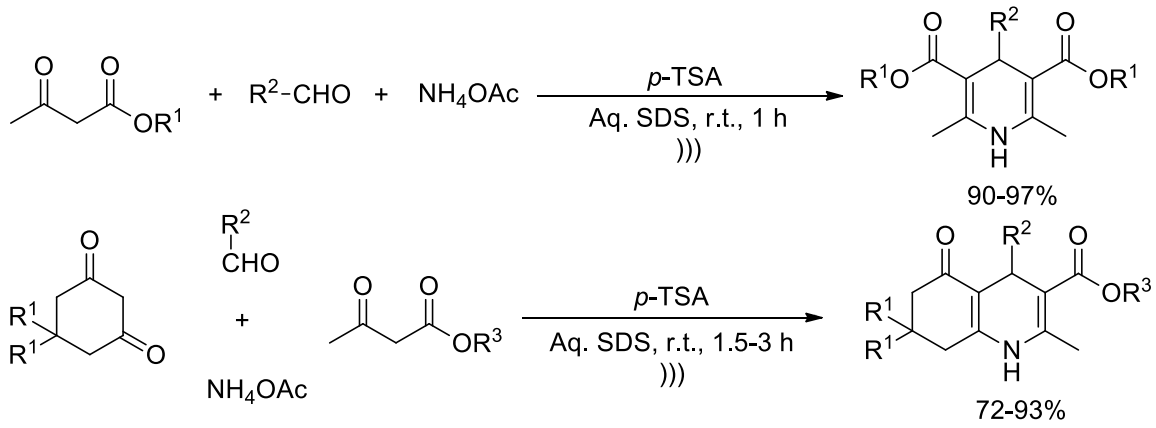

Scheme I.C.11 Ultrasound assisted synthesis of 1,4-DHPs and polyhydroquinolines in aqueous micelles.

I.C.3 Present work: Results and discussions

Graphene oxide (GO) catalyzed Hantzsch synthesis has been previously studied and reported.[51,52] However, these protocols resulted in the formation of both 1,4-dihydropyridines as well as its oxidized form, i.e. pyridine derivatives in different ratios. Moreover, the processes required elevated temperature (refluxing conditions) and no detailed recycling experiment has been performed. We supposed that GO being oxidising in nature, when used in excess, could lead to further oxidation of 1,4-DHPs to the corresponding pyridine derivatives. We therefore thought further functionalization of GO could prevent it from getting reduced and selectively form 1,4-DHP as the exclusive product. Amine functionalized graphene oxide nanosheets (AFGONs) was previously prepared, designated as NH_2–GO,[53] or

AP–GO (GO-supported primary amine),[54] and used as catalyst in Knoevenagel reaction and Henry-Michael reaction respectively. We have prepared AFGONs in our laboratory from GO and used it as an excellent bifunctional catalyst for the facile one-pot selective synthesis of dihydropyridines (DHPs), polyhydroacridines (PHAs) and polyhydroquinolines (PHQs) under ambient conditions (Scheme I.C.12). Moreover, we did not observe the formation of any oxidised pyridine derivative during the course of the reaction. We presumed that the high and selective catalytic activity of AFGONs might be due to the unique cooperative effect between amines on the basal plane of GO and the adjacent carboxylic acid functionalities on its edges.

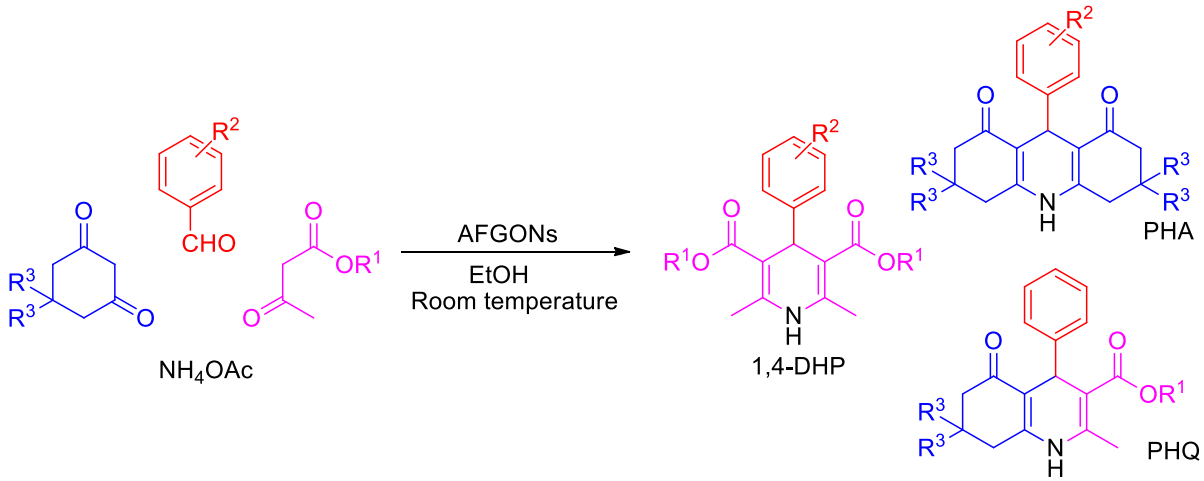

Scheme I.C.12 AFGONs catalyzed synthesis of 1,4-DHPs, PHAs and PHQs.

I.C.3.1 Preparation of the catalyst

The amine functionalized graphene oxide nanosheets (AFGONs) were prepared by following a reported procedure.[54] At first, graphene oxide was prepared by Tour's method.[55] It was then exfoliated in an ultrasonic bath for 2 h and then the amine groups were grafted onto the basal surface of GO through a facile amine-coupling reaction using (3-aminopropyl)triethoxysilane (Scheme I.C.13).

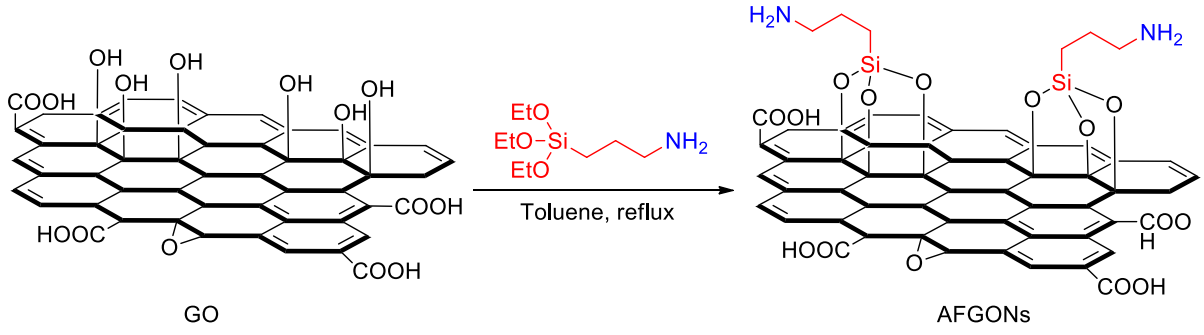

Scheme I.C.13 Illustration for the preparation of AFGONs.

I.C.3.2 Characterization of AFGONs

After the preparation of the catalyst it was characterized by FT-IR, Raman spectra, powder X-ray diffraction (XRD) and scanning electron microscopy (SEM). The FT-IR spectra of both GO and AFGONs were recorded in the range 4000-500 cm^{-1} (Figure I.C.2). The characterized bands in case of pristine GO at 3411, 1734 and 1628 cm^{-1} were due to the stretching vibrations of O–H, C=O and C=C bonds respectively.[55] The peaks in the range 1400-1000 cm^{-1} were due to the presence of C–O functionalities in GO.[55] In case of AFGONs the peaks at 2963 and 2924 cm^{-1} were due to the asymmetric and symmetric stretching modes of C–H bonds of aminopropyl groups.[53,56] The additional peak at 1593 cm^{-1} was due to the NH_2 scissor vibration, confirming the presence of terminal NH_2 in the material.[56] The band at 1123 cm^{-1} indicated Si–O–Si stretching, while the less intense band at 1198 cm^{-1} might be due to the rocking mode of SiO–C.[56] Moreover, the disappearance of the typical carbonyl band at 1734 cm^{-1} further confirmed that the carbonyl groups were converted to Si–O–C band, along with removal of oxygenated functional groups to form partially reduced graphene oxide (rGO).[57]

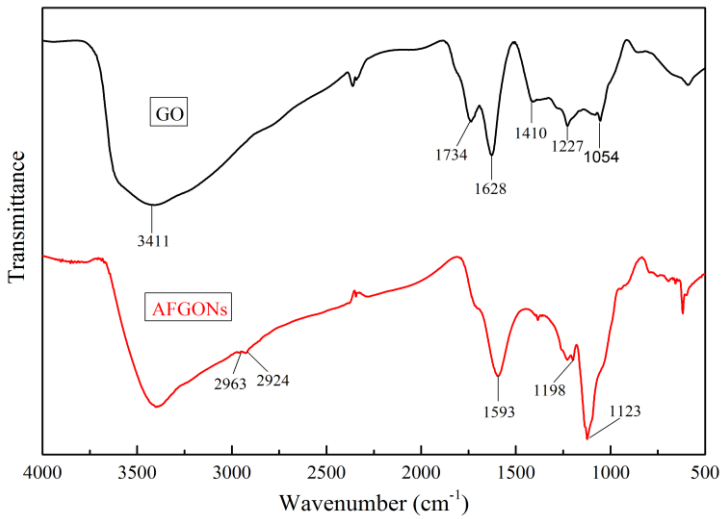

Figure I.C.2 FT-IR spectra of GO and AFGONs.

The Raman spectra of both GO and AFGONs showed characteristic D- (arising from A_{1g} vibrations of sp^2 carbon rings) and G- (arising from first order scattering of E_{2g} mode of sp^2 C atoms) bands at 1345 and 1592 cm^{-1} respectively (Figure I.C.3).[58] The intensity ratios of D- and G-bands (I_D/I_G) of GO and AFGONs were found to be 0.83 and 0.92 respectively. The higher intensity ratio (I_D/I_G) of AFGONs might indicate restoration of C=C bonds during the grafting process resulting in partial formation of rGO.[59,60]

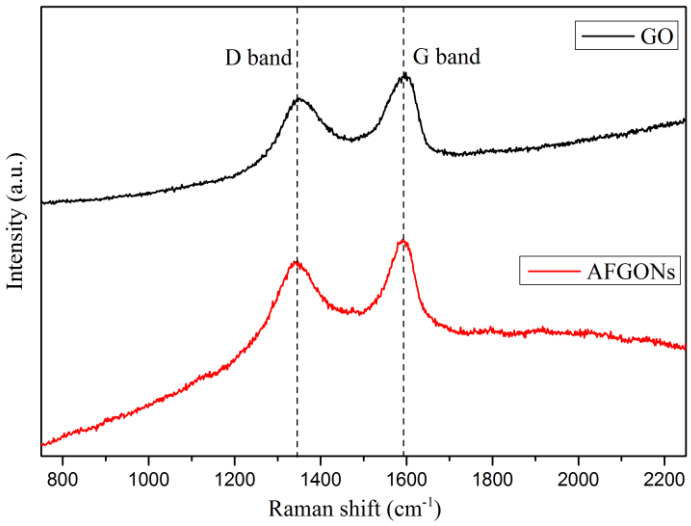

Figure I.C.3 Raman spectra of GO and AFGONs.

The X-ray diffraction (XRD) patterns of pristine GO showed a sharp peak at 2θ = 9.5° arising from the (001) plane of GO.[53] In the case of AFGONs a broad peak at 2θ = 22.1° was due to the effect of silica and the peak of GO has been shifted to 2θ = 11.9° (Figure I.C.4).[57] According to Bragg's law, 2dsinθ = nλ (λ = 0.154 nm), the interlayer distance (d) of AFGONs was found to be 7.4 Å (2θ = 11.9°) and that of GO was 9.2 Å (2θ = 9.5°) which could be attributed to the surface occupancy of aminopropyl-silica groups.[57] The characteristic peak of silica as well as the decrease in the d-spacing in case of AFGONs indicated that amino groups were fabricated on the surface of GO.[57]

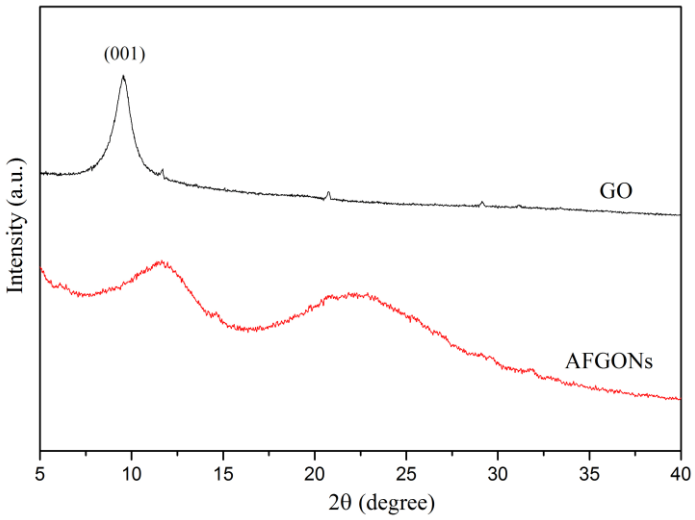

Figure I.C.4 X-ray diffraction patterns of GO and AFGONs.

The morphology of GO and AFGONs were analyzed by scanning electron microscopy (SEM). The SEM images along with the XRD patterns clearly indicated the amorphous and

fibrous nature of the catalyst (Figure I.C.5). Furthermore, the elemental composition of the AFGONs as determined by electron-dispersive X-ray spectroscopy (EDS), showed C (71.26 wt %), O (21.07 wt %), Si (3.96 wt %) and N (3.71 wt %), which confirmed the deposition of silica groups on the surface of GO (Figure I.C.6).

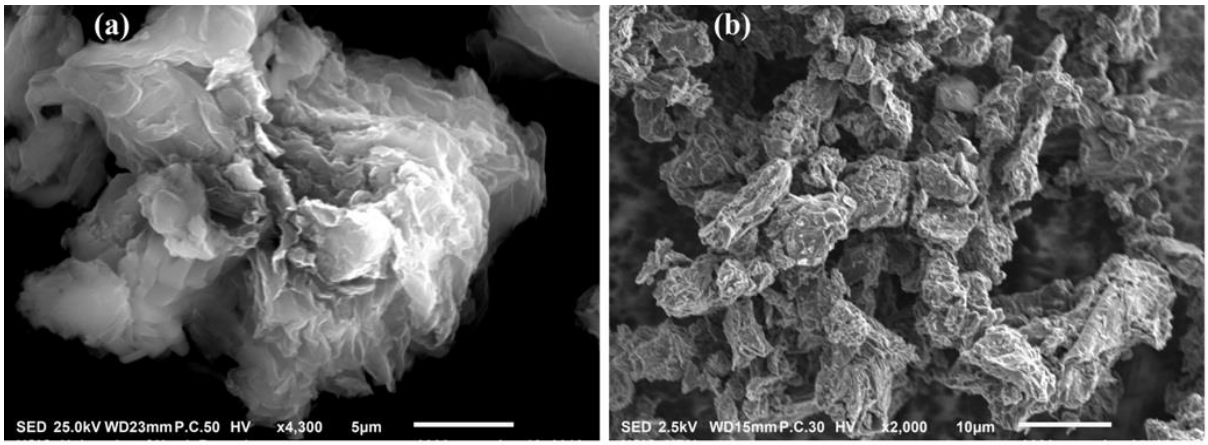

Figure I.C.5 SEM images of (a) GO and (b) AFGONs.

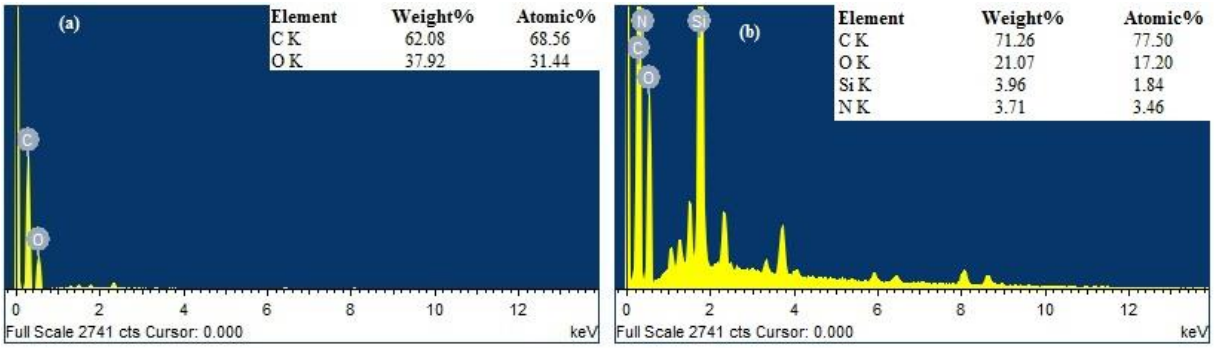

Figure I.C.6 EDS images of (a) GO and (b) AFGONs.

I.C.3.3 Catalytic activity of AFGONs: Optimization of reaction conditions

In order to optimize the reaction conditions, we began our investigation using ethyl acetoacetate (**1a**), 4-chlorobenzaldehyde (**2a**) and ammonium acetate as model substrates in the presence of AFGONs as catalyst. Initially, the reactants were screened with regard to different solvents and then the other parameters like temperature, catalyst loading and duration of reaction were varied (Table I.C.1). At first, we performed the reaction using AFGONs (50 mg) in ethanol at 78 °C. The desired product **4a** was obtained in 69% yield (entry 1). The formation of **4a** was confirmed by ^{1}H, ^{13}C NMR spectroscopy and HRMS analysis. The ^{1}H NMR peaks appearing as singlet at δ 2.33, 4.98 and 6.03 ppm were respectively due to the CH_3 groups, quaternary H and NH moieties of 1,4-DHP nucleus. Moreover, the compound **4a** was subjected to ESI-HRMS analysis and the (*m/z*) for

$C_{19}H_{22}ClNO_4$ $[M + H]^+$ was calculated at 364.1315 and found at 364.1299, which confirmed the formation of **4a**. To check the role of solvent, the reaction was carried out in various solvents like CH_3CN, H_2O and DMF (entries 2–5). The best result in terms of product yield was obtained using ethanol as solvent. Reducing the catalyst loading (25 mg) and carrying out the reaction at 50 °C increased the product yield to 72% (entry 6). Encouraged by the outcome, we carried out a reaction at room temperature (r.t.) which further increased the yield of the product to 88% (entry 7). The yield of the product was relatively lower at higher temperature as compared to room temperature. This could be due to some side reactions taking place at higher temperature as was observed on TLC. A neat mixture of the reactants without any solvent afforded the product in 52% yield (entry 8). The reaction when conducted without any catalyst resulted in poor conversion even after prolonged reaction time which indicated the imperative role of the catalyst (entry 9, 21%).

Table I.C.1 Optimization of reaction conditions[a]

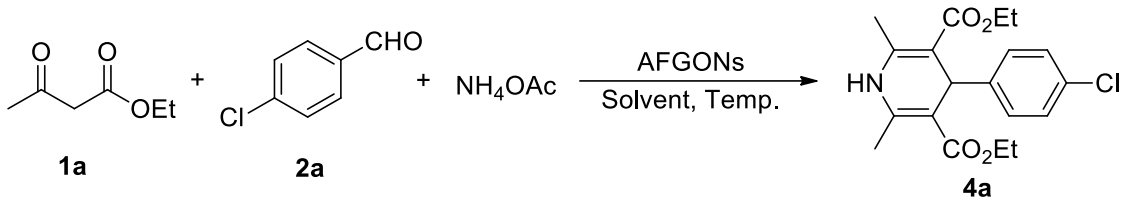

Entry	AFGONs (mg)	Solvent	Temp (°C) / time (h)	Yield (%)[b]
1	50	EtOH	78 / 8	69
2	50	CH_3CN	80 / 8	58
3	50	H_2O	90 / 8	42
4	50	H_2O	90 / 8	65[c]
5	50	DMF	80 / 8	68
6	25	EtOH	50 / 4	72
7	**25**	**EtOH**	**r.t. / 2**	**88**
8	25	–	r.t. / 2	52
9	–	EtOH	r.t. / 20	21

[a]Reaction conditions: **1a** (2 mmol), **2a** (1 mmol), NH_4OAc (2 mmol) and solvent (4 mL). [b]Isolated yield. [c]TBAB (10 mol%) was used.

I.C.3.4 Synthesis of 1,4-dihydropyridine derivatives

After the optimization of the reaction conditions, diverse 1,4-DHPs were synthesized and the results are presented in Table I.C.2. A series of different aldehydes reacted under the standard reaction conditions and in all cases the desired products were obtained in good to excellent

yields. Aromatic aldehydes substituted with both electron donating (–Cl, –Br, –CH_3, –OCH_3, –OH and –NMe_2) as well as electron withdrawing (–F and –NO_2) groups reacted efficiently to afford the corresponding products (**4a**-**k**). The substitution pattern on the aromatic moiety did not have any significant influence in the course of the reaction. We then checked the reaction with 2-naphthaldehyde and cinnamaldehyde, which furnished the desired products in 84% and 83% yield respectively (**4l** and **4m**). Further investigation with aliphatic aldehydes also worked efficiently affording the desired products (**4n** and **4o**). Fascinatingly, heterocyclic aldehydes like furfural and 5-bromo-2-thiophenecarboxaldehyde were found to be equally effective affording the anticipated products in 87% and 89% isolated yield respectively (**4p** and **4q**). In the ^{1}H NMR spectrum of **4c** the singlet peaks at δ 2.32, 3.64 and 4.95 ppm were respectively due to due to the CH_3 groups of 1,4-DHP nucleus, ester CH_3 groups and the quaternary H. The broad singlet peak δ 5.87 ppm was due to the NH moiety of 1,4-DHP nucleus. The four aromatic Hs appeared as two doublets at δ 7.14 (J = 8.4 Hz, 2H) and 7.32 (J = 8.4 Hz, 2H) ppm. In case of **4g**, the two terminal ester CH_3 groups appeared as triplets at δ 1.23 (J = 7.2 Hz) ppm. The peaks at δ 2.32 ppm were due to the two CH_3 groups of 1,4-DHP nucleus. The –NMe_2 group appeared as singlet at δ 2.88 ppm. The ester CH_2 groups appeared as quartet at δ 4.08 (J = 6.9 Hz) ppm. The quaternary H and the NH moiety appeared as singlet at δ 4.88 and 5.56 ppm. The four aromatic Hs appeared as two doublets at δ 6.60 (J = 78 Hz, 2H) and 7.14 (J = 8.4 Hz, 2H) ppm. In the ^{13}C NMR spectrum of **4g** the characteristic peak of –NMe_2 appeared at 38.3 ppm.

Table I.C.2 AFGONs catalyzed synthesis of 1,4-dihydropyridines[a]

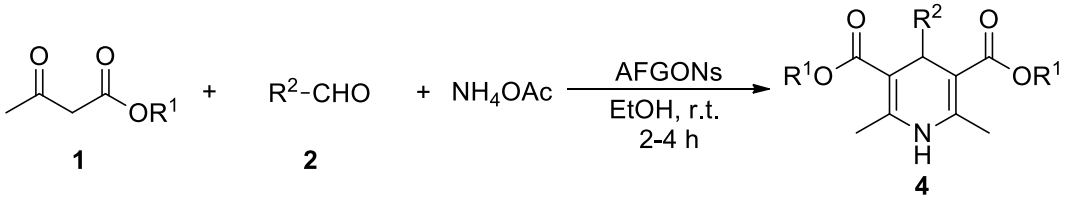

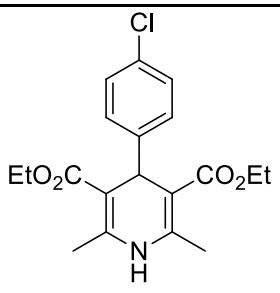	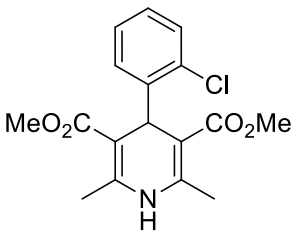	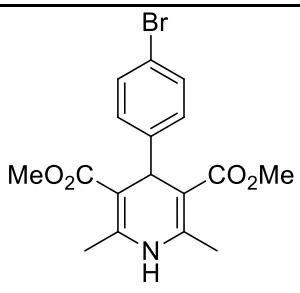
4a, 88%, 2 h	**4b**, 84%, 4 h	**4c**, 87%, 2 h

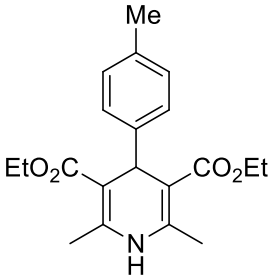

4d, 85%, 3h

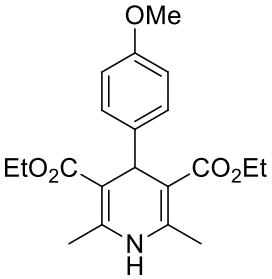

4e, 86%, 3 h

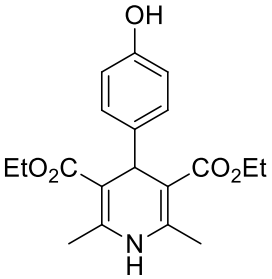

4f, 89%, 2 h

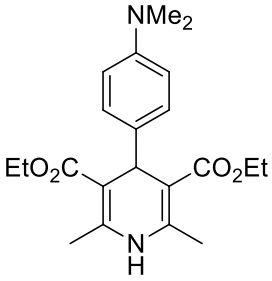

4g, 87%, 3 h

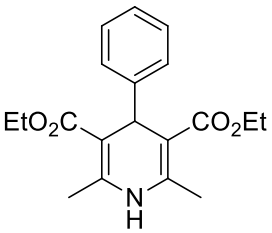

4h, 90%, 2h

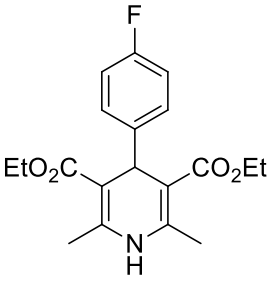

4i, 91%, 2 h

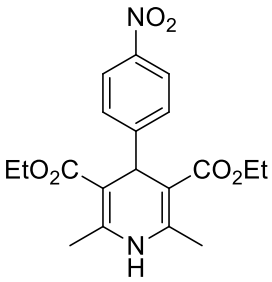

4j, 90%, 2 h

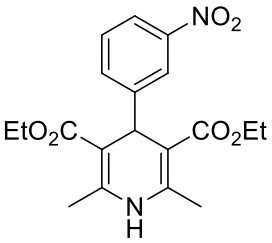

4k, 93%, 2 h

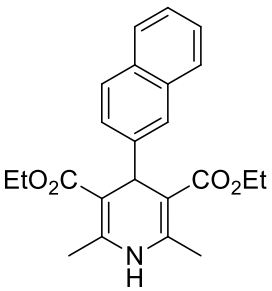

4l, 84%, 4 h

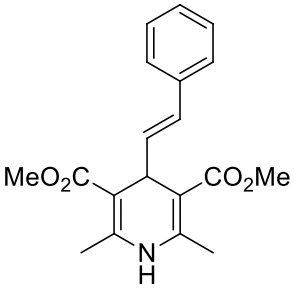

4m, 83%, 4 h

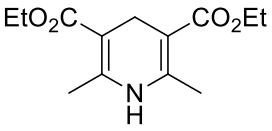

4n, 90%, 3 h

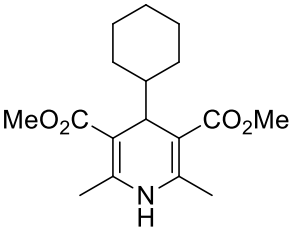

4o, 83%, 4 h

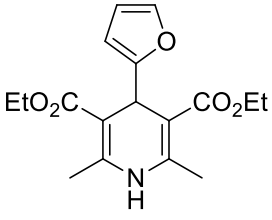

4p, 87%, 3 h

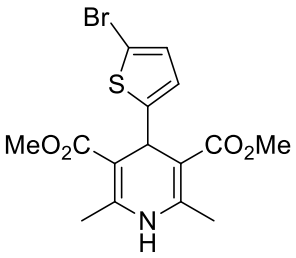

4q, 89%, 4 h

[a]Reaction conditions: **1** (2 mmol), **2** (1 mmol), NH_4OAc (2 mmol) and AFGONs (25 mg) in EtOH (4 mL) were stirred at r.t. for 2-4 h.

I.C.3.5 Synthesis of 1,8-dioxodecahydroacridine derivatives

The scope of the protocol was further extended towards the synthesis of 1,8-dioxodecahydroacridines (Table I.C.3). Acridinediones possesses potential biological and pharmacological properties. For instance 1,8-dioxodecahydroacridine derivatives exhibit a wide range of biological properties such as anti-malarial, anti-tumour, anticancer, anti-microbial activities and used as β-channel opener in case of cardiovascular diseases.[34,48] Moreover, some derivatives of acridinediones has been used in laser dyes and photo initiators because of their florescent properties.[46] The pseudo four-component reaction was accomplished with benzaldehydes bearing both electron withdrawing (–F, $–NO_2$) as well as electron donating (–Cl, –Br, –OH, –OMe) groups. The substitution pattern on the aldehyde partner did not affect the product yield. The formation of the desired products was confirmed by NMR spectroscopy. The compound **5d** showed distinct singlet peaks for the two dimedone CH_3 groups at δ 0.95 and 1.07 ppm. The quaternary H and the NH moiety appeared as singlet at δ 5.06 and 7.47 ppm respectively. The eight dimedone CH_2 hydrogen appeared as multiplet between 2.12-2.35 ppm. In the ^{13}C NMR spectrum heteronuclear coupling between ^{13}C and ^{19}F occurred and the peaks appeared at δ 32.8 (d, J = 28.5 Hz), 114.7 (d, J = 21.0 Hz) and 129.4 (d, J = 8.2 Hz) ppm.

Table I.C.3 AFGONs catalyzed synthesis of 1,8-dioxodecahydroacridine[a]

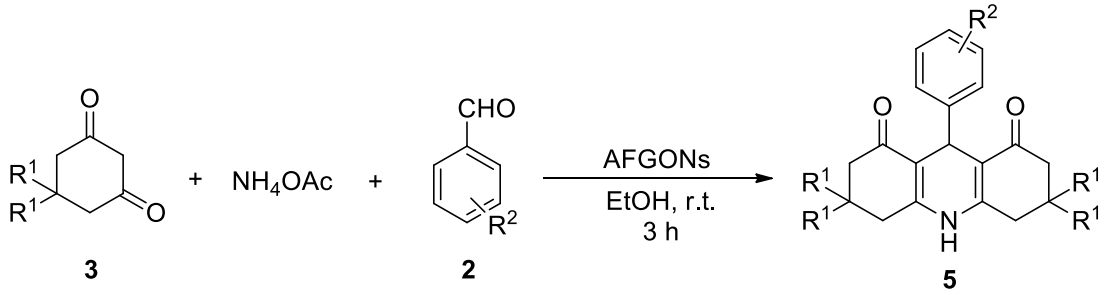

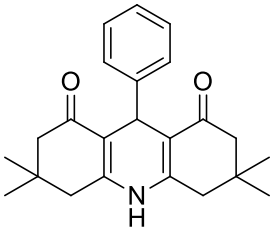	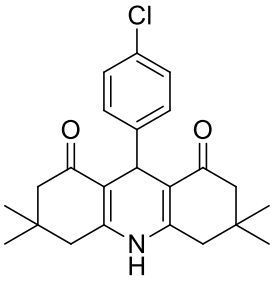	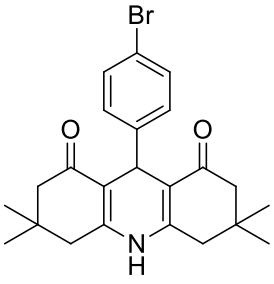
5a, 90%	**5b**, 89%	**5c**, 91%

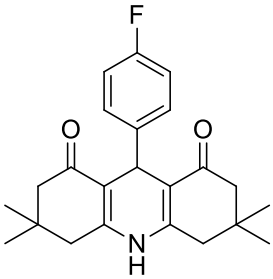

5d, 92%

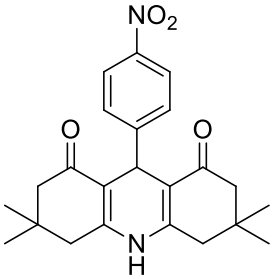

5e, 90%

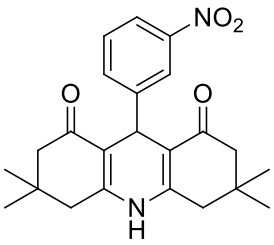

5f, 91%

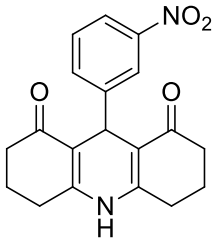

5g, 88%

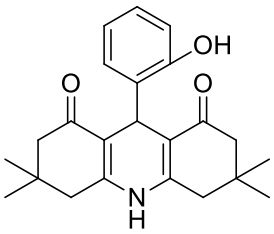

5h, 86%

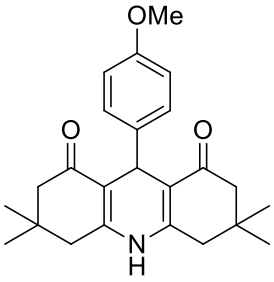

5i, 89%

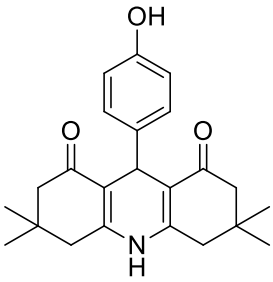

5j, 86%

[a]Reaction conditions: **3** (2 mmol), **2** (1 mmol), NH_4OAc (2 mmol), AFGONs (25 mg) and EtOH (4 mL) were stirred at r.t. for 3 h.

I.C.3.6 Synthesis of polyhydroquinoline derivatives

Polyhydroquinolines (PHQs) are unsymmetrical derivatives of 1,4-DHPs which displays prominent biological activities associated with cardiovascular diseases and hypertension.[37] Certain 2,4-disubstituted polyhydroquinoline derivatives are active glycogen phosphorylase inhibitors and exhibits anti-hyperglycemic activity.[61] We explored the synthesis of PHQs through four-component catalytic reaction between β-ketoester, aldehyde, dimedone/cyclohexan-1,3-dione and ammonium acetate. Gratifyingly, the reaction worked efficiently and the desired products were obtained in good to excellent yields (Table I.C.4). Benzaldehydes bearing both electron donating groups (–Me, $–CHMe_2$, –Br, –OH) as well as electron withdrawing groups (–F, $–NO_2$) were well tolerated in the course of the reaction. Furthermore, the four-component reaction did not result in the formation of any symmetrical 1,4-DHP derivatives. The compound **6c** was characterized by ^1H, ^{13}C spectroscopy and

HRMS analysis. The two terminal CH_3 moieties of isopropyl groups appeared as doublet at δ 1.17 (J = 6.9 Hz) ppm, and the CH hydrogen appeared as multiplet between δ 2.75-2.84 ppm. Furthermore, compound **6c** was analyzed by ESI-HRMS and the (m/z) $C_{23}H_{29}NO_3$ $[M + H]^+$ was calculated at 368.2225 and found at 368.2231, which confirmed the formation of **6c**.

Table I.C.4 AFGONs catalyzed four-component synthesis of polyhydroquinolines[a]

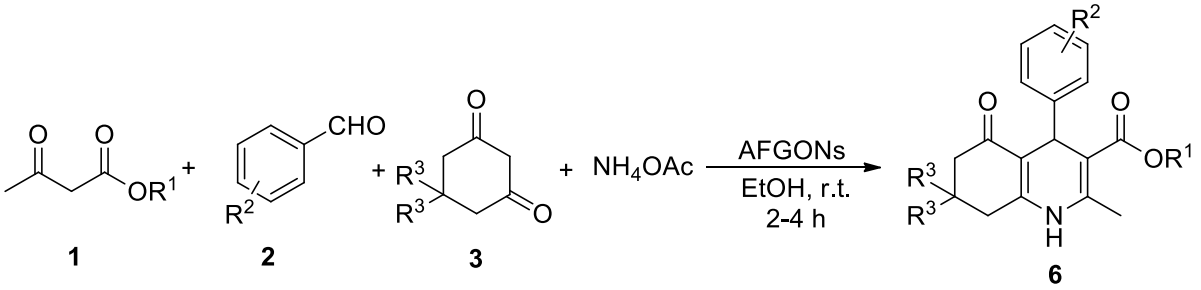

1 2 3 6

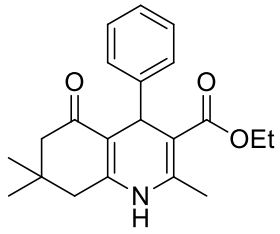

6a, 90%, 2 h

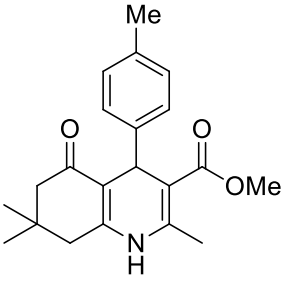

6b, 87%, 4 h

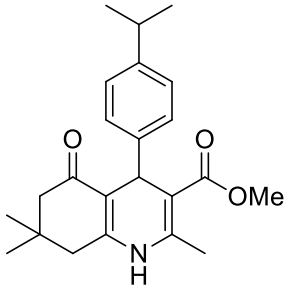

6c, 91%, 3 h

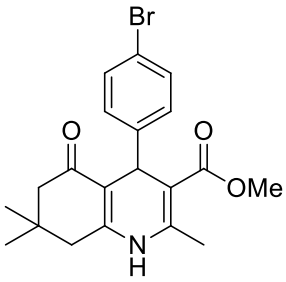

6d, 90%, 2 h

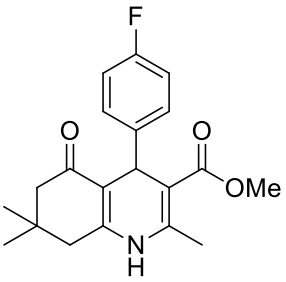

6e, 89%, 4 h

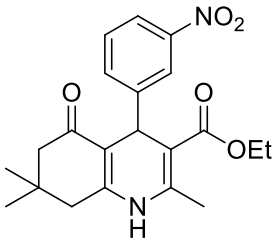

6f, 90%, 2 h

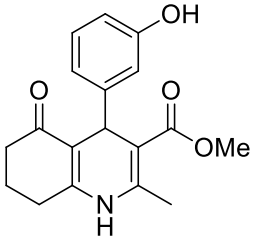

6g, 84%, 4 h

[a]Reaction conditions: **1** (1 mmol), **2** (1 mmol), **3** (1 mmol), NH_4OAc (2 mmol), AFGONs (25 mg) and EtOH (4 mL) were stirred at r.t. for 2-4 h.

I.C.3.7 Gram scale synthesis of 1,4-dihydropyridine (4a)

As an application of the newly developed methodology, we attempted a gram scale synthesis of 1,4-dihydropyridine (**4a**). For this purpose, ethyl acetoacetate (2.6 g, 20 mmol), 4-chlorobenzaldehyde (1.4 g, 10 mmol) and ammonium acetate (1.5 g, 20 mmol) were reacted under the standard reaction conditions using variable amounts of AFGONs (Table I.C.5). The desired product was formed in 84 % (3.05 g) isolated yield using 100 mg of catalyst (Scheme I.C.14). The results showed that proportionate increase of catalyst was not required for the gram scale synthesis.

Table I.C.5 Catalyst optimization in gram scale synthesis of 1,4-dihydropyridine (**4a**)

AFGONs (mg)	250	150	100	75
Isolated yield (%)	87	84	84	64

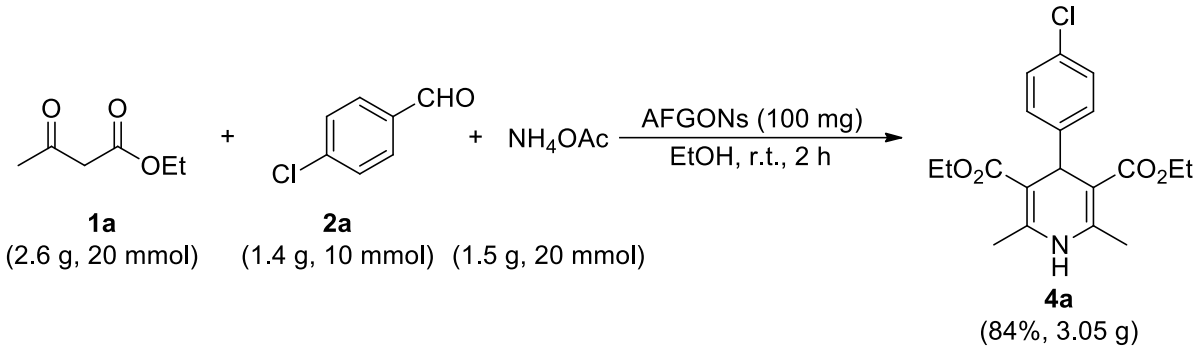

Scheme I.C.14 Gram scale synthesis of 1,4-dihydropyridine (**4a**).

I.C.3.8 Recyclability of AFGONs

We evaluated the reusability of AFGONs in the synthesis of **4a** under the optimized reaction condition. The catalyst was easily recovered from the reaction mixture by simple filtration. It was washed with ethyl acetate (3 x 5 mL) followed by water (5 mL) and was dried under vacuum for 6 h before being used for the next run. The catalyst could be used for five consecutive runs without significant loss in its catalytic activity and product yield (Figure I.C.7). Moreover, the recovered catalyst was characterized by FT-IR (Figure I.C.8 (a)), Raman spectroscopy (Figure I.C.8 (b)), X-ray powder diffraction (Figure I.C.9), SEM (Figure I.C.10) and EDS (Figure I.C.11) analysis and compared with the fresh catalyst. The results did not show any significant change in the spectral data and diffraction patterns of the catalyst before and after catalytic runs.

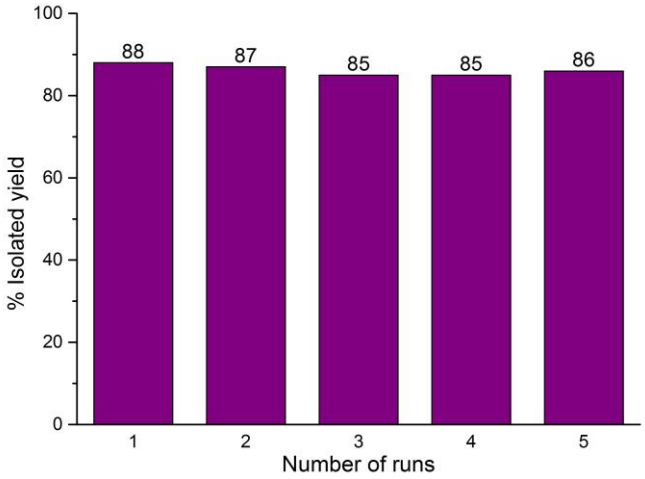

Figure I.C.7 Recyclability of AFGONs in the synthesis of 1,4-dihydropyridines.

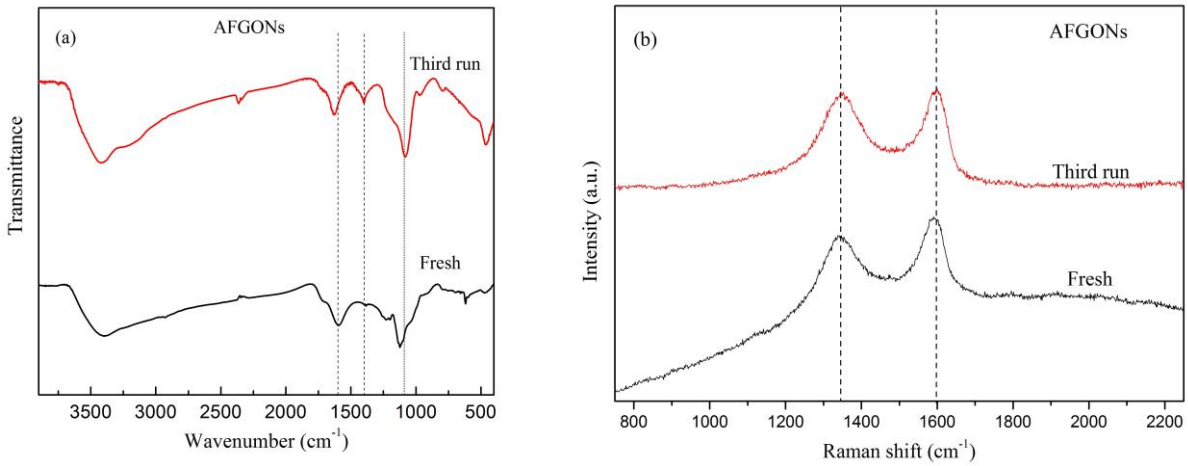

Figure I.C.8 (a) FT-IR and (b) Raman spectra of AFGONs fresh and after the third run.

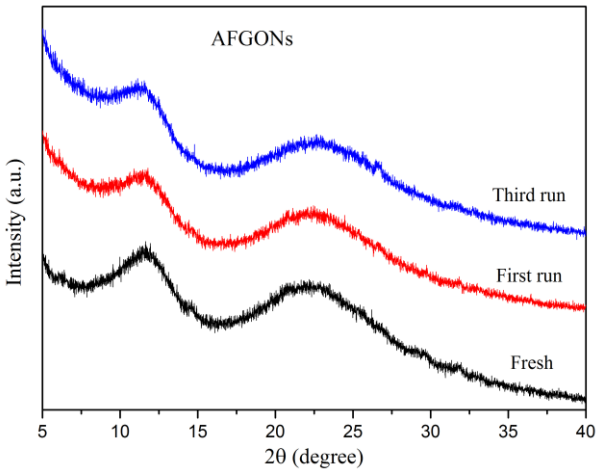

Figure I.C.9 X-ray diffraction patterns of AFGONs fresh, after first and third runs.

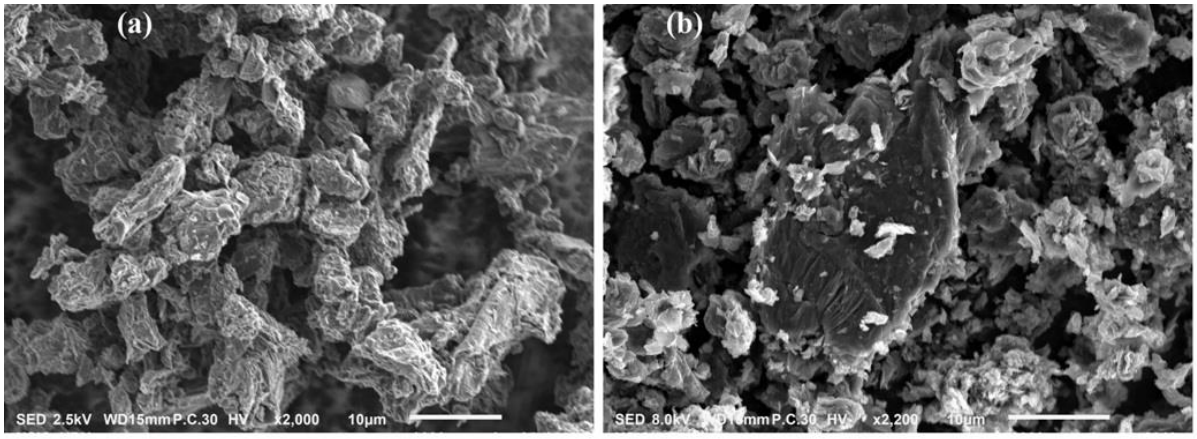

Figure I.C.10 SEM images AFGONs (a) fresh and (b) after the third run.

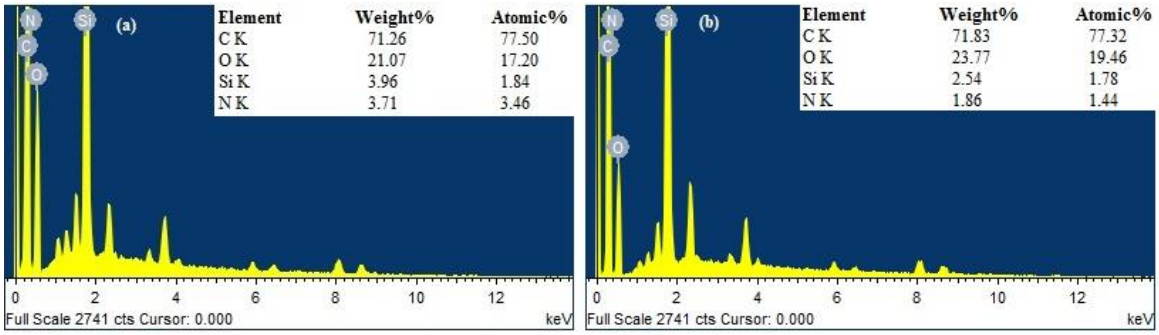

Figure I.C.11 EDS images of AFGONs (a) fresh and (b) third run.

I.C.3.9 Control experiments

The proposed mechanism for the formation of 1,4-DHP involves two key intermediates **7** and **8**, generated respectively by the aldol condensation of one equivalent of ethyl acetoacetate with aldehyde and the reaction of second equivalent of ethyl acetoacetate with ammonia.[38] We set up three control experiments under the optimized reaction conditions (Scheme I.C.14). The first reaction was performed by using ethyl acetoacetate (1 mmol) and 4-chlorobenzaldehyde (1 mmol) and the second reaction using 4-chlorobenzaldehyde (1 mmol) and NH_4OAc (2 mmol). The third reaction was carried out with ethyl acetoacetate (1 mmol) and NH_4OAc (2 mmol). The first and the second reaction did not result in the formation of any new products or intermediates even after 24 h. The HPLC analysis of the third reaction after 1 h indicated the presence of ethyl acetoacetate (31.1%) along with two new intermediates **8** and **9** (23.3% and 45.5% respectively). Although we were not able to isolate these two intermediates (**8** and **9**), it could be enamine (**8**) and bis-enamine (**9**), whose formation from 1,3-diketo ester and amine is reported in literature.[25,62,63] Furthermore, the formation of intermediate **9** was supported by HRMS data.[62] We added 4-chlorobenzaldehyde

in the third reaction after 1 h, which instantly gave the desired product (**4a**), which confirmed that the reaction proceeded through the formation of enamine intermediates. Moreover, the addition of **7** which was prepared by Knoevenagel condensation of ethyl acetoacetate and 4-chlorobenzaldehyde using piperidine,[64] to the third reaction after 1 h did not give **4a**, which further confirmed that the reaction mechanism does not involve intermediate **7**.

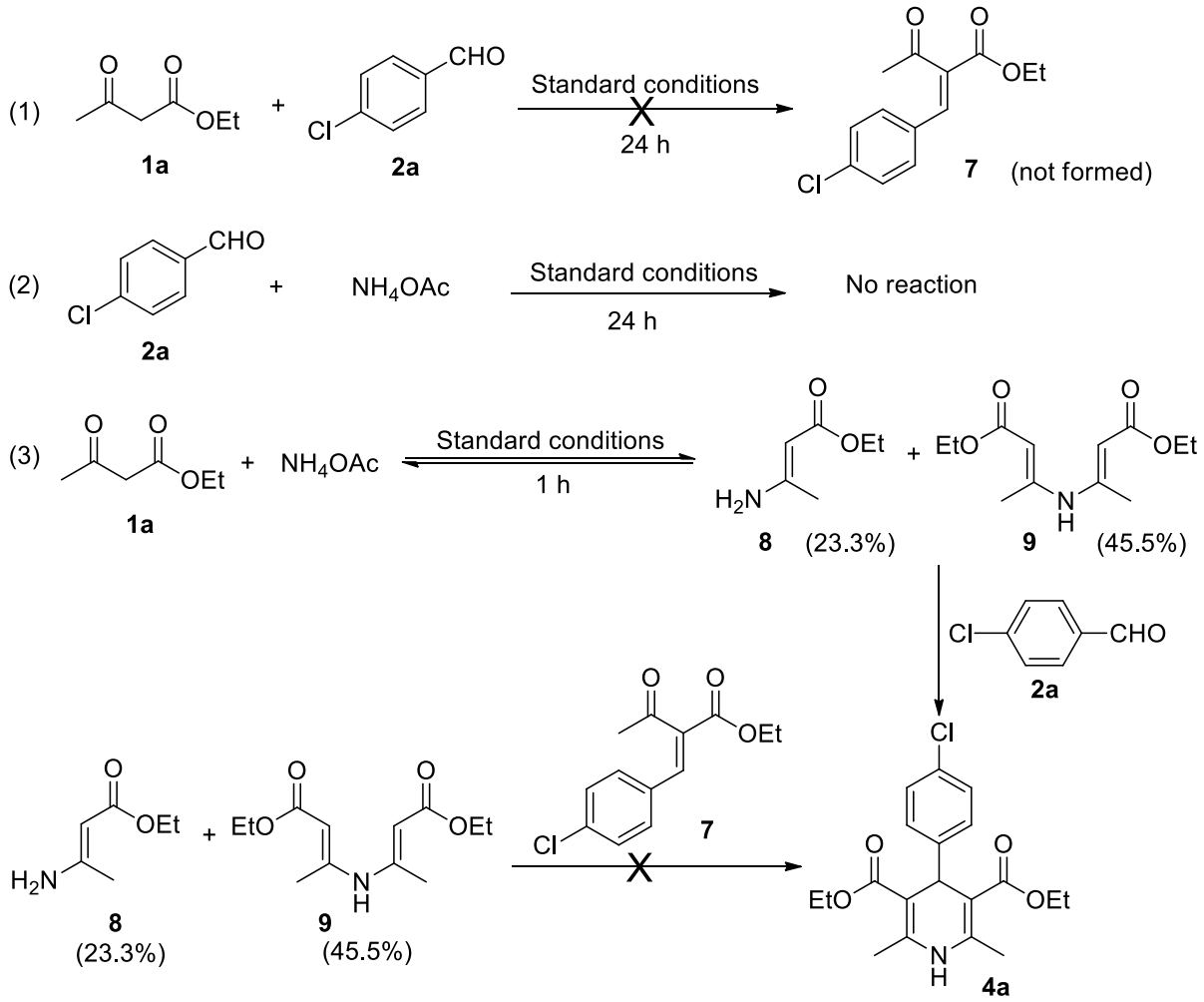

Scheme I.C.15 Control experimental analysis.

I.C.3.10 Plausible mechanism for the synthesis of 1,4-dihydropyridine

On the basis of the results obtained from control experiments, a mechanistic pathway for the 1,4-DHP synthesis was proposed (Scheme I.C.15). The acidic moiety present in the catalyst was involved in the activation of carbonyl groups of both ethyl acetoacetate and the aldehyde. Initially, the bis-enamine intermediate (**9**) was formed by the reaction of two equivalents of ethyl acetoacetate with ammonia generated from ammonium acetate. This was followed by the addition of aldehyde with bis-enamine (**9**) to form intermediate **10**. The basic moiety of the catalyst then abstracted a proton from **10** aiding in the cyclization to intermediate **11**

along with the elimination of one molecule of H_2O. Finally, the abstraction of another proton from **11** resulted in the formation of the desired 1,4-dihydropyridine.

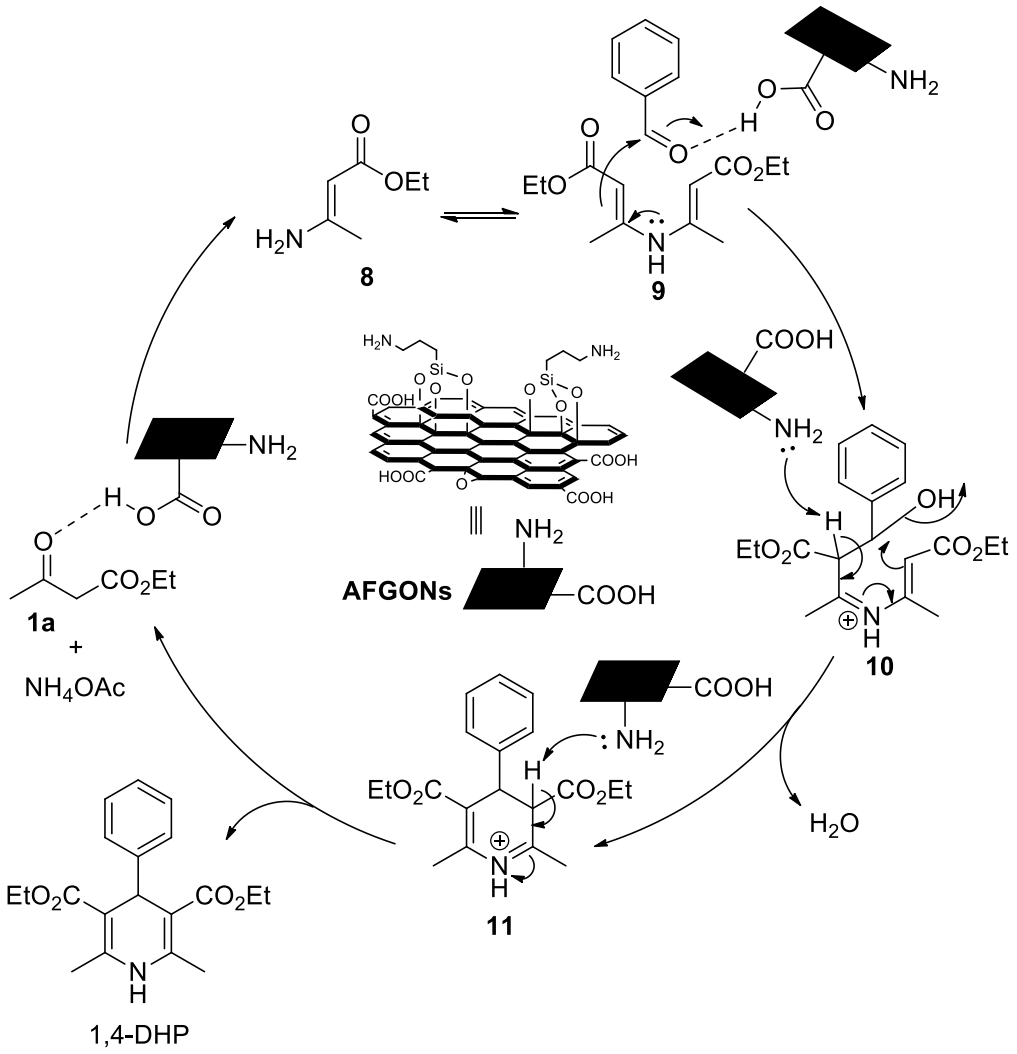

Scheme I.C.16 Plausible mechanism for the synthesis of 1,4-DHPs.

I.C.3.11 Comparison of AFGONs with previously reported catalytic systems

The efficiency of AFGONs was compared with previously reported catalytic systems for the synthesis of 1,4-DHPs (Table I.C.6). The reaction between benzaldehyde, ethyl acetoacetate and ammonium acetate was selected as the model reaction for this purpose. The results confirmed that AFGONs exhibited superior catalytic performance in terms low catalyst loading and ease of purification of products. Besides, room temperature reaction condition was an added advantage of this protocol.

Table I.C.6 Comparison of AFGONs with reported catalyst for the synthesis of 1,4-DHPs

Entry	Catalyst	Reaction conditions	Time	Yield (%)	Reference
1	$HClO_4$-SiO_2 (50 mg)	Solvent free/80 ^oC	20 min	95	65
2	ZrO_2-SO_3H (100 mg)	Solvent free/80 ^oC	12 min	94	66
3	Alginic acid (10 mol%)	EtOH/reflux	50 min	97	67
4	Cellulose sulfuric acid (50 mg)	Solvent free/80 ^oC	5 h	90	31†
5	Sulfated polyborate (5 wt%)	Solvent free/90 ^oC	15 min	95	41
6	Chitosan NPs (100 mg)	Solvent free/80 ^oC	20 min	90	68
7	PPh_3 (20 mol%)	EtOH/reflux	5 h	72	45†
8	$CeCl_3 \cdot 7H_2O$ (10 mol%)	CH_3CN/r.t.	3 h	80	69†
9	PdRuNi@GO (6 mg)	DMF/70 ^oC	45 min	88	36
10	AFGONs (25 mg)	EtOH/r.t.	2 h	90	This work

†Catalyst was not recyclable.

I.C.4 Conclusion

In conclusion, we have developed an eco-friendly route for the selective preparation of Hantzsch pyridines and related heterocyclic biomolecules via a one-pot multicomponent reaction using amine functionalized graphene oxide nanosheets (AFGONs). We have demonstrated that suitable tuning of GO prevented further oxidation of the product (1,4-DHP). Short reaction time, tolerance to wide range of functional groups, reusability of catalyst, green reaction profile and simple product purification procedure are the salient features of this protocol.

I.C.5 Experimental Section

I.C.5.1 General Information

All reagents were purchased from commercial suppliers and used as received. (3-Aminopropyl)triethoxysilane was purchased from TCI, India. The solvents were purchased from commercial suppliers and used after distillation. For TLC, Merck plates coated with silica gel 60, F_{254} were used. FT-IR spectra were recorded in FT-IR 8300 SHIMADZU spectrophotometer. The ^1H & ^{13}C NMR spectra were recorded at 300 MHz and 75 MHz respectively on Bruker AV 300 spectrometer in $CDCl_3$ and DMSO-d_6. Splitting patterns of protons were described as s (singlet), d (doublet), t (triplet), q (quartet), m (multiplet) and br (broad). Chemical shifts (δ) were reported in parts per million (ppm) relative to TMS as

internal standard. *J* values (coupling constant) were reported in Hz (Hertz). ^{13}C NMR spectra were recorded with complete proton decoupling ($CDCl_3$: δ 77.0 ppm and DMSO-d_6: 39.5 ppm). Centrifugation was done in REMI R-8C DX centrifuge. The X-ray diffraction studies (PXRD) were done by the Rigaku SmartLab (9 kW) diffractometer using CuKα radiation. Raman spectra of the samples were obtained with Renishaw InVia micro Raman spectroscopy with 514 nm laser source. Scanning Electron Microscopy (SEM) and Electron Dispersive X-ray Spectroscopy (EDS) were performed using JEOL JSM-IT 100 electron microscope.

I.C.5.2 Preparation of graphene oxide (GO)

Graphene oxide was prepared by following Tour's method.[55] In this method a 9:1 (v/v) mixture of H_2SO_4 / H_3PO_4 (180:20 mL) was added to a mixture of graphite powder (1.5 g) and $KMnO_4$ (9.0 g). The mixture was then stirred at 50 °C for 12 h. After cooling the mixture to room temperature, it was gradually poured into crushed ice (200 g), which was followed by the slow addition of H_2O_2 (30%, 1.5 mL). The solution was then centrifuged (5000 rpm) and the supernatant was discarded. The residual solid material was successively washed with deionised water (100 mL) and then with 30% HCl (100 mL). The solid material was then repeatedly washed with water and centrifuged. Finally, the solid brown material was collected and dried at 60 °C under vacuum to obtain solid graphene oxide.

I.C.5.3 Preparation of AFGONs

AFGONs were prepared by following literature reported method.[54] GO (500 mg) was dispersed in anhydrous toluene (20 mL) and ultrasonically treated for 2 h. After that, (3-aminopropyl)triethoxysilane (0.85 mmol) was added to it and stirred under reflux condition for 12 h. The solvent was evaporated in a vacuum rotary evaporator and the solid powder was washed with dichloromethane and vacuum dried at 60 °C for 12 h.

I.C.5.4 General procedure for the synthesis of 1,4-dihydropyridines (4a-q) using AFGONs

A 25 mL round bottomed flask was charged with β-ketoester (2mmol), aldehyde (1mmol), ammonium acetate (2 mmol) and ethanol (4 mL). This was followed by the addition of AFGONs (25 mg). The reaction mixture was stirred at room temperature until consumption of the reactants (2-4 h) monitored by TLC. After completion of the reaction the solvent was removed under vacuum. The reaction mixture was partitioned between ethyl acetate and water and the catalyst was separated by simple filtration. The combined organic layer was dried over anhydrous sodium sulfate and concentrated under vacuum. The residue obtained was recrystallized using either methanol or ethyl acetate to afford the solid products (**4a-q**).

I.C.5.5 General procedure for the synthesis of 1,8-dioxodecahydroacridines (5a-j) using AFGONs

The same methodology for the synthesis of 1,4-DHPs was followed here replacing β-ketoester with 1,3-diketone (2 mmol).

I.C.5.6 General procedure for the synthesis of polyhydroquinolines (6a-g) using AFGONs

In a 25 mL round bottomed flask, β-ketoester (1 mmol), 1,3-diketone (1 mmol), aldehyde (1 mmol), ammonium acetate (2 mmol) and ethanol (4 mL) were added. This was followed by the addition of the AFGONs (25 mg). The reaction mixture was stirred at room temperature for 2-4 h. After completion of the reaction, monitored by TLC, the solvent was removed under vacuum. The reaction mixture was partitioned between ethyl acetate and water and the catalyst was filtered off. The combined organic layer was dried over anhydrous sodium sulfate and concentrated under vacuum. The residue obtained was recrystallized using a mixture of ethyl acetate and petroleum ether to afford the desired solid products **(6a-g)**.

I.C.5.7 Characterization data of compounds listed in Table I.C.2-I.C.4

Diethyl 4-(4-chlorophenyl)-2,6-dimethyl-1,4-dihydropyridine-3,5-dicarboxylate (4a)[67]

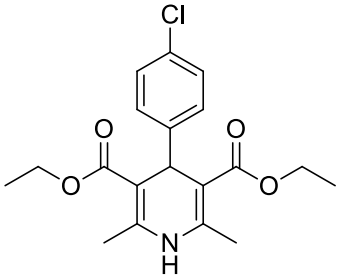

Yellow solid; m.p.: 144–146 °C (Lit. m.p.: 144–145 °C); **^{1}H NMR (300 MHz, $CDCl_3$)**: δ 1.22–1.27 (m, 6H), 2.33 (s, 6H), 4.06–4.18 (m, 4H), 4.98 (s, 1H), 6.03 (s, br, 1H), 7.18–7.30 (m, 4H); **^{13}C NMR (75 MHz, $CDCl_3$)**: δ 14.6, 19.8, 39.5, 60.2, 104.0, 128.2, 129.7, 132.0, 144.6, 146.7, 167.9; HRMS–ESI (*m/z*) calcd for $C_{19}H_{22}ClNO_4$ $[M + H]^+$ 364.1315 found 364.1299.

Dimethyl 4-(2-chlorophenyl)-2,6-dimethyl-1,4-dihydropyridine-3,5-dicarboxylate (4b)[67]

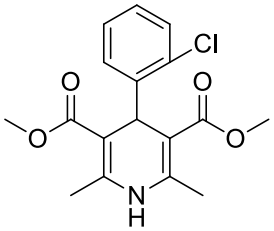

Yellow solid; m.p.: 185–186 °C (Lit. m.p.: 184–185 °C); **^{1}H NMR (300 MHz, $CDCl_3$)**: δ 2.13 (s, 3H), 2.50 (s, 3H), 3.62 (s, 3H), 3.70 (s, 3H), 5.75 (s, br, 1H), 5.96 (s, 1H), 7.20–7.26

(m, 3H), 7.36–7.38 (m, 1H); **^{13}C NMR (75 MHz, $CDCl_3$)**: δ 19.4, 21.3, 50.7, 51.2, 51.5, 103.6, 107.3, 127.1, 129.3, 129.7, 132.3, 137.6, 149.1, 154.6, 166.6, 168.0.

Dimethyl 4-(4-bromophenyl)-2,6-dimethyl-1,4-dihydropyridine-3,5-dicarboxylate (4c)[67]

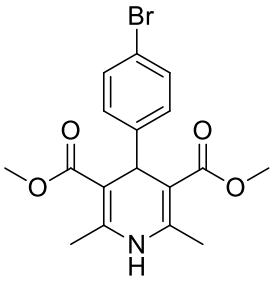

Yellow solid; m.p.: 199–200 °C (Lit. m.p.: 201–202 °C); **^{1}H NMR (300 MHz, $CDCl_3$)**: δ 2.32 (s, 6H), 3.64 (s, 6H), 4.95 (s, 1H), 5.87 (s, br, 1H), 7.14 (d, *J* = 8.4 Hz, 2H), 7.32 (d, *J* = 8.4 Hz, 2H); **^{13}C NMR (75 MHz, $CDCl_3$)**: δ 19.6, 39.0, 51.1, 103.4, 120.0, 129.5, 131.1, 144.5, 146.5, 167.8.

Diethyl 2,6-dimethyl-4-(*p*-tolyl)-1,4-dihydropyridine-3,5-dicarboxylate (4d)[67]

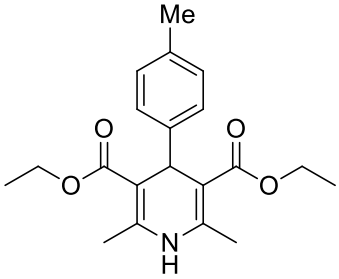

Yellow solid; m.p.: 135–136 °C (Lit. m.p.: 135–137 °C); **^{1}H NMR (300 MHz, $CDCl_3$)**: δ 1.22 (t, *J* = 6.9 Hz, 6H), 2.27–2.34 (m, 9H), 4.04–4.11 (m, 4H), 4.94 (s, 1H), 5.78 (s, br, 1H), 7.01 (d, *J* = 7.8 Hz, 2H), 7.16 (d, *J* = 7.8 Hz, 2H); **^{13}C NMR (75 MHz, $CDCl_3$)**: δ 14.2, 19.5, 21.0, 39.0, 59.6, 104.1, 127.7, 128.0, 128.5, 135.4, 143.8, 144.8, 167.6.

Diethyl 4-(4-methoxyphenyl)-2,6-dimethyl-1,4-dihydropyridine-3,5-dicarboxylate (4e)[67]

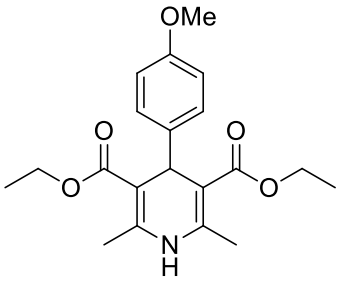

Yellow solid; m.p.: 160–161 °C (Lit. m.p.: 160–161 °C); **^{1}H NMR (300 MHz, $CDCl_3$)**: δ 1.20–1.28 (m, 6H), 2.31–2.34 (m, 6H), 3.76 (s, 3H), 4.06–4.17 (m, 4H), 4.96 (s, 1H), 5.85 (s, br, 1H), 6.78 (d, *J* = 8.7 Hz, 2H), 7.22 (d, *J* = 8.7 Hz, 2H); **^{13}C NMR (75 MHz, $CDCl_3$)**: δ 14.5, 19.8, 39.0, 55.4, 60.0, 104.5, 113.4, 129.2, 140.6, 144.0, 158.1, 168.0.

Diethyl 4-(4-hydroxyphenyl)-2,6-dimethyl-1,4-dihydropyridine-3,5-dicarboxylate (4f)[67]

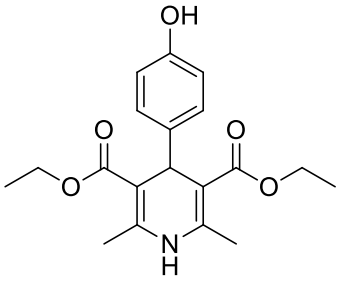

Pale yellow solid; m.p.: 229-230 °C (Lit. m.p.: 228–231 °C); **^{1}H NMR (300 MHz, DMSO–d_6)**: δ 1.12 (t, *J* = 6.6 Hz, 6H), 2.23 (s, 6H), 3.95–3.99 (m, 4H), 4.73 (s, 1H), 6.57 (d, *J* = 7.8 Hz, 2H), 6.92 (d, *J* = 7.8 Hz, 2H), 8.71 (s, br, 1H), 9.09 (s, br, 1H); **^{13}C NMR (75 MHz, DMSO–d_6)**: δ 14.1, 18.1, 37.8, 58.8, 102.2, 114.4, 128.2, 138.8, 144.6, 155.3, 167.0.

Diethyl 4-(4-dimethylaminophenyl)-2,6-dimethyl-1,4-dihydropyridine-3,5-dicarboxylate (4g)[70]

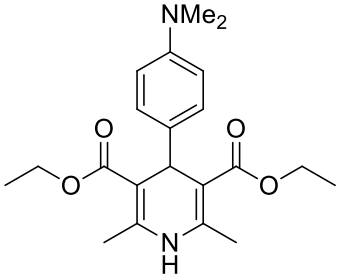

Pale yellow solid; m.p.: 158–161 °C (Lit. m.p.:158–162 °C); **^{1}H NMR (300 MHz, $CDCl_3$)**: δ 1.23 (t, *J* = 7.2 Hz, 6H), 2.32 (s, 6H), 2.88 (s, 6H), 4.08 (q, *J* = 6.9 Hz, 4H), 4.88 (s, 1H), 5.56 (s, 1H), 6.60 (d, *J* = 7.8 Hz, 2H), 7.14 (d, *J* = 8.4 Hz, 2H); **^{13}C NMR (75 MHz, $CDCl_3$)**: δ 14.3, 19.6, 38.3, 40.7, 59.6, 104.5, 112.3, 128.5, 136.4, 143.3, 149.1, 167.8.

Diethyl 2,6-dimethyl-4-phenyl-1,4-dihydropyridine-3,5-dicarboxylate (4h)[67]

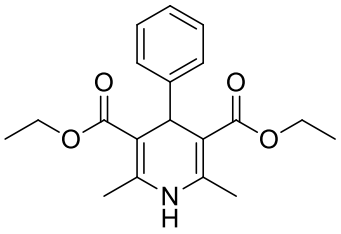

Yellow solid; m.p.: 156–158 °C (Lit. m.p.: 156–158 °C); **^{1}H NMR (300 MHz, $CDCl_3$)**: δ 1.21 (t, *J* = 7.2 Hz, 6H), 2.31 (s, 6H), 4.04–4.13 (m, 4H), 4.98 (s, 1H), 5.91 (s, br, 1H), 7.11–7.29 (m, 5H); **^{13}C NMR (75 MHz, $CDCl_3$)**: δ 14.6, 19.8, 39.9, 60.1, 104.3, 126.4, 128.1, 128.3, 144.4, 148.1, 168.1.

Diethyl 4-(4-fluorophenyl)-2,6-dimethyl-1,4-dihydropyridine-3,5-dicarboxylate (4i)[67]

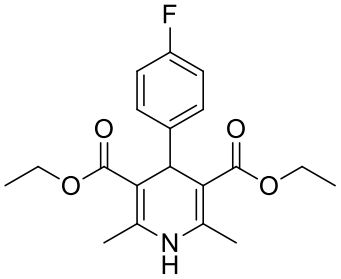

Yellow solid; m.p.: 152–153 °C (Lit. m.p.: 151–153 °C); **^{1}H NMR (300 MHz, $CDCl_3$)**: δ 1.21 (t, *J* = 7.2 Hz, 6H), 2.31 (s, 6H), 4.04–4.14 (m, 4H), 4.96 (s, 1H), 5.94 (s, br, 1H), 6.85–6.91 (m, 2H), 7.21–7.27 (m, 2H); **^{13}C NMR (75 MHz, $CDCl_3$)**: δ 14.1, 19.4, 38.9, 59.7, 103.9, 114.4 (d, *J* = 20.8 Hz), 129.3 (d, *J* = 7.7 Hz), 143.8 (d, *J* = 28.2 Hz), 159.6, 162.8, 167.5.

Diethyl 2,6-dimethyl-4-(4-nitrophenyl)-1,4-dihydropyridine-3,5-dicarboxylate (4j)[67]

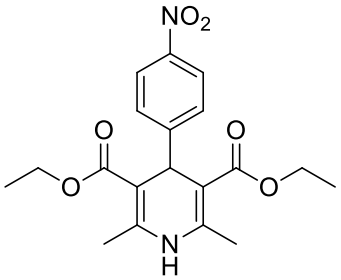

Yellow crystalline solid; m.p.: 125–126 °C (Lit. m.p.: 125–127 °C); **^{1}H NMR (300 MHz, $CDCl_3$)**: δ 1.22 (t, *J* = 6.9 Hz, 6H), 2.34 (s, 6H), 4.09 (d, *J* = 7.2 Hz, 4H), 5.01 (s, 1H), 6.16 (s, br, 1H), 7.46 (d, *J* = 8.1 Hz, 2H), 8.08 (d, *J* = 8.1 Hz, 2H); **^{13}C NMR (75 MHz, $CDCl_3$)**: δ 14.1, 19.4, 40.0, 59.9, 102.9, 123.2, 128.8, 144.8, 146.1, 155.1, 167.1.

Diethyl 2,6-dimethyl-4-(3-nitrophenyl)-1,4-dihydropyridine-3,5-dicarboxylate (4k)[67]

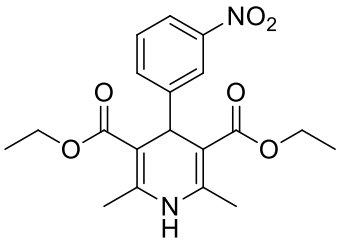

Yellow crystalline solid; m.p.: 165–166 °C (Lit. m.p.: 166–168 °C); **^{1}H NMR (300 MHz, $CDCl_3$)**: δ 1.22 (t, *J* = 7.2 Hz, 6H), 2.35 (s, 6H), 4.03–4.14 (m, 4H), 5.09 (s, 1H), 6.15 (s, br, 1H), 7.38 (t, *J* = 7.8 Hz, 1H), 7.65 (d, *J* = 7.8 Hz, 1H), 7.98–8.02 (m, 1H), 8.13 (t, *J* = 2.1 Hz, 1H); **^{13}C NMR (75 MHz, $CDCl_3$)**: δ 14.2, 19.5, 39.9, 60.0, 103.1, 121.3, 123.1, 128.6, 134.5, 145.0, 148.1, 150.0, 167.2.

Diethyl 2,6-dimethyl-4-(naphthalen-2-yl)-1,4-dihydropyridine-3,5-dicarboxylate (4l)[69]

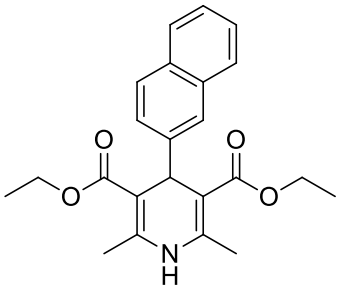

Yellow crystalline solid; m.p.: 192–193 °C (Lit. m.p.: 196 °C); **^{1}H NMR (300 MHz, $CDCl_3$)**: δ 1.21 (t, *J* = 7.2 Hz, 6H), 2.31 (s, 3H), 4.06 (q, *J* = 7.2 Hz, 4H), 5.16 (s, 1H), 6.08 (s, br, 1H), 7.36–7.49 (m, 3H), 7.66–7.75 (m, 4H); **^{13}C NMR (75 MHz, $CDCl_3$)**: δ 14.1, 19.4, 39.8, 59.7, 103.7, 125.0, 125.4, 126.1, 127.0, 127.3, 127.7, 132.1, 133.2, 144.1, 145.1, 167.7.

Dimethyl 2,6-dimethyl-4-styryl-1,4-dihydropyridine-3,5-dicarboxylate (4m)[67]

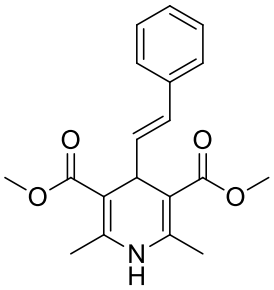

Yellow crystalline solid; m.p.: 172–174 °C (Lit. m.p.: 174–175 °C); **^{1}H NMR (300 MHz, $CDCl_3$)**: δ 2.33 (s, 6H), 3.72 (s, 6H), 4.61 (d, *J* = 4.2 Hz, 1H), 5.86 (s, br, 1H), 6.17 (d, *J* = 5.4 Hz, 2H), 7.09-7.20 (m, 1H), 7.23-7.33 (m, 4H); **^{13}C NMR (75 MHz, $CDCl_3$)**: δ 19.5, 36.1, 51.2, 101.2, 126.2, 126.9, 127.9, 128.4, 131.6, 137.6, 145.3, 168.0.

Diethyl 2,6-dimethyl-1,4-dihydropyridine-3,5-dicarboxylate (4n)[67]

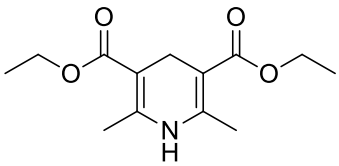

Yellow crystalline solid; m.p.: 177–179 °C (Lit. m.p.: 177–180 °C); **^{1}H NMR (300 MHz, $CDCl_3$)**: δ 1.28 (t, *J* = 8.1 Hz, 6H), 2.19 (s, 6H), 3.26 (s, 2H), 4.13–4.20 (m, 4H), 5.30 (s, br, 1H); **^{13}C NMR (75 MHz, $CDCl_3$)**: δ 14.4, 19.1, 24.7, 59.6, 99.4, 144.8, 168.0.

Dimethyl 4-cyclohexyl-2,6-dimethyl-1,4-dihydropyridine-3,5-dicarboxylate (4o)[37]

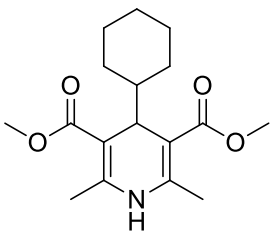

White solid; m.p.: 182–185 °C (Lit. m.p.: 184–185 °C); **^{1}H NMR (300 MHz, $CDCl_3$)**: δ 0.86–0.93 (m, 2H), 1.04–1.24 (m, 4H), 1.50–1.63 (m, 5H), 2.31 (s, 6H), 3.71 (s, 6H), 3.88 (d, *J* = 5.7 Hz, 1H), 5.93 (s, br, 1H); **^{13}C NMR (75 MHz, $CDCl_3$)**: δ 19.2, 26.5, 28.5, 38.2, 45.5, 50.8, 101.3, 144.9, 169.1.

Diethyl 4-(furan-2-yl)-2,6-dimethyl-1,4-dihydropyridine-3,5-dicarboxylate (4p)[67]

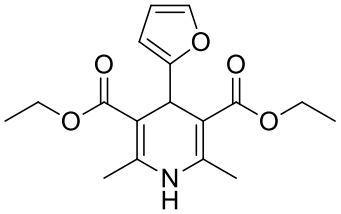

Brown solid; m.p.: 159–161 °C (Lit. m.p.: 160–161 °C); **^{1}H NMR (300 MHz, $CDCl_3$)**: δ 1.262 (t, *J* = 7.2 Hz, 6H), 2.32 (s, 6H), 4.07–4.21 (m, 4H), 5.19 (s, 1H), 5.93–6.02 (m, 2H), 6.20 (s, br, 1H), 7.20 (s, 1H); **^{13}C NMR (75 MHz, $CDCl_3$)**: δ 14.3, 19.4, 33.3, 59.8, 100.6, 104.4, 110.0, 140.8, 145.2, 158.6, 167.5.

Dimethyl 4-(5-bromothiophen-2-yl)-2,6-dimethyl-1,4-dihydropyridine-3,5-dicarboxylate (4q)[63]

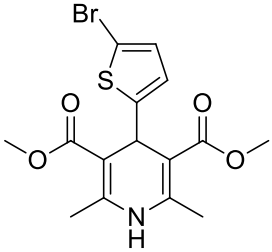

White solid; m.p.: 149–152 °C (Lit. m.p.: 150–154 °C); **^{1}H NMR (300 MHz, DMSO–d_6)**: δ 2.27 (s, 6H), 3.62 (s, 6H), 5.08 (s, 1H), 6.47 (d, *J* = 3.3 Hz, 1H), 6.93 (d, *J* = 3.6 Hz, 1H), 9.16 (s, br, 1H); **^{13}C NMR (75 MHz, DMSO–d_6)**: δ 18.5, 34.6, 51.3, 100.7, 108.9, 123.6, 130.2, 147.2, 153.8, 167.3.

3,3,6,6-Tetramethyl-9-phenyl-3,4,6,7,9,10-hexahydroacridine-1,8(2*H*,5*H*)-dione (5a)[46]

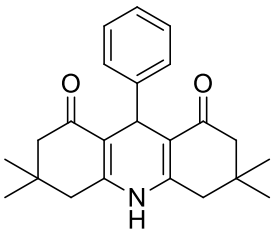

Yellow solid; m.p.: >220 °C (Lit. m.p.: 272 °C); **^{1}H NMR (300 MHz, $CDCl_3$)**: δ 0.95 (s, 6H), 1.07 (s, 6H), 2.08–2.35 (m, 8H), 5.08 (s, 1H), 7.068 (t, *J* = 6.9 Hz, 1H), 7.19 (t, *J* = 7.2 Hz, 2H), 7.33 (d, *J* = 6.9 Hz, 3H); **^{13}C NMR (75 MHz, $CDCl_3$)**: δ 27.1, 29.5, 32.6, 33.5, 40.8, 50.7, 113.4, 125.9, 127.9, 146.4, 148.4, 195.7.

9-(4-Chlorophenyl)-3,3,6,6-tetramethyl-3,4,6,7,9,10-hexahydroacridine-1,8(2*H*,5*H*)-dione (5b)[46]

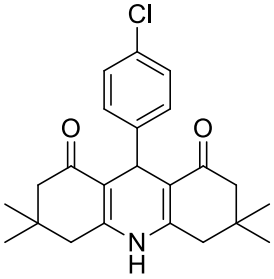

Yellow solid; m.p.: >220 °C (Lit. m.p.: 302–303 °C); **^{1}H NMR (300 MHz, $CDCl_3$)**: δ 0.93 (s, 6H), 1.05 (s, 6H), 2.03–2.28 (m, 8H), 5.05 (s, 1H), 7.15 (d, *J* = 8.4 Hz, 2H), 7.27 (d, *J* = 8.7 Hz, 2H), 8.58 (s, br, 1H); **^{13}C NMR (75 MHz, $CDCl_3$)**: δ 27.0, 29.5, 32.5, 33.3, 40.5, 50.8, 112.6, 128.0, 129.4, 131.5, 145.3, 149.8, 196.2.

9-(4-Bromophenyl)-3,3,6,6-tetramethyl-3,4,6,7,9,10-hexahydroacridine-1,8(2*H*,5*H*)-dione (5c)[46]

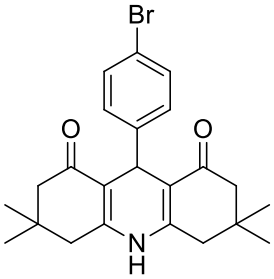

Yellow crystalline solid; m.p.: >220 °C (Lit. m.p.: >300 °C); **^{1}H NMR (300 MHz, $CDCl_3$)**: δ 0.95 (s, 6H), 1.07 (s, 6H), 2.12–2.35 (m, 8H), 5.03 (s, 1H), 7.22 (d, *J* = 8.4 Hz, 2H), 7.31 (d, *J* = 8.1 Hz, 2H), 7.43 (s, br, 1H); **^{13}C NMR (75 MHz, $CDCl_3$)**: δ 27.1, 29.5, 32.6, 33.4, 40.8, 50.7, 113.0, 119.7, 129.8, 131.0, 145.5, 148.7, 195.7.

9-(4-Fluorophenyl)-3,3,6,6-tetramethyl-3,4,6,7,9,10-hexahydroacridine-1,8(2*H*,5*H*)-dione (5d)[46]

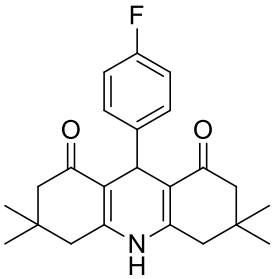

Yellow solid; m.p.: > 220 °C (Lit. m.p.: 246–248 °C); **^{1}H NMR (300 MHz, $CDCl_3$)**: δ 0.95 (s, 6H), 1.07 (s, 6H), 2.12–2.35 (m, 8H), 5.06 (s, 1H), 6.87 (t, *J* = 8.7 Hz, 2H), 7.26–7.32 (m, 2H), 7.47 (s, br, 1H); **^{13}C NMR (75 MHz, $CDCl_3$)**: δ 27.0, 29.5, 32.8 (d, *J* = 28.5 Hz), 40.8, 50.7, 113.3, 114.7 (d, *J* = 21.0 Hz), 129.4 (d, *J* = 8.2 Hz), 142.4, 148.6, 195.3.

3,3,6,6-Tetramethyl-9-(4-nitrophenyl)-3,4,6,7,9,10-hexahydroacridine-1,8(2*H*,5*H*)-dione (5e)[46]

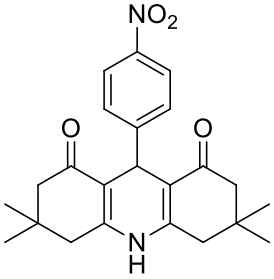

Yellow crystalline solid; m.p.: >220 °C (Lit. m.p.: 268–270 °C); **^{1}H NMR (300 MHz, $CDCl_3$)**: δ 1.12 (s, 6H), 1.24 (s, 6H), 2.30–2.52 (m, 8H), 5.54 (s, 1H), 7.25 (d, *J* = 8.4 Hz, 2H), 8.13 (d, *J* = 8.7 Hz, 2H), 11.81 (s, br, 1H); **^{13}C NMR (75 MHz, $CDCl_3$)**: δ 27.4, 29.4, 31.2, 31.4, 33.2, 46.3, 47.0, 114.8, 123.4, 127.5, 146.1, 146.5, 189.5, 190.8.

3,3,6,6-Tetramethyl-9-(3-nitrophenyl)-3,4,6,7,9,10-hexahydroacridine-1,8(2*H*,5*H*)-dione (5f)[46]

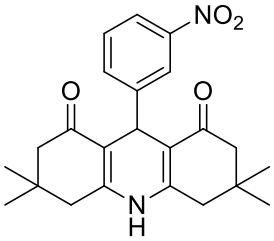

Yellow solid; m.p.: >220 °C (Lit. m.p.: 298–300 °C); **^{1}H NMR (300 MHz, $CDCl_3$)**: δ 0.97 (s, 6H), 1.10 (s, 6H), 2.13–2.45 (m, 8H), 5.17 (s, 1H), 6.41 (s, br, 1H), 7.39 (t, *J* = 7.8 Hz, 1H), 7.86–8.05 (m, 3H); **^{13}C NMR (75 MHz, $CDCl_3$)**: δ 27.1, 29.4, 32.7, 34.0, 41.2, 50.6, 112.9, 121.2, 122.2, 128.6, 135.5, 147.9, 148.1, 148.4, 195.1, 195.3; HRMS–ESI (*m/z*) calcd for $C_{23}H_{26}N_2O_4$ $[M + H]^+$ 395.1971 found 395.1978.

9-(3-Nitrophenyl)-3,4,6,7,9,10-hexahydroacridine-1,8(2*H*,5*H*)-dione (5g)[71]

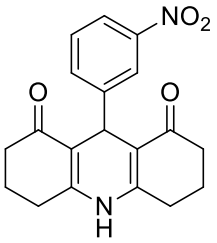

Yellow solid; m.p.: >220 °C (Lit. m.p.: 280–282 °C); **^{1}H NMR (300 MHz, DMSO–d_6)**: δ 1.04–1.90 (m, 5H), 1.95–2.19 (m, 5H), 2.23–2.43 (m, 2H), 3.86–3.95 (m, 1H), 6.95 (d, *J* = 9.6 Hz, 1H), 7.32–7.44 (m, 1H), 7.56–7.63 (m, 1H), 7.82–7.90 (m, 2H); **^{13}C NMR (75 MHz, DMSO–d_6)**: δ 20.1, 20.7, 29.1, 33.3, 37.0, 59.8, 58.9, 100.5, 101.6, 115.2, 123.5, 129.1, 147.9, 169.0, 196.1, 205.5.

9-(2-Hydroxyphenyl)-3,3,6,6-tetramethyl-3,4,6,7,9,10-hexahydroacridine-1,8(2*H*,5*H*)-dione (5h)[72]

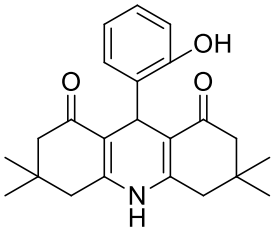

Yellow solid; m.p.: 218–219 °C (Lit. m.p.: 219–222 °C); **^{1}H NMR (300 MHz, CDCl$_3$)**: δ 0.98–1.02 (m, 8H), 1.12 (s, 3H), 1.26 (t, *J* = 7.2 Hz, 1H), (s, 3H), 2.32 (s, 3H), 2.44–2.62 (m, 2H), 4.08–4.15 (m, 1H), 4.68 (s, 1H), 7.00–7.02 (m, 3H), 7.12–7.27 (m, 1H); **^{13}C NMR (75 MHz, CDCl$_3$)**: δ 14.1, 27.1, 27.7, 29.1, 30.0, 32.2, 41.5, 49.9, 60.3, 111.0, 115.7, 118.3, 124.5, 127.4, 128.0, 151.0, 169.0, 200.7.

9-(4-Methoxyphenyl)-3,3,6,6-tetramethyl-3,4,6,7,9,10-hexahydroacridine-1,8(2*H*,5*H*)-dione (5i)[46]

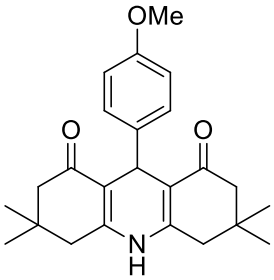

Yellow solid; m.p.: >220 °C (Lit. m.p.: >300 °C); **^{1}H NMR (300 MHz, CDCl$_3$)**: δ 1.09 (s, 5H), 1.22 (s, 7H), 2.40 (s, 8H), 3.76 (s, 3H), 5.48 (s, 1H), 6.80 (d, *J* = 7.5 Hz, 2H), 7.00 (d, *J* = 7.5 Hz), 11.91 (s, br, 1H); **^{13}C NMR (75 MHz, CDCl$_3$)**: δ 14.1, 21.0, 22.5, 27.1, 29.5, 32.5, 40.7, 50.8, 55.0, 60.3, 113.3, 128.9, 139.1, 148.7, 157.6, 171.1, 195.9.

9-(4-Hydroxyphenyl)-3,3,6,6-tetramethyl-3,4,6,7,9,10-hexahydroacridine-1,8(2*H*,5*H*)-dione (5j)[46]

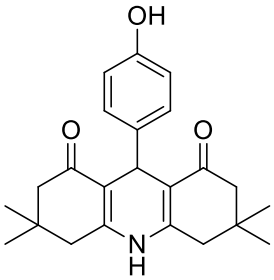

White solid; m.p.: >220 °C (Lit. m.p.: >300 °C); **^{1}H NMR (300 MHz, CDCl$_3$)**: δ 0.91 (s, 6H), 1.21 (s, 6H), 5.47 (s, 1H), 6.65 (d, *J* = 6.9 Hz, 2H), 6.90 (d, *J* = 7.2 Hz, 2H), 11.88 (s, br, 1H); **^{13}C NMR (75 MHz, CDCl$_3$)**: δ 27.3, 29.4, 31.4, 31.9, 115.2, 115.8, 127.8, 129.2, 153.9, 189.6, 190.6.

Ethyl 2,7,7-trimethyl-5-oxo-4-phenyl-1,4,5,6,7,8-hexahydroquinoline-3-carboxylate (6a)[43]

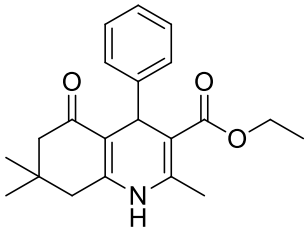

White solid; m.p.: 186–187 °C (Lit. m.p.: 186–188 °C); **^{1}H NMR (300 MHz, $CDCl_3$)**: δ 0.92 (s, 3H), 1.05 (s, 3H), 1.20 (t, *J* = 7.2 Hz, 3H), 2.15–2.25 (m, 4H), 2.31 (s, 3H), 4.06 (q, *J* = 7.2 Hz, 2H), 5.04 (s, 1H), 7.06–7.11 (m, 2H), 7.19 (t, *J* = 7.5 Hz, 2H), 7.30 (d, *J* = 7.2 Hz, 2H); **^{13}C NMR (75 MHz, $CDCl_3$)**: δ 14.2, 19.2, 27.1, 29.5, 32.6, 36.6, 40.7, 50.7, 59.8, 105.8, 111.7, 126.0, 127.8, 128.0, 144.0, 147.2, 149.3, 167.6, 195.9.

Methyl 2,7,7-trimethyl-5-oxo-4-(*p*-tolyl)-1,4,5,6,7,8-hexahydroquinoline-3-carboxylate (6b)[43]

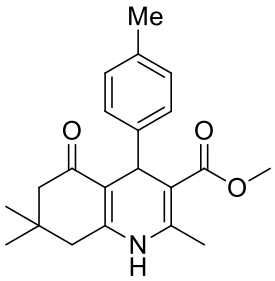

Yellow solid; m.p.: >220 °C (Lit. m.p.: 272–273 °C); **^{1}H NMR (300 MHz, $CDCl_3$)**: δ 0.94 (s, 3H), 1.07 (s, 3H), 2.18–2.23 (m, 3H), 2.25–2.31 (m, 4H), 2.37 (s, 3H), 3.61 (s, 3H), 5.02 (s, 1H), 5.84 (s, br, 1H), 7.01 (d, *J* = 7.5 Hz, 2H), 7.1 (d, *J* = 8.1 Hz, 2H); **^{13}C NMR (75 MHz, $CDCl_3$)**: δ 19.5, 21.0, 27.2, 29.4, 32.7, 35.7, 41.2, 50.7, 51.0, 105.9, 112.5, 127.6, 128.7, 135.4, 143.4, 143.8, 147.6, 167.9, 195.4.

Methyl 4-(4-isopropylphenyl)-2,7,7-trimethyl-5-oxo-1,4,5,6,7,8-hexahydroquinoline-3-carboxylate (6c)

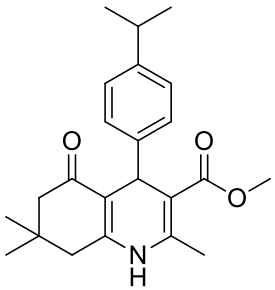

Yellow crystalline solid; m.p.: 209–213 °C; **^{1}H NMR (300 MHz, $CDCl_3$)**: δ 0.95 (s, 3H), 1.06 (s, 3H), 1.17 (d, *J* = 6.9 Hz, 6H), 2.13–2.21 (m, 2H), 2.28–2.36 (m, 5H), 2.75–2.84 (m, 1H), 3.61 (s, 3H), 5.03 (s, 1H), 7.03 (d, *J* = 8.1 Hz, 3H), 7.19 (d, *J* = 8.1 Hz, 2H); **^{13}C NMR**

(75 MHz, $CDCl_3$): δ 19.2, 23.9, 27.3, 29.4, 32.7, 33.5, 35.7, 40.8, 50.8, 51.0, 105.7, 111.8, 126.0, 127.5, 144.1, 144.3, 146.3, 149.3, 168.1, 196.0; HRMS–ESI (*m/z*) calcd for $C_{23}H_{29}NO_3$ $[M + H]^+$ 368.2225 found 368.2231.

Methyl 4-(4-bromophenyl)-2,7,7-trimethyl-5-oxo-1,4,5,6,7,8-hexahydroquinoline-3-carboxylate (6d)[43]

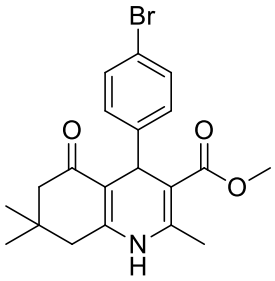

Yellow crystalline solid; m.p.: >220 °C (Lit. m.p.: 263–265 °C); **^{1}H NMR (300 MHz, $CDCl_3$)**: δ 0.93 (s, 3H), 1.08 (s, 3H), 2.13–2.39 (m, 7H), 3.62 (s, 3H), 5.03 (s, 1H), 6.21 (s, br, 1H), 7.19 (d, *J* = 8.4 Hz, 2H), 7.33 (d, *J* = 8.4 Hz, 2H); **^{13}C NMR (75 MHz, $CDCl_3$)**: δ 19.4, 27.1, 29.4, 32.7, 36.0, 41.1, 50.6, 51.0, 105.3, 111.8, 119.8, 129.6, 131.0, 143.9, 145.8, 148.1, 167.6, 195.4.

Methyl 4-(4-fluorophenyl)-2,7,7-trimethyl-5-oxo-1,4,5,6,7,8-hexahydroquinoline-3-carboxylate (6e)[73]

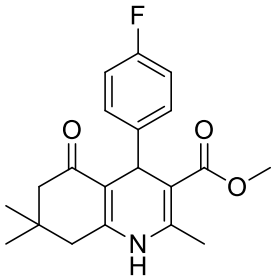

Yellow solid; m.p.: >220 °C (Lit. m.p.: 235–238 °C); **^{1}H NMR (300 MHz, DMSO–d_6)**: δ 0.81 (s, 3H), 0.99 (s, 3H), 2.00-2.49 (m, 7H), 3.51 (s, 3H), 4.85 (s, 1H), 7.00 (t, *J* = 8.7 Hz, 2H), 7.12–7.17 (m, 2H), 9.14 (s, br, 1H); **^{13}C NMR (75 MHz, DMSO–d_6)**: δ 18.2, 26.3, 29.0, 32.1, 35.0, 50.1, 50.6, 103.0, 109.8, 114.4 (d, *J* = 20.7 Hz), 117.6, 128.9 (d, *J* = 7.7 Hz), 143.6, 145.5, 149.5, 167.1, 194.3; HRMS–ESI (*m/z*) calcd for $C_{20}H_{22}FNO_3$ $[M + H]^+$ 344.1662 found 344.1672.

Methyl 2,7,7-trimethyl-4-(3-nitrophenyl)-5-oxo-1,4,5,6,7,8-hexahydroquinoline-3-carboxylate (6f)[43]

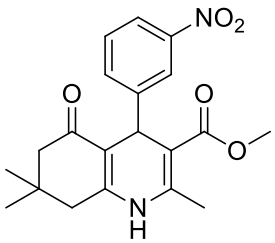

Yellow solid; m.p.: 174–176 °C (Lit. m.p.: 175–176 °C); **^{1}H NMR (300 MHz, $CDCl_3$)**: δ 0.93 (s, 3H), 1.08 (s, 3H), 1.20 (t, *J* = 7.2 Hz, 3H), 2.06–2.42 (m, 7H), 4.07 (q, *J* = 7.2 Hz, 2H), 5.16 (s, 1H), 6.91 (s, br, 1H), 7.38 (t, *J* = 7.8 Hz, 1H), 7.72 (d, *J* = 7.8 Hz, 1H), 7.98 (d, *J* = 8.1 Hz, 1H), 8.13 (s, 1H); **^{13}C NMR (75 MHz, $CDCl_3$)**: δ 14.1, 19.3, 27.0, 29.3, 32.7, 37.0, 40.7, 50.5, 60.0, 104.9, 111.0, 121.2, 122.8, 134.7, 144.7, 148.1, 149.2, 149.4, 167.0, 195.7.

Methyl 4-(3-hydroxyphenyl)-2-methyl-5-oxo-1,4,5,6,7,8-hexahydroquinoline-3-carboxylate (6g)

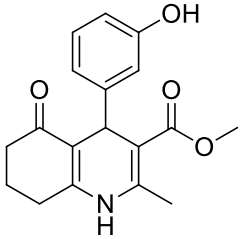

Yellow solid; m.p.: 218–220 °C; **^{1}H NMR (300 MHz, DMSO–d_6)**: δ 1.78–1.98 (m, 3H), 2.20 (s, 3H), 2.24–2.27 (m, 3H), 3.61 (s, 3H), 4.85 (s, 1H), 6.42–6.47 (m, 1H), 6.55–6.58 (m, 2H), 6.89–7.08 (m, 1H), 9.08–9.16 (m, 1H), 9.43 (s, br, 1H); **^{13}C NMR (75 MHz, DMSO–d_6)**: δ 21.2, 26.8, 35.5, 37.2, 51.1, 103.6, 111.5, 112.9, 114.7, 118.3, 129.0, 129.1, 145.4, 149.3, 151.6, 157.4, 167.9, 195.1.

I.C.5.8 Scanned copies of ^{1}H, ^{13}C NMR and HRMS spectra of a representative compound (6c)

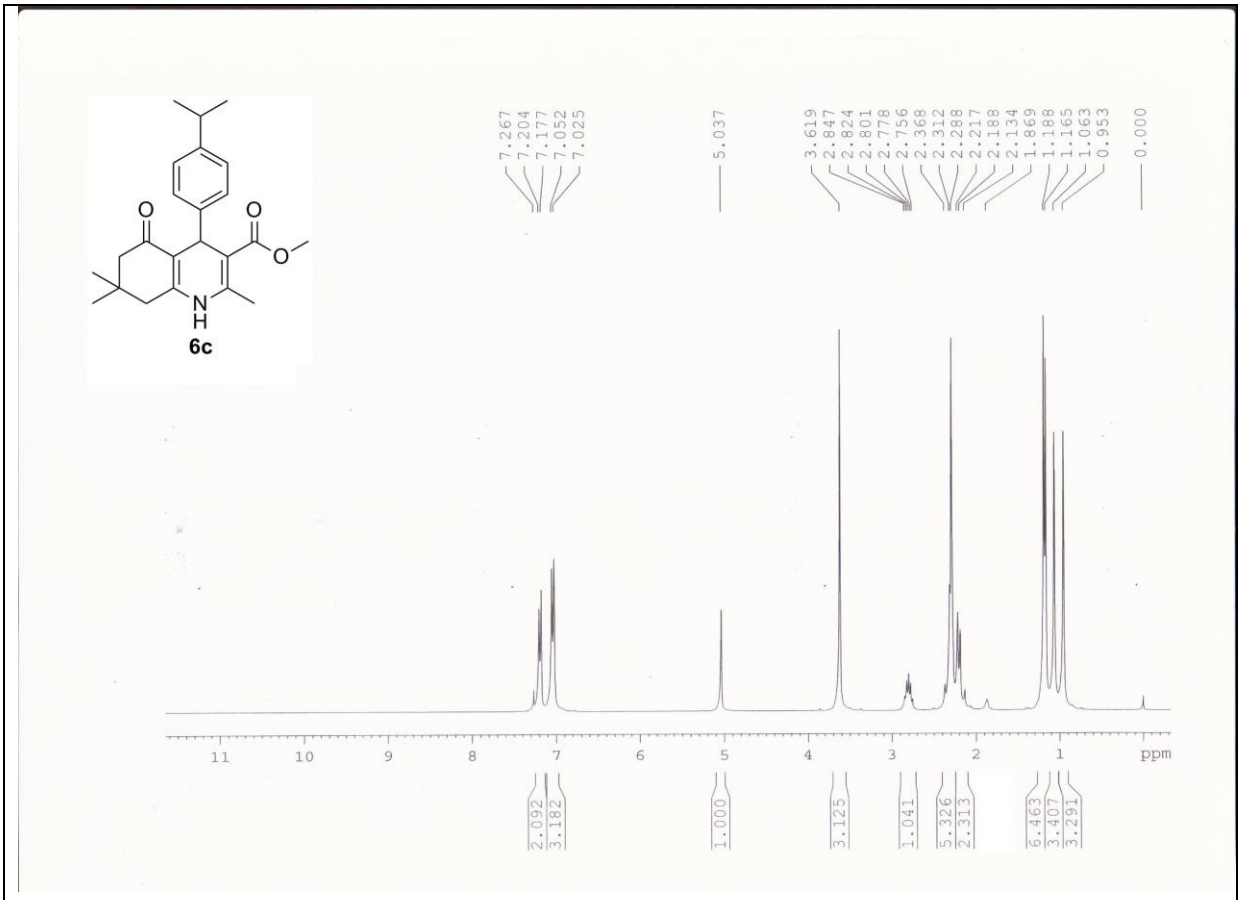

Figure I.C.12 Scanned copy of ^{1}H NMR spectrum of methyl 4-(4-isopropylphenyl)-2,7,7-trimethyl-5-oxo-1,4,5,6,7,8-hexahydroquinoline-3-carboxylate **(6c)**

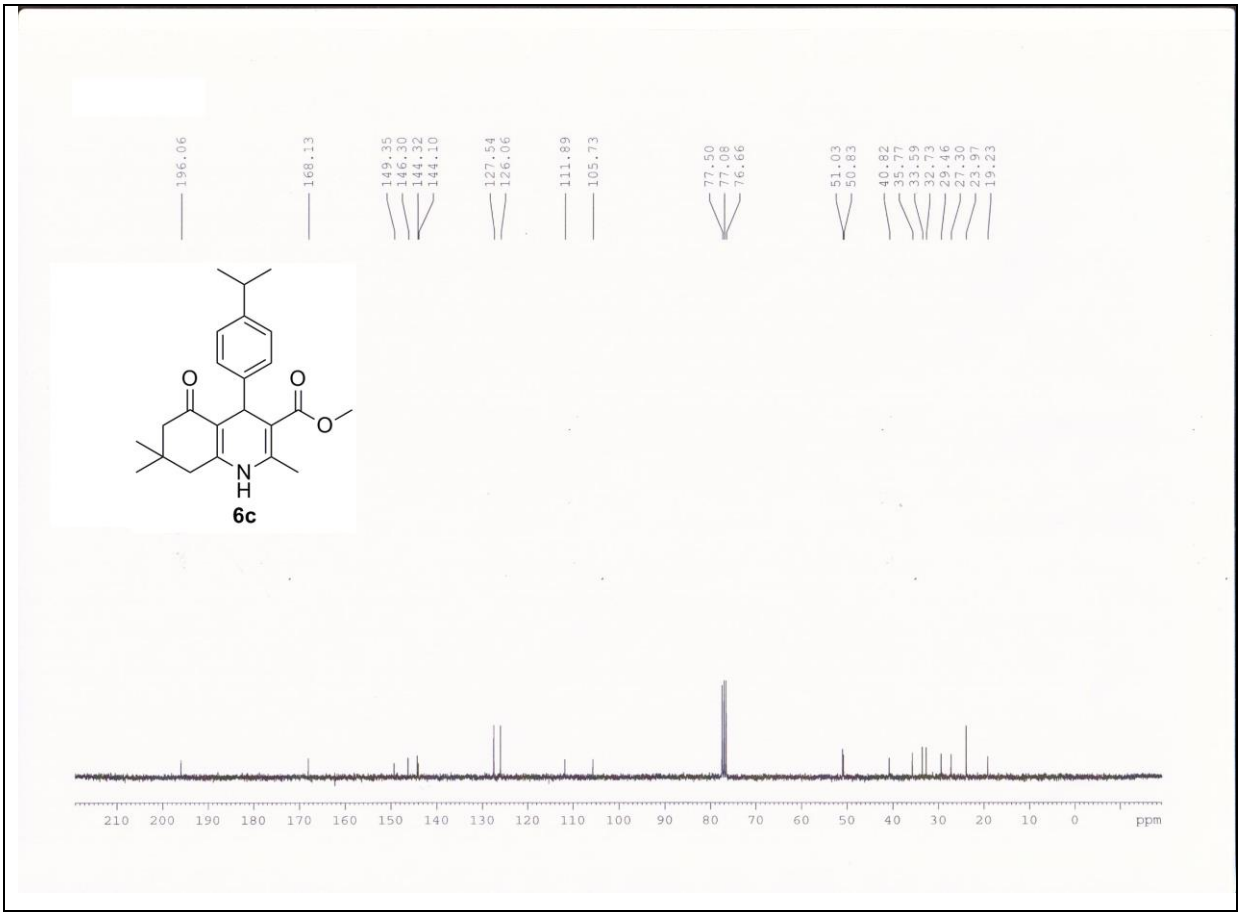

Figure I.C.13 Scanned copy of ^{13}C NMR spectrum of methyl 4-(4-isopropylphenyl)-2,7,7-trimethyl-5-oxo-1,4,5,6,7,8-hexahydroquinoline-3-carboxylate **(6c)**

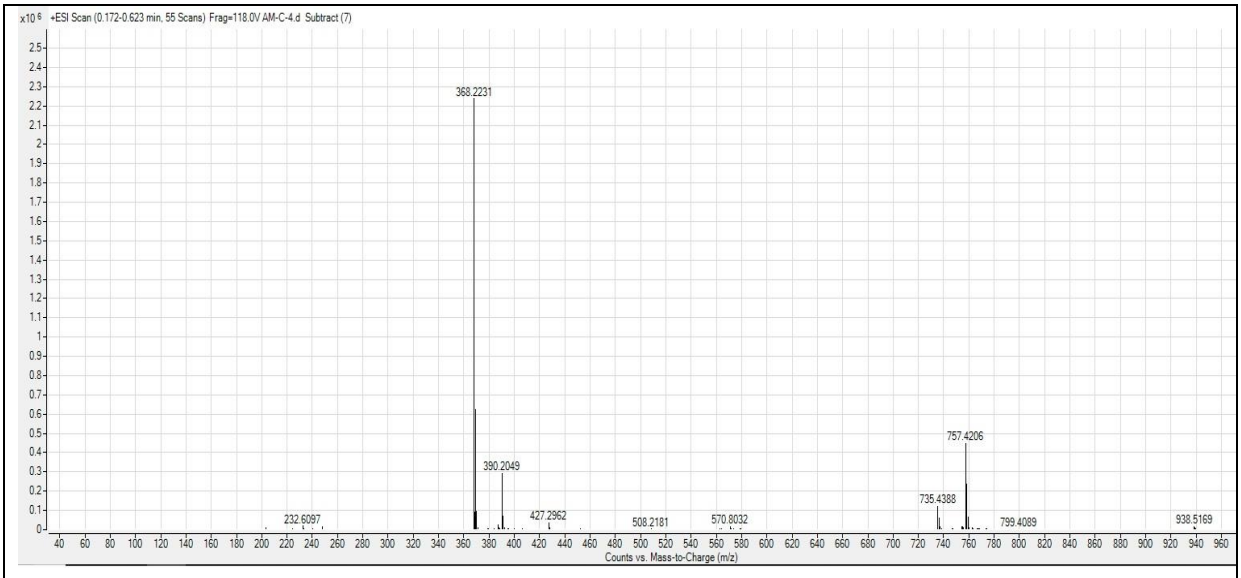

Figure I.C.14 Scanned copy of HRMS spectrum of methyl 4-(4-isopropylphenyl)-2,7,7-trimethyl-5-oxo-1,4,5,6,7,8-hexahydroquinoline-3-carboxylate **(6c)**

I.C.6 References

References are given in BIBLIOGRAPHY under Chapter I, Section C.

Chapter I

Section D

Graphene Oxide (GO) Catalyzed Synthesis of Thioethers under Continuous Flow Mode

I.D.1 Introduction

Flow chemistry also referred to as continuous flow chemistry is a term commonly utilized to describe the performance of a reaction in a narrow tube or pipe.[1-3] Continuous flow reactors have dimensions in the range 10^2-10^3 μm and can contain a few μL to several mL of chemical entities. The starting materials, reagents and homogeneous catalysts are injected into the reactor through the inlets by pumping. The heterogeneous or solid catalysts are supported inside the reactor in predefined columns or tubes, which are designed as a part of the instrumentation. These columns are filled with optimized amount of heterogeneous catalysts (packed beds) which can be manipulated as per the requirement of the reaction. The synthetic transformation in a flow reactor takes place in a continuously flowing stream of chemicals. An important parameter associated with flow chemistry is the residence time.[4] It is the amount of time during which a reaction is either heated or cooled inside the reactor. It is calculated from the volume of the reactor and the flow rate through it (residence time = reactor volume/flow rate). Thus the residence time can be reduced by shortening the length of the reactor channel or tube. In flow reaction, short residence time could be extremely useful in controlling reactions involving transient species. The flow reactor is a relatively newer technology that affects fluid dynamics, heat and mass transfers for streams of chemicals. The advantages of flow chemistry are elucidated below:

(i) Faster assemblies of molecules: The flow reaction is generally carried out under pressure in well defined reactors. This enables reactions to be heated above the normal boiling range of the reactants, thereby making the reaction proceed faster.

(ii) Safer reactions: Since the reaction takes place in certain tubes, there are less chances of exposure of certain chemicals or fumes to the outer environment. Moreover, flow chemistry allows formation of small amount of hazardous intermediates at any instant. This is achieved due to increased temperature control and short residence times.

(iii) Rapid optimization of reactions: The evolution of sophisticated instruments enables variation of reaction conditions swiftly on micro molar scales. Different parameters like ratio of reagents, concentration, temperature and reaction time can be rapidly varied and monitored. The course of addition of substrates and reagents can also be automated.

(iv) Integrated synthesis and analysis: After completion of the reaction the products can be flowed directly into a workup system. Thereafter, the products can be analyzed by means of an in-line analyzer (UV, FT-IR, LCMS, etc).

(v) Cleaner products: The rapid diffusion mixing ensures excellent reaction selectivity, eliminating issues found in batch reactors. The high surface to volume ratio enables instantaneous heating or cooling preventing side reactions and giving almost cleaner products.

(vi) Easy scale-up: The kilogram scale synthesis can be achieved easily due to excellent mixing and heat transfer. Industrial scale syntheses are performed in large reactors having higher flow rates.

Several reactions that are not possible in traditional batch procedure can be achieved by using flow reactors. These include reactions that occur instantaneously (second scale) at relatively higher temperature. The multistep procedures such as rapid deprotonation followed by instantaneous addition of an electrophile at high temperature are made easy in flow reactors.[5] Another important advantage of flow chemistry is the simultaneous work of several smaller reactors in parallel towards a common product.[6,7] This reduces time and effort and a large amount of product can be synthesized in shorter time.

Continuous flow chemistry does not mean simple transposition of batch procedures through narrow channels. It involves comprehensive redesign and improvisation of conventional batch processes. This is generally implemented through knowledge of chemical engineering and practical aspects of chemistry.[8] A general diagram for continuous flow set-up is presented in Figure I.D.1. Initially, the reagents are separately pumped through a micromixer into the reaction zone also called reactor. The reaction zone can be customized as per the needs of the reaction. This is the region where the temperature can be controlled. The different types of reactors that are commonly used are agitating microsphere reactors, fixed-bed reactors, tube-in-tube reactors, coils, etc. The reaction zone is succeeded by a back pressure regulator, which is installed to maintain the reaction pressure at a desired value. Thereafter, an in-line analyzer is attached, which leads to the purification bed via a phase separator. Thus, purified products can be obtained from crude reaction mixtures.

Modern instruments even allow microwave irradiation for flow synthesis.[9] Besides, traditional piston pumps have been replaced with magnetohydrodynamic actuators.[10] Moreover, in some instruments electroosmotic flow has been employed to ascend the reagents into the reactor.[11] Several spectroscopic techniques have been used under flow conditions. For instance, stopped-flow kinetic measurements have been used with circular dichroism (CD), FT-IR and NMR for the detection of intermediates.[12-14] Although several

commercially available flow set-ups are widely in use, simpler flow set-ups can be conveniently organized by using PFA capillaries and HPLC connectors.[15]

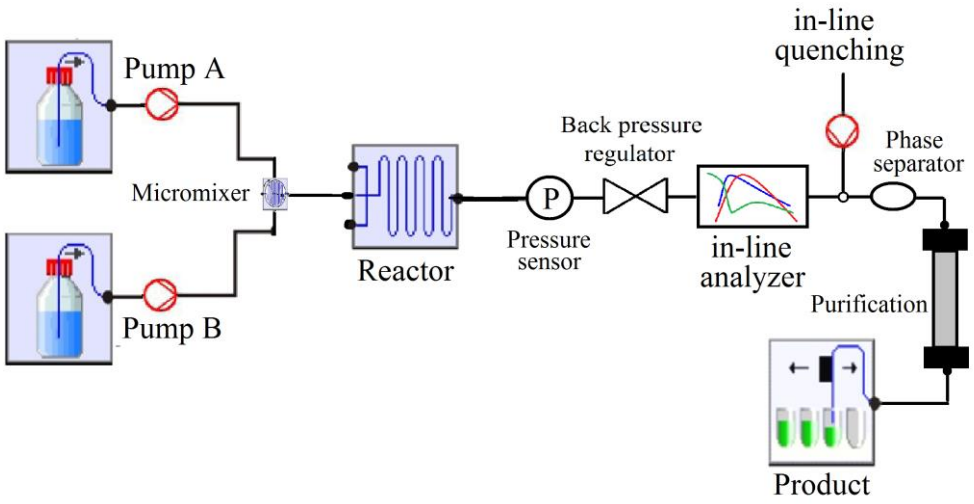

Figure I.D.1 Schematic diagram of a continuous flow set-up.

Although flow chemistry when applied appropriately helps in reducing time and effort, it is associated with certain limitations. Not all reactions can be performed with same efficacy in flow reactors and a careful analysis must be undertaken before carrying out any chemical transformation. Besides, handling of highly viscous materials or suspensions often becomes a challenging task.[16]

Ever since the discovery of flow chemistry, enormous steps have been taken to implement this technology in pharmaceutical industries for preparative organic synthesis. Moreover, multistep continuous flow systems have improved the syntheses of active pharmaceutical ingredients (API),[17] natural products, commodity chemicals and value added chemical entities (VACE).[5] Figure I.D.2 lists some active pharmaceutical ingredients that are in the WHO list of essential medicines and are synthesized by using flow chemistry. Thus flow chemistry has evolved from single step reactions to complex multistep processes in areas of preparative organic chemistry.[18-20]

Continuous flow chemistry has been utilised as a technology for implementing green and sustainable processes.[21-23] Since flow chemistry increases the overall safety of chemical processes, many organic chemists are developing new strategies aiming at transition towards a bio based chemical industries.[24] In this context, glycerol which is a waste product of biodiesel industry has been used as starting material for the preparation of several chemical building blocks using flow chemistry.[25] Myriads of heterogeneous catalysts in the form of packed beds are used for the flow synthesis of lower alcohols like methanol, propanol, allyl

alcohol, etc. The heterogeneous catalysts include CeO_2, $Pt/TiPO_4$, Ag/Al_2O_3, Ag/ZSM-5, Fe-silicalite, modified SBA and others.[3]

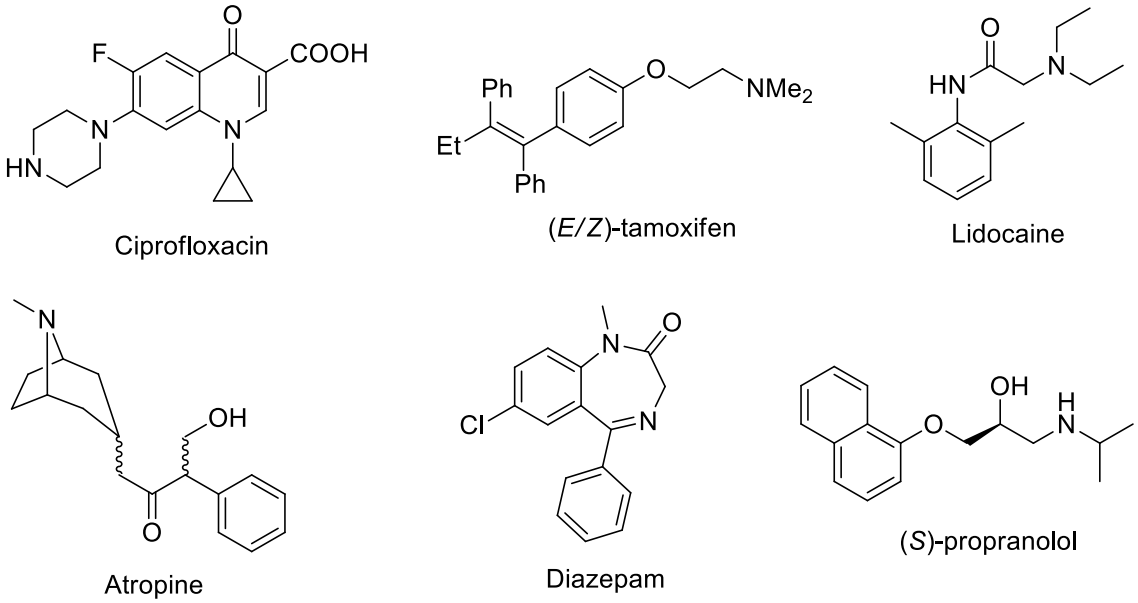

Figure I.D.2 Examples of active pharmaceutical ingredients synthesized via flow chemistry.

Flow chemistry has also been used in chemical processing methods for water and waste water treatment. The methodology mainly involves UV irradiation either in the presence or absence of catalysts.[26] Moreover, photocatalytic degradation of bio-resistant dyes under flow mode has been demonstrated by using TiO_2 catalyst supported on cement matrix.[27] Other methods like electrochemical oxidation, sonolysis and bombardment with high energy accelerated electrons have been used for the decomposition of organic pollutants in waste water.[28,29] Thus continuous flow chemistry is a revolution of the present and future so as to perform chemical synthesis through a machine assisted process.

On the other hand, the construction of C–S bond represents a fundamental step in chemical synthesis owing to their prevalence in a variety of organic compounds possessing potential pharmacological activity.[30-32] They have remarkable pharmacological efficiency and find application against the treatment of a wide range of diseases like Alzheimer's, Parkinson's, malaria, cancer and diabetes.[33-36] Apart from multifaceted biological and therapeutic applications, functionalized thioethers are also used as important intermediates in contemporary organic synthesis.[37] Few representative bioactive molecules possessing functionalized C–S bond are shown in Figure I.D.3.

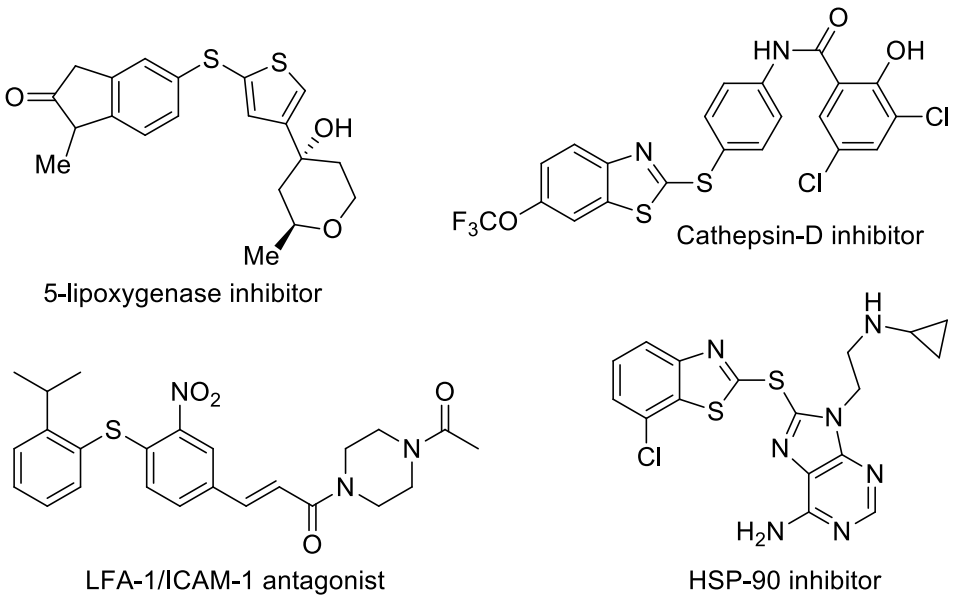

Figure I.D.3 Functionalized thioethers possessing bioactive properties.

There are numerous methods available for the synthesis of thioethers, the traditional approach involves reduction of diaryl sulfones or sulfoxides in presence of strong reducing agents,[38] which requires stringent reaction conditions. The most prominent and synthetically reliable method is based on transition metal (Pd, Cu, Ni) catalyzed cross coupling reaction of aryl halides and thiols or disulfides.[39,40] However, transition metal catalyzed C–S coupling often requires high temperature, strong bases, expensive ligands, oxidants and hazardous solvents.[40] An alternative metal free protocol for the synthesis of thioethers involves the cross coupling of arene diazonium salts and thiols or disulfides, also known as Stadler-Ziegler reaction.[41,42] Diazonium compounds serves as an important intermediate in diverse organic transformations owing to their multifarious reactivity.[43-45] Traditional Stadler-Ziegler reaction involves the reaction between aryl diazonium salt (derived in situ from aniline using an acid) and thiolate anion (derived from thiol/disulfide using a base).[41,42] Recently, a variety of different protocols have been developed for the transition metal free catalyzed Stadler-Ziegler reaction.[46,47] However, the continuous flow synthesis of thioethers via Stadler-Ziegler reaction has been limited.[48] For instance, a visible light mediated arylation of cysteine via diazotization has been accomplished by using eosin Y as photocatalyst under continuous flow conditions.[49] Although, the Stadler-Ziegler reaction offers easy access to unsymmetrical thioethers, the use of strong acids, bases for making the thiolate anion and the use of metal catalysts restrict its wide applicability.[50-53]

In recent times, nanocarbon materials like graphene oxide (GO) as carbocatalysts in diverse organic reactions have been well studied since the first seminal paper by Bielawaski in 2010.[54] The sustainable 2D honeycomb structure of carbonaceous graphene on oxidation and subsequent exfoliation provides an easy access to graphene oxide, which bears several oxygenated functional groups, particularly –COOH on its peripheral sides and –OH, epoxy groups on its basal plane.[55] Both oxidative and acidic properties of GO have been exploited in several catalytic organic transformations.[56-58] However, this carbocatalyst (GO) has not been used in a flow reaction so far.

I.D.2 Background and objectives

The use of the term 'flow synthesis' was reported for the first time in organic chemistry paper in 1970, where the investigators carried out the synthesis of polypeptides in a column.[59] However, the first comprehensive use of flow chemistry in chemical synthesis or analytical analysis came in the late 1990s.[60] In the 2000s, continuous flow microreactors with fluid propulsion technology was used in for the amplification of DNA through polymerase chain reaction (PCR).[10] Although the use of the term 'flow chemistry' has been in use since the last two decades, the first use of flow reactor in chemistry dates back to 1932, where phosphoric acid catalyst on silica gel was employed for the dehydration of diethylcarbinol.[61] Moreover, the synthesis of natural products via flow chemistry was reported by G. K. Tranmer and co-workers.[62] They carried out the multistep synthesis of natural product oxomaritidine using flow reactor assembly. Few examples of Stadler-Ziegler reaction and also the use of flow chemistry in organic synthesis are illustrated below.

A one-pot Stadler-Ziegler synthesis of thioethers has been developed by following continuous flow technique as well as through batch procedure (Scheme I.D.1). The investigators have used $[Ru(bpy)_3Cl_2]\cdot 6H_2O$ as photocatalyst in presence of blue LEDs as light source.[48] In the case of flow synthesis the reaction has been carried out in capillary microreactor. Moreover, a plausible mechanism has been proposed which suggested that the reaction proceeds through single electron transfer (SET).

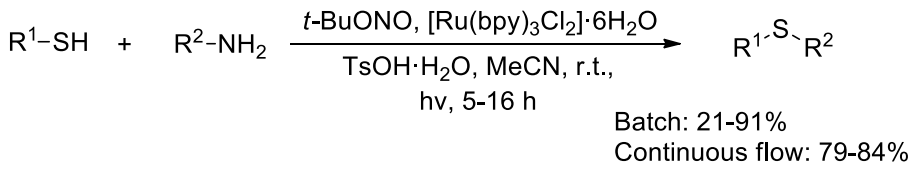

Scheme I.D.1 Photocatalytic Stadler-Ziegler reaction using $[Ru(bpy)_3Cl_2]\cdot 6H_2O$ catalyst.

A light emitting diode irradiated Stadler-Ziegler reaction has been reported under metal-free, catalyst-free and solvent-free condition (Scheme I.D.2). Diverse diaryl sulfides have been synthesized in 33-96%. The authors also carried out a gram scale synthesis of diaryl sulphide and extended the protocol towards the synthesis of diaryl selenides. Moreover, a late stage selenylation of sulfa drugs have been achieved using the standard reaction condition.[46]

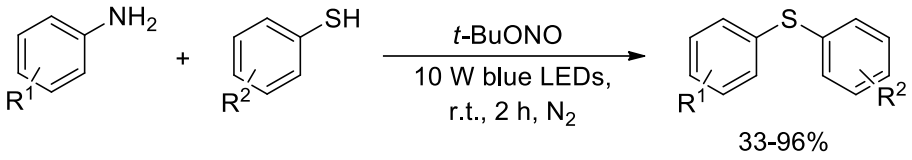

Scheme I.D.2 Synthesis of thioethers in presence of blue LEDs.

An organo-photocatalytic protocol for the synthesis of diaryl sulfides has been developed.[47] Eosin Y has been used as organo-photocatalyst in presence of green LEDs and the reaction has been carried out under ambient condition. Moreover, one of the sulfide has been further functionalized to the corresponding sulfone derivative (Scheme I.D.3). The protocol could be scaled up for and a plausible mechanism has been presented.

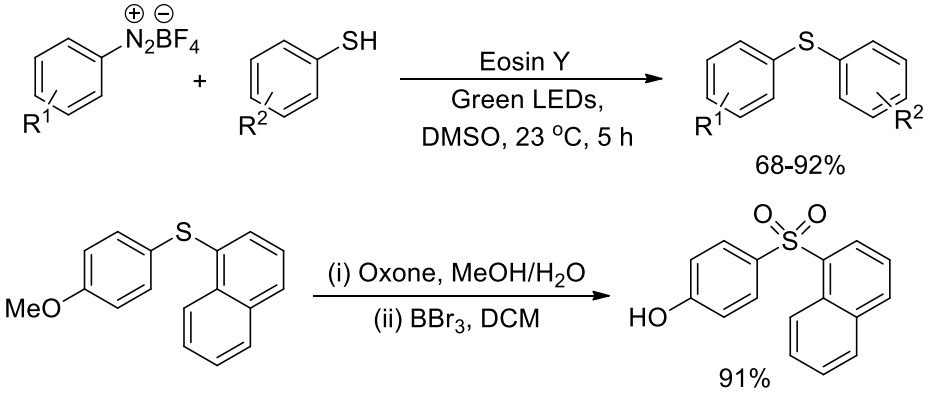

Scheme I.D.3 Organo-photocatalytic method for the synthesis of diaryl sulfides.

The synthesis of diaryl sulfides has been accomplished under mechanochemical condition in alumina surface. Diazonium tetrafluoroborates and diaryl disulfides have been reacted in presence of KOH over neutral alumina under ball milling condition (Scheme I.D.4). The protocol has been further extended towards the synthesis of diaryl selenides, diaryl tellurides and S-aryl dithiocarbamates.[51]

A modified form of the Stadler-Ziegler reaction has been reported from arenediazonium *o*-benzenedisulfonimides and sodium thiolates under catalyst-free condition.[53] A library of sixty three different thioethers has been synthesized and a plausible mechanism has been proposed

(Scheme I.D.5). After the completion of the reaction *o*-benzenedisulfonimides could be regenerated by passing through ion exchange resin and can be re-used after diazotization.

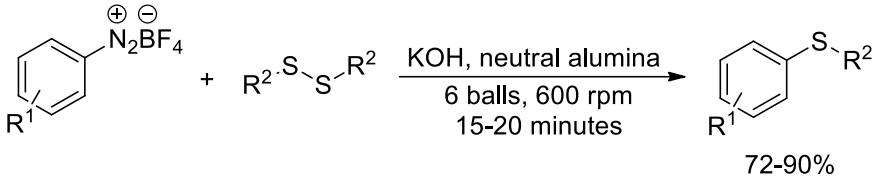

Scheme I.D.4 Synthesis of diaryl sulfides under ball milling conditions.

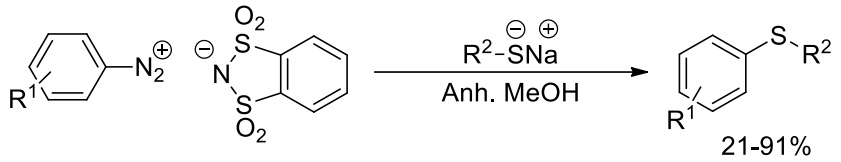

Scheme I.D.5 Stadler-Ziegler reaction from arenediazonium *o*-benzenedisulfonimides.

An expedient synthesis of aryl sulfides under metal-free condition and promoted by ascorbic acid has been achieved. The reaction conditions involve stirring of anilines and disulfides in presence of ascorbic acid under ambient temperature (Scheme I.D.6). The investigators also conducted few control experiments to establish the reaction pathway. The use of TEMPO (a radical quencher) inhibited the reaction suggesting the formation of radical during the course of the reaction. Furthermore, the protocol has been extended for the synthesis of aryl selenides.[63]

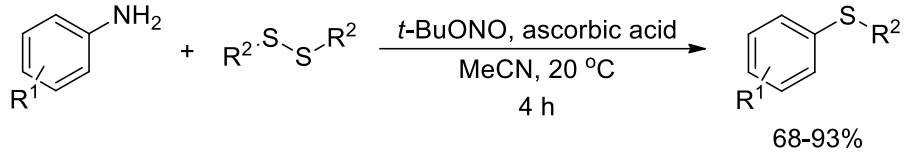

Scheme I.D.6 Ascorbic acid promoted Stadler-Ziegler synthesis of aryl sulfides.

Sodium acetate mediated metal-free synthesis of thioethers has been reported by Wangelin and co-workers.[50] Different sulfur sources like disulfide, elemental sulfur and thiols have been used for the reaction; however, disulfide gave the best yield. A detailed mechanistic study and further extension of the protocol towards the synthesis of selenides and tellurides has been performed. The same methodology has also been used for radical cyclization-thiolation (Scheme I.D.7).

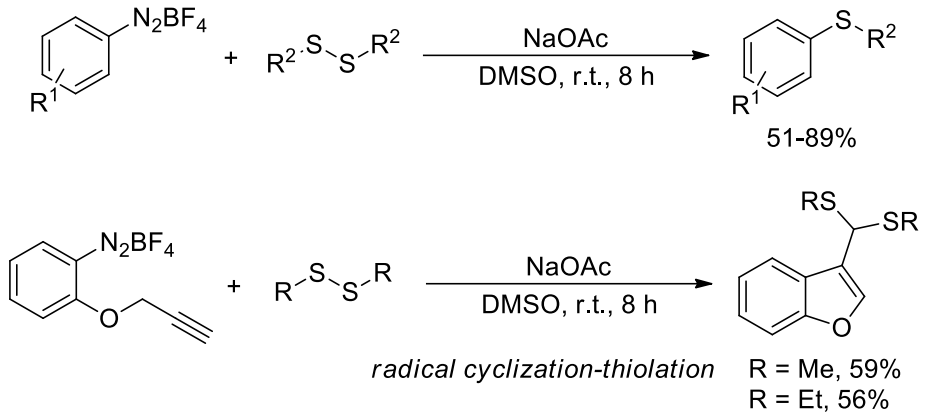

Scheme I.D.7 NaOAc mediated of aryldiazonium tetrafluoroborates.

An efficient copper catalyzed sulfur transfer reaction for the synthesis of thioethers has been developed.[64] The methodology results in the simultaneous formation of two C–S bonds using sodium thiosulfate as the sulfenylation reagent. Diverse thioethers have been synthesized from aryl amines and alkyl halides in 40-99% yields (Scheme I.D.8). Moreover, the investigators also carried out late-stage sulfenylation of aryl amines and carried out to get detail insights into the mechanism.

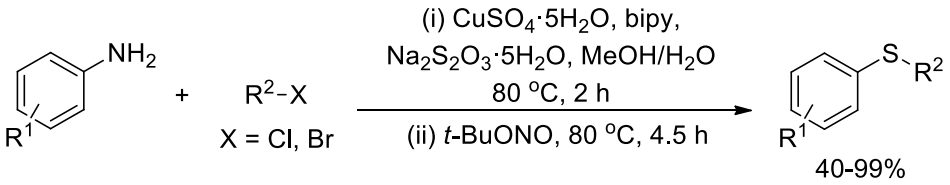

Scheme I.D.8 Copper catalyzed synthesis of thioethers.

I.D.3 Present work: Results and discussions

Graphene oxide (GO) exhibits dual properties i.e. both acidic and oxidative properties, we therefore have employed GO as a heterogeneous acid catalyst in the Stadler-Ziegler reaction under flow conditions. The particle size of GO was measured previously by DLS studies and found to be 544 ± 37 nm for 82% of the GO particles.[65] Organyl nitrites,[43] and supported nitrites,[66] have been shown to be efficient and better diazotizing agents than inorganic nitrites in terms of safer handling, cost effectiveness and by-product formation. We in our studies have found *tert*–butylnitrite (*t*-BuONO) as the cheaper and best nitrosation agent. Thus we have developed GO catalyzed flow reaction as a sustainable protocol for making unsymmetrical thioethers (Scheme I.D.9). Although several commercially available flow systems mediate continuous flow transformations, we have fabricated our own flow equipment from affordable and readily available laboratory apparatus.

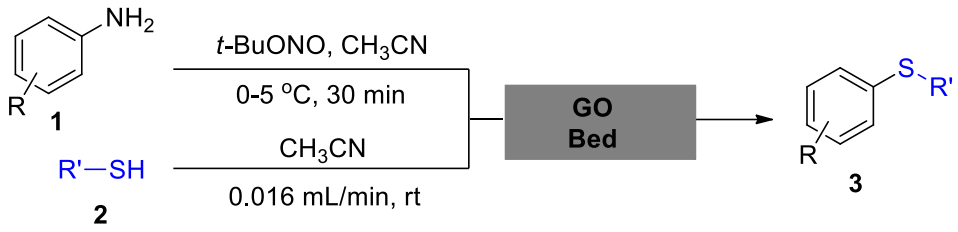

Scheme I.D.9 GO catalyzed continuous flow synthesis of thioethers.

The flow reaction bed of graphene oxide was prepared in a chromatographic column, the base of which was plugged with a thick cotton bed followed by packing with GO. The glass column had provisions for wrapping with ice jacket that could maintain low temperature (0-5 °C). Firstly, a solution of aromatic amine in CH_3CN was placed on GO bed followed by the addition of the nitrosation reagent in CH_3CN. The reaction bed was then kept at 0-5 °C for 30 minutes using the ice jacket. Then the ice jacket was removed and a solution of thiol in CH_3CN was added at room temperature (r.t.) to the reactor column drop wise at different flow rates (mL/min) and the reaction mixture was allowed to pass through the flow reaction column to afford the desired thioether (Figure I.D.4).

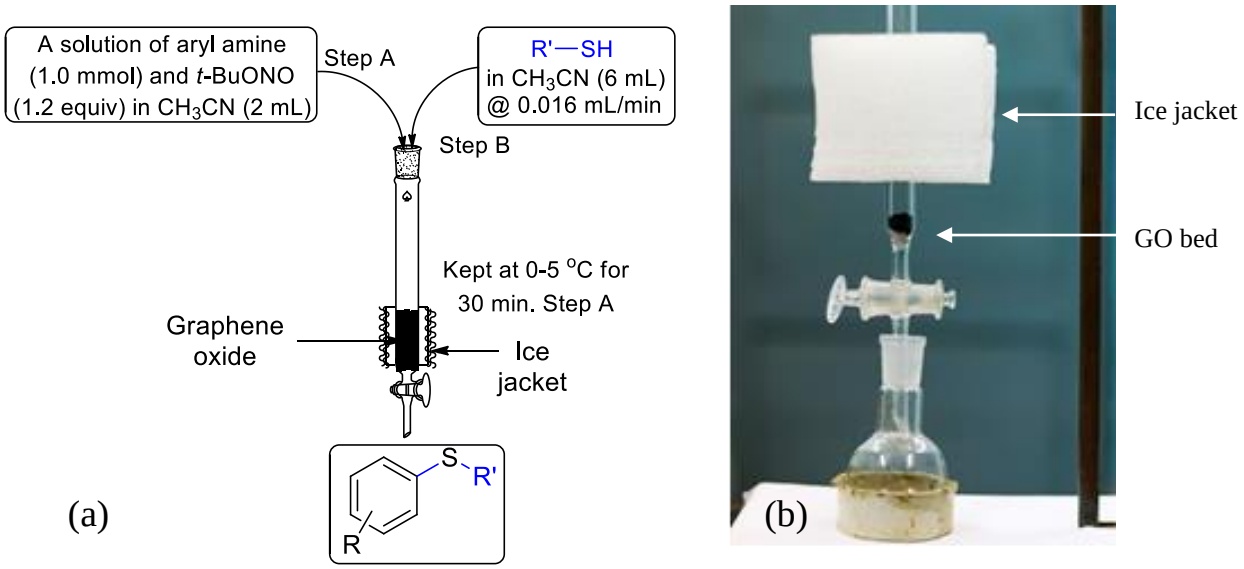

Figure I.D.4 Experimental setup for continuous flow two-step synthesis of thioether: (a) schematic, (b) digital image.

I.D.3.1 Optimization of reaction conditions

In the optimization process, we used 4-methoxyaniline **1a** (1 mmol) and thiophenol **2a** (1 mmol) as model substrates, *tert*–butylnitrite (*t*-BuONO) (1.2 mmol) as the nitrosation reagent, and the catalyst bed of 2 mm height was prepared with GO (300 mg). The reaction

protocol involves primarily two steps: (i) a solution of aryl amine and *tert*–butylnitrite in solvent was soaked on to the GO bed and kept at 0-5 °C for 30 minutes (step A), (ii) the thiol in the same solvent was added at different flow rates to the resulting diazonium species on GO (step B). After the addition was complete, the desired product was eluted with the solvent. The results are presented in Table I.D.1. Use of CH_3OH at a flow rate of 0.050 mL/min (6 mL solution during 2 h) gave the desired thioether **3a** in 60% yield along with diphenyl disulfane (23%) (entry 1). The formation of **3a** was confirmed by ^1H and ^{13}C NMR spectroscopy. In the ^1H NMR spectrum the singlet peak at δ 3.82 ppm was due to the OCH_3 group. The five aromatic Hs of the thiol moiety appeared as multiplet in between 7.11-7.26 ppm. The four aromatic Hs of the aniline moiety appeared as two doublet of doublet at δ 6.90 (dd, J = 6.6 and 2.1 Hz) and 7.42 (dd, J = 6.9 and 2.1 Hz) ppm. The ^{13}C NMR spectrum of **3a** showed a peak at δ 55.3 ppm due to the presence of OCH_3 group. Changing the solvent from CH_3OH to CH_3CN resulted in increase of the product yield to 77% (entry 2). The reaction carried out in H_2O afforded the desired diaryl sulfide in 21% yield only (entry 3). This might be due to the poor solubility of aryl amine in H_2O. Next, the effect of other nitrosation agents on the course of the reaction was studied. The use of butylnitrite (BuONO) instead of *t*-BuONO did not show any pronounced effect in the course of the reaction (entry 4, 76%). Since the CH_3CN solvent was found to be better, we examined addition of solution of thiol in CH_3CN (step B) at different flow rates. These experiments resulted in further developments in terms of higher yield of the desired diaryl sulfide as well as suppression of conversion to disulfides via oxidative dimerization. Thus, addition of the thiol solution at a flow rate of 0.025 mL/min formed the desired diaryl sulfide **3a** in 82% yield (entry 5) and further decreasing the flow rate to 0.016 mL/min increased the product yield to 86% along with the diaryl disulfide in 8% (entry 6). However, the flow rate at 0.012 mL/min resulted in a lower yield of the desired product (entry 7, 75%), presumably due to the fact that the diazonium intermediate is decomposed under longer exposure on to the surface of GO catalyst. We conducted an experiment under the optimized reaction condition by conventional method under stirring. A one-pot two-step strategy was employed, where **1a** (1 mmol), GO (25 mg), *t*-BuONO (1.2 equiv) and CH_3CN (2 mL) were stirred at 0 °C for 30 minutes and then the thiol (1 mmol) was added to this diazotization mixture and the reaction was continued for 6 h at room temperature. The desired thioether **3a** in this conventional method was formed in 72% isolated yield along with 17% of the disulfane (entry 8). Furthermore, the reaction did not occur when carried out in the absence of nitrosation reagent (entry 9). In order to examine the scalability of the flow reaction, we performed the reaction in 5 mmol scale taking 4-

methoxyaniline, GO (1.0 g) and keeping the flow over a period of 10 h that gave the unsymmetrical thioether **3a** in 81% yield (entry 10). This indicates that large scale flow reactions can be performed within standard time limit.

Table I.D.1 Optimization of the continuous flow reaction conditions[a]

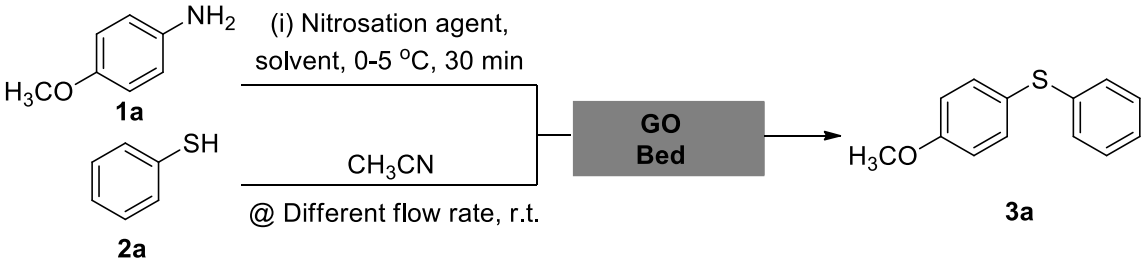

Entry	Solvent	Nitrosation reagent	Flow rate (mL/min)[b]	Yield (%)[c]
1	CH_3OH	*t*-BuONO	0.050	60
2	CH_3CN	*t*-BuONO	0.050	77
3	H_2O	*t*-BuONO	0.050	21
4	CH_3CN	BuONO	0.050	76
5	CH_3CN	*t*-BuONO	0.025	82
6	**CH_3CN**	***t*-BuONO**	**0.016**	**86**[d]
7	CH_3CN	*t*-BuONO	0.012	75
8	CH_3CN	*t*-BuONO	–	72[e]
9	CH_3CN	–	0.016	No reaction
10	CH_3CN	*t*-BuONO	0.016	81[f]

[a]Reaction conditions: (i) **1a** (1 mmol), nitrosation reagent (1.2 equiv), solvent (2 mL); (ii) **2a** (1 mmol), solvent (6 mL). [b]The rate at which thiol solution was added to the flow reactor column. [c]Isolated yield. [d]Diphenyl disulfane was formed in 8% yield. [e]Reaction conducted by conventional method under stirring. Diphenyl disulfane was formed in 17% yield. [f]Reaction performed with **1a** (5 mmol), GO (1.0 g), **2a** (5 mmol) in solvent (10 mL) and flow time 10 h.

I.D.3.2 Synthesis of thioethers through flow reaction

After optimization of the continuous flow reaction conditions, the protocol was extended towards the synthesis of diverse unsymmetrical thiothers from different aromatic amines and aryl/alkyl thiols. The results have been presented in Table I.D.2. Aromatic amines containing both electron donating groups ($–OCH_3$, $–CH_3$, –Br and –Cl) as well as electron withdrawing groups ($–NO_2$ and $–COCH_3$) were tolerated under the reaction conditions. In the case of aromatic thiols, substitution pattern comprising of electron donating and electron withdrawing groups also did not affect the course of the reaction resulting significant conversion to the desired product (entries 1-8). The reaction was also successful with

aliphatic thiols. For example, long chain aliphatic thiols like heptanethiol and pentanethiol gave the corresponding thioethers (**3g**-**3i**) in 82-87% yield (entries 9-11). Moreover, the reactions involving heterocyclic substrates (both heterocyclic amines and heterocyclic thiols) were also explored. The reaction between 4-aminopyridine and 4-methylbenzenethiol or between 4-methoxyaniline and pyridine-2-thiol went smoothly to afford the corresponding unsymmetrical diayl sulfides in 79-84% yield (entries 12 and 13). Thus, GO appears to be innocuous to heterocyclic moiety in comparison to other acids normally used in the diazotization process. Again, the reaction between 2-naphthylamine with 4-tolylthiol or between 4-toluidine and naphthalene-2-thiol worked efficiently affording the same product **3l** in nearly similar yields (79-82%) (entries 14 and 15). The study manifested that the reaction conditions i.e. the diazotization of aryl amine followed by continuous flow of thiols over the catalyst bed (GO) did not affect much or had any significant effect in the course of the reaction. The products were characterized by ^{1}H and ^{13}C NMR spectroscopy. For instance compound **3c** showed a singlet peak at δ 3.81 ppm corresponding to the OCH_3 group. All the aromatic protons appeared as doublet of doublet at 6.89 (dd, *J* = 6.6 and 2.1 Hz, 2H), 7.06 (dd, *J* = 6.6 and 2.1 Hz, 2H), 7.18 (dd, *J* = 6.6 and 2.1 Hz, 2H) and 7.40 (dd, *J* = 6.7 and 2.4 Hz, 2H) due to coupling between adjacent Hs. In the ^{1}H NMR spectrum of **3e** the peak at δ 3.55 ppm was due to the $COCH_3$ group. In the ^{13}C NMR spectrum the same peak appeared at 26.5 ppm. The heteronuclear coupling occurred between ^{13}C and ^{19}F and the peaks appeared at δ 116.6 (d, *J* = 87 Hz), 134.82 (d, *J* = 33 Hz) and 138.0 (d, *J* = 129 Hz) ppm. The compound **3h** showed two triplets at δ 0.89 (*J* = 6.6 Hz) and 2.83 (*J* = 7.2 Hz) ppm due to the terminal CH_3 and SCH_2 groups of thiol moiety respectively. The same peaks appeared at δ 13.9 and 32.6 ppm in ^{13}C NMR spectrum.

Table I.D.2 GO catalyzed synthesis of thioethers under continuous flow reaction[a]

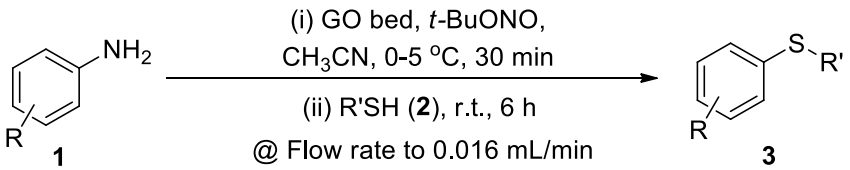

Entry	Aromatic amine	Thiol	Product	Yield (%)[b]
1	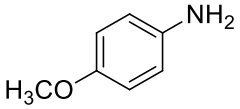	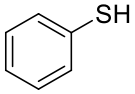	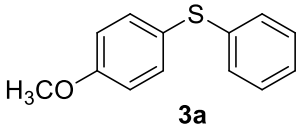 **3a**	86

2	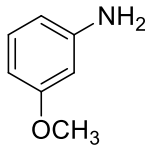	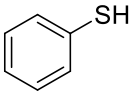	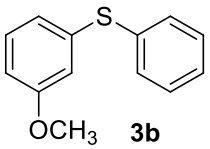 **3b**	83
3	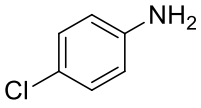	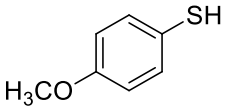	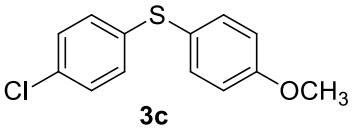 **3c**	84
4	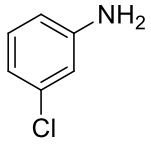	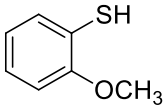	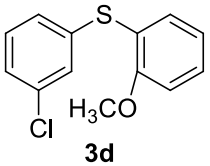 **3d**	81
5	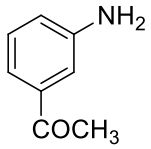	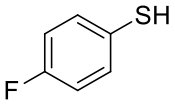	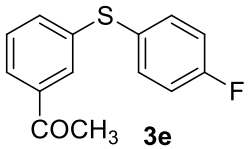 **3e**	88
6	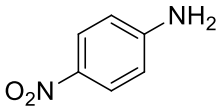	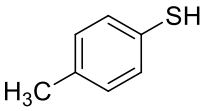	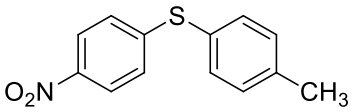 **3f**	84
7	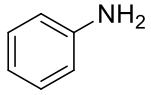	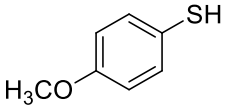	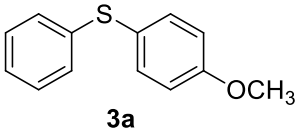 **3a**	87
8	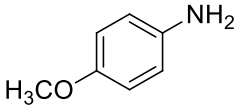	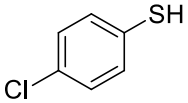	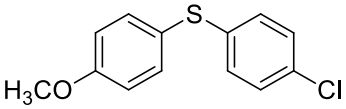 **3c**	83
9	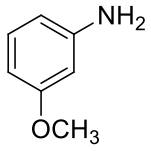	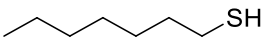	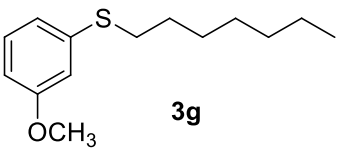 **3g**	82
10	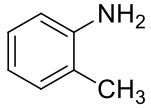	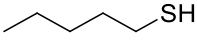	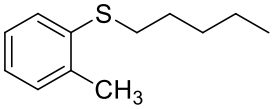 **3h**	87
11	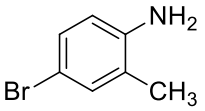	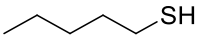	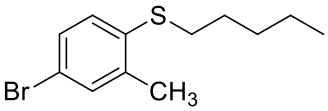 **3i**	87

12	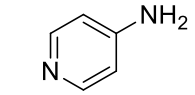	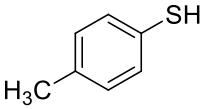	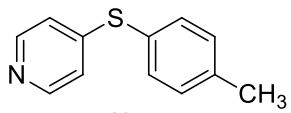 **3j**	79
13	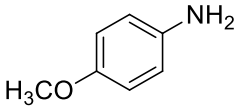	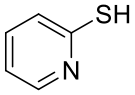	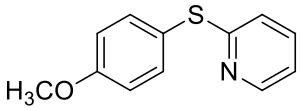 **3k**	84
14	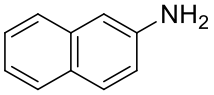	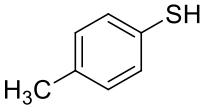	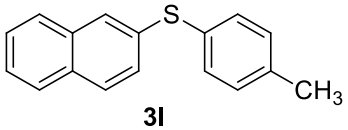 **3l**	79
15	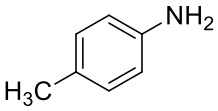	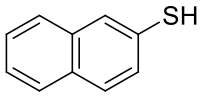	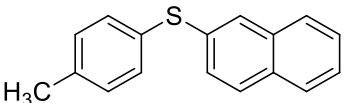 **3l**	82

[a]Reaction conditions: (i) **1** (1 mmol), *t*-BuONO (1.2 equiv), CH_3CN (2 mL); (ii) **2** (1 mmol), CH_3CN (6 mL). [b]Isolated yield after purification through column chromatography.

I.D.3.3 Recyclability of the GO flow reaction bed

We carried out the recyclability test of the catalyst bed after the completion of the reaction. The flow reactor catalyst bed (GO) was reused for ten consecutive runs without any appreciable loss in the yield of the products (Figure I.D.5). After completion of the reaction, the reaction mixture was eluted with ethyl acetate from the flow reactor column. For use in recycling experiments, the GO bed in the column was washed with ethyl acetate (3 x 5 mL) followed by acetone (1 x 5 mL) and dried with an external hot air blower. We even compared the FT-IR spectra of the fresh GO with the recovered GO (after fifth run) and did not observe any significant change in the spectral pattern (Figure I.D.6).

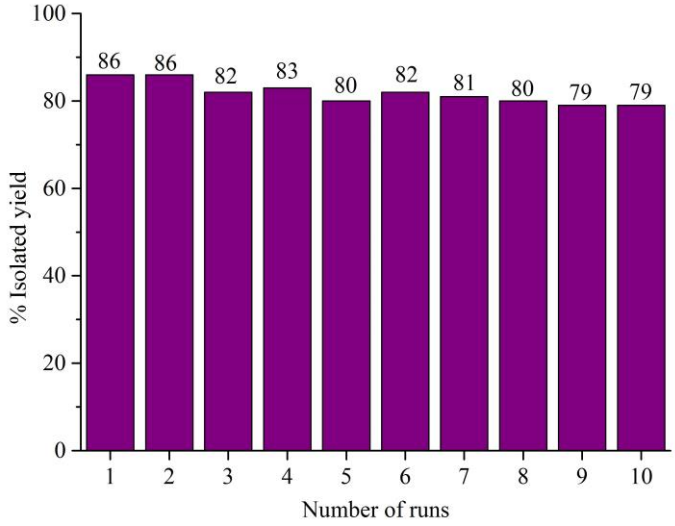

Figure I.D.5 Recyclability of GO flow reactor bed in Stadler-Ziegler reaction.

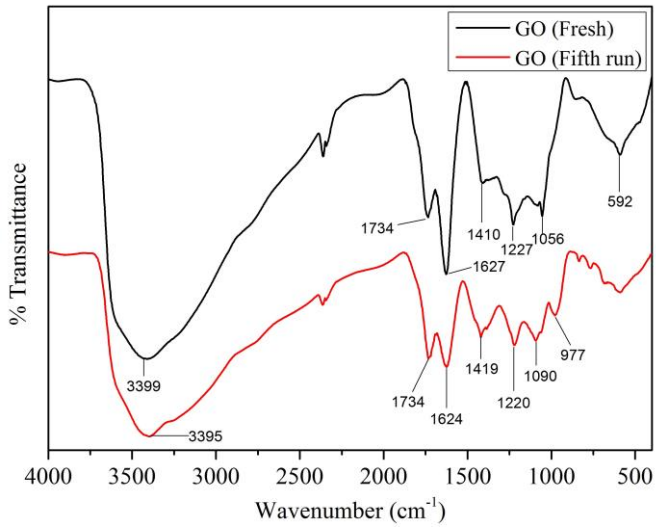

Figure I.D.6 FT-IR spectra of GO catalyst: fresh and after the fifth run.

I.D.3.4 Control experiments

To get some insights into the mechanistic pathway for the reaction, we conducted some control experiments (Scheme I.D.10). The Stadler-Ziegler reaction is believed to proceed via radical intermediates.[63] Firstly, we set up one reaction under the optimized conditions using 4-methoxyaniline (**1a**) and thiophenol (**2a**) in presence of a radical scavenger, TEMPO. In this case, the desired product (**3a**) was isolated in 17% yield only, suggesting clear evidence that the reaction might proceed through aryl radical intermediate. Since we observed partial formation of diaryl disulfide, which could originate via oxidative dimerization of aryl thiol, we performed one reaction between **1a** (1 mmol) and 1,2-diphenyldisulfane **4** (0.5 mmol) under the standard continuous flow conditions. This reaction afforded **3a** in 85% yield suggesting that the disulfide could be other intermediate in the reaction.

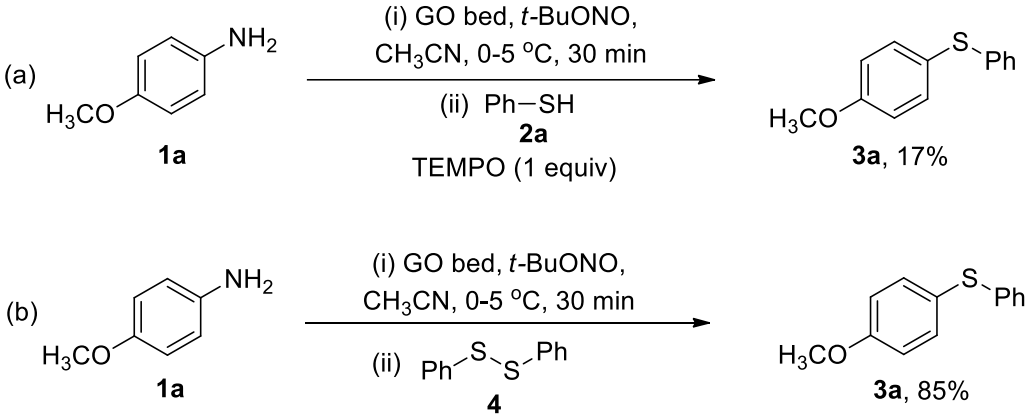

Scheme I.D.10 Control experimental analysis.

I.D.3.5 Plausible mechanism for the flow synthesis of thioethers

Based on the results obtained from control experiments and keeping analogy with literature reports,[63,67] we proposed a plausible mechanism (Scheme I.D.11). The diazotization of aromatic amine **1a** using *t*-BuONO in presence of GO gives rise to the formation of the diazonium salt **6**, which underwent homolytic dediazotization to provide the aryl radical **7**. It is believed that the formation of the aryl radical **7** is facilitated by graphene oxide.[68,69] On the other hand, the oxidative dimerization of thiol **2a** to the disulfide intermediate **4** has been facilitated in the presence of GO,[70] which subsequently formed the thiyl radical **5**. Finally, the reaction between aryl radical **7** and thiyl radical **5** resulted in the formation of the product **3a**.

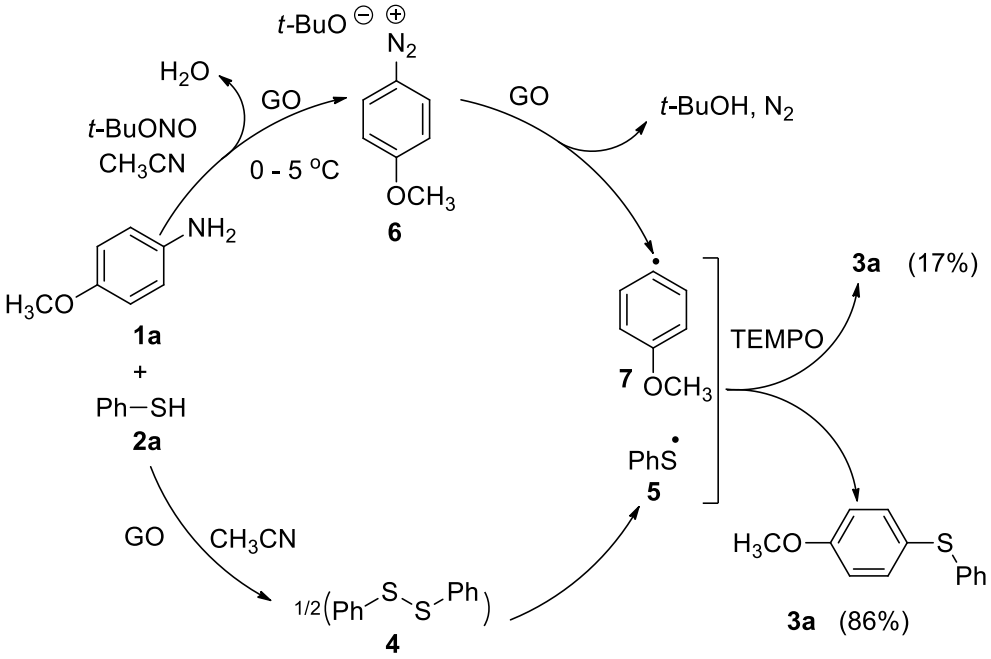

Scheme I.D.11 Plausible mechanism for Stadler-Ziegler reaction.

I.D.4 Conclusion

We have developed GO catalyzed Stadler-Ziegler synthesis of thioethers under continuous flow technique. The technique offers the advantages of affording the final thioether under metal-free condition, suppresses the formation of common by-product (disulfides), and is applicable to variety of aryl amines and thiols providing a facile access to various unsymmetrical diaryl/aryl-alkyl sulfanes in very good yields. Moreover, the catalytic bed (GO) can be reused for ten consecutive runs without any loss in its catalytic performance. Graphene oxide has been used as a sustainable carbocatalyst in various organic reactions; however, to the best of our knowledge, this example of continuous flow reaction technique of

GO catalyst is reported for the first time. The results are expected to encourage further applications of GO catalyzed reactions in flow reactor designed in common laboratory.

I.D.5 Experimental Section

I.D.5.1 General Information

For the construction of flow reactor, chromatographic glass column of 2 cm diameter was used. All reagents were purchased from commercial suppliers and used directly without further purification. The solvents were of AR grade and used after distillation. All the products were purified by column chromatography on 60-120 mesh silica gel (Merck, India). For TLC, Merck plates coated with silica gel 60, F_{254} were used. FT-IR spectra were recorded in FT-IR 8300 SHIMADZU spectrophotometer. The ^{1}H & ^{13}C NMR spectra were recorded at 300 MHz and 75 MHz respectively on Bruker AV 300 spectrometer in $CDCl_3$. Splitting patterns of protons were described as s (singlet), d (doublet), t (triplet), q (quartet), m (multiplet) and dd (doublet of doublet). Chemical shifts (δ) were reported in parts per million (ppm) relative to TMS as internal standard. *J* values (coupling constant) were reported in Hz (Hertz). ^{13}C NMR spectra were recorded with complete proton decoupling ($CDCl_3$: δ 77.0 ppm). Centrifugation was performed in REMI R-8C DX centrifuge.

I.D.5.2 Preparation of graphene oxide (GO)

Graphene oxide was prepared by following Tour's method.[71] In this method a 9:1 (v/v) mixture of H_2SO_4 / H_3PO_4 (180:20 mL) was added to a mixture of graphite powder (1.5 g) and $KMnO_4$ (9.0 g). The mixture was then stirred at 50 °C for 12 h. After cooling the mixture to room temperature, it was gradually poured into crushed ice (200 g), which was followed by the slow addition of H_2O_2 (30%, 1.5 mL). The solution was then centrifuged (5000 rpm) and the supernatant was discarded. The residual solid material was successively washed with deionised water (100 mL) and then with 30% HCl (100 mL). The solid material was then repeatedly washed with water and centrifuged. Finally, the solid brown material was collected and dried at 60 °C under vacuum to obtain solid graphene oxide.

I.D.5.3 Typical procedure for the synthesis of thioethers using flow reaction technique

The flow reactor was prepared in a chromatographic column, the base of which was plugged with a thick layer of cotton. It was then supported with graphene oxide catalyst (300 mg) and the height of the catalyst bed was 2 mm. A solution of the aromatic amine (1 mmol) and *t*-BuONO (1.2 equiv, 0.14 mL) in CH_3CN (2 mL) was added to the reactor column. The temperature of the reactor column was maintained at 0-5 °C for 30 minutes. After that a solution of thiol (1 mmol) in CH_3CN (6 mL) was added to the reaction bed drop wise at a

flow rate of 0.016 mL/min. Once the addition had been completed, the reactor bed was eluted with ethyl acetate (3 x 5 mL) and all organic parts were collected in a flask. Evaporation of the solvents under vacuum afforded the residue, which was again passed through a short column of silica gel using light petroleum ether and ethyl acetate as eluent to afford the desired unsymmetrical thioethers. All products were characterized by ^{1}H and ^{13}C NMR spectroscopy and compared with the reported melting points for known solid compounds.

I.D.5.4 Characterization data for various thioethers (**3a-3l**)

(4-Methoxyphenyl)(phenyl)sulfane (3a)[47]

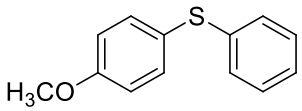

Orange liquid; **^{1}H NMR (300 MHz, CDCl$_3$)**: δ 3.82 (s, 3H), 6.90 (dd, *J* = 6.6 and 2.1 Hz, 2H), 7.11–7.26 (m, 5H), 7.42 (dd, *J* = 6.9 and 2.1 Hz, 2H); **^{13}C NMR (75 MHz, CDCl$_3$)**: δ 55.3, 114.9, 124.1, 125.6, 128.0, 128.8, 135.3, 138.5, 159.7.

(3-Methoxyphenyl)(phenyl)sulfane (3b)[47]

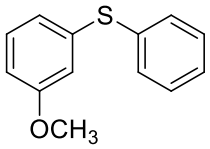

Yellow liquid; **^{1}H NMR (300 MHz, CDCl$_3$)**: δ 3.71 (s, 3H), 6.74 (dd, *J* = 8.1 and 2.7 Hz, 1H), 6.85–6.90 (m, 2H), 7.14–7.29 (m, 4H), 7.34–7.37 (m, 2H); **^{13}C NMR (75 MHz, CDCl$_3$)**: δ 55.1, 112.6, 115.8, 122.8, 127.1, 129.1, 129.8, 131.2, 135.1, 137.1, 159.9.

(4-Chlorophenyl)(4-methoxyphenyl)sulfane (3c)[47]

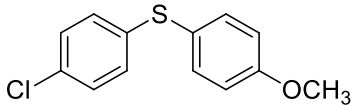

White solid; m.p.: 62–63 °C; **^{1}H NMR (300 MHz, CDCl$_3$)**: δ 3.81 (s, 3H), 6.89 (dd, *J* = 6.6 and 2.1 Hz, 2H), 7.06 (dd, *J* = 6.6 and 2.1 Hz, 2H), 7.18 (dd, *J* = 6.6 and 2.1 Hz, 2H), 7.40 (dd, *J* = 6.7 and 2.4 Hz, 2H); **^{13}C NMR (75 MHz, CDCl$_3$)**: δ 55.3, 115.1, 123.7, 128.9, 129.2, 131.5, 135.4, 137.3, 160.0.

(3-Chlorophenyl)(2-methoxyphenyl)sulfane (3d)

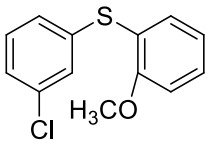

Orange liquid; **^{1}H NMR (300 MHz, $CDCl_3$)**: δ 3.83 (s, 3H), 6.89–6.94 (m, 2H), 7.11–7.18 (m, 3H), 7.20–7.34 (m, 3H); **^{13}C NMR (75 MHz, $CDCl_3$)**: δ 55.8, 111.2, 121.3, 121.5, 126.4, 127.6, 129.2, 129.7, 129.9, 133.6, 134.6, 137.9, 158.2.

1-(3-((4-Fluorophenyl)thio)phenyl)ethanone (3e)

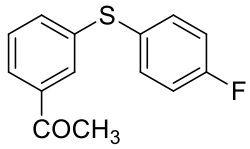

Colourless liquid; **^{1}H NMR (300 MHz, $CDCl_3$)**: δ 2.55 (s, 3H), 7.03–7.08 (m, 2H), 7.35–7.44 (m, 4H), 7.75–7.82 (m, 2H); **^{13}C NMR (75 MHz, $CDCl_3$)**: δ 26.5, 116.5, 116.7, 118.0, 126.3, 128.7, 129.2, 133.4, 134.7, 134.8, 137.7, 38.2, 132.2, 134.3, 197.3.

(4-Nitrophenyl)(*p*-tolyl)sulfane (3f)[72]

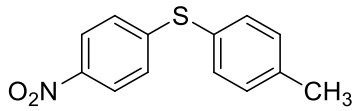

Yellow solid; m.p.: 81–83 °C; **^{1}H NMR (300 MHz, $CDCl_3$)**: δ 1.79 (s, 3H), 6.50 (d, *J* = 7.5 Hz, 2H), 6.65 (d, *J* = 7.8 Hz, 2H), 6.81 (d, *J* = 7.8 Hz, 2H), 7.41 (d, *J* = 7.5 Hz, 2H); **^{13}C NMR (75 MHz, $CDCl_3$)**: δ 20.7, 123.3, 125.6, 130.2, 134.4, 139.6, 144.6, 148.6.

Heptyl(3-methoxyphenyl)sulfane (3g)[73]

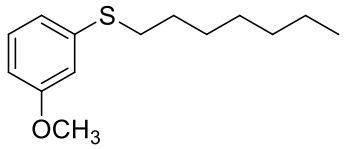

Yellow liquid; **^{1}H NMR (300 MHz, $CDCl_3$)**: δ 0.85–0.90 (m, 3H), 1.25–1.32 (m, 8H), 1.39–1.41 (m, 2H), 1.60–1.68 (m, 1H), 2.91 (t, *J* = 7.2 Hz, 2H), 6.86–6.71 (m, 1H), 6.85–6.91 (m, 2H), 7.15–7.25 (m, 1H); **^{13}C NMR (75 MHz, $CDCl_3$)**: δ 14.0, 22.6, 28.8, 29.1, 31.3, 31.7, 33.3, 55.2, 111.2, 114.0, 120.8, 129.6, 138.5, 159.8.

Pentyl(*o*-tolyl)sulfane (3h)[74]

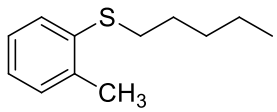

Colourless liquid; **^{1}H NMR (300 MHz, $CDCl_3$)**: δ 0.89 (t, *J* = 6.6 Hz, 3H), 1.31–1.41 (m, 4H), 1.64–1.68 (m, 2H), 2.35 (s, 3H), 2.87 (t, *J* = 6.9 Hz, 2H), 7.03–7.07 (m, 1H), 7.13 (s, 2H), 7.23 (d, *J* = 7.5 Hz, 1H); **^{13}C NMR (75 MHz, $CDCl_3$)**: δ 13.9, 20.2, 22.2, 28.6, 31.1, 32.7, 125.1, 126.2, 127.2, 129.9, 136.3, 137.1.

(4-Bromo-2-methylphenyl)(pentyl)sulfane (3i)

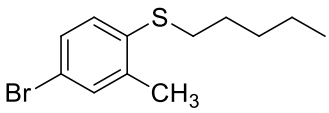

Orange liquid; **^{1}H NMR (300 MHz, CDCl$_3$)**: δ 0.89 (t, *J* = 6.9 Hz, 3H), 1.31–1.42 (m, 4H), 1.58–1.66 (m, 2H), 2.30 (s, 3H), 2.83 (t, *J* = 7.2 Hz, 2H), 7.06 (d, *J* = 8.4 Hz, 1H), 7.23–7.27 (m, 2H); **^{13}C NMR (75 MHz, CDCl$_3$)**: δ 13.9, 20.0, 22.2, 28.4, 31.0, 32.6, 118.6, 128.4, 129.1, 132.5, 135.6, 138.9, 162.1.

4-(*p*-Tolylthio)pyridine (3j)[75]

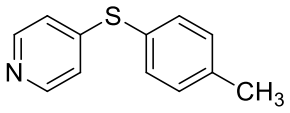

Yellow solid; m.p.: 56–57 °C; **^{1}H NMR (300 MHz, CDCl$_3$)**: δ 2.41 (s, 3H), 6.89–6.91 (m, 2H), 7.26 (d, *J* = 7.2 Hz, 2H), 7.43 (d, *J* = 7.2 Hz, 2H), 8.30–8.31 (m, 2H); **^{13}C NMR (75 MHz, CDCl$_3$)**: δ 21.3, 120.4, 125.5, 130.7, 135.3, 140.1, 149.2, 151.0.

2-((4-Methoxyphenyl)thio)pyridine (3k)[51]

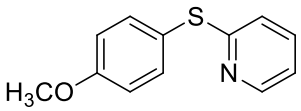

Orange solid; m.p.: 50–52 °C; **^{1}H NMR (300 MHz, CDCl$_3$)**: δ 3.84 (s, 3H), 6.76–6.78 (m, 1H), 6.93–6.97 (m, 3H), 7.39–7.54 (m, 3H), 8.39–8.40 (m, 1H); **^{13}C NMR (75 MHz, CDCl$_3$)**: δ 55.3, 115.2, 118.0, 119.3, 120.2, 120.9, 136.5, 137.1, 149.3, 160.5, 162.7.

Naphthalen-2-yl(*p*-tolyl)sulfane (3l)[72]

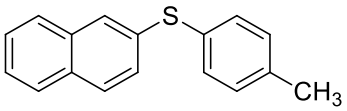

White solid; m.p.: 70–71 °C; **^{1}H NMR (300 MHz, CDCl$_3$)**: δ 2.35 (s, 3H), 7.14 (d, *J* = 7.8 Hz, 2H), 7.31–7.36 (m, 3H), 7.40–7.47 (m, 2H), 7.68–7.79 (m, 4H); **^{13}C NMR (75 MHz, CDCl$_3$)**: δ 20.5, 122.2, 125.8, 126.6, 127.0, 127.2, 127.7, 128.0, 129.4, 130.7, 131.3, 131.4, 133.1, 133.6, 136.9.

I.D.5.5 Scanned copies of ^{1}H and ^{13}C NMR spectra of (4-chlorophenyl)(4-methoxyphenyl)sulfane (3c)

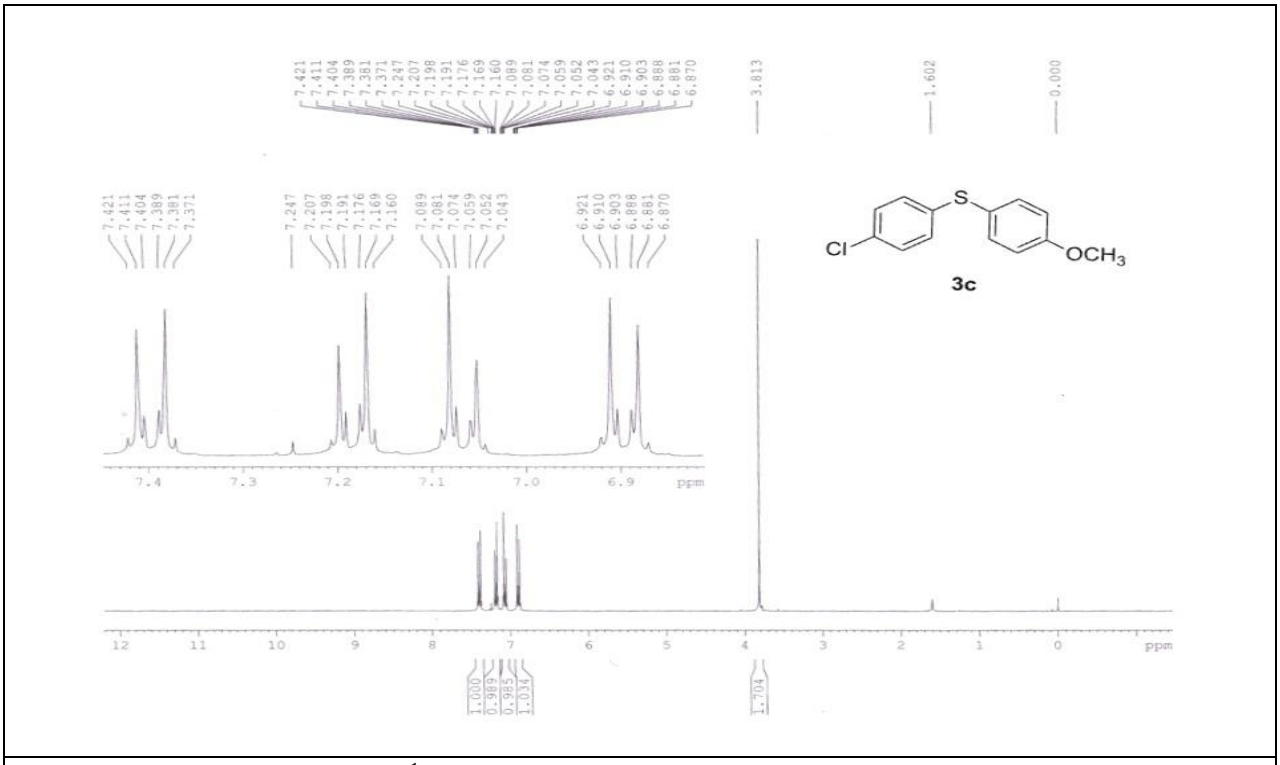

Figure I.D.7 Scanned copy of ^{1}H NMR spectrum of (4-chlorophenyl)(4-methoxyphenyl)sulfane (**3c**)

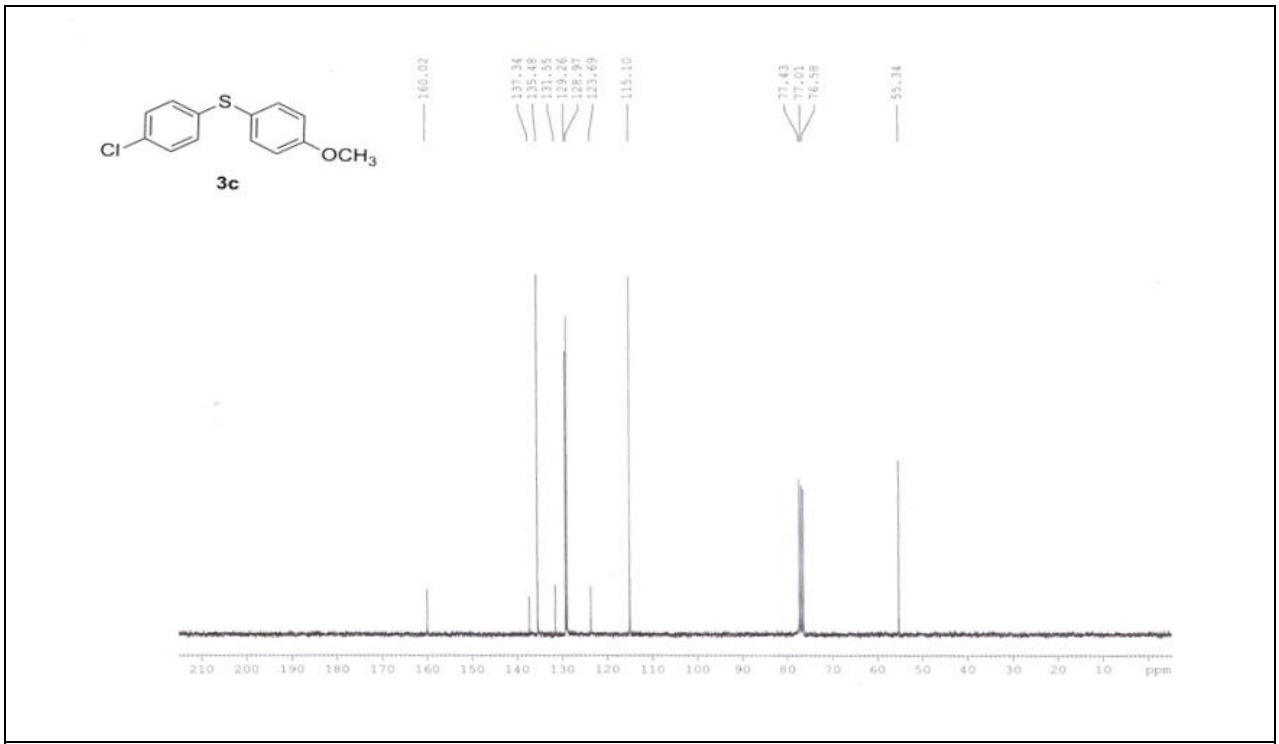

Figure I.D.8 Scanned copy of ^{13}C NMR spectrum of (4-chlorophenyl)(4-methoxyphenyl)sulfane (**3c**)

I.D.6 References

References are given in BIBLIOGRAPHY under Chapter I, Section D.

Chapter II

Section A

Graphene-based Composites in Heterogeneous Catalysis

II.A.1 Graphene-based nanocomposites

Owing to the high surface area, excellent conductivity, heterogeneous nature and low manufacturing cost, graphene-based materials have emerged as a new dimension in catalysis.[1] Pristine graphene has two-dimensional structure which easily aggregates due to the π-π interaction between individual graphene layers.[2,3] This stacking of individual layers limits its applications in different fields. Thus it is necessary to surmount graphene's extreme hydrophobic nature which leads to its aggregation. This has been done by the functionalization of graphene nanosheets with other mesoporous/microporous materials.[4] Graphene-based composites have received paramount attention as they are promising candidates for the fabrication of energy conversion devices due to their high energy density.[5] The catalytic efficiency of conventional catalysts largely depends on its surface to volume ratio. In this context, graphene-based catalysts have been found to be extremely useful due to its high surface to volume ratio. This results in an increase in the number of catalytically active sites.

The graphene nanosheets can be blended with different other functional components or materials to form nanocomposites. Most graphene-based composites are composed of two different materials, although ternary composites consisting of more than two materials are also known. The incorporation of a second component could result in the formation of new materials with unique properties due to the synergistic effects of individual components. This provides with a new opportunity for the design and development of new materials and catalysts. Other materials that are used with graphene for the design and development of new functional materials include metal nanoparticles (NPs),[6-8] metal oxides,[9,10] metal-organic framework (MOF),[11,12] polymers,[13,14] bio-materials,[15,16] small organic molecules,[17,18] other nanomaterials like carbon nanotubes and fullerenes,[19,20] mesoporous materials like zeolites, silica, etc.[21-22]

II.A.1.1 Graphene-zeolite composites

Apart from direct functionalization of graphenes with metal and metal oxide NPs, carbonaceous graphene-based composite materials are also used as suitable supports to immobilize metal species for further uses in catalysis.[23] In this context, zeolites have been considered to be a well structured material for blending with graphene.[24] Zeolites are micro-mesoporous and crystalline aluminosilicates with an infinite, three-dimensional framework having large surface area, widely used in catalysis.[5] The catalytic activity of zeolites has been widely used in the petroleum refining industry due to its acid-base properties and hierarchical

structure which can be modulated during its synthesis.[25] Moreover, zeolite supported metal species are used in the production of high-octane gasoline and in hydrocracking process.[26] The immobilization of metal NPs onto graphene-zeolite composites could prevent agglomeration of the NPs and accelerate charge transfer. Over the last few years, composite materials from two-dimensional graphene oxide (GO) or reduced GO (rGO) and three-dimensional zeolite have drawn enormous interests because of noticeable morphological changes found in the resulting composites, and primarily they have been used as metal scavengers, membranes or in water purification.[27-31]

II.A.1.2 Graphene-silica composites

Graphene silica hybrid materials have attracted significant attention because of their remarkable properties.[32,33] Graphene-silica nanocomposite has become one of the superior materials because of their outstanding peoperties.[34] They have been used as adsorbents,[35] catalysts,[36] fillers,[37] and toxic metal ion scavengers.[38] For instance, graphene-silica nanocomposite has been employed for the selective adsorption of Pb^{2+} ions.[39] The most common method for the preparation of graphene-silica nanocomposite has been based on hydrothermal treatments either in presence or absence of surfactants.[22,40] Furthermore, Ag NPs decorated graphene oxide-silica nanocomposite has been synthesized via sol-gel method and employed for the detection of H_2O_2 and glucose.[41]

Chen and co-workers,[42] have synthesized magnetic porous silica-graphene oxide hybrid composites (Fe_3O_4@mSiO_2/GO) and employed it as a potential adsorbent for removal of *p*-nitrophenol from aqueous solutions. R. L. Oliveira described the functionalization of GO surface with organosilanes bearing amine or thiol functionalities and used them as support to immobilize Pd nanoparticles. These new Pd-GO/SiO_2 nanocomposite has been effectively used as a catalyst for the Mizoroki-Heck and Suzuki-Miyaura cross-coupling reactions.[43] The synthesis of ultra-small gold nanoparticles immobilized on mesoporous silica coated graphene oxide (GO) nanosheet has been reported by Zhang and his group.[44] This Au/SiO_2/GO nanocomposite could efficiently catalyze the reduction of *p*-nitrophenol.

II.A.1.3 Graphene-metal composites

Graphenes or functionalized graphenes decorated with metal NPs is an emerging area in catalysis and other versatile applications. There are different strategies that are employed for the immobilization of metal NPs on the surface of graphene. The most common among them has been based on solution based techniques where the liquid wets the surface. Another

approach to construct graphene-metal nanocomposites has been based on chemical functionalization of graphitic surface in order to generate anchoring sites. Graphene oxide (GO) has been generally used for this purpose because the presence of oxygenated groups allows easy functionalization. It has been found that GO is better than its reduced form for the growth of NPs.[45] GO and metal salts or metal precursors are chemically reduced to generate graphene-metal composites.[46,47] An alternate method for the synthesis of metal-graphene composite involves simultaneous reduction of both GO and metals NPs under microwave irradiation.[48,49] Other approaches for the deposition of metal NPs on graphene are electro-deposition,[50] thermal evaporation,[51] photochemical,[52] and solvent-less bulk synthesis.[53] The deposition of metal NPs using this technique depends on several factors like nature of the solvent, type of metal precursor, reducing agents used and the deposition time and temperature. A wide range of noble metal NPs like Au,[54] Pt,[55] Ag,[56] etc., have been immobilized onto graphene surface. Graphene-metal composites based on first row transition metals like Fe,[57] Cu,[58] Ni,[59] and Co,[60] are widely used in catalysis. In addition other reactive metals that are commonly used for preparation of graphene-metal nanocomposites include Pd,[61] Ru,[62] Rh,[63] and Ir.[63] Few examples of graphene-metal nanocomposites that have been used as catalysts are illustrated below.

Dandia and co-workers,[64] have immobilized Ag NPs on the surface of graphene oxide (Ag NPs/GO). The nanocomposite material has been used for the synthesis of pyranopyrazolones in aqueous media. Diverse pyrano[2,3-*c*:6,5-*c*′]dipyrazol-2-ones have been synthesized in 84-96% under ambient conditions (Scheme II.A.1).

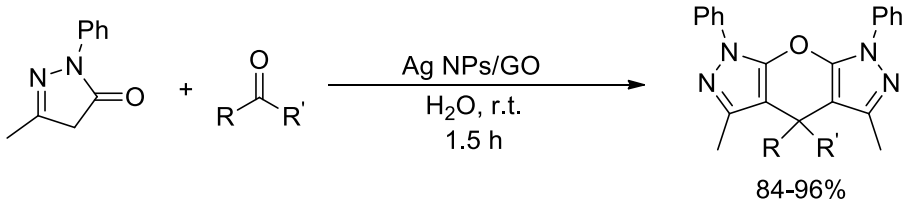

Scheme II.A.1 Ag NPs/GO catalyzed synthesis of pyranopyrazolones.

Palladium nanoparticles immobilized on reduced graphene oxide has been prepared in ionic liquid, [BMIM]PF_6 by phase transfer method (Pd/rGO-IL).[65] The microscopic analysis revealed uniform distribution of Pd NPs on the surface of rGO with average particle size being 2 nm. The nanocomposite catalyst showed excellent activity in Heck coupling reaction (Scheme II.A.2).

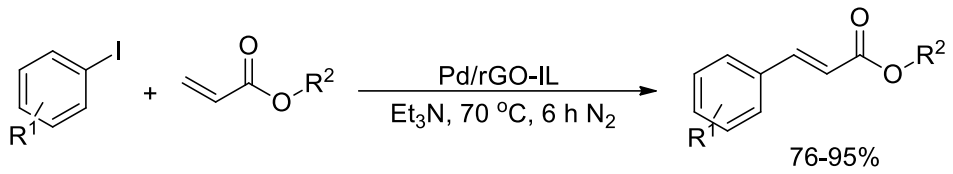

Scheme II.A.2 Pd/rGO-IL catalyzed Heck coupling reaction.

An expedient synthesis of substituted biphenyls via Hiyama cross-coupling reaction (Scheme II.A.3) has been developed by using Pd decorated GO nanosheets under micellar media (Pd-GO/P123). Among the various surfactants, triblock copolymer P123 showed the best results in terms of product yield. The enhanced catalytic activity has been due to the well exfoliation of the graphene oxide layers.[66]

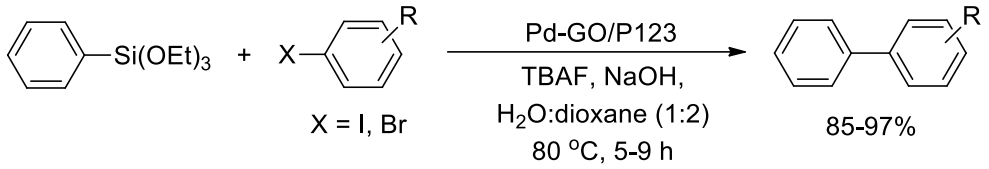

Scheme II.A.3 Hiyama cross-coupling reaction using Pd decorated GO nanosheets.

Gold nanoparticles immobilized on thiol functionalized reduced graphene oxide (AuNPs@rGO-SH) has been prepared and employed for the synthesis of tetrahydro-4*H*-chromenes in aqueous media (Scheme II.A.4). The reaction proceeds through the formation of Knoevenagel intermediate, where gold nanoparticles facilitates polarisation of carbonyl moieties.[67]

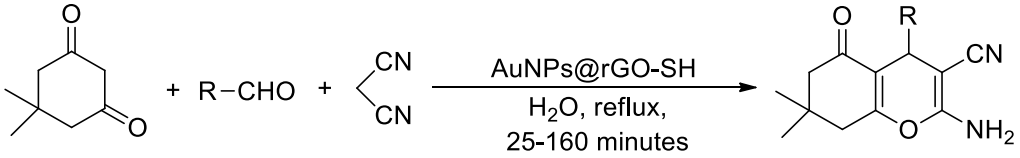

Scheme II.A.4 Synthesis of tetrahydro-4*H*-chromenes using AuNPs@rGO-SH.

The synthesis of propargylamines via A^3 coupling reaction has been accomplished by using $CuCl_2$ immobilized on aminopropyl silane functionalized GO (GO-$CuCl_2$) under microwave irradiation.[68] The heterogeneous nature of the catalyst allowed it to be recycled for five runs without significant loss in its activity (Scheme II.A.5).

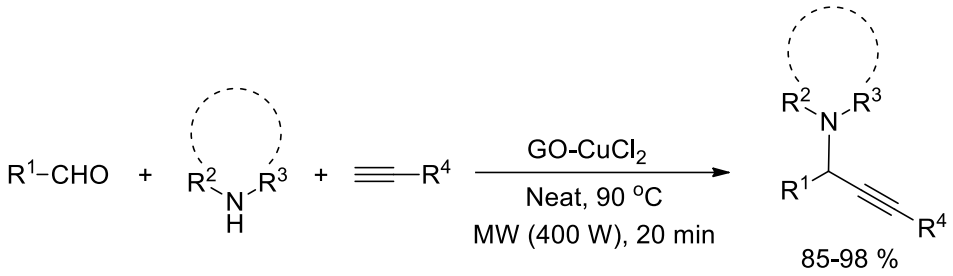

Scheme II.A.5 GO-$CuCl_2$ catalyzed synthesis of propargylamines.

II.A.1.4 Graphene-metal oxide composites

Graphene-metal oxide nanocomposite has been used for energy harvesting, storage devices, nano-optics and in catalysis. Several metal oxide supported graphene nanocomposites have been developed over the last few years. This include TiO_2,[69] MnO_2,[70] SnO_2,[71] Fe_3O_4,[72] Cu_2O,[73] etc. Orth and his group,[74] modified the surface of graphene oxide with thiols for the preparation of sulfur functionalized graphene oxide. The sulfur-functionalized GO has been converted to sorbent by the treatment of TiO_2 or SiO_2. The synthesized sorbent has been used for the removal of Pb^{2+}, Cd^{2+}, Ni^{2+} and Zn^{2+} as heavy metal ions from aqueous solution in batch method.[75]

Reddy and co-workers,[76] have synthesized 1,4-disubstituted-1,2,3-triazoles by using copper oxide supported graphene oxide (CuO-GO) nanocomposite as a heterogeneous catalyst (Scheme II.A.6) in aqueous media at ambient temperature.

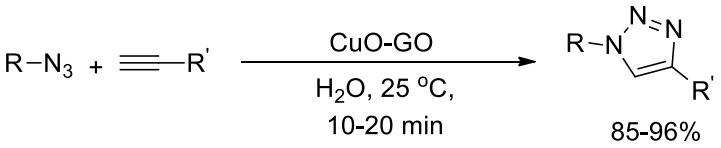

Scheme II.A.6 CuO-GO catalyzed synthesis of 1,4-disubstituted-1,2,3-triazoles.

Magnetic graphene oxide anchored sulfonic acid ($CoFe_2O_4$/GO-SO_3H) has been prepared and used in the synthesis of pyrazolopyridines in deep eutectic solvent under microwave irradiation.[77] A three-component reaction in choline chloride/glycerol as a green solvent afforded the desired products in 84-95% yield (Scheme II.A.7).

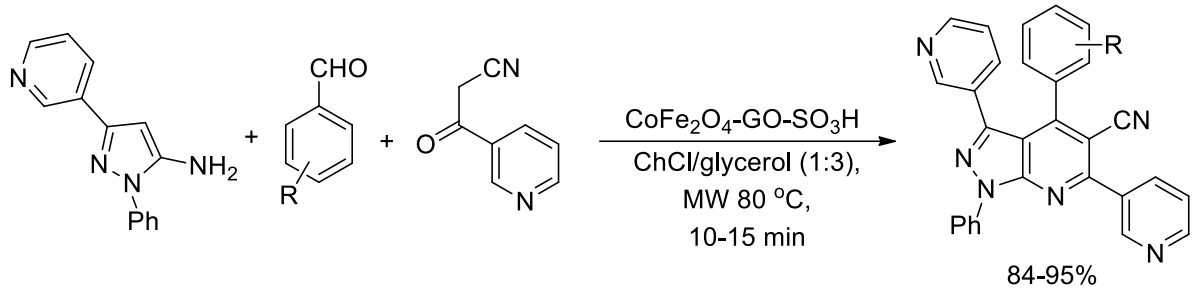

Scheme II.A.7 Microwave assisted synthesis of pyrazolopyridines in deep eutectic solvent.

An efficient synthesis of tetrasubstituted imidazoles using sulfonic acid functionalized magnetic graphene oxide (Fe_3O_4@GO-Pr-SO_3H) nanocomposite has been accomplished.[78] The methodology involves a four-component approach using benzil, aromatic aldehydes, primary amines and ammonium acetate (Scheme II.A.8). A wide range of imidazole derivatives has been formed in 89-94% yields.

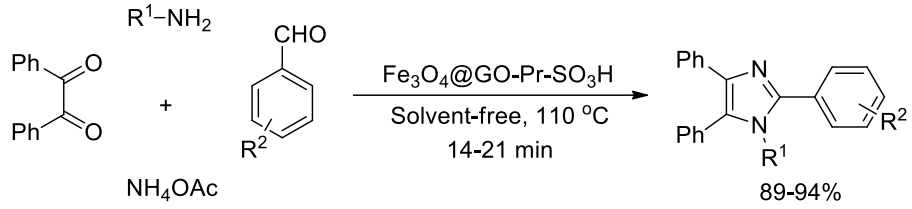

Scheme II.B.8 Synthesis of imidazoles using magnetic graphene oxide nanocomposite.

II.A.2 Conclusion

The trend towards 'green chemistry' necessitates an entire shift from traditional concepts of process efficiency that largely focuses on chemical yield, to the one that assigns economic value to eliminating waste at the source and avoids use of toxic and/or hazardous substances. Keeping in mind the principles of green chemistry, catalysis via nanomaterials has emerged as a revolutionary way to address multifarious challenges. The fundamental aim of nanocatalysis research is to understand mechanisms at molecular level, and then to design and synthesize catalysts with desired activity. To effect the transition from conventional techniques to modern methods, graphene-based nanomaterials have emerged as an important tool. We believe that novel approaches based on nanomaterials could transform the technology used in modern heterogeneous catalysis.

II.A.3 References

References are given in BIBLIOGRAPHY under Chapter II, Section A.

Chapter II

Section B

Ni Decorated Reduced Graphene Oxide Zeolite Nanocomposite Catalyzed Synthesis of 1,2,3-Triazoles

II.B.1 Introduction

Triazoles are ubiquitous in a wide range of biologically active compounds.[1] Unsubstituted triazoles with the molecular formula $C_2H_3N_3$ exhibit two isomeric forms, 1,2,3-triazole and 1,2,4-triazole (Figure II.B.1). The 1,2,3-triazole further exists in three different tautomeric forms: 1,2,3-1*H*-triazole, 1,2,3-2*H*-triazole and 1,2,3-4*H*-triazole (Figure II.B.1). There are numerous examples of triazoles with anti-HIV, anti-inflammatory, anti-cancer, anti-microbial and anti-bacterial activities (Figure II.B.2).[2-5] Apart from their widespread biological properties, functionalized triazoles are also acknowledged for their therapeutic effects and are extensively used as clinical drugs.[2,6] Some of the commonly marketed drug molecules possessing triazole unit are fluconazole (anti-fungal), ravuconazole (anti-fungal), caboxyamidotriazole (anti-cancer), tazobactum (β-lactum antibiotic), cefatrizine (β-lactum antibiotic) and alprazolam (for treating anxiety disorders) (Figure II.B.3). Moreover, 3-amino-1,2,4-triazole has been used as herbicide, cotton defoliant and as inhibitor of mitochondrial and chloroplast functions.[7]

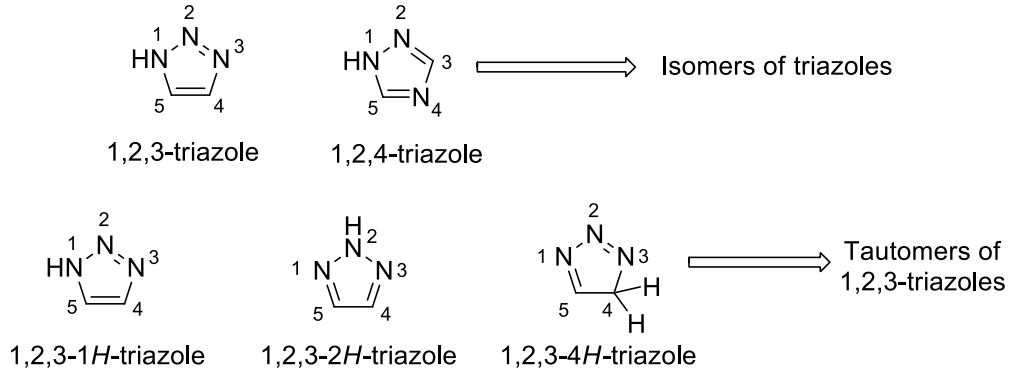

Figure II.B.1 Isomeric and tautomeric forms of various triazoles.

In addition to their biological and pharmacological activities, triazole derivatives like 4-amino-5-mercapto-3-ethyl-1,2,4-triazole (AMET) has been tested as corrosion inhibitors for muntz alloy in solutions.[8] They are also used as water replacements in proton conductors used in fuel cells.[9] Another important application of triazole is in the synthesis of dendrimers.[10] Dendrimers are three dimensional branched macromolecules and are made up of three components, an exterior surface with functional groups, interior branched chains and the central core. They are radially symmetric molecules and their size typically ranges in the nanometer scale. The core of several dendrimers consists of triazole unit (Figure II.B.4). Dendrimers are used for medicinal purposes, in material science, in the stabilization of metal nanoparticles (NPs), etc.[10]

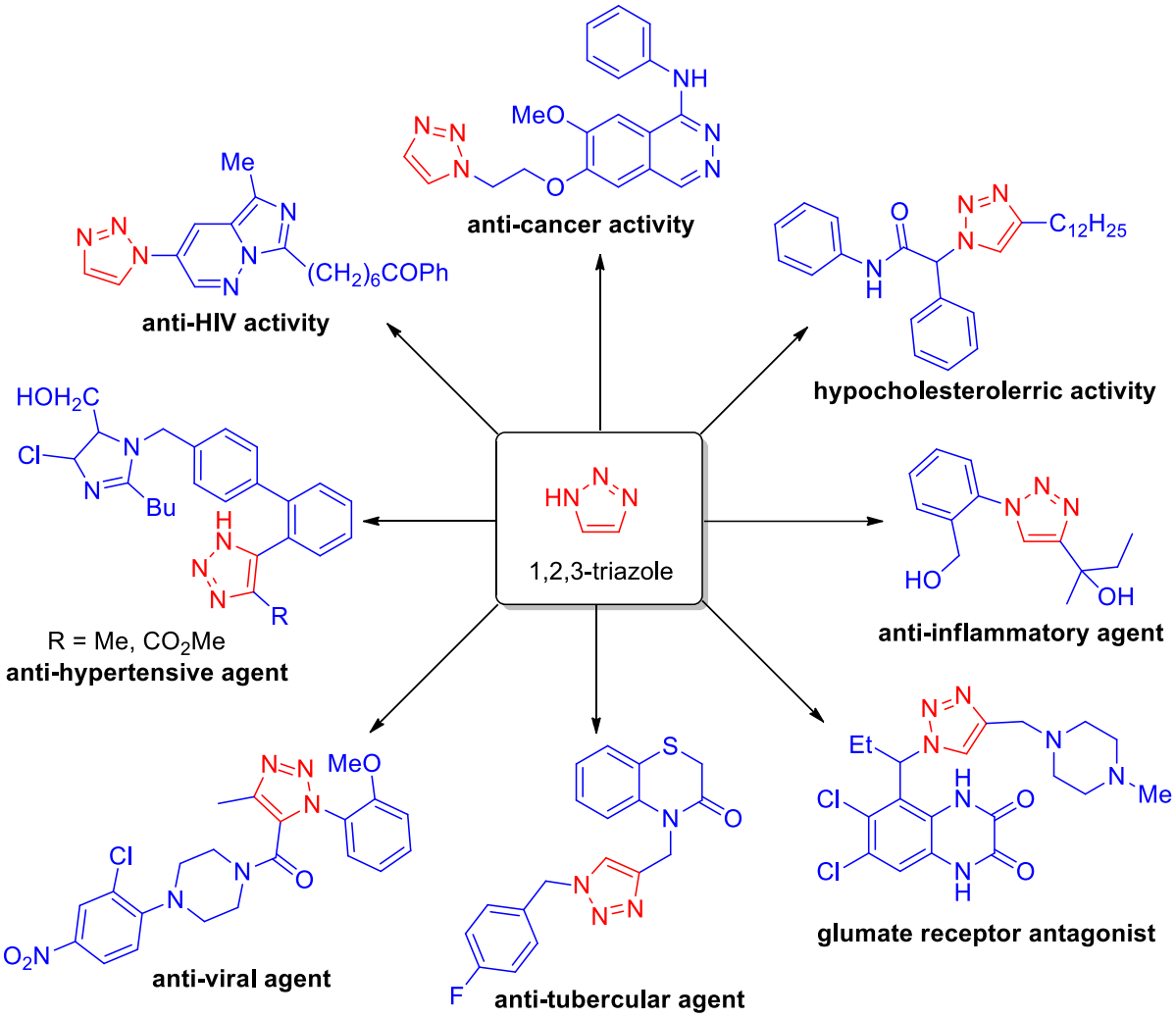

Figure II.B.2 Biologically active triazoles and their potential activities.

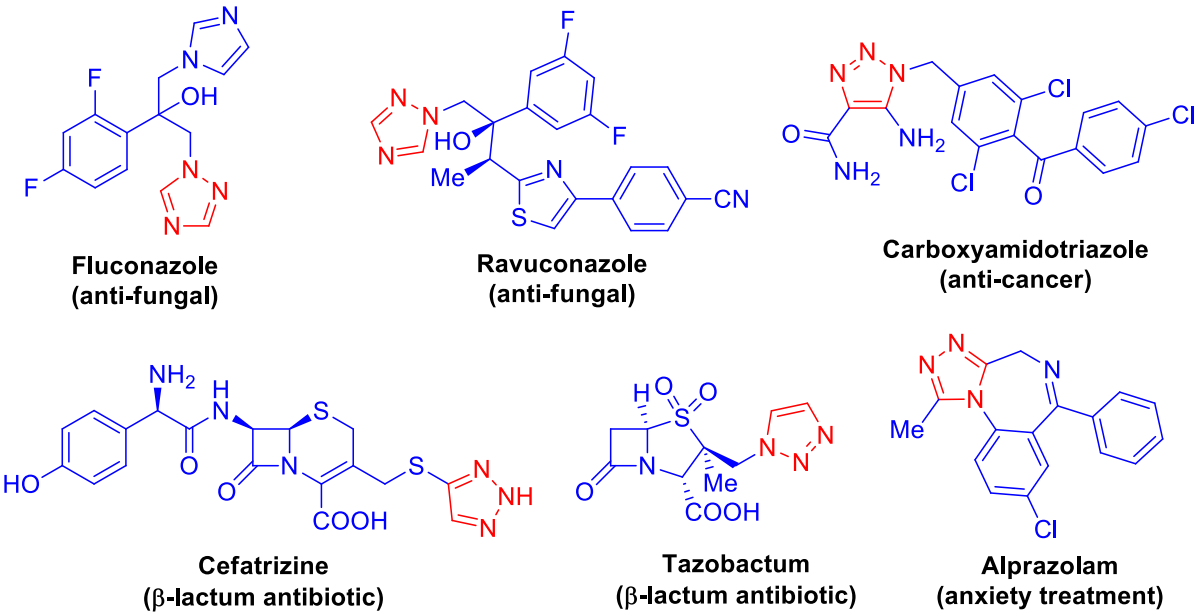

Figure II.B.3 Clinical drugs based on triazole unit.

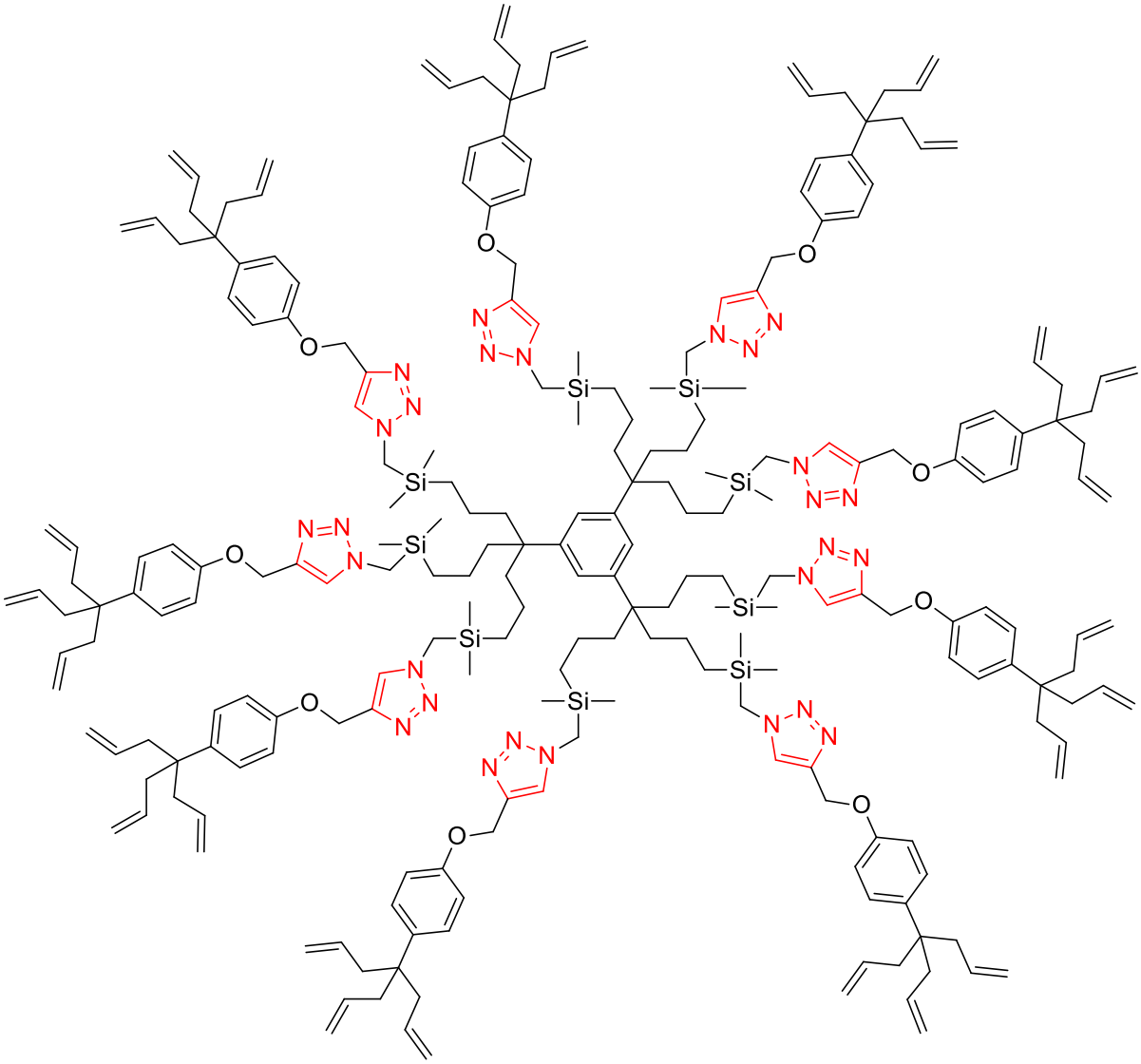

Figure II.B.4 Typical example of a triazole based dendrimer.

Owing to their diverse applications ranging from medicinal chemistry to material science, the synthesis of this scaffold has always been a challenging task for synthetic organic chemists. The most common way of synthesizing 1,2,3-triazole moiety is by employing Huisgen [3+2] cycloaddition reaction between azides and alkynes (Scheme II.B.1).[11-13]

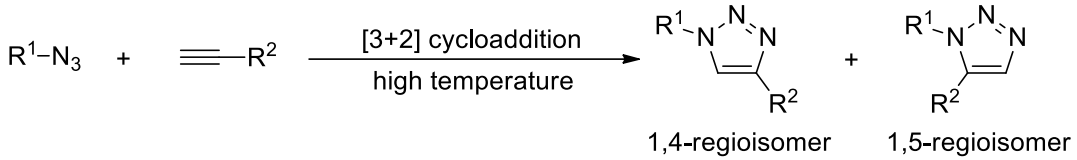

Scheme II.B.1 Huisgen cycloaddition.

However, Huisgen cycloaddition have certain limitations like requirement of high temperature and lack of regioselectivity between 1,4- and 1,5-disubstituted-1,2,3-triazoles. In

2002, Sharpless-Fokin from Scripps Research Institute,[14] and Meldal groups from Carlsberg Laboratory,[15] have independently reported the copper(I) catalyzed version of the Huisgen cycloaddition, which is popularly known as 'click' reaction. The advantage of their protocol lies in the regioselective formation of 1,4-disubstituted-1,2,3-triazole. The reaction employs alkyl azide and alkyne in presence of copper(I) catalyst, which is either added directly or is alternatively generated in situ from copper(II) salt by using a reducing agent. Owing to the toxicity and explosive nature of organyl azides,[16] their direct use is often avoided and an alternative three-component approach involving alkyl halide, sodium azide and terminal alkyne has been adopted (Scheme II.B.2).[17] The reaction between alkyl halide and sodium azide forms alkyl azide, which subsequently reacts with terminal alkyne, furnishing 1,4-disubstituted-1,2,3-triazole as the ultimate product. Thus, the Cu(I) catalyzed azide alkyne cycloaddition (CuAAC) has emerged as one of the fundamental route for the regioselective formation of 1,2,3-triazole scaffolds.[18,19]

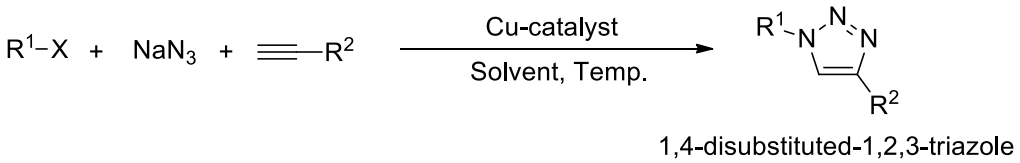

Scheme II.B.2 Copper catalyzed three-component synthesis of 1,2,3-triazole.

II.B.2 Background and objectives

Since the discovery of copper-catalyzed click reaction, various catalytic systems (homogeneous or heterogeneous) have been developed.[20,21] Homogeneous catalysts mainly include copper(I) or copper(II) salts and copper complexes.[20] On the other hand, copper immobilized on diverse insoluble supports like magnetic nanoparticles,[22-24] clay,[25,26] organic polymers,[27,28] silica,[29,30] and zeolites,[31,32] have been used as heterogeneous catalysts. Polymer blended with silica has also been used as support for the preparation of catalysts in CuAAC.[33,34] There are also reports of bimetallic NPs in CuAAC, where one of the congeners acts as a support for the other metal.[34,36] Carbonaceous nanomaterials like graphene oxide (GO),[37-39] reduced graphene oxide (rGO),[40-42] and charcoal,[43,44] are also employed for immobilization of copper in CuAAC. Few representative strategies for click reactions are discussed below.

The synthesis of 1,4-disubstituted-1,2,3-triazoles has been accomplished by using 2-pyrrolecarbaldiminato-Cu(II) complex in aqueous media.[45] The methodology involves three-component reaction between alkyl halides, sodium azide and alkynes and the corresponding

products were obtained in 55-97% yield (Scheme II.B.3). Low catalyst loading (1 mol%), ambient reaction conditions and synthesis of bis-/tris- triazoles are the prominent features of this protocol.

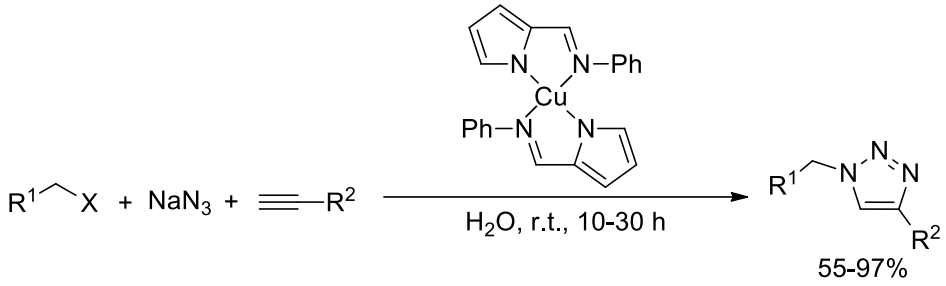

Scheme II.B.3 2-Pyrrolecarbaldiminato-Cu(II) complex catalyzed AAC.

An amphiphilic catalyst derived from tris(triazolyl)-poly(ethylene glycol) and $CuSO_4 \cdot 5H_2O$ (PEG-tristz-Cu^I) has been prepared. The catalyst has been employed for the synthesis of 1,2,3-triazoles (Scheme II.B.4). The protocol was further extended towards the synthesis of diverse functionalized triazoles bearing medicinal and biological importance.[46] Moreover, the catalyst could be reused for six cycles without decomposition.

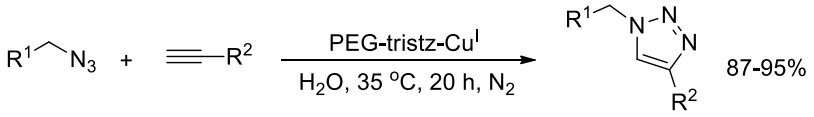

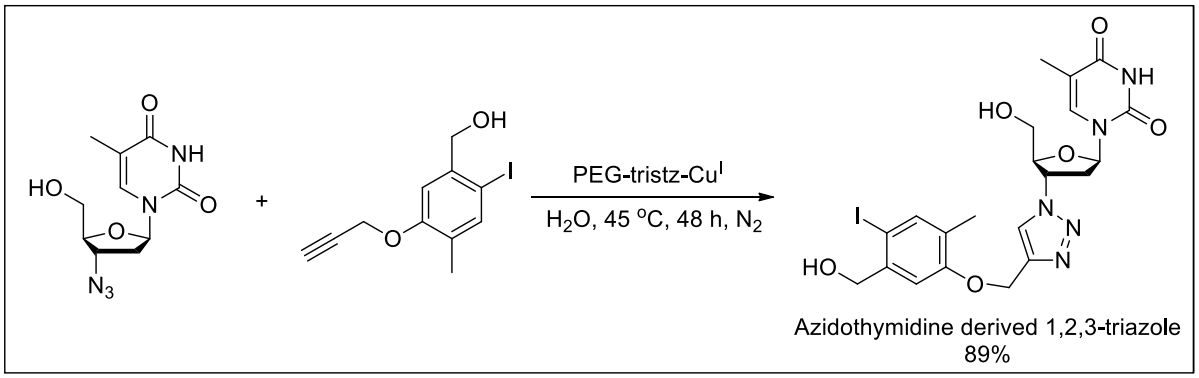

Scheme II.B.4 Synthesis of 1,2,3-triazole derivatives using amphiphilic copper catalyst.

A copper(II) coordinated phenanthroline complex based on SBA-15 framework [Cu(II)phen@SBA-15] has been prepared and characterized by different spectroscopic and microscopic techniques. The hybrid material was used as heterogeneous catalyst for the multicomponent synthesis of 1,2,3-triazoles from terminal alkynes, NaN_3 and alkyl halides (Scheme II.B.5). Moreover, the reaction has been successfully accomplished when alkyl halide was substituted with aryl diazonium salts or epoxides.[47]

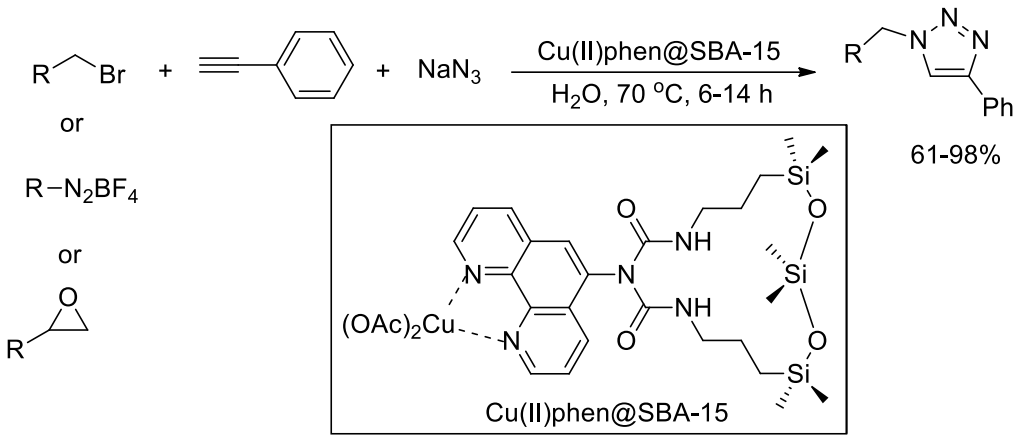

Scheme II.B.5 Multicomponent synthesis of triazoles using Cu(II)phen@SBA-15.

Graphene oxide (GO) decorated with copper(II) porphyrin (GO-CuPPh) has been prepared by cross linking GO and porphyrin in the presence of $Cu(OAc)_2$. The nanocomposite material has been characterized in detail by different spectroscopic techniques. The catalyst was then used for the synthesis of 1,2,3-triazoles under ultrasonic irradiation in aqueous ethanol (Scheme II.B.6).[48] In another report, Reddy and co-workers[37] have prepared graphene oxide supported copper oxide (CuO-GO) nanocomposite. The catalyst has been employed in the synthesis of 1,4-disubstituted-1,2,3-triazoles in water at ambient temperature (Scheme II.B.6). The investigators suggested that the oxygenated functional groups present on the surface of GO prevent the aggregation of CuO during the course of the reaction.

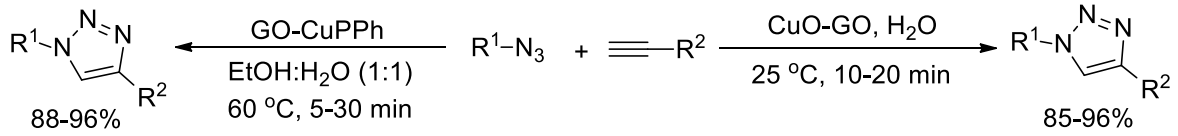

Scheme II.B.6 Graphene based materials in the synthesis of 1,2,3-triazoles.

Microwave assisted synthesis of 1,4-disubstituted-1,2,3-triazoles using copper(II) precatalyst in methanol has been achieved under ligand-free conditions (Scheme II.B.7). Copper(II) catalyzed click reactions are facile and generally requires the presence of a reducing source. However, the present system represents a reductant free protocol where Cu(II) species are efficiently reduced by methanol in presence of alkynes to form polymeric alkynylcopper(I) precatalyst, which subsequently reacts with azides, leading to the formation of triazoles.[49]

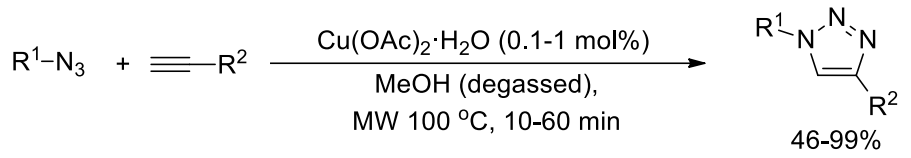

Scheme II.B.7 Microwave assisted synthesis of 1,2,3-triazoles.

Ionic liquid mediated green synthesis of 1,2,3-triazoles has been demonstrated by using copper iodide as catalyst (Scheme II.B.8). The authors have employed 1-methyl-3-butylimidazolium hydroxide [Bmim]OH, as an alternative to traditional solvents and the corresponding products were obtained in 30-99% yield.[50]

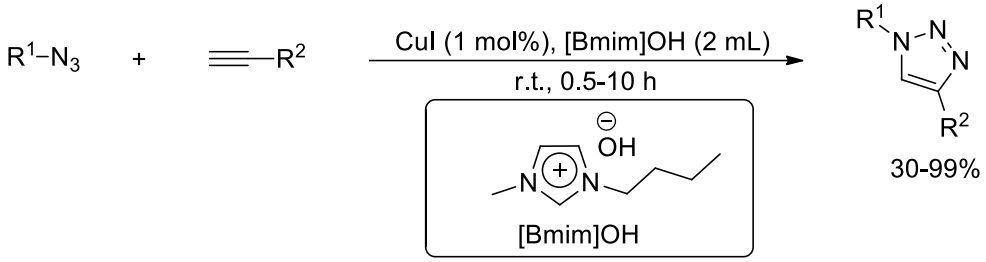

Scheme II.B.8 [Bmim]OH mediated CuI catalyzed synthesis of triazoles.

Copper iodide in combination with eosin Y (photoredox catalyst) has been used in the three-component synthesis of 1,4-disubstituted-1,2,3-triazoles (Scheme II.B.9). The reaction conditions involve photo-irradiation using compact fluorescent lamp (CFL, 23 W) in aqueous ethanol as solvent. Diverse 1,2,3-triazoles were obtained in 69-87% yield and a plausible mechanism involving single electron transfer (SET) has been proposed.[51]

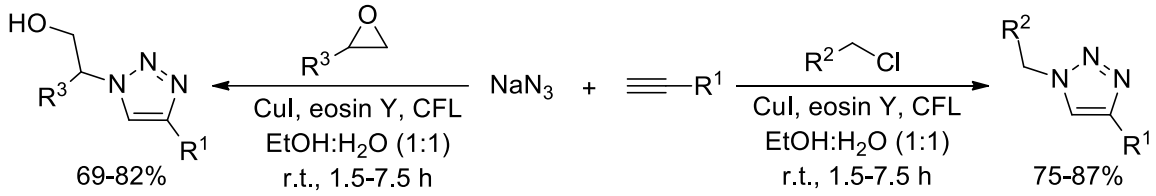

Scheme II.B.9 Synthesis of 1,2,3-triazoles using CuI in presence of eosin Y.

A four-component strategy involving sequential Ugi, cycloaddition and Knoevenagel condensation leading to the formation of diverse 3-triazolyl-quinolin-2-(1*H*)-ones has been accomplished by using $Cu(OAc)_2 \cdot H_2O$ (Scheme II.B.10). The reaction conditions are mild and the products can be obtained in one-pot without isolation of intermediates.[52]

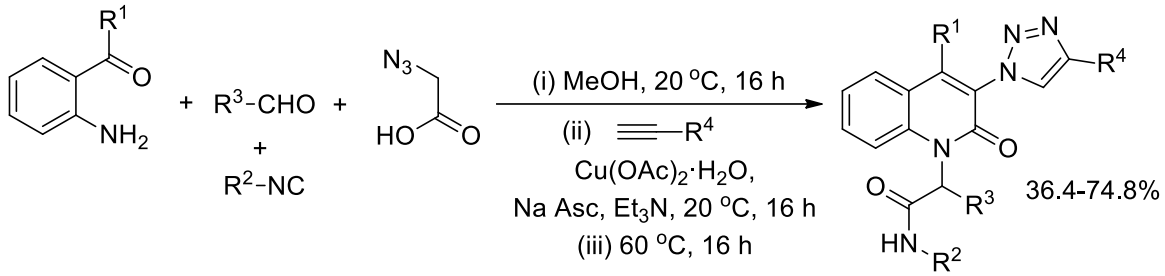

Scheme II.B.10 One-pot four-component synthesis of 3-triazolyl-quinolin-2-(1*H*)-ones.

A series of diverse polycyclic triazoles has been synthesized by using Cu/Pd dual metal catalysis.[53] The first step of the reaction involves CuI catalyzed azide alkyne cycloaddition, followed by palladium catalyzed C–H bond functionalization (Scheme II.B.11). The catalytic system has been successfully applied for the gram scale synthesis of polycyclic triazoles.

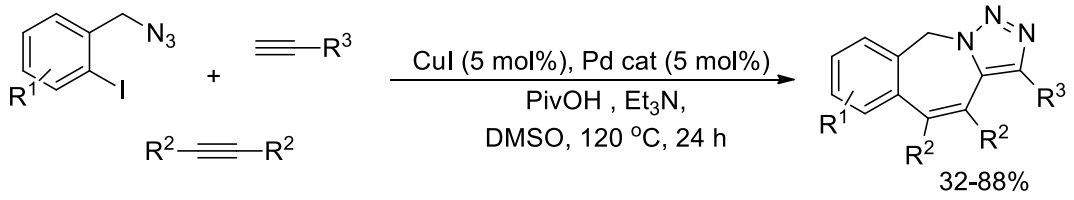

Scheme II.B.11 Synthesis of functionalized triazoles by Cu/Pd dual metal catalysis.

The use of copper based catalytic systems has been the primary choice when it comes to regioselective synthesis of 1,2,3-triazoles. However, copper catalysts are often associated with certain limitations. The mechanistic studies of CuAAC showed that the reaction proceeds through the formation of Cu-acetylide intermediate.[19] This intermediate tends to polymerize, which has a detrimental effect on the rate of the reaction and overall yield of the product.[18] Moreover, when CuAAC is carried out using Cu(II) species, the use of a reducing agent becomes indispensable. In view of these shortcomings, the development of new catalysts based on transition metals other than copper has been gaining popularity. There are few examples where transition metals like Ru, Ag, Au, Ir and Zn are used for azide alkyne cycloaddition.[54-56] Ruthenium is the second most widely employed transition metal for click reaction.[57] However, the Ru-catalyzed version, unlike, CuAAC, regioselectively forms 1,5-disubstituted-1,2,3-triazole as the major product. Jia and co-workers[58] while experimenting with ruthenium complexes discovered that certain complexes could efficiently catalyze the AAC (RuAAC). The reaction between alkyl azides and terminal alkynes using $Cp^*RuCl(PPh_3)_2$ (1-2 mol%) affords 1,5-disubstituted-1,2,3-triazoles, in almost 100% regioselectivity (Scheme II.B.12). Moreover, the catalyst also proved to be effective when

terminal alkynes have been replaced by diphenyl acetylene leading to the formation of 1,4,5-trisubstituted triazoles. The authors proposed a plausible mechanism involving the formation of ruthenacycle intermediate. This intermediate then undergoes reductive elimination to form the desired triazole product. Another microwave assisted protocol for the synthesis of 1,5-disubstituted-1,2,3-triazoles has been accomplished by using the same catalyst [Cp*RuCl(PPh_3)$_2$].[59]

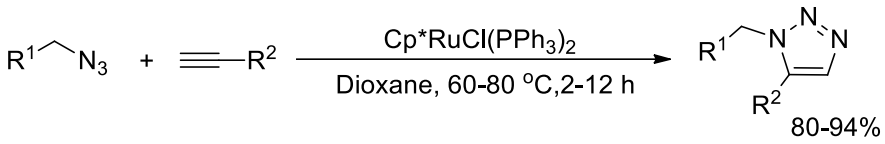

Scheme II.B.12 Cp*RuCl(PPh_3)$_2$ catalyzed synthesis of 1,5-disubstituted-1,2,3-triazoles.

While nickel catalysts have been used in several organic reactions its application towards triazole synthesis via azide alkyne cyaloaddition has been less explored. Literature reports reveal that there are two homogeneous catalytic systems, and one heterogeneous catalytic system have been reported for AAC.[60-63] Raney nickel has been used as catalyst for the [3+2] cycloaddition reaction between alkyl azide and terminal alkyne.[60] However, the lack of regioselectivity in case of some substrates resulted in a mixture of 1,4- and 1,5-disubstituted-1,2,3-triazoles, thereby limiting the scope of the reaction (Scheme II.B.13). Besides, Raney nickel contains certain amount of Al_2O_3, which could lead to side reactions thereby lowering the yield of the products.[64] Moreover, its stringent storage condition and pyrophoric nature renders difficulty in handling this compound. The authors conducted control experiments to probe into the mechanistic pathway, which ruled out the formation of Ni-acetylide intermediate. On the basis of isotopic experiments the authors proposed a mechanism which involved π-complexation of alkyne with nickel followed by the formation of metallacycle intermediate.

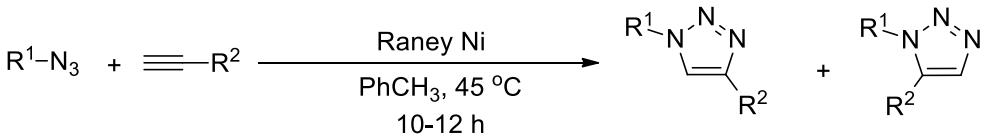

Scheme II.B.13 Raney nickel catalyzed azide alkyne cycloaddition.

Recently, Hong and co-workers developed another Ni-catalyzed azide alkyne cycloaddition (NiAAC) using a combination of nickelocene (Cp_2Ni) and Xantphos, which however leads to the formation of 1,5-disubstituted-1,2,3-triazoles as the major product.[61] The actual catalyst in this case is Ni(Xantphos)$_2$, generated in situ from Cp_2Ni and Xantphos. Although, this

expensive catalytic system (Cp_2Ni-Xantphos) can be used for both terminal and internal alkynes, its ligand-specific nature and non-recoverability limits its further uses. Besides, Cp_2Ni is moisture sensitive and decomposes on exposure to air. In another report the same group reported NiAAC using the same catalyst Cp_2Ni, however, in this case internal alkyne has been used in place of terminal alkynes (SchemeII.B.14).[62]

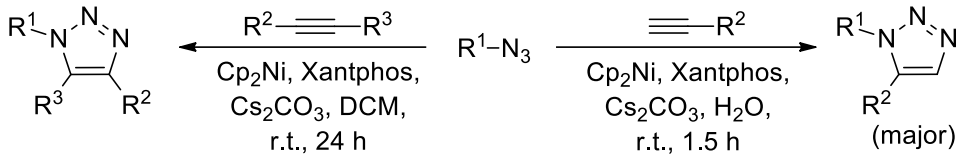

Scheme II.B.14 Cp_2Ni catalyzed azide alkyne cycloaddition.

The heterogeneous Ni catalyst has been based on triazole linked organic polymer (Ni-TLOP).[63] This catalyst has been employed as a photocatalyst in AAC under visible light irradiation (Scheme II.B.15). Although the heterogeneous catalyst (Ni-TLOP) exhibits high catalytic performance in AAC, the catalyst preparation requires some expensive chemicals; the catalyst becomes active only under visible light irradiation, and studied in a two-component AAC process. Moreover, the exact wavelength of light used during the photochemical reaction has not been indicated.

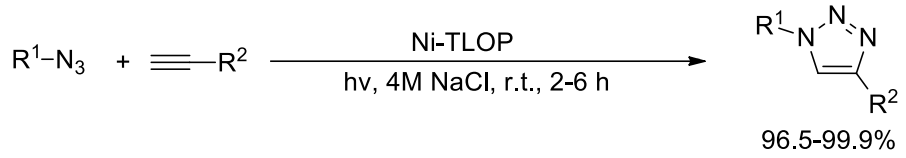

Scheme II.B.15 Ni-TLOP catalyzed AAC.

II.B.3 Present work: Results and discussions

Graphene-based composites are often used as suitable supports to immobilize metal species for further uses in catalysis.[65,66] On the other hand, zeolites are microporous and crystalline aluminosilicates with an infinite, three-dimensional framework having large surface area, widely used in catalysis.[67] However, such composite nanomaterials with large surface area, rich π-electron networks and/or diverse functionalities have not been explored to decorate with metallic species and subsequent uses in catalysis. This work is primarily aimed at developing new ternary composite nanomaterials for use as sustainable catalyst in organic transformations. The triazole synthesis via click chemistry has been a continuous field of development. The previously reported Ni-catalyzed AAC (NiAAC) employs two-component strategy for the synthesis of triazoles from azides and alkynes. Now, the synthesis of azide

requires and additional step, which can be subdued by employing a three-component strategy involving alkyl halides, NaN_3 and terminal alkynes. The primary focus of this advancement has been directed towards easy accessibility and stability of the heterogeneous Ni catalysts that could eliminate the above limitations, and exhibit versatile applications in the three-component click triazole synthesis under sustainable reaction conditions. We have prepared the nanocomposite from graphene oxide (GO) and NaY Zeolite, which has been subsequently decorated with nickel species in presence of $NaBH_4$ resulting in situ reduction of GO to rGO to obtain finally a ternary composite material, designated as Ni–rGO–zeolite. The new ternary composite (Ni–rGO–zeolite) has been employed as an efficient and sustainable heterogeneous catalyst in three-component azide alkyne cycloaddition (NiAAC) in aqueous conditions (Scheme II.B.16).

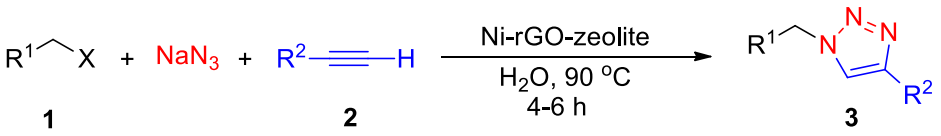

Scheme II.B.16 Ni–rGO–zeolite catalyzed three-component click reaction.

II.B.3.1 Preparation of Ni–rGO–zeolite nanocomposite

The GO–zeolite composite was prepared by adding an aqueous suspension of sodium Y (NaY) zeolite (pH ~ 11.2) to an aqueous dispersion of GO (pH ~ 3.4), so as to obtain nearly neutral pH of the overall aqueous suspension. The aqueous suspension containing GO and NaY zeolite was then heated at 60 °C for 16 h under gentle magnetic stirring followed by evaporation of water and drying under vacuum to afford the GO–zeolite composite (details are in the experimental section).

The nickel decorated rGO–zeolite material (Ni–rGO–zeolite) was then prepared by the addition of nickel acetate to a suspension of finely powdered GO–zeolite material in ethylene glycol followed by the addition of sodium borohydride. The contents were then stirred at 180 °C for 3 h (details are in the experimental section).

II.B.3.2 Characterization of Ni–rGO–zeolite nanocomposite

The presence of nickel in the ternary nanocomposite was measured by inductively coupled plasma atomic emission spectroscopy (ICP-AES). For this purpose, the nanocomposite catalyst (5 mg) was digested with aqua regia (6 mL) and the nickel content was estimated to be 0.887 mmol g^{-1} of the Ni–rGO–zeolite nanocomposite.

The FT-IR spectra of Ni–rGO–zeolite, GO–zeolite, NaY zeolite and GO were recorded in the range 4000-400 cm^{-1} (Figure II.B.5). In the case of GO, the peaks at 1729 and 1627 cm^{-1} were due to the stretching vibrations of C=O and C=C bonds respectively.[68] The broad peak at around 3432 cm^{-1} was related to the stretching vibration of hydroxyl groups present in GO.[68] On the contrary, GO–zeolite and Ni–rGO–zeolite, showed peaks at 1022, 578 and 454 cm^{-1}. These peaks were due to the internal vibrations of TO_4 (T = Si, Al) tetrahedral moiety of NaY zeolite.[69,70] Furthermore, the typical carbonyl band of GO at 1729 cm^{-1} also disappeared which indicates that the carbonyl groups might have been converted to Al/Si–O–C band resulting in the formation of the nanocomposite.[71]

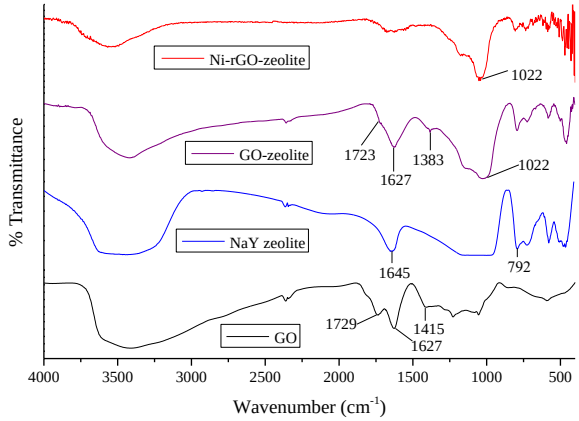

Figure II.B.5 FT-IR spectra of GO, NaY zeolite, GO–zeolite and Ni–rGO–zeolite.

It is worth mentioning that transformation of GO to rGO is expected during the hydrothermal treatment of GO–zeolite composite. The hydrothermal treatment was performed to ensure incorporation of nickel into the nanocomposite material. A comparative Raman spectral analysis has been undertaken to get detail insight into the conversion of GO to rGO (Figure II.B.6). The presence of D and G band along with the 2D related bands in Raman spectrum of the nanocomposite conform to the transformation of GO to rGO. The Raman spectrum of GO–zeolite composite shows sharp 2D peak along with the obvious D and G bands. As expected the higher intensity of G band (I_G) than that of D band (I_D) has been observed here. Whereas, after the hydrothermal treatment not only the intensity of D band has increased resulting in $I_D/I_G>1$ but also the 2D band (appeared at 2705 cm^{-1} in case of GO–zeolite) slightly shifted towards lower wavenumber at 2690 cm^{-1} (Figure II.B.6). Such observation corroborated transformation of GO to rGO via reformation of graphitic regions in the sheet.[72,73]

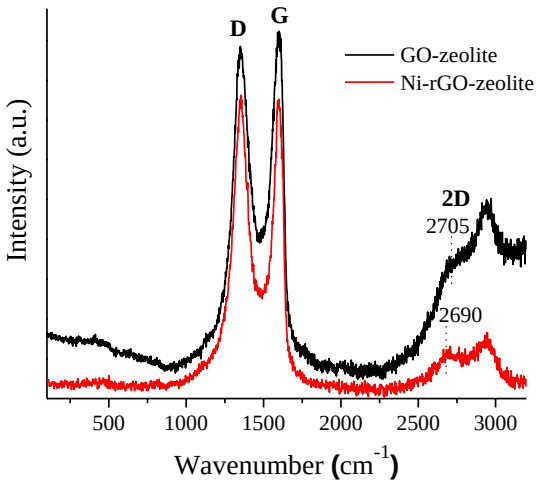

Figure II.B.6 Raman spectra of Ni–rGO–zeolite catalyst and GO–zeolite (as control).

The XRD (X-ray diffraction) pattern of the Ni–rGO–zeolite nanocomposite has been shown in the Figure II.B.7. The XRD peaks could be assigned to the reflection of NaY zeolite crystal planes, and thus confirm the formation of NaY zeolite phase.[74,75] The diffraction pattern of the composite catalyst (Ni–rGO–zeolite) was also compared with that of GO–zeolite control sample (Figure II.B.7) where similar pattern revealed retention of NaY crystal structure after incorporation of Ni moiety in GO–zeolite composite system. Similar trend of I_{220} and I_{311} in both the cases also indicated that there was probably no encapsulation of Ni in the zeolite cage.[76] However, the chemical characteristics of Ni component could not be recognized presumably due to the presence of NaY zeolite reflection peaks in the pattern.

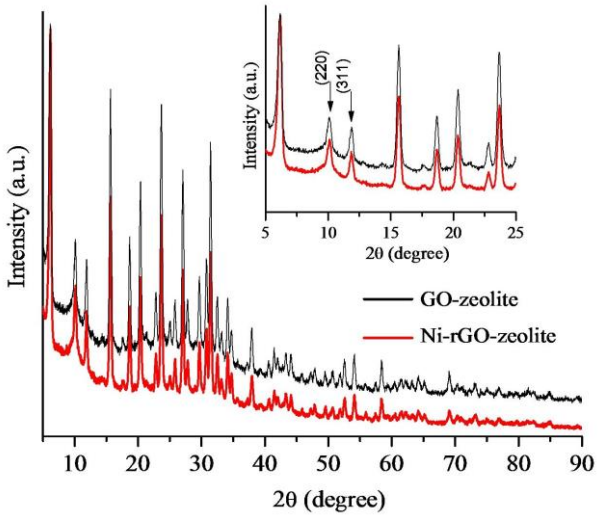

Figure II.B.7 XRD patterns of GO–zeolite and Ni–rGO–zeolite composites.

The chemical composition of the Ni–rGO–zeolite composite was further investigated by XPS (X-ray photoelectron spectroscopy) analysis. The survey scan of the material in Figure II.B.8.1 showed binding energy peaks of Al2p, Si2p, Na1s corresponding to zeolite, C1s from rGO, and Ni2p from Ni NPs. For detail insight into the composition, deconvolution of high resolution C1s and Ni2p spectra were undertaken to check the interaction between rGO and Ni species. Deconvoluted C1s spectrum (Figure II.B.8.2a) showed binding energy peaks corresponding to C=C and C–C arising from rGO. In addition to that peaks 285.98, 287, 287.80 and 289.04 eV indicated presence of C–OH, epoxy C–O–C, C=O and O=C–O functional groups on rGO, respectively.[73,77,78] Moreover, the peak at 286.50 eV could be attributed to the Ni–C bonding. The Ni2p high resolution spectrum with $Ni2p_{1/2}$ and $Ni2p_{3/2}$ core levels has been shown in Figure II.B.8.2b. In this spectrum the $Ni2p_{3/2}$ and $Ni2p_{1/2}$ core level peaks at 853.17 and 870.54 eV, respectively correspond to the free metallic Ni(0).[79] Furthermore, the pair of binding energy peaks at 856.95 ($Ni2p_{3/2}$) and 874.46 ($Ni2p_{1/2}$) eV, and 862.68 ($Ni2p_{3/2}$) and 880.80 eV ($Ni2p_{1/2}$) could be assigned for Ni–O–C and Ni–C bonds, respectively.[79] Thus detailed XPS analysis confirmed an intrinsic interaction between the rGO and Ni species.

The morphology and microstructure of Ni–rGO–zeolite was analyzed by scanning electron microscopy (SEM). By comparing the SEM images of GO–zeolite and Ni–rGO–zeolite nanocomposites it could be understood only the existence of crystal aggregates of zeolites along with the rGO plates (Figure II.B.9a and II.B.9b). In the Ni–rGO–zeolite nanocomposite, nickel NPs were uniformly dispersed on the surface of rGO sheets through chemical bonding with the functional groups and zeolite crystals (Figure II.B.9b). The SEM-energy dispersive X-ray scattering analysis (SEM-EDS) of Ni–rGO–zeolite confirmed the presence of Ni along with C, O, Si and Al (FigureII.B.9c). The transmission electron microscopy (TEM) analysis of Ni–rGO–zeolite was also carried out to detect the presence of distinguishable nanoparticles. The TEM image (Figure II.B.9d), revealed uniform distribution of quasi hexagonal plate-like nanostructures of zeolites (a few are shown by yellow arrow in Figure II.B.9d),[80,81] on the rGO sheets. XPS has confirmed that a major amount of the nickel is bonded with the functional groups (ionic state/Ni^{2+}) and existence of small amount of metallic nickel (Ni^0). As a result, visibility of metallic nickel in the TEM is insignificant, however, the SEM-EDS confirmed the existence of Ni (0.31 At%) in the nanocomposite.

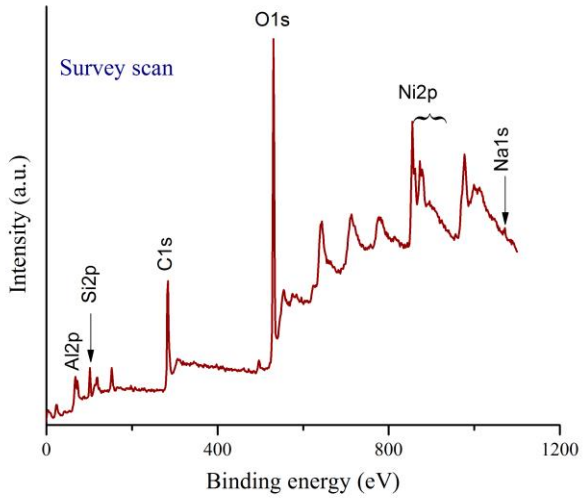

FigureII.B.8.1 XPS survey scan of Ni–rGO–zeolite catalyst.

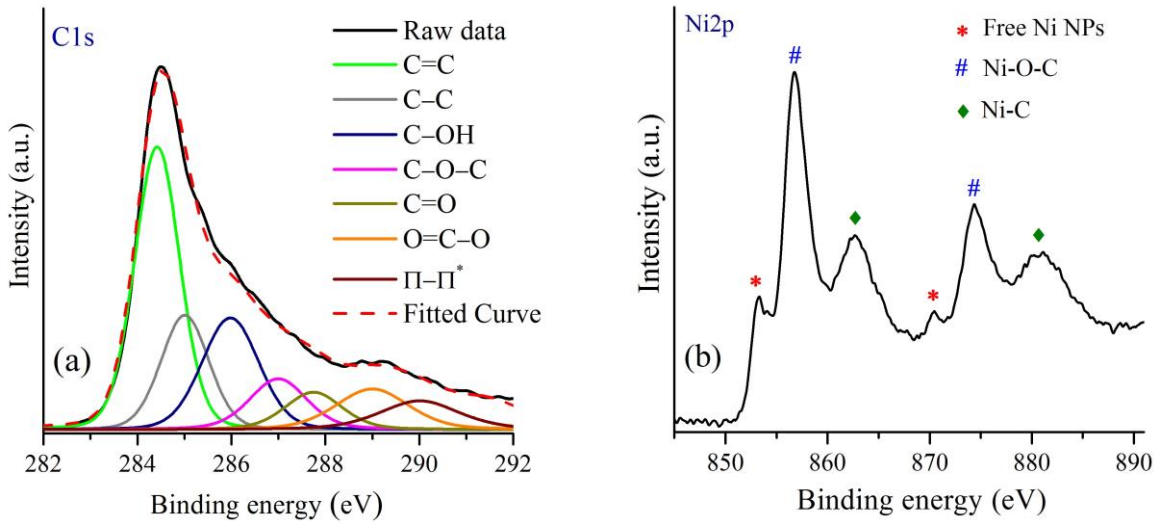

Figure II.B.8.2 XPS spectra of Ni–rGO–zeolite composite: (a) high resolution C1s spectrum (b) high resolution Ni2p spectrum.

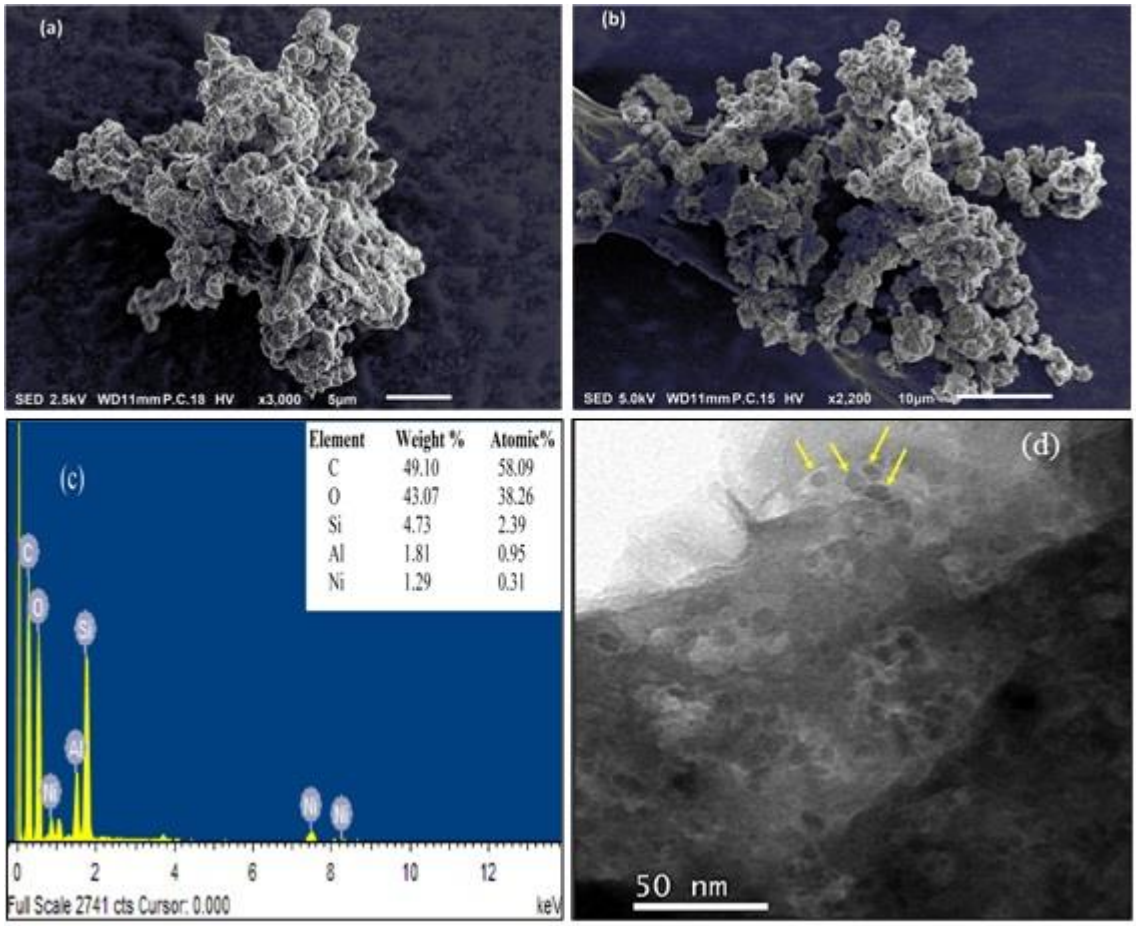

Figure II..B.9 (a) SEM image of GO–zeolite, (b) SEM image of Ni–rGO–zeolite, (c) EDS of Ni–rGO–zeolite and (d) TEM image of Ni–rGO–zeolite.

II.B.3.3 Catalytic activity of Ni–rGO–zeolite: Optimization of reaction conditions

The catalytic activity of Ni–rGO–zeolite was examined was examined in the three-component click reaction. For this purpose, benzyl bromide (**1a**) and phenylacetylene (**2a**) were selected as the model substrates (Table II.B.1). Initially, **1a**, **2a** and sodium azide were reacted in presence of Ni–rGO–zeolite (50 mg per mmol of the substrate) in CH_3CN at 80 °C for 8 h. The desired product 1-benzyl-4-phenyl-1*H*-1,2,3-triazole (**3a**) was isolated in 67% yield (entry 1). We assumed poor solubility of sodium azide in CH_3CN might be the cause of lower yield. To overcome the solubility issue, the same reaction was carried out in a mixture of CH_3CN:H_2O (1:1 v/v) and the yield of the product increased to 81% (entry 2). The catalyst loading was then lowered to 30 mg and the reaction was carried out in H_2O at 90 °C. This resulted in an excellent conversion of 94% (entry 3). Further reducing the amount of catalyst to 15 mg and lowering the temperature to 60 °C, decreased the yield of the product to 82% and 69% respectively (entries 4 and 5). We even carried out a reaction in presence of an additive, tetrabutylammonium bromide (TBAB, 10 mol%) but did not observe any significant

improvement in the yield of product (entry 6, 95%). A solvent-less approach using only the reactants and catalyst formed the desired product in modest yield (entry 7, 77%). The reaction when conducted without any catalyst resulted in meagre conversion emphasizing the imperative role of the catalyst (entry 8, 16%). It is noteworthy to mention that $Ni(OAc)_2 \cdot 4H_2O$ also catalyzed the reaction and the triazole product was obtained in a relatively lower yield (entry 9, 53%). Finally, we scaled up the reaction under the optimized conditions which resulted in good conversion (entry 10, 89%). For comparison of the catalytic activity, we conducted two experiments using Ni–zeolite and Ni–rGO that resulted in the formation of the desired 1,4-disubstituted triazole derivative **3a** in 52% and 40% yield respectively (entries 11 and 12). The formation of **3a** was confirmed by ^{1}H and ^{13}C NMR spectroscopy. The two singlet peaks at δ 5.48 and 7.58 ppm were respectively due to the two benzylic Hs and the hydrogen present in the triazole unit. The same peaks appeared at δ 54.1 and 130.5 ppm in the ^{13}C NMR spectrum.

Table II.B.1 Optimization of the reaction conditions[a]

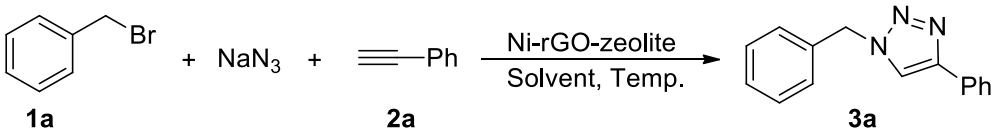

1a **2a** **3a**

Entry	Catalyst (mg)	Solvent	Temp (°C) / time (h)	Yield (%)[b]
1	50	CH_3CN	80 / 8	67
2	50	CH_3CN:H_2O (1:1)	80 / 8	81
3	**30**	**H_2O**	**90 / 4**	**94**
4	15	H_2O	90 / 4	82
5	30	H_2O	60 / 4	69
6	30	H_2O	90 / 4	95[c]
7	30	–	90 / 4	77
8	–	H_2O	90 / 24	16
9	–	H_2O	90 / 4	53[d]
10	100	H_2O	90 / 4	89[e]
11	30	H_2O	90 / 4	52[f]
12	30	H_2O	90 / 4	40[g]

[a]Reaction conditions: **1a** (1 mmol), **2a** (1 mmol), NaN_3 (1.5 mmol) and solvent (2 mL). [b]Isolated yield. [c]TBAB (10 mol%) was used. [d]$Ni(OAc)_2 \cdot 4H_2O$ (15 mol%) was used. [e]Reaction was performed in 5 mmol scale. [f]Reaction carried out using Ni–zeolite catalytic system. [g]Reaction carried out using Ni–rGO catalytic system.

II.B.3.4 Synthesis of 1,4-disubstituted-1,2,3-triazoles

Diverse triazole derivatives were synthesized from alkyl halides and terminal alkynes using Ni–rGO–zeolite catalyst. The results obtained have been presented in Table II.B.2. Initially, we varied the alkyl halides for the reaction, keeping the terminal alkyne fixed. Afterwards, we tested the effect of substituent on the alkyne partner for the reaction. Both benzyl bromide and benzyl chloride gave the triazole **3a** in 94% and 90% isolated yield respectively (entry 1). Benzyl bromide bearing isopropyl, bromo and iodo groups in the ring reacted efficiently with phenylacetylene affording the desired products (**3b**-**3d**) in 88-91% yield (entries 2-4). When cinnamyl bromide was employed, the yield of the triazole **3e** was comparatively low (entry 5, 77%). We presumed that the lower yield might be due to the tendency of cinnamyl azide undergoing intramolecular rearrangement.[82] 1-Chloromethyl naphthalene also reacted under the standard condition furnishing the product **3f** in 85% yield (entry 6). The reaction also went smoothly when allyl bromide was used and the desired product **3g** was obtained in 83% isolated yield (entry 7). Further attempt with activated functionalized organic halides, such as 4-chlorophenacyl bromide was also accomplished (entry 8, 79%). Next, terminal alkynes other than phenylacetylene such as 4-ethynyltoluene, 1-bromo-4-ethynylbenzene and 1-ethynyl-4-nitrobenzene were employed. In the reaction between 4-ethynyltoluene with different alkyl halides, under the standard reaction conditions, the corresponding triazoles (**3i**-**3m**) were obtained in 78-94% yield (entries 9-13). 1-Bromo-4-ethynylbenzene and 1-ethynyl-4-nitrobenzene were also transformed into the corresponding triazoles (**3n** and **3o**) in 87% and 80% yield respectively (entries 14 and 15). The catalyst thus exhibited superior catalytic activity regardless of the electronic nature and substitution pattern on the alkyl as well as alkyne moiety. The ^{1}H NMR spectrum of **3e** showed a doublet of doublet at δ 5.12 (J = 0.9, 6.3 Hz) ppm due to the benzylic Hs. The cinnamyl sp^{2}C–H linked with the phenyl group appeared as a doublet at δ 6.66 (J = 15.9 Hz) ppm. The coupling constant value of 15.9 Hz indicated the *trans*- geometry of the cinnamyl double bond. In case of compound **3g** the peaks at δ 4.96 (d, J = 5.7 Hz) and 5.95-6.08 (m, 1H) ppm were respectively due to the due to the two benzylic Hs and the hydrogen present in the triazole unit. In the ^{13}C NMR spectrum of the same compound the peak at δ 52.7 ppm was due to the benzylic carbon and the peaks at δ 119.7 and 131.3 ppm could be assigned to the allylic carbons. In compound **3h** the benzylic Hs appeared as a singlet at δ 6.24 ppm in the ^{1}H NMR spectrum. The same peak appeared at δ 56.4 ppm in the ^{13}C NMR spectrum.

Table II.B.2 Ni–rGO–zeolite catalyzed synthesis of 1,4-disubstituted-1,2,3-triazoles [a]

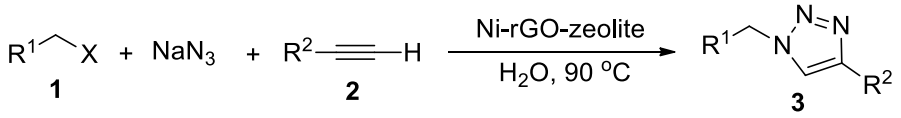

Entry	Alkyl halide	Alkyne	Triazole	Time (h)	Yield (%)[b]
1	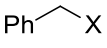	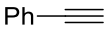	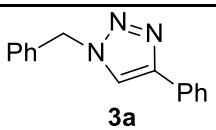 **3a**	4	X = Br, 94 X = Cl, 90
2	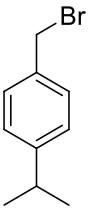	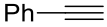	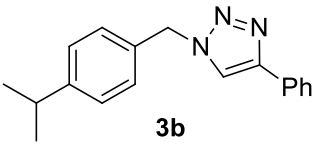 **3b**	5	88
3	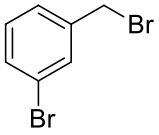	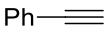	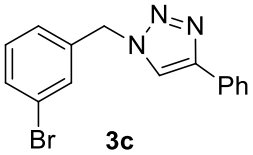 **3c**	4	90
4	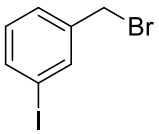	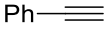	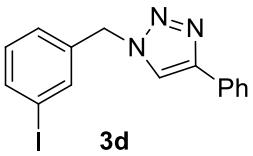 **3d**	4	91
5	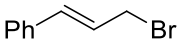	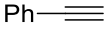	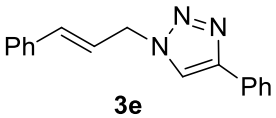 **3e**	5	77
6	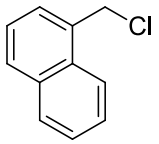	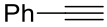	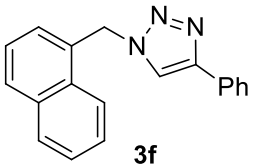 **3f**	6	85
7[c]	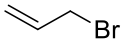	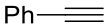	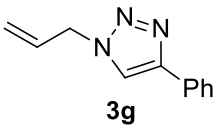 **3g**	4	83
8	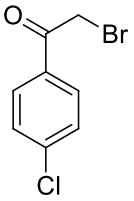	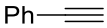	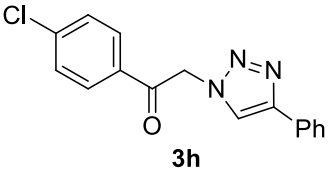 **3h**	4	79

9	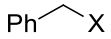	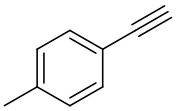	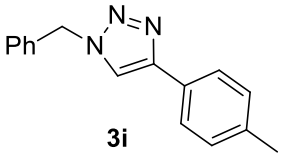 **3i**	4	X = Br, 87 X = Cl, 84
10	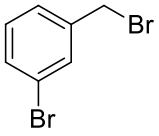	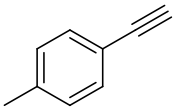	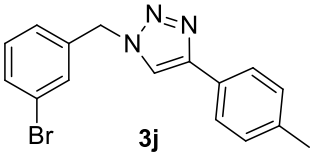 **3j**	4	88
11	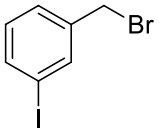	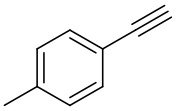	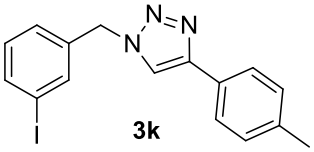 **3k**	4	90
12	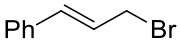	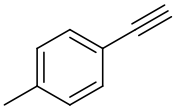	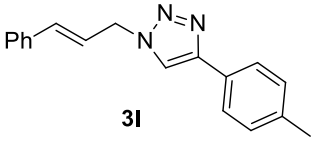 **3l**	5	78
13[c]	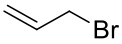	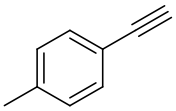	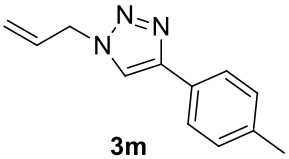 **3m**	4	94
14	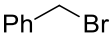	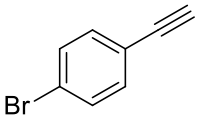	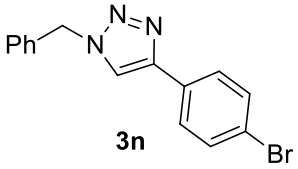 **3n**	4	87
15	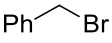	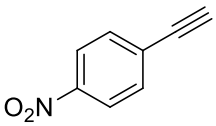	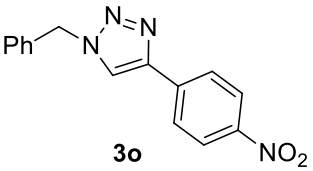 **3o**	4	80

[a]Reaction conditions: **1** (1 mmol), **2** (1 mmol), NaN_3 (1.5 mmol), Ni–rGO–zeolite (30 mg) and H_2O (2 mL) were stirred at 90 °C. [b]Isolated yield. [c]Reaction was carried out at 70 °C.

II.B.3.5 Recyclability of the catalyst

We checked the recyclability of Ni–rGO–zeolite catalyst in the three-component click reaction between **1a**, **2a** and NaN_3 in aqueous medium under the optimized condition. After the first run the catalyst was separated from the reaction mixture by simple filtration, washed with ethyl acetate (5 x 5 mL) and dried under vacuum for 24 h. It was then re-used for the second run. The catalyst was re-used for four consecutive runs without any significant drop in the yield of the product (Figure II.B.10). Moreover, we estimated the nickel content in Ni–rGO–zeolite before and after the recycle runs. As could be seen from ICP-AES analysis,

before the reaction the nickel content in Ni–rGO–zeolite (30 mg) was 0.026 mmol, while that after the first and third run were 0.026 and 0.022 mmol respectively. This indicated that no significant leaching of nickel occurred from the nanocomposite during the course of the reaction.

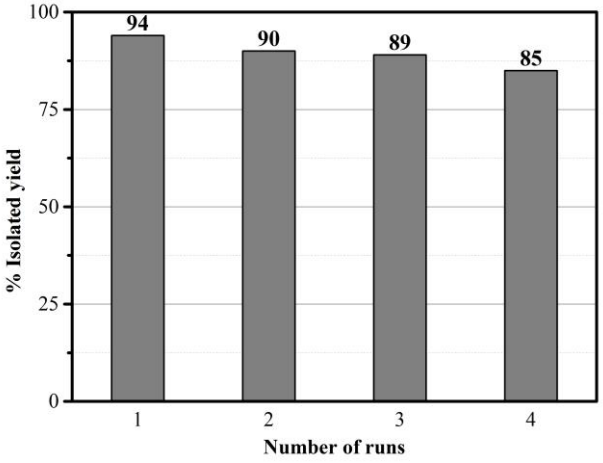

Figure II.B.10 Recyclability of Ni–rGO–zeolite in the click synthesis of triazoles.

Furthermore, XPS analysis of the catalyst was also carried out after the first run to determine any change in the chemical state of nickel. Figure II.B.11a showed the survey scan where presence of binding energy peaks corroborated recyclability result. However in Ni2p high resolution spectrum increase in free nickel NPs related binding energy peaks were observed without any significant change in binding energy values (Figure II.B.11b). Whereas, the peak intensity of Ni–O–C and Ni–C were found to decrease, it is noteworthy that under similar kind of reaction condition NaN_3 has the ability to modify the oxygen containing functional groups of rGO.[83] So this might have resulted in the formation of greater number of free nickel NPs in the composite. However, the ICP-AES analysis confirmed the retention of total nickel content, so no significant loss in catalytic activity of the catalyst was observed.

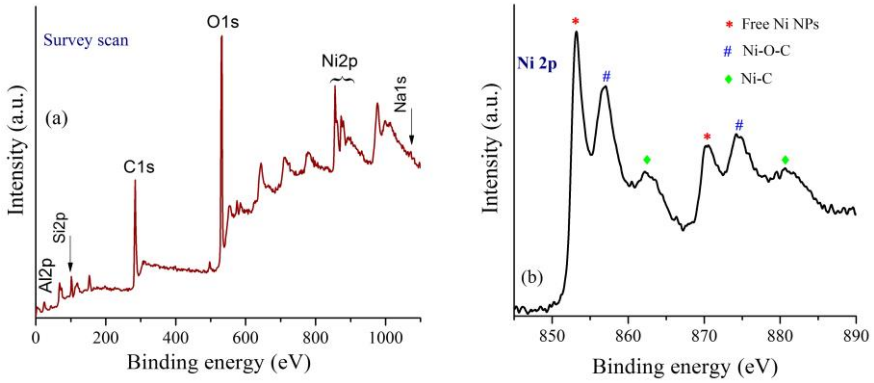

Figure II.B.11 XPS analysis of Ni–rGO–zeolite after first run: (a) survey scan (b) high resolution Ni2p spectrum.

II.B.3.6 Plausible mechanism for the reaction

The copper catalyzed version of the Huisgen cycloaddition (CuAAC) involves the formation of copper acetylide as one of the key intermediate, which then undergoes cycloaddition with azide moiety leading to the formation of triazole.[14,19] However, as previously reported by Sommer et al. when the reaction occurred in zeolite surface, it did not involve such Cu-acetylide intermediate. The reaction proceeded through π-complexation between alkyne and the metal and finally via the formation of a metallacycle intermediate.[32] The formation of similar metallacycle intermediate was also evident in Raney nickel catalyzed AAC.[60] Raney nickel contains finely divided Ni(0) particles, so the active species in the mechanistic pathway might be the zero-valent state of nickel.

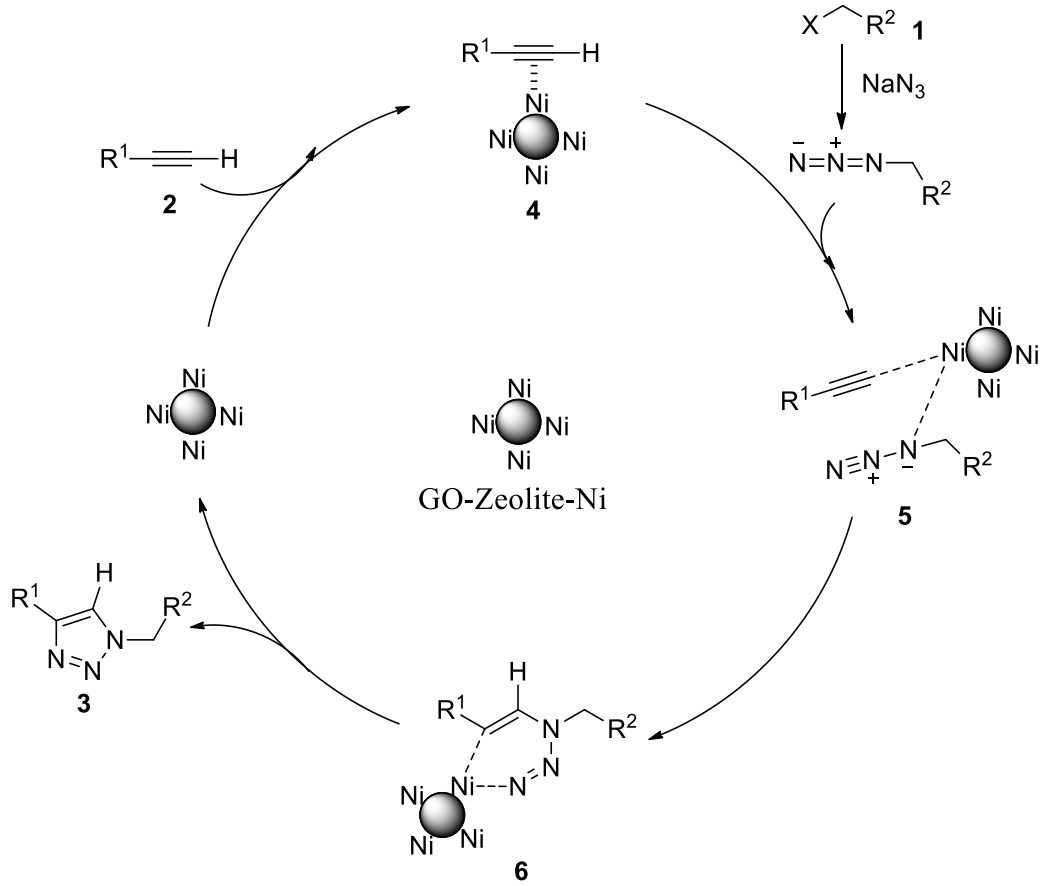

Scheme II.B.17 Plausible mechanism for Ni–rGO–zeolite catalyzed click reaction.

Based on these reports we presumed that the free nickel NPs present in Ni–rGO–zeolite might be responsible for exerting such catalytic activity in click reaction. Therefore, the first step of the reaction presumably involved a π–complex (**4**) formed by the reaction between alkyne and Ni(0) species. This was followed by coordination of the incoming azide with nickel leading to the formation of a new coordinated species (**5**), which subsequently

underwent cycloaddition to form the metallacycle intermediate (**6**). Finally, reductive elimination of the metallacycle intermediate led to the formation of the desired triazole product (**3**) and regenerated the Ni(0) active species to effect the next catalytic cycle (Scheme II.B.17).

II.B.4 Conclusion

In conclusion, we have developed a new heterogeneous ternary nanocomposite catalyst based on nickel (Ni–rGO–zeolite). As compared to the previously reported very few Ni-catalysts used in AAC and only one heterogeneous photoactive Ni catalyst, the present heterogeneous catalytic system offers certain advantages like easy preparation from cheap and sustainable materials, stable at room temperature, high catalytic efficiency in aqueous medium, regioselective formation of 1,4-disubstituted-1,2,3-triazoles, recovery by simple filtration and recyclability, etc. The enhanced catalytic performance of this heterogeneous Ni catalyst in AAC presumably originates from the concurrent supports and stabilization of the active Ni(0) species by an unique combination of π-electron rich rGO and microporous zeolitic surface. Among very few Ni catalysts studied in [3+2] AAC, the present catalytic system not only eliminates some of the shortcomings but certainly will pave the way for further applications of Ni-catalyzed 'click' reactions.

II.B.5 Experimental Section

II.B.5.1 General Information

All reagents were purchased from Sigma-Aldrich and used directly without further purification. NaY zeolite was purchased from Sigma-Aldrich. The solvents were purchased from commercial suppliers and used after distillation. All the products were purified by column chromatography on 60-120 mesh silica gel (Merck, India). For TLC, Merck plates coated with silica gel 60, F_{254} were used. FT-IR spectra were recorded in FT-IR 8300 SHIMADZU spectrophotometer. The ^{1}H & ^{13}C NMR spectra were recorded at 400 MHz and 100 MHz respectively on Bruker Ascend 400 spectrometer in $CDCl_3$ and DMSO-d_6. Splitting patterns of protons were described as s (singlet), d (doublet), dd (doublet of doublet) and m (multiplet). Chemical shifts (δ) were reported in parts per million (ppm) relative to TMS as internal standard. *J* values (coupling constant) were reported in Hz (Hertz). ^{13}C NMR spectra were recorded with complete proton decoupling ($CDCl_3$: δ 77.0 ppm and DMSO-d_6: 39.5 ppm). Centrifugation was done in REMI R-8C DX centrifuge. Inductively Coupled Plasma Atomic Emission Spectroscopy (ICP-AES) was measured by using SPECTRO analytical

instruments GmbH, Germany. The X-ray diffraction studies (XRD) were done by the Rigaku SmartLab (9 kW) diffractometer using CuKα radiation. Raman spectra of the samples were obtained with Renishaw InVia micro Raman spectroscopy with 514 nm laser source. Scanning Electron Microscopy (SEM) and Electron-Dispersive X-ray Spectroscopy (EDS) were performed using JEOL JSM-IT 100 electron microscope. Transmission electron microscopy (TEM) measurements were carried out using a JEOL JEM-2100F high-resolution electron microscope. X-ray photoelectron spectroscopic (XPS) measurements were done on a PHI 5000 Versaprobe II XPS system with an Al Kα source and a charge neutralizer at room temperature.

II.B.5.2 Preparation of graphene oxide (GO)

Graphene oxide was prepared by following Tour's method.[68] In this method a 9:1 (v/v) mixture of H_2SO_4 / H_3PO_4 (180:20 mL) was added to a mixture of graphite powder (1.5 g) and $KMnO_4$ (9.0 g). The mixture was then stirred at 50 °C for 12 h. After cooling the mixture to room temperature, it was gradually poured into crushed ice (200 g), which was followed by the slow addition of H_2O_2 (30%, 1.5 mL). The solution was then centrifuged (5000 rpm) and the supernatant was discarded. The residual solid material was successively washed with deionised water (100 mL) and then with 30% HCl (100 mL). The solid material was then repeatedly washed with water and centrifuged. Finally, the solid brown material was collected and dried at 60 °C under vacuum to obtain solid graphene oxide.

II.B.5.3 Preparation of GO–zeolite nanocomposite

Graphene oxide (275 mg) was dispersed in distilled water (100 mL) and ultrasonically treated for 1 h. Subsequently, NaY zeolite (400 mg) was proportionately added to the GO dispersion ensuring neutral pH of the overall dispersion. The dispersion was then placed in an oil bath at 60 °C and stirred for 16 h. The solvent was then removed under reduced pressure and the solid mass was dried under vacuum for 24 h.

II.B.5.4 Preparation of Ni–rGO–zeolite nanocomposite

A Teflon-capped sealed tube containing GO–zeolite (500 mg) dispersion in ethylene glycol (10 mL) was charged with $Ni(OAc)_2 \cdot 4H_2O$ (124 mg, 0.5 mmol). The contents were then gently stirred at 60 °C for 30 minutes. After that, $NaBH_4$ (37 mg, 1 mmol) was added to the mixture portion wise. The sealed tube was again Teflon capped and placed in a preheated oil bath at 180 °C. After stirring for 3 h, the mixture was cooled to room temperature, diluted with water and centrifuged at 5000 rpm. The supernatant was discarded and the solid composite material was washed alternatively with water and ethanol (3 times each). The solid composite material was then dried under vacuum for 48 h.

II.B.5.5 Preparation of Ni–zeolite catalyst

Ni–zeolite composite catalyst was prepared by a literature reported method with minor modifications.[84] A 250 mL RB flask was charged with ethylene glycol (50 mL) and $NiNO_3 \cdot 6H_2O$ (290 mg). The mixture was ultrasonicated for 30 minutes, sealed, purged with nitrogen and placed in an oil bath at 200 °C. This was followed by the rapid addition of $NaBH_4$ (200 mg) into the flask. The mixture is then stirred at this temperature for 2 h and cooled to room temperature. The solid was separated by centrifugation, washed with ethanol and distilled water (3 times each) and dried under vacuum for 24 h.

II.B.5.6 Preparation of Ni–rGO catalyst

Ni–rGO catalyst was prepared by following a previously reported procedure.[85] Graphene oxide (2.75 g) was ultrasonically dispersed in 800 mL of water. To the GO dispersion, a solution of $NiCl_2 \cdot 6H_2O$ (2.08 g, 8.75 mmol) in 600 mL water and hexamethylenetetramine (2.453 g, 17.5 mmol) solution in 250 mL water were added. The mixture was stirred at room temperature at for 10 minutes and finally sealed in 2 L Teflon-lined stainless steel autoclave for hydrothermal reaction at 120 °C for 4 h. The black powder was washed several times with water to remove excess Ni salt and hexamethylenetetramine and dried. The powder was then heated in air 380 °C for 1 h to obtain NiO–rGO nanocomposite. The reduction of this material in presence of rGO at 350 °C with a continuous flow of H_2 gas gives Ni–rGO nanocomposite catalyst.

II.B.5.7 Typical procedure for the synthesis of 1,2,3-triazoles

A round bottomed flask (25 mL) equipped with a magnetic stir bar, was charged with alkyl halide (1 mmol), terminal alkyne (1 mmol), NaN_3 (1.5 mmol) and Ni–rGO–zeolite (30 mg). Freshly distilled water (2 mL) was added to it and the reaction mixture was gently stirred at 90 °C for 4-6 h. After completion of the reaction (monitored by TLC), the reaction mixture was cooled to room temperature. The catalyst was recovered through simple filtration and the reaction mixture was extracted with ethyl acetate (3 x 5 mL). The combined organic layer was dried over anhydrous Na_2SO_4 and concentrated under vacuum. The residue obtained was purified by column chromatography using light petroleum ether / ethyl acetate as eluent to afford the desired product. All products were characterized by ^1H, ^{13}C NMR data and also compared with reported melting points for solid compounds.

II.B.5.8 Characterization data of various 1,2,3-triazole derivatives

1–Benzyl–4–phenyl–1*H*–1,2,3-triazole (3a)[86]

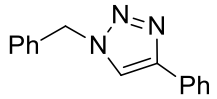

White crystalline solid; m.p.: 128–130 °C (Lit. m.p.: 128–129 °C)[86]; **^{1}H NMR (400 MHz, $CDCl_3$)**: δ 5.53 (s, 2H), 7.29–7.37 (m, 8H), 7.67 (s, 1H), 7.78–7.79 (m, 2H); **^{13}C NMR (100 MHz, $CDCl_3$)**: δ 54.2, 119.7, 125.7, 128.0, 128.2, 128.8, 128.9, 129.2, 130.5, 134.7, 148.2.

1-(4-Isopropylbenzyl) –4–phenyl-1*H*–1,2,3-triazole (3b)[87]

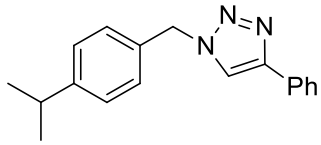

White solid; m.p.: 177–178 °C (Lit. m.p.: 175 °C)[87]; **^{1}H NMR (400 MHz, $CDCl_3$)**: δ 1.20–1.58 (m, 6H), 2.97–2.99 (m, 1H), 5.52 (s, 2H), 7.00–7.15 (m, 1H), 7.23-7.27 (m, 2H), 7.38–7.42 (m, 2H), 7.65 (m, 3H), 7.73-7.82 (m, 2H); **^{13}C NMR (100 MHz, $CDCl_3$)**: δ 23.9, 26.2, 33.9, 54.1, 119.4, 125.7, 126.9, 127.29, 128.1, 128.8, 128.9, 129.4, 131.9, 133.1.

1–(3–Bromo benzyl)–4–phenyl–1*H*–1,2,3-triazole (3c)[88]

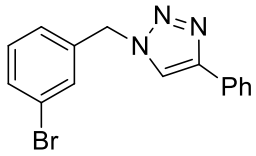

Light yellow solid; m.p.: 92–94 °C (Lit. m.p.: 91–93 °C)[88]; **^{1}H NMR (400 MHz, $CDCl_3$)**: δ 5.53 (s, 2H), 7.22–7.25 (m, 2H), 7.32 (d, *J* = 7.2 Hz, 1H), 7.38–7.49 (m, 4H), 7.69 (s, 1H), 7.79–7.81 (m, 2H); **^{13}C NMR (100 MHz, $CDCl_3$)**: δ 53.5, 119.6, 123.1, 125.7, 126.6, 128.3, 128.9, 130.3, 130.7, 131.0, 132.0, 136.9, 148.5.

1–(3–Iodo benzyl)–4–phenyl–1*H*–1,2,3–triazole (3d)[89]

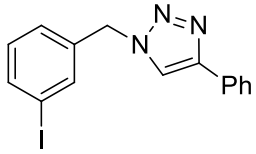

White solid; m.p.: 120–122 °C (Lit. m.p.: 122–124 °C)[89]; **^{1}H NMR (400 MHz, $CDCl_3$)**: δ 5.50 (s, 2H), 7.10–7.12 (m, 1H), 7.24 (d, *J* = 8 Hz, 2H), 7.32 (d, *J* = 7.2 Hz, 1H), 7.40 (t, *J* = 7.2 Hz, 2H), 7.66–7.70 (m, 3H), 7.79–7.81 (m, 2H); **^{13}C NMR (100 MHz, $CDCl_3$)**: δ 53.3, 94.8, 119.6, 125.8, 127.2, 128.3, 128.9, 130.4, 130.8, 136.8, 136.9, 137.9, 148.4.

1–Cinnamyl–4–phenyl–1*H*–1,2,3–triazole (3e)[90]

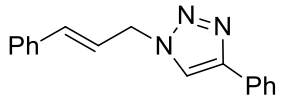

White solid; m.p.: 136–138 °C (Lit. m.p.: 132–134 °C)[90]; **^{1}H NMR (400 MHz, $CDCl_3$)**: δ 5.15 (dd, *J* = 1.2, 7.6 Hz, 2H), 6.35–6.41 (m, 1H), 6.69 (d, *J* = 16 Hz, 1H), 7.29–7.43 (m, 8H), 7.80–7.84 (m, 3H); **^{13}C NMR (100 MHz, $CDCl_3$)**: δ 52.4, 119.5, 121.9, 125.7, 126.8, 128.2, 128.6, 128.8, 128.9, 130.6, 135.4, 135.5, 148.1.

1–(Naphthalen–1–ylmethyl)–4–phenyl–1*H*–1,2,3–triazole (3f)[91]

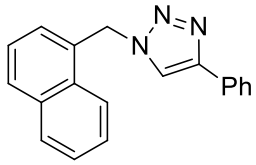

White solid; m.p.: 133–134 °C (Lit. m.p.: 135 °C)[91]; **^{1}H NMR (400 MHz, $CDCl_3$)**: δ 5.99 (s, 2H), 7.26–7.34 (m, 3H), 7.46–7.72 (m, 5H), 7.90 (s, 2H), 7.99 (s, 2H), 8.0 (s, 1H); **^{13}C NMR (100 MHz, $CDCl_3$)**: δ 52.4, 119.6, 122.9, 125.4, 125.7, 126.5, 127.4, 127.9, 128.1, 128.8, 129.0, 129.9, 130.1, 130.5, 131.2, 134.0, 148.0.

1–Allyl–4–phenyl–1*H*–1,2,3–triazole (3g)[86]

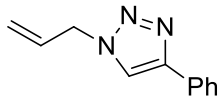

White crystalline solid; m.p.: 62–64 °C (Lit. m.p.: 57–58 °C)[86]; **^{1}H NMR (400 MHz, $CDCl_3$)**: δ 4.96 (d, *J* = 6 Hz, 2H), 5.26–5.34 (m, 2H), 5.99–6.01 (m, 1H), 7.29–7.31 (m, 1H), 7.36–7.40 (m, 2H), 7.44–7.80 (m, 3H); **^{13}C NMR (100 MHz, $CDCl_3$)**: δ 52.7, 119.6, 120.1, 125.7, 128.1, 128.8, 130.6, 131.3, 147.9.

1–(4–Chlorophenyl)–2–(4–phenyl–1*H*–1,2,3–triazol–1–yl)ethanone (3h)[92]

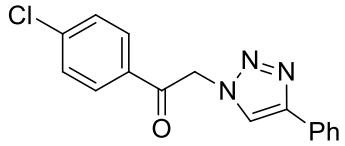

White solid; m.p.: 104–106 °C (Lit. m.p.: 106–109 °C)[92]; **^{1}H NMR (400 MHz, DMSO-d_6)**: δ 6.24 (s, 2H), 7.33 (s, 1H), 7.44 (s, 2H), 7.68–7.69 (m, 2H), 7.85 (s, 2H), 8.08–8.09 (m, 2H), 8.50 (s, 1H); **^{13}C NMR (100 MHz, DMSO-d_6)**: δ 56.5, 123.5, 125.6, 128.4, 129.5, 129.6, 130.6, 131.2, 133.3, 139.7, 146.8, 191.8.

1–Benzyl–4–(*p*–tolyl)–1*H*–1,2,3–triazole (3i)[86]

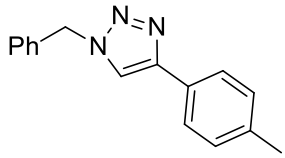

White crystalline solid; m.p.: 152–154 °C (Lit. m.p.: 154–155 °C)[86]; **^{1}H NMR (400 MHz, $CDCl_3$)**: δ 2.35 (s, 3H), 5.52 (s, 2H), 7.19 (d, *J* = 8 Hz, 2H), 7.27–7.36 (m, 5H), 7.62 (s, 1H), 7.68 (d, *J* = 8 Hz, 2H); **^{13}C NMR (100 MHz, $CDCl_3$)**: δ 21.3, 54.1, 119.3, 125.6, 127.7, 128.0, 128.7, 129.1, 129.5, 134.8, 13809, 148.3.

1–(3–Bromo benzyl)–4–(*p*–tolyl)–1*H*–1,2,3–triazole (3j)[91]

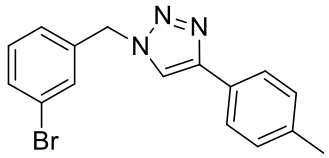

Light yellow solid; m.p.: 132–134 °C (Lit. m.p.: 132–134 °C)[91]; **^{1}H NMR (400 MHz, $CDCl_3$)**: δ 2.37 (s, 3H), 5.53 (s, 2H), 7.23–7.26 (m, 5H), 7.46–7.49 (m, 2H), 7.65–7.70 (m, 3H); **^{13}C NMR (100 MHz, $CDCl_3$)**: δ 21.3, 53.4, 119.1, 123.1, 125.7, 126.5, 127.5, 129.5, 130.7, 131.0, 131.9, 137.0, 138.2, 148.6.

1–(3–Iodo benzyl)–4–(*p*–tolyl)–1*H*–1,2,3–triazole (3k)[91]

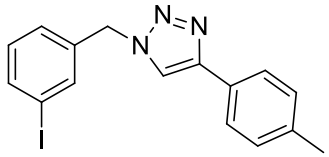

White solid; m.p.: 130–132 °C (Lit. m.p.: 130 °C)[91]; **^{1}H NMR (400 MHz, $CDCl_3$)**: δ 2.37 (s, 3H), 5.50 (s, 2H), 7.1 (m, 1H), 7.20–7.26 (m, 3H), 7.64–7.71 (m, 5H); **^{13}C NMR (100 MHz, $CDCl_3$)**: δ 21.3, 53.3, 94.8, 119.1, 125.7, 127.2, 127.6, 129.5, 130.8, 136.9, 137.0, 137.9, 138.2, 148.5.

1–Cinnamyl–4–(*p*–tolyl)–1*H*–1,2,3–triazole (3l)[91]

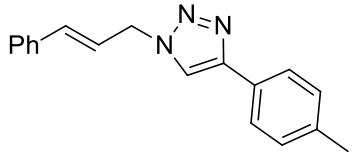

White solid; m.p.: 145–147 °C (Lit. m.p.: 145–147 °C)[91]; **^{1}H NMR (400 MHz, $CDCl_3$)**: δ 2.33 (s, 3H), 5.13 (dd, *J* = 1.2, 8 Hz, 2H), 6.34–6.39 (m, 1H), 6.68 (d, *J* = 16 Hz, 1H), 7.21 (d, *J* = 8 Hz, 2H), 7.25–7.40 (m, 5H), 7.71 (d, *J* = 8 Hz, 2H), 7.76 (s, 1H); **^{13}C NMR (100 MHz, $CDCl_3$)**: δ 21.3, 52.4, 119.1, 122.0, 125.6, 126.7, 127.8, 128.6, 128.8, 129.5, 135.3, 135.5, 138.0, 148.2.

1–Allyl–4–(*p*–tolyl)–1*H*–1,2,3–triazole (3m)[91]

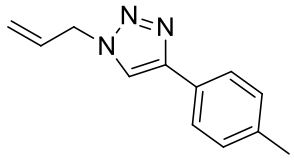

Pale yellow solid; m.p.: 88–90 °C (Lit. m.p.: 88–90 °C)[91]; **^{1}H NMR (400 MHz, $CDCl_3$)**: δ 2.34 (s, 3H), 4.95 (d, *J* = 6 Hz, 2H), 5.27–5.34 (m, 2H), 5.97–6.01 (m, 1H), 7.19 (d, *J* = 8 Hz, 2H), 7.69 (d, *J* = 9.2 Hz, 3H); **^{13}C NMR (100 MHz, $CDCl_3$)**: δ 21.3, 52.7, 119.2, 120.1, 125.6, 127.8, 129.5, 131.4, 138.0, 148.1.

1-Benzyl–4–(4–bromophenyl)–1*H*–1,2,3–triazole (3n)[86]

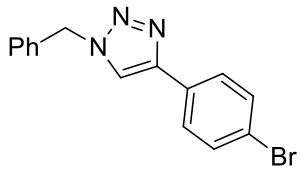

White solid; m.p.: 142–143 °C (Lit. m.p.: 144 °C)[86]; **^{1}H NMR (400 MHz, $CDCl_3$)**: δ 5.54 (s, 2H), 7.29 (s, 2H), 7.36 (s, 3H), 7.49 (d, *J* = 1.6 Hz, 2H), 7.64 (d, *J* = 8 Hz, 3H); **^{13}C NMR (100 MHz, $CDCl_3$)**: δ 54.3, 119.7, 122.0, 127.2, 128.1, 128.9, 129.2, 129.5, 131.9, 134.5, 147.1.

1–Benzyl–4–(4–nitrophenyl)–1*H*–1,2,3–triazole (3o)[93]

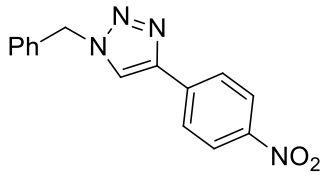

Yellow solid; m.p.: 166–168 °C (Lit. m.p.: 171–172 °C)[93]; **^{1}H NMR (400 MHz, DMSO-d_6)**: δ 5.66 (s, 2H), 7.34 (d, *J* = 6.8 Hz, 5H), 8.09–8.10 (m, 2H), 8.26–8.28 (m, 2H), 8.88 (s, 1H); **^{13}C NMR (100 MHz, DMSO-d_6)**: δ 53.7, 124.1, 124.8, 126.4, 128.5, 128.7, 129.3, 136.1, 137.5, 145.2, 147.0.

II.B.5.9 Scanned copies of ^{1}H and ^{13}C NMR spectra of 1–benzyl–4–phenyl–1*H*–1,2,3-triazole (3a)

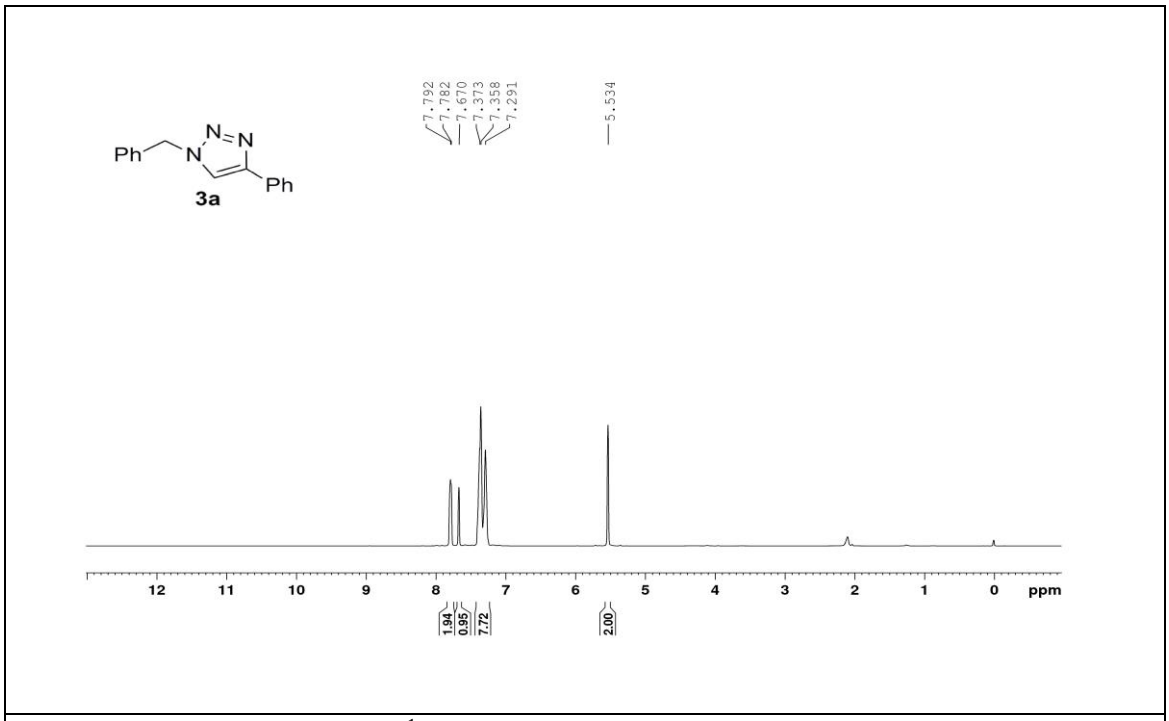

Figure II.B.12 Scanned copy of ^{1}H NMR spectrum of 1-benzyl-4-phenyl-1*H*-1,2,3-triazole (**3a**)

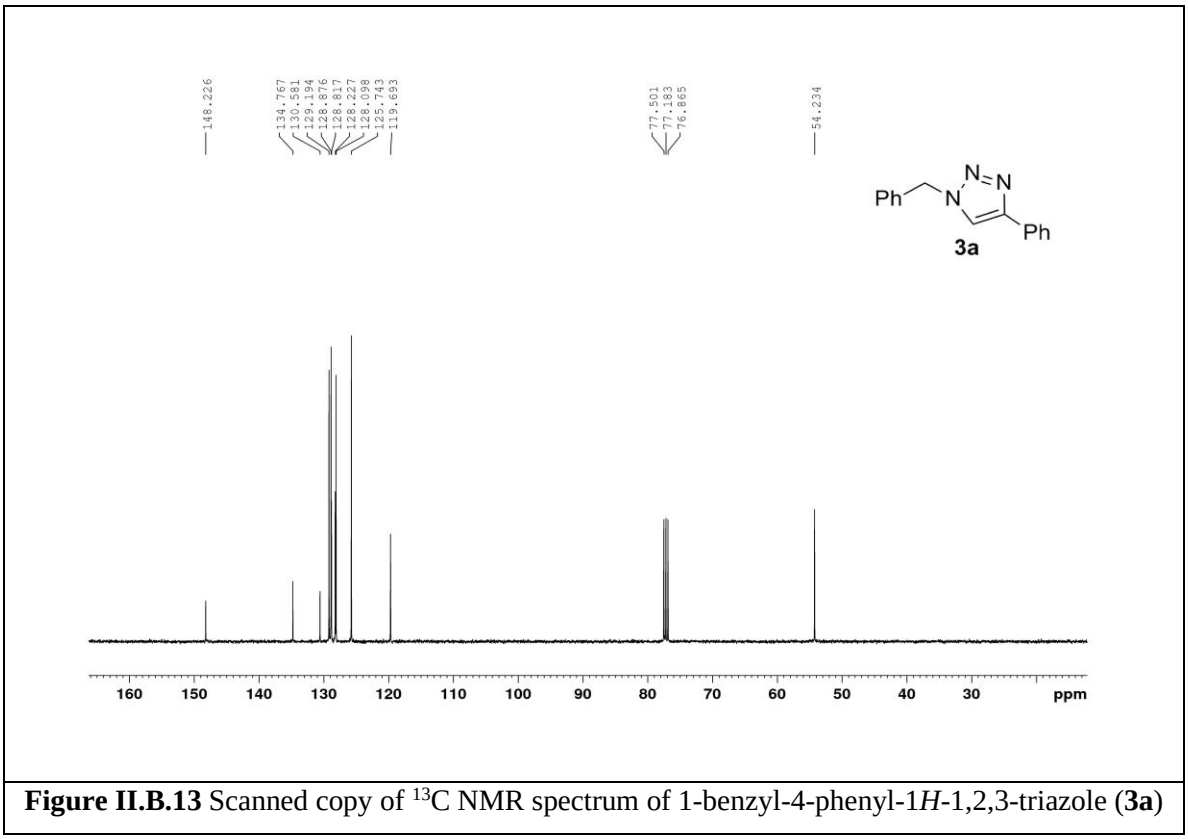

Figure II.B.13 Scanned copy of ^{13}C NMR spectrum of 1-benzyl-4-phenyl-1*H*-1,2,3-triazole (**3a**)

II.B.6 References

References are given in BIBLIOGRAPHY under Chapter II, Section B.

Chapter II

Section C

Cu@GO–SiO_2 Nanocomposite Catalyzed Diverse Cross-Coupling Reactions

II.C.1 Introduction

Transition metal catalyzed C–C and C–X (X = N, S, O) cross-coupling reactions represents a unique dimension in contemporary organic synthesis.[1] Remarkable progress has taken place over the last few decades owing to their widespread application in the synthesis of simple as well as highly complex molecules.[1] While carrying out the synthesis of active pharmaceutical ingredients (API), at least one of the steps involve transition metal catalyzed cross-coupling reactions. Several transition metals pioneering palladium followed by copper and to some extent nickel have been employed as catalyst for various organic transformations.[2-4] In this context, metallic nanoparticles (NPs) have received paramount attention from academia and industry because of their excellent catalytic activity. Metallic NPs possesses high surface area to volume ratio which plays a key role in catalyzing organic transformations. There are also reports of bimetallic nanoparticles as catalyst where the synergism between two different metals facilitates the overall catalytic process.[5,6]

In addition, the development of catalytic systems which are heterogeneous in nature has been another interesting area of research.[7] Heterogeneous catalysts are robust, highly efficient and if appropriately designed can prevent contamination of final products from toxic metals. They efficiently catalyze organic reactions and can be repeatedly used without substantial loss in its catalytic activity. Several polymers loaded with metallic nanoclusters are used as heterogeneous catalysts in diverse cross-coupling reactions.[8,9] The emergence of diverse protocols associated with simpler catalytic systems and enhanced catalytic activity has been gaining much attention these days.

The use of carbon nanomaterials in catalysis is most demanding area in chemical science due to their stability and high surface area.[10] From last two decades graphene oxide (GO) has attracted immense attention in the field of catalysis due to its high surface area, high thermal, chemical and mechanical stability.[10] Graphene oxide (GO), a two-dimensional (2D) honeycomb lattice carbon nanomaterial with a flat mono or few layer structure, has attracted enormous attention in the field of organic synthesis.[11-13] Due to the presence of unique multiple oxygen moieties, GO has been used to prepare many functional materials for adsorption, catalysis, sensors, electronics and optics.[14] Additionally, metal/graphene oxide nanocomposites play a crucial role in diverse fields like catalysis, fabrication of sensors, toxic metal ion scavenging, cellular imaging and drug delivery.[15] The chemical properties of the graphene oxide can be manipulated or tuned by chemical modifications. Other carbonaceous materials are also used as solid supports for immobilization of metal/metal oxide nanoparticles (NPs). The use of supported metallic NPs as heterogeneous catalysts in organic

reactions has attracted substantial attention in the recent years. Palladium has been the mostly used metal because of its excellent catalytic activity in various cross-coupling reactions.[2] However, its toxicity and expensive nature limits its use in certain cases. Recently, copper based catalysts have been widely used in organic synthesis owing to its unique features like low toxicity and relatively low cost.[3] Considering the above challenges we have prepared a ternary nanocomposite Cu@GO–SiO_2 and employed it in diverse cross-coupling reactions.

II.C.2 Background and objectives

Transition metal catalyzed cross-coupling reactions have been studied in detail by several research groups for the last few decades.[1] Among the multifarious cross-coupling reactions, the one that has by far received the most attention has been the Suzuki-Miyaura cross-coupling reaction.[16] Traditional Suzuki-Miyaura cross-coupling reaction involves alkenyl boranes and alkyl/aryl halides as the coupling partners in presence of palladium catalysts.[17,18] However, several newer modifications of this reaction have evolved over the course of last two decades.[19,20] This reaction has rapidly become one of the most efficient processes for the formation of C–C bonds owing to its versatile applications and non-toxic nature of the reactants. After the Suzuki-Miyaura cross-coupling reaction, another important cross-coupling reaction has been the Buchwald-Hartwig cross-coupling reaction for the formation of C–N bonds.[21] Other transition metal catalyzed cross-coupling reactions that are also widely studied involves the formation of C–S, C–O and C–Se.[22-24] Few representative examples of different cross-coupling reactions have been illustrated below.

An efficient protocol for the Mizoroki-Heck cross-coupling reaction using palladium NPs supported chemically modified graphene has been accomplished (Scheme II.C.1). The investigators have prepared nitrogen and sulfur functionalized graphene oxide and immobilized palladium NPs on its surface (GL-Pd). The excellent catalytic activity of the nanocomposite has been attributed to the coordination from N and S to Pd.[25,26]

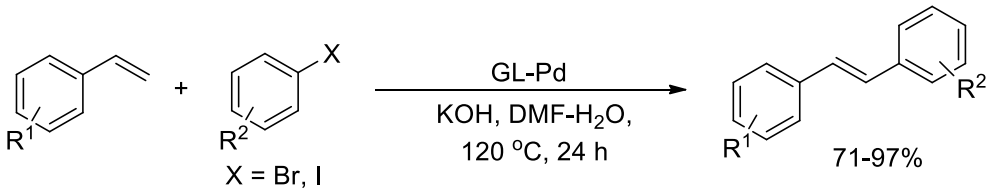

Scheme II.C.1 Heck cross-coupling reaction using Pd supported chemically modified graphene.

Palladium chloride supported on graphene oxide (GO-$PdCl_2$) has been prepared and used as a heterogeneous catalyst for C–C and C–N cross coupling reactions.[27] The reaction conditions

involve coupling of heteroaryl sulfonates with arylboronic acids, terminal alkynes and anilines to form the corresponding cross-coupled products (Scheme II.C.2).

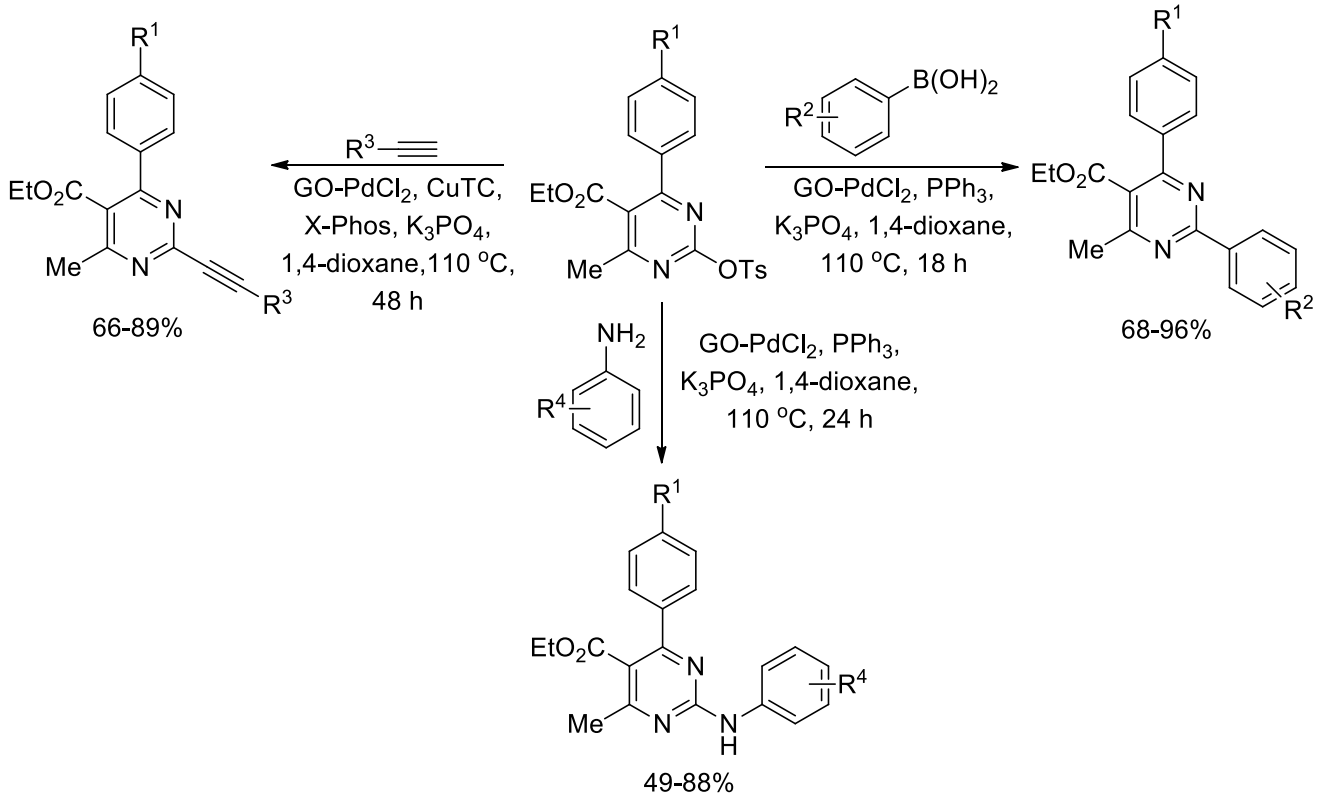

Scheme II.C.2 GO-$PdCl_2$ catalyzed C–C and C–N cross coupling reactions.

Nickel nanoparticles supported on reduced graphene oxide surface (Ni-rGO-40) has been used as a heterogeneous catalyst for the synthesis of thioethers from thiols and aryl iodides/bromides (Scheme II.C.3). The catalyst has been recycled for six cycles without apparent loss in the yield of products. The corresponding thioethers have been obtained in 75-93% yields.[28]

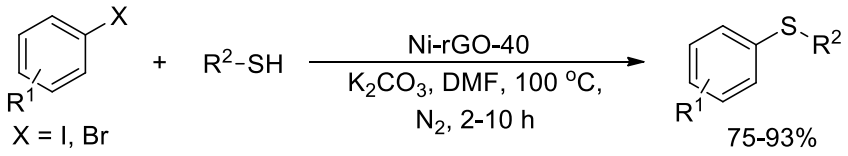

Scheme II.C.3 Ni-rGO-40 catalyzed C–S cross-coupling reaction.

Copper nanoparticles immobilized on carbon nanofibers (Cu NPs/CNFs) has been prepared and used for the arylation of phenols via C–O cross-coupling reaction (Scheme II.C.4). The protocol has been further extended for the C–N cross-coupling reaction.[29]

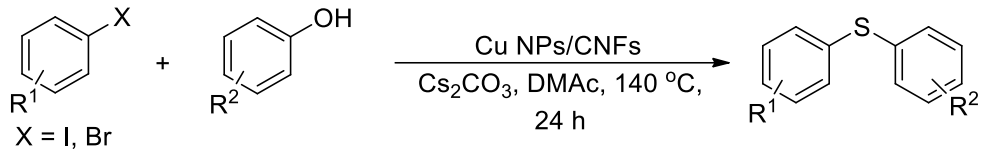

Scheme II.C.4 Cu NPs/CNFs catalyzed C–O cross-coupling reaction.

Nanocrystalline copper oxide (CuO NPs) has been used as catalyst for the C–Se cross-coupling reaction (Scheme II.C.5). The reaction conditions involve aryl iodides and diaryl diselenides as the coupling partners using KOH as base under inert atmosphere. The corresponding diaryl selenides have been synthesized in 82-94% yields.[30]

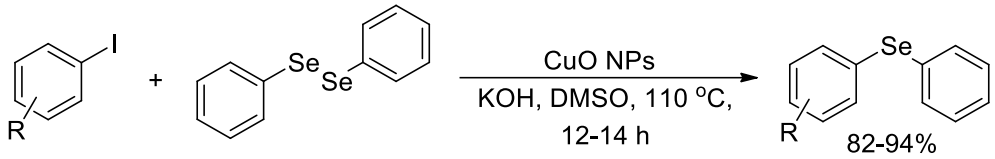

Scheme II.C.5 CuO NPs catalyzed synthesis of diaryl diselenides.

II.C.3 Present work: Results and discussions

II.C.3.1 Preparation of Cu@GO–SiO_2 nanocomposite

We have prepared the GO–SiO_2 composite according to the procedure developed by Choi and co-workers.[31] Graphene oxide was chosen as a support due to its high stability, high surface area and the presence of oxygenated functional groups which allowed further functionalization. The functionalization of graphene oxide with silica was effectively carried out by the hydrolysis of tetraethylorthosilicate (TEOS) in the presence of hydrophilic GO dispersion. After that copper species were immobilized on to the surface of GO–SiO_2 via in situ reduction of copper acetate using $NaBH_4$. This new ternary nanocomposite (Cu@GO–SiO_2) was used as a heterogeneous catalyst for C–S, C–C, C–O and C–N cross-coupling reactions.

II.C.3.2 Characterization of Cu@GO–SiO_2 nanocomposite

The synthesized ternary nanocomposite (Cu@GO–SiO_2) was characterized by different spectroscopic methods such as FT-IR, Raman spectroscopy, powder X-ray diffraction patterns (XRD) and X-ray photoelectron spectroscopy (XPS). Furthermore, the morphology of Cu@GO–SiO_2 nanocomposite was analyzed by transmission electron microscopy (TEM).

To determine the various functional groups, the FT-IR spectra of the synthesized GO, GO–SiO_2 and Cu@GO–SiO_2 were recorded. The comparative FT-IR spectrum of GO, GO–SiO_2

and Cu@GO–SiO_2 nanocomposite has been shown in Figure II.C.1. The peaks at 3423 cm^{-1} and 1397 cm^{-1} were attributed due to the stretching and deformation of –OH bond in the GO.[32] The band centered at 1046 cm^{-1} was associated with the stretching of the C–O bond.[32] The stretching vibration of the C=O bond of carboxyl groups was observed at 1721 cm^{-1}.[32] When GO–SiO_2 has been formed after the reaction with TEOS, the characteristic peaks of silica were observed.[31] It indicates the fabrication of silica on GO surface. The sharp peak at 471 cm^{-1} was attributed to Si–O–Si bending vibration.[33] The typical carbonyl group band at 1721 cm^{-1} disappeared which indicated that the carbonyl groups were converted to Si–O–C bands.[33] In the FT-IR spectrum of Cu@GO–SiO_2 nanocomposite, the intensity of –OH stretching was reduced significantly during the reduction process of metal nanoparticles. When the FT-IR spectra of GO, GO–SiO_2 and Cu@GO–SiO_2 were compared the characteristic peaks between 1300 cm^{-1} and 1600 cm^{-1} were absent in the spectrum of Cu@GO–SiO_2 nanocomposite, which indicated that the oxygen containing functional groups were unfixed.

The X-ray diffraction (XRD) patterns of GO–SiO_2 hybrid composite and Cu@GO–SiO_2 nanocomposite has been shown in Figure II.C.2. A sharp peak at 10.65° and 42.49° was observed in GO–SiO_2 hybrid and was in accordance with the literature report.[15] A broad peak at 23.24° was due to the leading effect of silica particles in graphene oxide.[31] In the XRD pattern of the Cu@GO–SiO_2 nanocomposite (Figure II.C.2) showed that the presence of diffraction peaks at 2θ ~ 36.47°, 43.44°, 50.73° due to Cu_2O (JCPDS# 01-073-6371) and 73.96° due to metallic Cu (JCPDS# 01-071-4609) nanoparticles.[34]

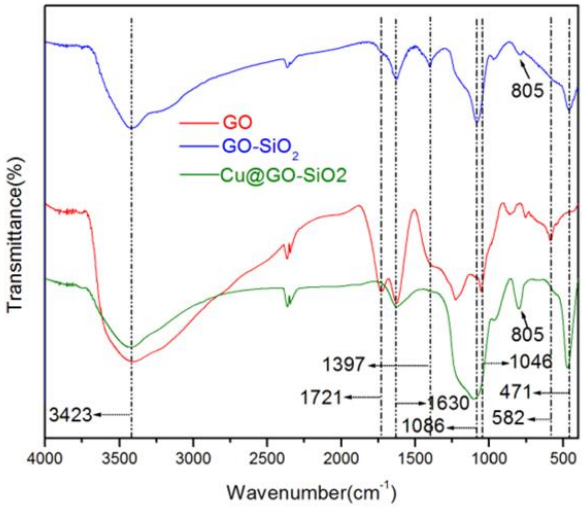

Figure II.C.1 FT-IR spectra of GO, GO–SiO_2 and Cu@GO–SiO_2.

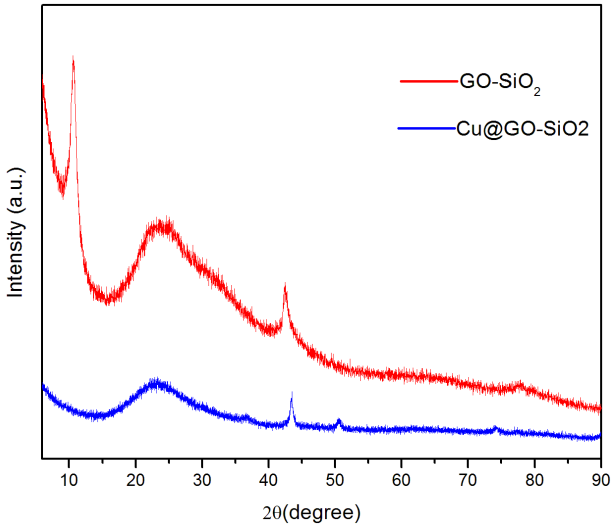

Figure II.C.2 XRD patterns of GO–SiO_2 and Cu@GO–SiO_2.

Raman spectroscopy has been another powerful technique in the characterization of graphene-based materials. As can be seen from the Raman spectra (Fig II.C.3), the D- and G-bands of the GO–SiO_2 and Cu@GO–SiO_2 gave almost same values. However, the intensity ratio of the D- and G- bands (I_D/I_G) has been found to decrease which corroborates the successful incorporation of copper NPs in the nanocomposite.[35]

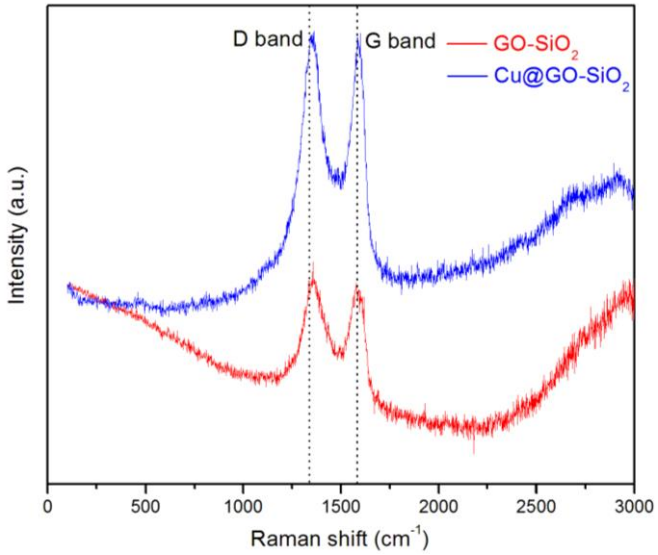

Figure II.C.3 Raman spectra of GO–SiO_2 and Cu@GO–SiO_2.

The morphology and microstructure of the Cu@GO–SiO_2 was analyzed from transmission electron microscopy (TEM) analysis (Figure II.C.4). The Figure II.C.4a shows the nano sized copper particles were distributed uniformly in the GO–SiO_2 surface. At higher magnification the deposition of Cu NPs was clearly observed (Figure II.C.4b and Figure II.C.4c). The

average size of copper NPs was shown in the inset of Figure II.C.4b which showed that most of the NPs were distributed in the range of 5-10 nm. The clear image of metal NPs depositions on GO–SiO_2 surface was observed with the help of HRTEM image at 5 nm magnification (Figure II.C.4d). Moreover, the selected area electron diffraction patterns (SAED) of Cu@GO–SiO_2 depicted the lattice fringes of Cu_2O and Cu NPs, which clearly indicated its crystalline nature. The chemical composition of the as-prepared nanocomposite was analyzed by energy dispersive X-ray spectroscopy (EDS). The EDS spectrum showed the presence of Cu, O, C and Si species which further confirms the deposition of copper NPs on GO–SiO_2 surface (Figure II.C.4e).

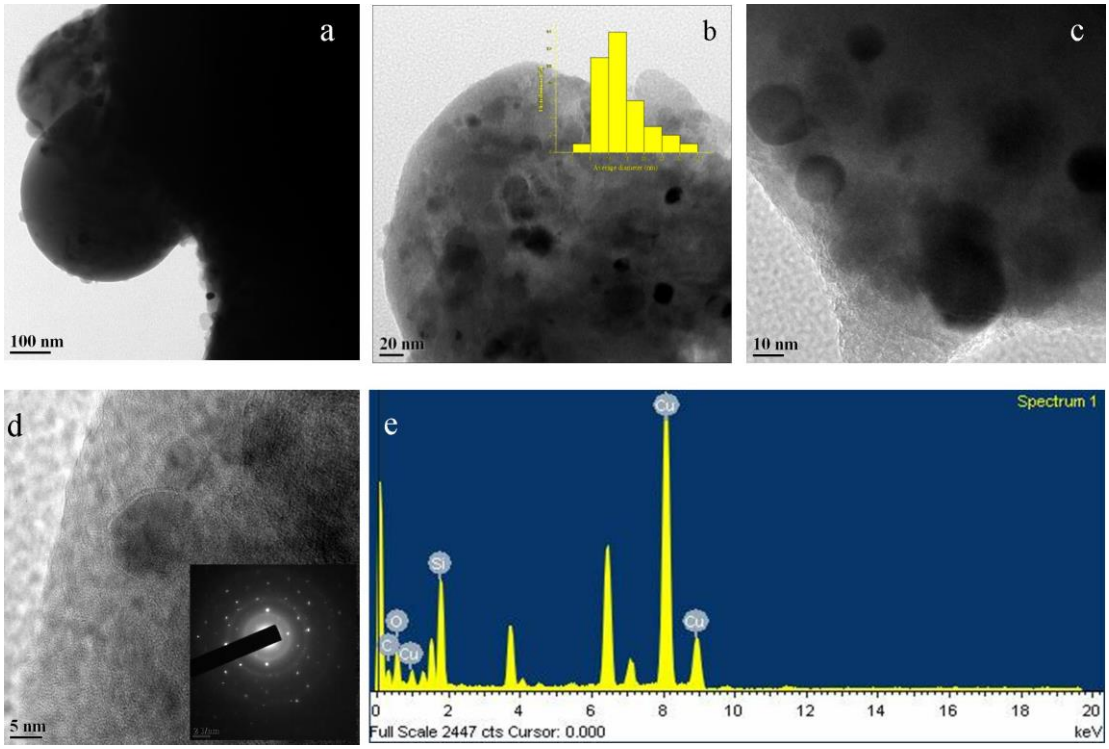

Figure II.C.4 (a-d) HR-TEM images and (e) EDS image of Cu@GO–SiO_2.

The X-ray photoelectron spectroscopy (XPS) analysis of Cu@GO–SiO_2 was performed to get more details about the nanocomposite (Figure II.C.5). The peak at 934.4 eV corresponds to the Cu $2p_{3/2}$ peak of Cu^+ and Cu^{2+} species. The peaks at 952.3 and 954.3 eV, corresponding to Cu $2p_{1/2}$ were also due to the presence of Cu^+ and Cu^{2+} species. Moreover, satellite peaks of Cu $2p_{3/2}$ and Cu $2p_{1/2}$ were also observed at 943.0 and 962.4 eV.[36]

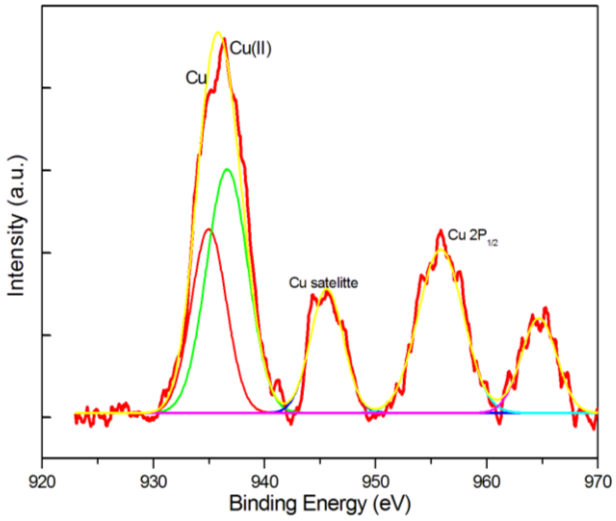

Figure II.C.5 XPS analysis of Cu@GO–SiO_2 nanocomposite.

II.C.3.3 Catalytic activity of Cu@GO–SiO_2 nanocomposite

II.C.3.3a Cu@GO–SiO_2 nanocomposite catalyzed C–S cross-coupling reaction

The as-prepared Cu@GO–SiO_2 nanocomposite was then employed for various cross-coupling reactions. At first, we have used the catalyst for the C–S cross-coupling reaction. For this purpose, 4-iodoanisole (**1a**) and thiophenol (**2a**) were selected as the model substrates. The results have been presented in Table II.C.1. Initially, the reaction was carried out in aqueous media with K_2CO_3 and sodium dodecyl sulfate (SDS) at 90 °C which furnished the desired thioether **3a** in 87% yield (entry 1). In the absence of SDS, the yield of the product decreased to 63% (entry 2). Next, the reaction was performed in polar aprotic solvents like DMF and CH_3CN which afforded the desired product in 79% and 82% yields respectively (entries 3 and 4). In presence of tetrabutylammonium bromide (TBAB), the yield of the product did increase to 91% in aqueous media (entry 5). The change of base from K_2CO_3 to Na_2CO_3 and KOH in water gave lower yield (entries 6 and 7, 84% and 87%). The same reaction at room temperature gave a trace amount of product after 24 h of the reaction (entry 8). While increasing the quantity of the catalyst to 35 mg gave similar conversion (entry 9, 92%), and lowering catalyst loading to 15 mg resulted in good conversion (entry 10, 82%). The reaction did not proceed in the absence of the catalyst, keeping other conditions unchanged (entry 11). However, carrying out the reaction without solvent and additive, the yield of the product got significantly lowered (entry 12, 54%). The absence of base also resulted in similar observation (entry 13, 48%).

Table II.C.1 Optimization of the reaction conditions[a]

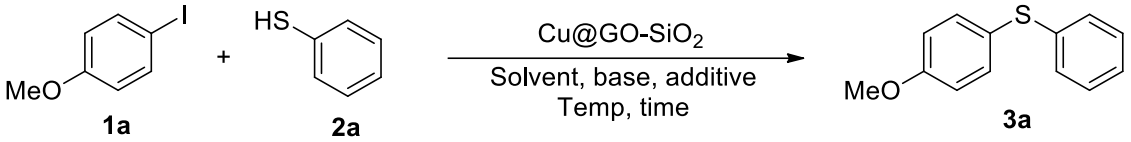

Entry	Catalyst (mg)	Solvent	Base	Additive	Temp (°C)/ time (h)	Yield (%)[b]
1	25	H_2O	K_2CO_3	SDS	90 / 8	87
2	25	H_2O	K_2CO_3	–	90 / 8	63
3	25	DMF	K_2CO_3	–	90 / 8	79
4	25	CH_3CN	K_2CO_3	–	80 / 8	82
5	**25**	**H_2O**	**K_2CO_3**	**TBAB**	**90 / 8**	**91**
6	25	H_2O	Na_2CO_3	TBAB	90 / 8	84
7	25	H_2O	KOH	TBAB	90 / 8	87
8	25	H_2O	K_2CO_3	TBAB	r.t. / 24	trace
9	35	H_2O	K_2CO_3	TBAB	90 / 8	92
10	15	H_2O	K_2CO_3	TBAB	90 / 8	82
11	–	H_2O	K_2CO_3	TBAB	90 / 8	no reaction
12	25	–	K_2CO_3	–	90 / 8	54
13	25	H_2O	–	TBAB	90 / 8	48

[a]Reaction conditions: **1a** (1 mmol), **2a** (1 mmol), base (2 mmol), solvent (2 mL) and additive (10 mol%). [b]Isolated yield after purification through column chromatography.

With the optimized reaction conditions in hand, the substrate scope with various aryl halides and thiols was thoroughly explored (Table II.C.2). Aryl iodides bearing electron donating as well as electron withdrawing groups such gave good to excellent yield of the corresponding thioethers (entries 1 to 9). The same reaction with aryl bromides with aryl thiols gave relatively lower yield of the corresponding sulfides (entries 1 and 2). The reaction of aryl iodides with alkyl thiols gave lower yields than that of aryl thiols (entries 10 and 11). Moreover, the reaction also worked efficiently with heteroaryl thiol and the desired product was formed in 87% yield (entry 12).

Table II.C.2 Cu@GO–SiO_2 catalyzed synthesis of thioethers[a]

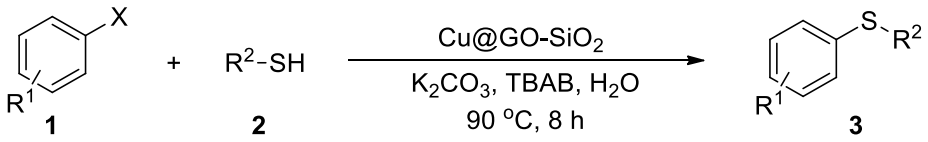

Entry	Aryl halide	Thiol	Thioether	Yield (%)[b]
1	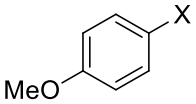 (X = I, Br)	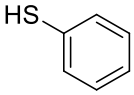	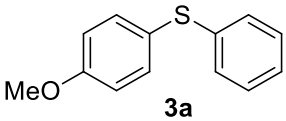 **3a**	91 (X = I) 84 (X = Br)
2	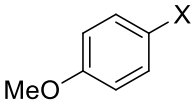 (X = I, Br)	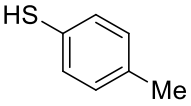	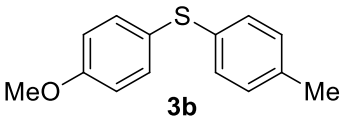 **3b**	88 (X = I) 82 (X = Br)
3	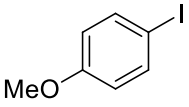	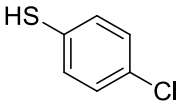	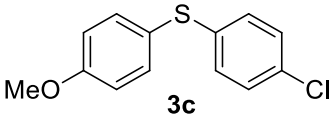 **3c**	93
4	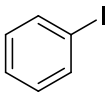	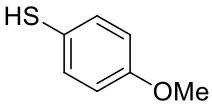	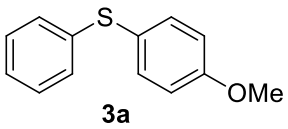 **3a**	87
5	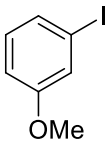	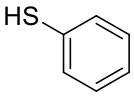	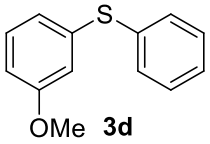 **3d**	89
6	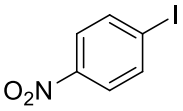	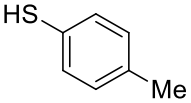	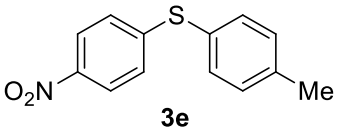 **3e**	88
7	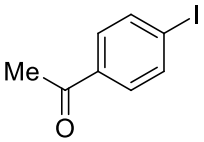	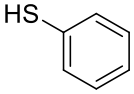	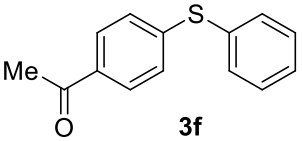 **3f**	90
8	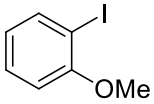	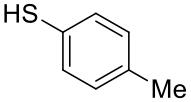	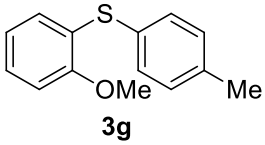 **3g**	86
9	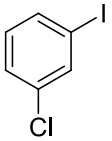	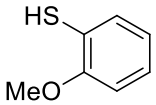	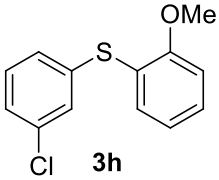 **3h**	85
10	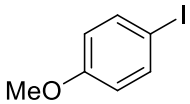	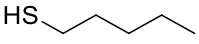	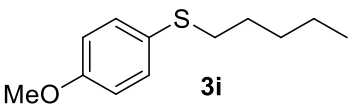 **3i**	80
11	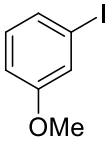	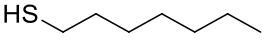	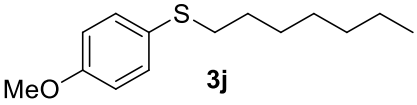 **3j**	83

12	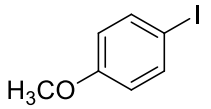	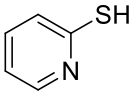	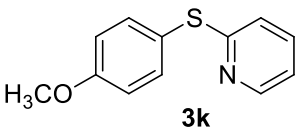 **3k**	87

[a]Reaction conditions: **1** (1 mmol), **2** (1 mmol), Cu@GO–SiO_2 (25 mg), K_2CO_3 (2 mmol), TBAB (10 mol%) and H_2O (2 mL) were stirred at 90 °C for 8 h. [b]Isolated yield after purification through column chromatography.

II.C.3.3b Cu@GO–SiO_2 nanocomposite catalyzed C–C cross-coupling reaction

The Suzuki-Miyura coupling reaction was also investigated with the as-prepared Cu@GO–SiO_2 nanocomposite. Initially, the reaction was carried out with 4-iodoanisole (**1a**) and phenylboronic acid (**4a**) using Cu@GO–SiO_2 nanocomposite (25 mg), K_2CO_3 (1 mmol) and tetrabutylammonium bromide, TBAB (10 mol%) at 100 °C. The desired product **5a** was formed in 34% isolated yield (entry 1). The change of solvent from water to DMF and then to DMSO significantly increased the yield of the product to 78% and 72% respectively (entries 2 and 3). The change of base from K_2CO_3 to Na_2CO_3 and KOH under the same condition gave lower yields (entries 4 and 5, 61% and 65% respectively). When the catalyst loading was increased from 25 to 40 mg the desired product was isolated in 79% yield (entry 6). The reaction did not occur in the absence of the catalyst (entry 7).

Table II.C.3 Optimization of the reaction conditions[a]

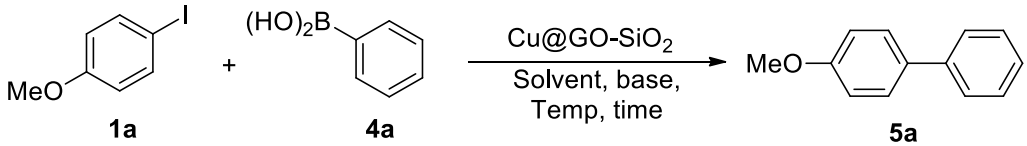

1a **4a** **5a**

Entry	Catalyst (mg)	Solvent	Base	Temp (°C)/ time (h)	Yield (%)[b]
1	25	H_2O	K_2CO_3	100 / 8	34[c]
2	**25**	**DMF**	**K_2CO_3**	**110 / 8**	**78**
3	25	DMSO	K_2CO_3	110 / 8	72
4	25	DMF	Na_2CO_3	110 / 8	61
5	25	DMF	KOH	110 / 8	65
6	40	DMF	K_2CO_3	110 / 8	79
7	–	DMF	K_2CO_3	110 / 8	no reaction

[a]Reaction conditions: **1a** (0.5 mmol), **4a** (0.5 mmol), base (1 mmol) and solvent (2 mL). [b]Isolated yield after purification through column chromatography. [c]TBAB (10 mol%) was used.

With the optimized reaction conditions in hand, the substrate scope of aryl iodides and phenylboronic acids was thoroughly explored (Table II.C.4). Aryl iodides bearing electron

donating as well as electron withdrawing groups resulted in the formation of the desired products in 69-78% yield (entries 1 to 7). This indicated that imperative role of the catalyst towards catalyzing Suzuki cross coupling reaction.

Table II.C.4 Cu@GO–SiO_2 catalyzed synthesis of substituted biphenyls[a]

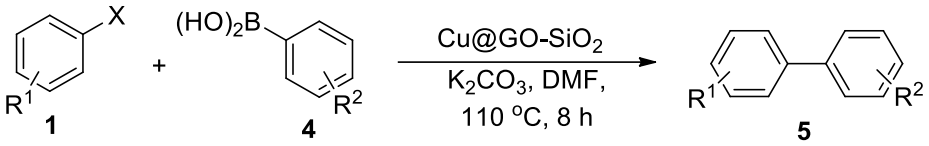

Entry	Aryl halide	Phenylboronic acid	Product	Yield (%)[b]
1	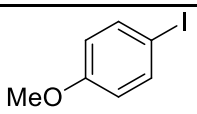	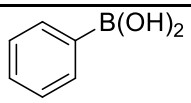	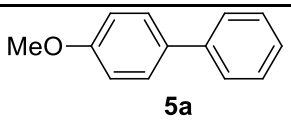 **5a**	78
2	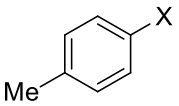 (X = I, Br)	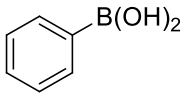	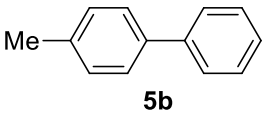 **5b**	73 (X = I) 69 (X = Br)
3	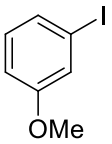	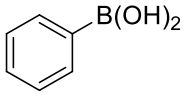	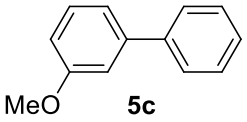 **5c**	72
4	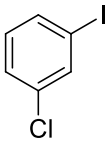	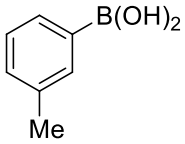	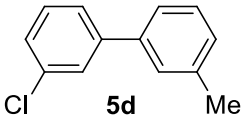 **5d**	76
5	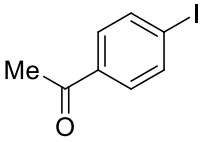	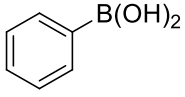	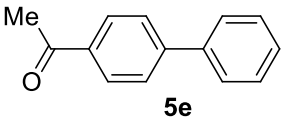 **5e**	78
6	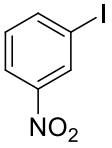	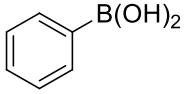	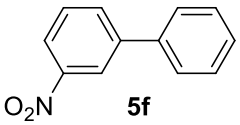 **5f**	76
7	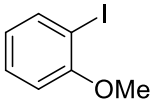	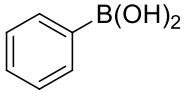	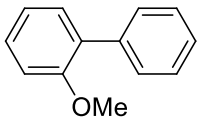 **5g**	70

[a]Reaction conditions: **1** (1 mmol), **4** (1 mmol), Cu@GO–SiO_2 (25 mg), K_2CO_3 (2 mmol) and DMF (2 mL) were stirred at 110 °C for 8 h. [b]Isolated yield after purification through column chromatography.

II.C.3.3c Cu@GO–SiO_2 nanocomposite catalyzed C–O cross-coupling reaction

We next attempted the C–O cross-coupling reaction with Cu@GO–SiO_2 nanocomposite. For this reaction 4-iodoanisole (**1a**) and 4-hydroxytoluene (**6a**) were selected as the model coupling partners. The catalytic activity of the catalyst was studied under various solvents, bases, ligands and additives at different temperatures (Table II.C.5). In each reaction **1a** (0.5 mmol), **6a** (0.5 mmol), ligand (10 mol%) and base (1.0 mmol) were taken. The best condition was achieved in presence of K_3PO_4 as base and 2,2′-bipyridine as ligand in DMF at 110 °C.

Table II.C.5 Optimization of the reaction conditions[a]

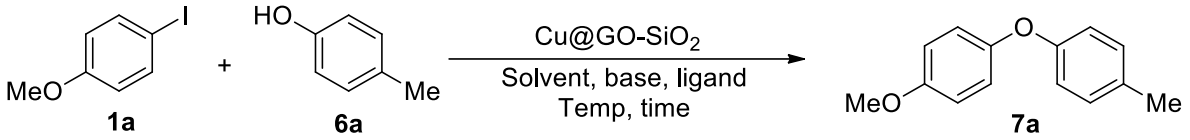

Entry	Catalyst (mg)	Solvent	Base	Ligand[b]	Temp (°C)/ time (h)	Yield (%)[c]
1	25	DMF	K_2CO_3	L1	110 / 24	71
2	25	DMSO	K_2CO_3	L1	110 / 24	65
3	25	PhMe	K_2CO_3	L1	110 / 24	41
4	25	DMF	Cs_2CO_3	L1	110 / 24	58
5	25	DMF	KF	L1	110 / 24	38
6	**25**	**DMF**	**K_3PO_4**	**L1**	**110 / 24**	**91**
7	25	DMF	K_3PO_4	L2	110 / 24	87
8	25	DMF	K_3PO_4	L3	110 / 24	40
9	25	DMF	K_3PO_4	L1	r.t. / 24	no reaction
10	35	DMF	K_3PO_4	L1	110 / 24	93
11	15	DMF	K_3PO_4	L1	110 / 24	79
12	–	DMF	K_3PO_4	L1	110 / 24	no reaction
13	25	DMF	–	L1	110 / 24	trace
14	25	DMF	K_3PO_4	–	110 / 24	43

[a]Reaction conditions: **1a** (0.5 mmol), **6a** (0.5 mmol), base (1 mmol), ligand (10 mol%) and solvent (2 mL). [b]Ligand: L1 = 2,2′-bipyridine, L2 = 1,10-phenanthroline and L3 = L-proline. [c]Isolated yield after purification through column chromatography.

With the optimized reaction conditions we have studied the substrate scope with various aryl halides with substituted phenols (Table II.C.6). Aryl iodides showed better response than aryl bromides towards the reaction (entries 2 and 5).

Table II.C.6 Cu@GO–SiO_2 catalyzed synthesis of diarylethers[a]

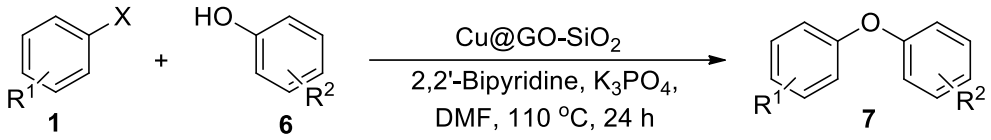

Entry	Aryl halide	Phenol	Diarylether	Yield (%)[b]
1	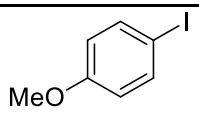	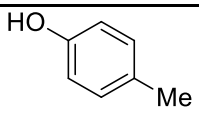	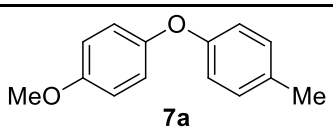 **7a**	91
2	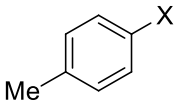 (X = I, Br)	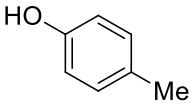	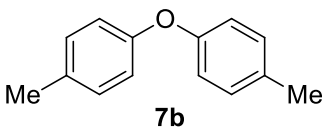 **7b**	93 (X = I) 84 (X = Br)
3	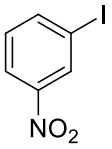	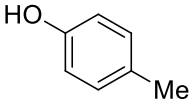	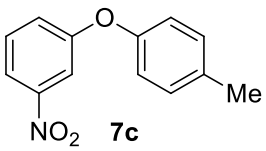 **7c**	89
4	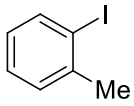	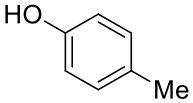	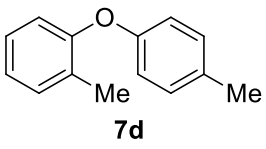 **7d**	79
5	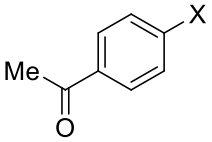 (X = I, Br)	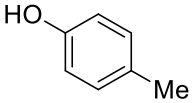	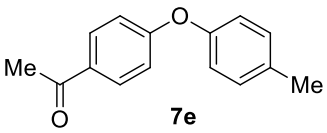 **7e**	92 (X = I) 86 (X = Br)
6	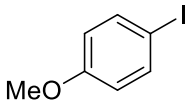	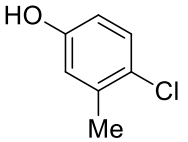	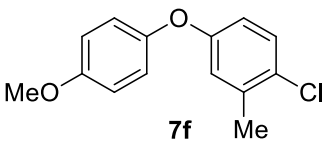 **7f**	87

[a]Reaction conditions: **1** (1 mmol), **6** (1 mmol), Cu@GO–SiO_2 (25 mg), K_3PO_4 (2 mmol), 2,2′-bipyridine (10 mol%) and DMF (2 mL) were stirred at 110 °C for 24 h. [b]Isolated yield after purification through column chromatography.

II.C.3.3d Cu@GO–SiO_2 nanocomposite catalyzed C–N cross-coupling reaction

We next employed the nanocomposite for C–N cross-coupling reaction with aryl halides and imidazoles (Table II.C.7). The as-synthesized Cu@GO–SiO_2 catalyst was used by taking 4-iodotoluene (**1b**) and imidazole (**8a**) as coupling partners. The catalytic activity of the catalyst was examined under various solvents, bases and additives at different temperatures. The best condition was achieved in presence of KOH in CH_3CN at 80 °C (entry 5, 86% yield).

Table II.C.7 Optimization of reaction conditions[a]

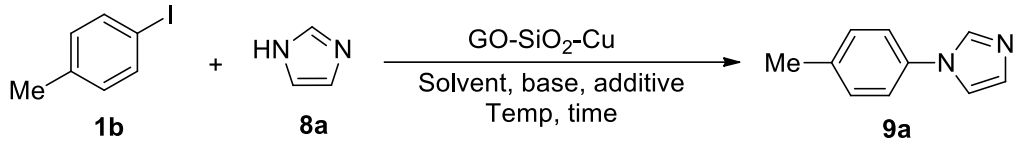

Entry	Cu@GO–SiO_2 (mg)	Solvent	Base	Temp (°C)/ time (h)	Yield (%)[b]
1	25	DMF	K_2CO_3	110 / 24	68
2	25	DMSO	K_2CO_3	110 / 24	73
3	25	H_2O	K_2CO_3	100 / 24	32
4	25	MeCN	K_2CO_3	80 / 24	79
5	**25**	**MeCN**	**KOH**	**80 / 24**	**86**
6	25	MeCN	NaOH	80 / 24	75
7	–	MeCN	KOH	80 / 24	no reaction

[a]Reaction conditions: **1b** (1 mmol), **8a** (1 mmol), base (2 mmol) and solvent (2 mL). [b]Isolated yield after purification through column chromatography.

With the optimized reaction conditions we have studied the substrate scope with various aryl iodides with imidazole or benzimidazole (Table II.C.8). The corresponding C–N cross coupled products were synthesized in 80-89% isolated yield (entries 1 to 8).

Table II.C.8 Cu@GO–SiO_2 catalyzed C–N cross coupling reaction[a]

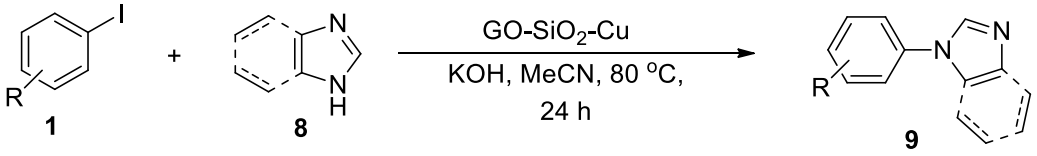

Entry	Aryl halide	Amine	Product	Yield (%)[b]
1	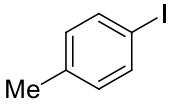	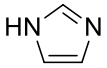	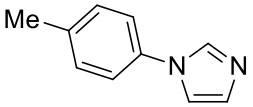 **9a**	86
2	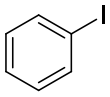	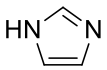	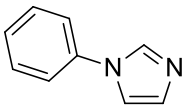 **9b**	89
3	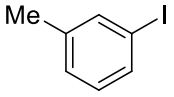	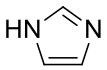	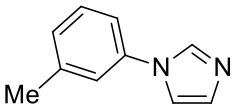 **9c**	81

4	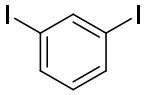	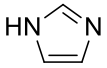	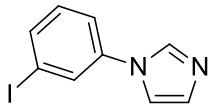 **9d**	80
5	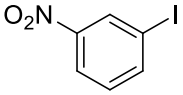	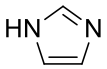	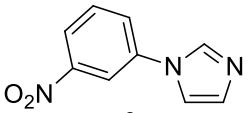 **9e**	85
6	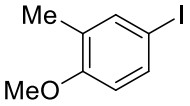	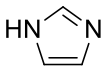	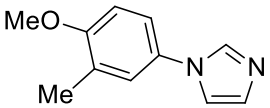 **9f**	86
7	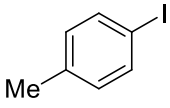	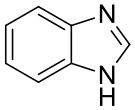	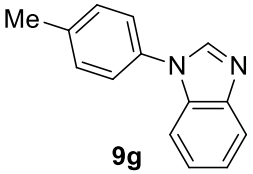 **9g**	88
8	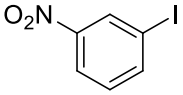	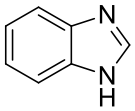	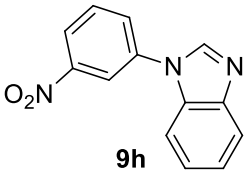 **9h**	84

[a]Reaction conditions: **1** (1 mmol), **8** (1 mmol), Cu@GO–SiO_2 (25 mg), KOH (2 mmol) and MeCN (2 mL) were stirred at 80 °C for 24 h. [b]Isolated yield after purification through column chromatography.

II.C.3.4 Recyclability of Cu@GO–SiO_2 nanocomposite

We have checked the recyclability of Cu@GO–SiO_2 catalyst in the C–S cross-coupling reaction under the optimized condition. After the first run the catalyst was separated from the reaction mixture by simple filtration, washed with ethyl acetate (3 x 5 mL) and dried under vacuum for 24 h. It was then re-used for the next catalytic run. The catalyst was re-used for four consecutive runs without any significant drop in the yield of the product (Figure II.C.6). Moreover, we characterized the catalyst after the third run by using XRD patterns and Raman spectroscopy. The morphology of the catalyst was also studied by using HRTEM analysis.

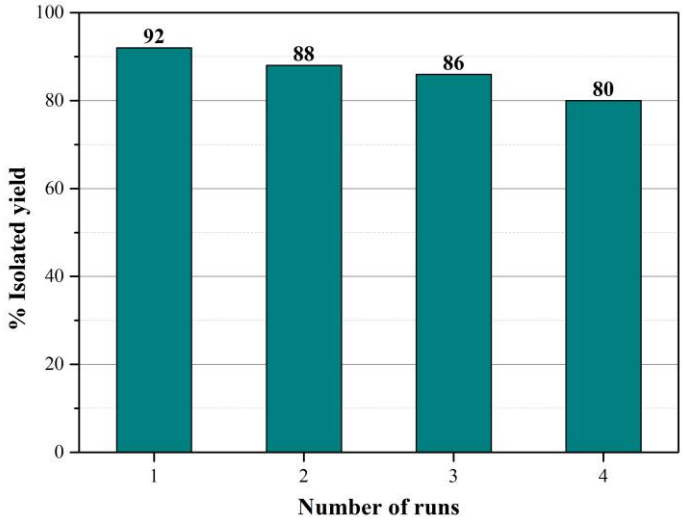

Figure II.C.6 Recyclability of Cu@GO–SiO_2 nanocomposite in C–S cross-coupling reaction.

II.C.4 Conclusion

In conclusion, we have prepared a robust catalyst based on graphene oxide silica hybrid surface. The catalyst exhibited excellent catalytic activity towards different cross-coupling reactions. Moreover, the catalyst was also found recyclable without appreciable loss in its performance. We presumed that the superior catalytic activity of the catalyst was due to the presence of copper species in different oxidation states. Furthermore, we believe that this heterogeneous catalytic system would also be effective towards other copper catalyzed processes.

II.C.5 Experimental section

II.C.5.1 General Information

All reagents were purchased from Sigma-Aldrich and used directly without further purification. Tetraethyl orthosilicate (TEOS) was procured from Sigma-Aldrich and used as received. The solvents were purchased from commercial suppliers and used after distillation. All the products were purified by column chromatography on 60-120 mesh silica gel (Merck, India). For TLC, Merck plates coated with silica gel 60, F_{254} were used. FT-IR spectra were recorded in FT-IR 8300 SHIMADZU spectrophotometer. The ^{1}H & ^{13}C NMR spectra were recorded at 300 MHz and 75 MHz respectively on Bruker AV 300 spectrometer in $CDCl_3$. Splitting patterns of protons were described as s (singlet), d (doublet), dd (doublet of doublet) and m (multiplet). Chemical shifts (δ) were reported in parts per million (ppm) relative to TMS as internal standard. *J* values (coupling constant) were reported in Hz (Hertz). ^{13}C NMR spectra were recorded with complete proton decoupling ($CDCl_3$: δ 77.0 ppm). Centrifugation

was done in REMI R-8C DX centrifuge. The X-ray diffraction studies (XRD) were done by the Rigaku SmartLab (9 kW) diffractometer using CuKα radiation. Raman spectra of the samples were obtained with Renishaw InVia micro Raman spectroscopy with 514 nm laser source. Scanning Electron Microscopy (SEM) and Electron-Dispersive X-ray Spectroscopy (EDS) were performed using JEOL JSM-IT 100 electron microscope. Transmission electron microscopy (TEM) measurements were carried out using a JEOL JEM-2100F high-resolution electron microscope. X-ray photoelectron spectroscopic (XPS) measurements were done on a PHI 5000 Versaprobe II XPS system with an Al Kα source and a charge neutralizer at room temperature.

II.C.5.2 Preparation of graphene oxide (GO)

Graphene oxide was prepared by following Tour's method.[32] In this method a 9:1 (v/v) mixture of H_2SO_4 / H_3PO_4 (180:20 mL) was added to a mixture of graphite powder (1.5 g) and $KMnO_4$ (9.0 g). The mixture was then stirred at 50 ℃ for 12 h. After cooling the mixture to room temperature, it was gradually poured into crushed ice (200 g), which was followed by the slow addition of H_2O_2 (30%, 1.5 mL). The solution was then centrifuged (5000 rpm) and the supernatant was discarded. The residual solid material was successively washed with deionised water (100 mL) and then with 30% HCl (100 mL). The solid material was then repeatedly washed with water and centrifuged. Finally, the solid brown material was collected and dried at 60 ℃ under vacuum to obtain solid graphene oxide.

II.C.5.3 Preparation of GO–SiO_2 hybrid nanocomposite

GO–SiO_2 hybrid nanocomposite was prepared by following a reported method.[31] For this purpose, the well-known hydrolysis of tetraethylorthosilicate (TEOS) was then employed. Briefly, GO (300 mg) prepared via the Tour's method and TEOS (5 g) were dispersed separately in ethanol (30 g) to produce stable suspensions. Subsequently, the two suspensions were mixed together and placed into a water bath at 40 ℃ for 10 min to ensure a constant temperature. Hydrous ammonia ($NH_3 \cdot H_2O$, 0.76 g) was added quickly into the mixture, and the products were displaced after 15 h, washed 3 times with de-ionized water and ethanol each, and finally dried in a vacuum oven at 60 ℃ 48 h.

II.C.5.4 Preparation of Cu@GO–SiO_2 composite

GO–SiO_2 (1.0 g) was taken in a Teflon-capped sealed tube. To it $Cu(OAc)_2 \cdot H_2O$ (1 mmol, 200 mg) and $NaBH_4$ (200 mg) was added followed by the addition of 5 mL of water. It was then placed in a pre-heated oil bath at 100 ℃ and gently stirred for 3 h. The mixture was then cooled to room temperature and centrifuged at 5000 rpm. The supernatant was discarded and

the residue was washed with distilled water (3 times) and finally with acetone (2 times). The solid mass was then dried under vacuum for 48 h.

II.C.5.5 Typical procedure for the cross-coupling reactions

In a Teflon-capped sealed tube equipped with a magnetic stir bar, aryl halides (1.0 or 0.5 mmol), thiols/phenylboronic acids/phenols/imidazoles (1.0 or 0.5 mmol), Cu@GO–SiO_2 (25 mg), base (2 equiv), ligand (10 mol%, only in case of C–O coupling), TBAB (10 mol%, only in case of C–S coupling) and solvent (2 mL) were added. The resulting reaction mixture was stirred at 80-110 °C for 8-24 h. After completion of the reaction (monitored by TLC), the reaction mixture was cooled to room temperature. The catalyst was then recovered through simple filtration. The reaction mixture was diluted with water and extracted by ethyl acetate (3 x 5 mL). Finally, the combined organic layer was dried over anhydrous Na_2SO_4 and concentrated. The residue was then further purified by column chromatography on silica gel using the light petroleum ether and ethyl acetate as eluent to afford the desired products. All products were characterized by ^{1}H and ^{13}C NMR spectroscopy.

II.C.5.6 Characterization data of various products listed in Table II.C.2, II.C.4, II.C.6 and II.C.8

(4-Methoxyphenyl)(phenyl)sulfane (3a)

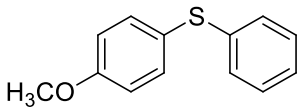

^{1}H NMR (300 MHz, $CDCl_3$): δ 3.82 (s, 3H), 6.90 (dd, *J* = 6.6 and 2.1 Hz, 2H), 7.11-7.26 (m, 5H), 7.42 (dd, *J* = 6.9 and 2.1 Hz, 2H); **^{13}C NMR (75 MHz, $CDCl_3$)**: δ 55.3, 114.9, 124.1, 125.6, 128.0, 128.8, 135.3, 138.5, 159.7.

(4-Methoxyphenyl)(*p*-tolyl)sulfane (3b)

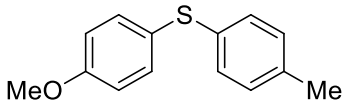

^{1}H NMR (300 MHz, $CDCl_3$): δ 2.29 (s, 3H), 3.79 (s, 3H), 6.85 (d, *J* = 9 Hz, 2H), 7.05 (d, *J* = 8.1 Hz, 2H), 7.12 (d, J = 8.1 Hz, 2H), 7.35 (d, *J* = 9 Hz, 2H); **^{13}C NMR** (**75 MHz, $CDCl_3$**): δ 20.9, 55.3, 114.8, 125.6, 129.3, 129.7, 134.3, 136.1, 159.4.

(4-Chlorophenyl)(4-methoxyphenyl)sulfane (3c)

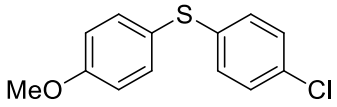

^{1}H NMR (300 MHz, $CDCl_3$): δ 3.81 (s, 3H), 6.89 (d, *J* = 8.7 Hz, 2H), 7.05-7.08 (m, 2H), 7.16-7.19 (m, 2H), 7.39 (d, *J* = 9 Hz, 2H); **^{13}C NMR (75 MHz, $CDCl_3$)**: δ 55.3, 115.1, 123.6, 128.9, 129.2, 131.5, 135.4, 137.3, 160.0.

(3-Methoxyphenyl)(phenyl)sulfane (3d)

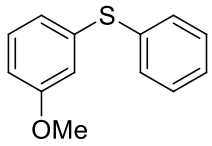

^{1}H NMR (300 MHz, $CDCl_3$): δ 3.69 (s, 3H), 6.72-6.76 (m, 1H), 6.85-6.90 (m, 2H), 7.14-7.37 (m, 6H); **^{13}C NMR (75 MHz, $CDCl_3$)**: δ 55.1, 112.6, 115.8, 122.8, 127.1, 129.1, 129.8, 131.2, 135.1, 137.1, 159.9.

(4-Nitrophenyl)(*p*-tolyl)sulfane (3e)

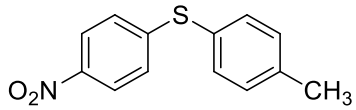

^{1}H NMR (300 MHz, $CDCl_3$): δ 1.79 (s, 3H), 6.50 (d, *J* = 7.5 Hz, 2H), 6.65 (d, *J* = 7.8 Hz, 2H), 6.81 (d, *J* = 7.8 Hz, 2H), 7.41 (d, *J* = 7.5 Hz, 2H); **^{13}C NMR (75 MHz, $CDCl_3$)**: δ 20.7, 123.3, 125.6, 130.2, 134.4, 139.6, 144.6, 148.6.

1-(4-(Phenylthio)phenyl)ethanone (3f)

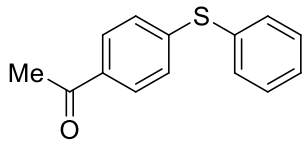

^{1}H NMR (300 MHz, $CDCl_3$): δ 2.52 (s, 3H), 7.18 (d, *J* = 8.7 Hz, 2H), 7.36-7.47 (m, 5H), 7.79 (d, *J* = 8.7 Hz, 2H); **^{13}C NMR (75 MHz, $CDCl_3$)**: δ 26.3, 127.3, 128.6, 128.7, 129.5, 131.9, 133.7, 134.3, 144.7, 196.9.

(2-Methoxyphenyl)(*p*-tolyl)sulfane (3g)

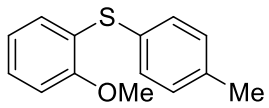

^{1}H NMR (300 MHz, $CDCl_3$): δ 2.35 (s, 3H), 3.88 (s, 3H), 6.79-6.88 (m, 2H), 6.92-6.95 (m, 1H), 7.13-7.20 (m, 3H), 7.30-7.32 (m, 2H); **^{13}C NMR (75 MHz, $CDCl_3$)**: δ 21.1, 55.8, 110.6, 121.2, 125.7, 127.4, 129.7, 129.8, 130.1, 132.9, 137.7, 156.5.

(3-Chlorophenyl)(2-methoxyphenyl)sulfane (3h)

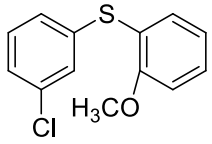

^{1}H NMR (300 MHz, $CDCl_3$): δ 3.83 (s, 3H), 6.89-6.94 (m, 2H), 7.11-7.18 (m, 3H), 7.20-7.34 (m, 3H); **^{13}C NMR (75 MHz, $CDCl_3$)**: δ 55.8, 111.2, 121.3, 121.5, 126.4, 127.6, 129.2, 129.7, 129.9, 133.6, 134.6, 137.9, 158.2.

(4-Methoxyphenyl)(pentyl)sulfane (3i)

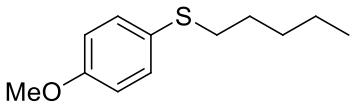

^{1}H NMR (300 MHz, $CDCl_3$): δ 0.85-0.90 (m, 3H), 1.25-1.40 (m, 6H), 1.58 (t, *J* = 7.8 Hz, 2H), 6.82-6.85 (m, 2H), 7.31-7.34 (m, 2H); **^{13}C NMR (75 MHz, $CDCl_3$)**: δ 13.9, 22.2, 29.0, 30.8, 35.7, 55.2, 114.4, 126.8, 132.8, 158.6.

Heptyl(3-methoxyphenyl)sulfane (3j)

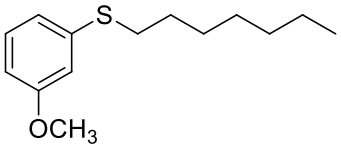

^{1}H NMR (300 MHz, $CDCl_3$): δ 0.85-0.90 (m, 3H), 1.25-1.32 (m, 8H), 1.39-1.41 (m, 2H), 1.60-1.68 (m, 1H), 2.91 (t, *J* = 7.2 Hz, 2H), 6.86-6.71 (m, 1H), 6.85-6.91 (m, 2H), 7.15-7.25 (m, 1H); **^{13}C NMR (75 MHz, $CDCl_3$)**: δ 14.0, 22.6, 28.8, 29.1, 31.3, 31.7, 33.3, 55.2, 111.2, 114.0, 120.8, 129.6, 138.5, 159.8.

2-((4-Methoxyphenyl)thio)pyridine (3k)

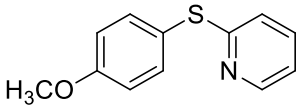

^{1}H NMR (300 MHz, $CDCl_3$): δ 3.84 (s, 3H), 6.76-6.78 (m, 1H), 6.93-6.97 (m, 3H), 7.39-7.54 (m, 3H), 8.39-8.40 (m, 1H); **^{13}C NMR (75 MHz, $CDCl_3$)**: δ 55.3, 115.2, 118.0, 119.3, 120.2, 120.9, 136.5, 137.1, 149.3, 160.5, 162.7.

4-Methoxy-1,1'-biphenyl (5a)

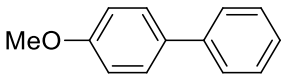

^{1}H NMR (300 MHz, $CDCl_3$): δ 3.84 (s, 3H), 6.95-6.99 (m, 2H), 7.23-7.31 (m, 1H), 7.38-7.43 (m, 2H), 7.51-7.56 (m, 4H); **^{13}C NMR (75 MHz, $CDCl_3$)**: δ 55.3, 114.2, 126.6, 126.7, 128.1, 128.7, 113.8, 140.8, 159.1.

4-Methyl-1,1'-biphenyl (5b)

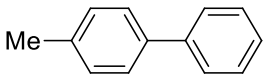

^{1}H NMR (300 MHz, $CDCl_3$): δ 2.34 (s, 3H), 7.29-7.33 (m, 4H), 7.41-7.52 (m, 5H); **^{13}C NMR (75 MHz, $CDCl_3$)**: δ 21.3, 127.6, 127.8, 127.9, 129.2, 129.5, 130.6, 137.8, 140.8.

3-Methoxy-1,1'-biphenyl (5c)

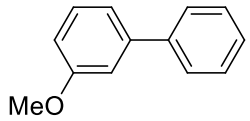

^{1}H NMR (300 MHz, $CDCl_3$): δ 3.84 (s, 3H), 6.87-6.90 (m, 1H), 7.12-7.18 (m, 2H), 7.31-7.36 (m, 2H), 7.39-7.44 (m, 2H), 7.56-7.59 (m, 2H); **^{13}C NMR (75 MHz, $CDCl_3$)**: δ 55.3, 112.7, 112.9, 119.7, 127.2, 127.4, 128.7, 129.8, 141.1, 142.8, 159.9.

3-Chloro-3'-methyl-1,1'-biphenyl (5d)

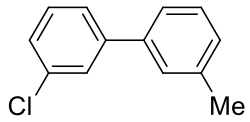

^{1}H NMR (300 MHz, $CDCl_3$): δ 2.38 (s, 3H), 7.15-7.19 (m, 1H), 7.27-7.34 (m, 5H), 7.40-7.44 (m, 1H), 7.54-7.55 (m, 1H); **^{13}C NMR (75 MHz, $CDCl_3$)**: δ 21.5, 124.2, 125.3, 127.2, 127.3, 127.9, 128.6, 128.8, 129.9, 134.6, 138.5, 139.8, 143.2.

1-([1,1'-Biphenyl]-4-yl)ethanone (5e)

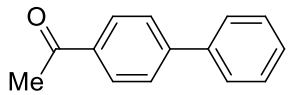

^{1}H NMR (300 MHz, $CDCl_3$): δ 2.62 (s, 3H), δ 7.39-7.49 (m, 3H), 7.60-7.7.68 (m, 4H), 8.00-8.03 (m, 2H); **^{13}C NMR (75 MHz, $CDCl_3$)**: δ 127.2, 127.2, 128.2, 128.94, 128.98, 135.8, 139.8, 145.7, 197.8.

3-Nitro-1,1'-biphenyl (5f)

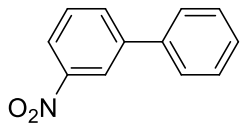

^{1}H NMR (300 MHz, $CDCl_3$): δ 7.40-7.59 (m, 6H), 7.86-7.89 (m, 1H), 8.14-8.17 (m, 1H), 8.40-8.41 (m, 1H); **^{13}C NMR (75 MHz, $CDCl_3$)**: δ 121.9, 122.0, 127.1, 128.5, 129.2, 129.7, 133.0, 138.6, 142.8, 148.7.

2-Methoxy-1,1'-biphenyl (5g)

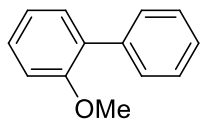

^{1}H NMR (300 MHz, $CDCl_3$): δ 3.96 (s, 3H), 7.16-7.28 (m, 2H), 7.52-7.56 (m, 3H), 7.59-7.62 (m, 2H), 7.75-7.79 (m, 2H); **^{13}C NMR (75 MHz, $CDCl_3$)**: δ 55.6, 11.4, 121.6, 127.1, 128.2, 128.8, 129.78, 130.9, 131.1, 138.7, 156.6.

1-Methoxy-4-(*p*-tolyloxy)benzene (7a)

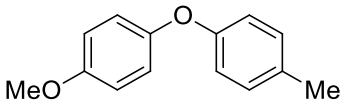

^{1}H NMR (300 MHz, $CDCl_3$): δ 2.30 (s, 3H), 3.77 (s, 3H), 6.78-6.86 (m, 4H), 6.88-6.97 (m, 2H), 7.02-7.11 (m, 2H); **^{13}C NMR (75 MHz, $CDCl_3$)**: δ 20.6, 55.6, 114.8, 117.8, 120.3, 130.1, 132.0, 150.7, 155.6, 156.1.

4,4'-Oxybis(methylbenzene) (7b)

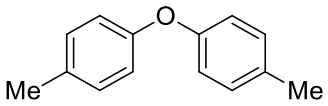

^{1}H NMR (300 MHz, $CDCl_3$): δ 2.32 (s, 6H), 6.88 (d, *J* = 8.1 Hz, 4H), 7.11 (d, *J* = 7.8 Hz, 4H); **^{13}C NMR (75 MHz, $CDCl_3$)**: δ 20.7, 118.6, 130.1, 132.4, 155.3.

1-Nitro-3-(*p*-tolyloxy)benzene (7c)

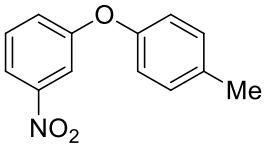

^{1}H NMR (300 MHz, $CDCl_3$): δ 2.35 (s, 3H), 6.94 (d, *J* = 8.4 Hz, 2H), 7.19 (d, *J* = 8.3 Hz, 2H), 7.26-7.29 (m, 1H), 7.43 (t, *J* = 8.2 Hz, 1H), 7.73 (s, 1H), 7.85-7.89 (m, 1H); **^{13}C NMR (75 MHz, $CDCl_3$)**: δ 20.8, 121.2, 117.2, 119.9, 123.7, 130.2, 130.7, 134.6, 149.2, 153.0, 159.0.

1-Methyl-2-(*p*-tolyloxy)benzene (7d)

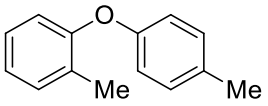

^{1}H NMR (300 MHz, $CDCl_3$): δ 2.24 (s, 3H), 2.30 (s, 3H), 6.79-6.87 (m, 3H), 7.00-7.15 (m, 3H), 7.21-7.24 (m, 2H); **^{13}C NMR (75 MHz, $CDCl_3$)**: δ 16.2, 20.6, 117.5, 119.2, 123.6, 127.0, 129.7, 130.1, 131.3, 131.9, 155.0, 155.5.

1-(4-(*p*-Tolyloxy)phenyl)ethanone (7e)

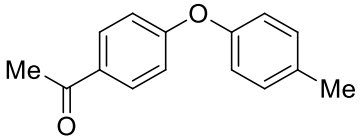

^{1}H NMR (300 MHz, $CDCl_3$): δ 2.36 (s, 3H), 2.55 (s, 3H), 6.94-6.99 (m, 4H), δ 7.18 (d, *J* = 8.1 Hz, 2H), 7.90-7.94 (m, 2H); **^{13}C NMR (75 MHz, $CDCl_3$)**: δ 20.8, 26.4, 116.8, 120.2, 130.5, 130.6, 131.5, 134.4, 153.0, 162.5, 196.9.

1-Chloro-4-(4-methoxyphenoxy)-2-methylbenzene (7f)

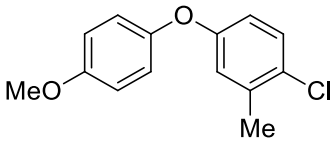

^{1}H NMR (300 MHz, $CDCl_3$): δ 2.30 (s, 3H), 3.79 (s, 3H), 6.68-6.72 (m, 1H), 6.81 (d, *J* = 2.1 Hz), 6.85-6.89 (m, 2H), 6.92-6.96 (m, 2H), 7.22 (d, *J* = 8.6 Hz, 1H), **^{13}C NMR (75 MHz, $CDCl_3$)**: δ 114.9, 116.2, 119.9, 120.7, 127.6, 129.8, 137.3, 149.9, 156.0, 157.0.

1-(*p*-Tolyl)-1*H*-imidazole (9a)

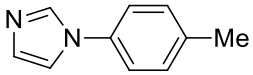

^{1}H NMR (300 MHz, $CDCl_3$): δ 2.39 (s, 1H), 7.18 (s, 1H), 7.23-7.28 (m, 5H), 7.81 (s, 1H); **^{13}C NMR (75 MHz, $CDCl_3$)**: δ 20.9, 118.3, 121.4, 130.1, 130.3, 134.9, 135.6, 137.4.

1-Phenyl-1*H*-imidazole (9b)

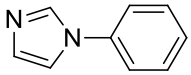

^{1}H NMR (300 MHz, $CDCl_3$): δ 7.24-7.28 (m, 2H), 7.35-7.39 (m, 3H), 7.46-7.51 (m, 2H), 7.90 (s, 1H); **^{13}C NMR (75 MHz, $CDCl_3$)**: δ 118.7, 121.9, 127.7, 128.0, 130.1, 130.2, 133.9, 135.7.

1-(*m*-Tolyl)-1*H*-imidazole (9c)

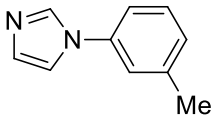

^{1}H NMR (300 MHz, $CDCl_3$): δ 2.32 (s, 3H), 6.92-7.38 (m, 5H), 7.85 (s, 1H); **^{13}C NMR (75 MHz, $CDCl_3$)**: δ 21.3, 118.2, 118.5, 122.1, 128.2, 129.6, 130.2, 135.6, 137.3, 140.0.

1-(3-Iodophenyl)-1*H*-imidazole (9d)

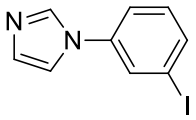

^{1}H NMR (300 MHz, $CDCl_3$): δ 7.07-7.12 (m, 2H), 7.16-7.17 (m, 1H), 7.26-7.28 (m, 1H), 7.57-7.65 (m, 2H), 7.75 (s, 1H); **^{13}C NMR (75 MHz, $CDCl_3$)**: δ 94.7, 117.9, 120.5, 130.1, 130.6, 131.2, 135.3, 136.4, 138.2.

1-(3-Nitrophenyl)-1*H*-imidazole (9e)

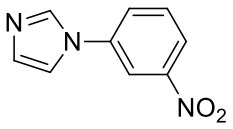

^{1}H NMR (300 MHz, $CDCl_3$): δ 7.28 (s, 1H), 7.40 (s, 1H), 7.70-7.81 (m, 2H), 7.99 (s, 1H), 8.23-8.26 (m, 1H), 8.30 (t, *J* = 2.1 Hz, 1 H); **^{13}C NMR (75 MHz, $CDCl_3$)**: δ 116.2, 117.9, 122.0, 126.8, 131.1, 131.3, 135.4, 138.1, 149.0.

1-(4-Methoxy-3-methylphenyl)-1*H*-imidazole (9f)

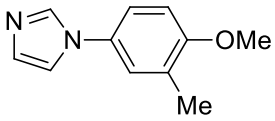

^{1}H NMR (300 MHz, $CDCl_3$): δ 2.26 (s, 3H), 3.87 (s, 3H), 6.85-6.89 (m, 1H), 7.14-7.27 (m, 4H), 7.78 (s, 1H); **^{13}C NMR (75 MHz, $CDCl_3$)**: δ 16.3, 55.6, 110.2, 110.4, 120.2, 124.4, 125.6, 128.3, 129.7, 130.2, 157.1.

1-(*p*-Tolyl)-1*H*-benzo[*d*]imidazole (9g)

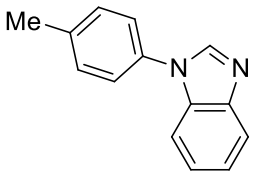

^{1}H NMR (300 MHz, $CDCl_3$): δ 2.44 (s, 3H), 7.26-7.40 (m, 6H), 7.48-7.52 (m, 1H), 7.84-7.88 (m, 1H), 8.09 (s, 1H); **^{13}C NMR (75 MHz, $CDCl_3$)**: δ 21.1, 110.5, 120.4, 122.7, 123.6, 124.0, 130.5, 133.7, 138.1, 142.3, 143.7.

1-(3-Nitrophenyl)-1*H*-benzo[*d*]imidazole (9h)

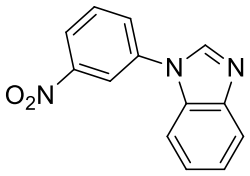

^{1}H NMR (300 MHz, $CDCl_3$): δ 7.37-7.42 (m, 2H), 7.55-7.58 (m, 1H), 7.77-7.83 (m, 1H), 7.88-7.94 (m, 2H), 8.1 (s, 1H), 8.31-8.34 (m, 2H); **^{13}C NMR (75 MHz, $CDCl_3$)**: δ: 110.0, 118.7, 121.0, 122.5, 123.5, 124.5, 129.4, 131.2, 133.0, 137.4, 141.7, 144.1, 149.2.

II.C.5.7 Scanned copies of ^{1}H and ^{13}C NMR spectra of 1-nitro-3-(*p*-tolyloxy)benzene (7c)

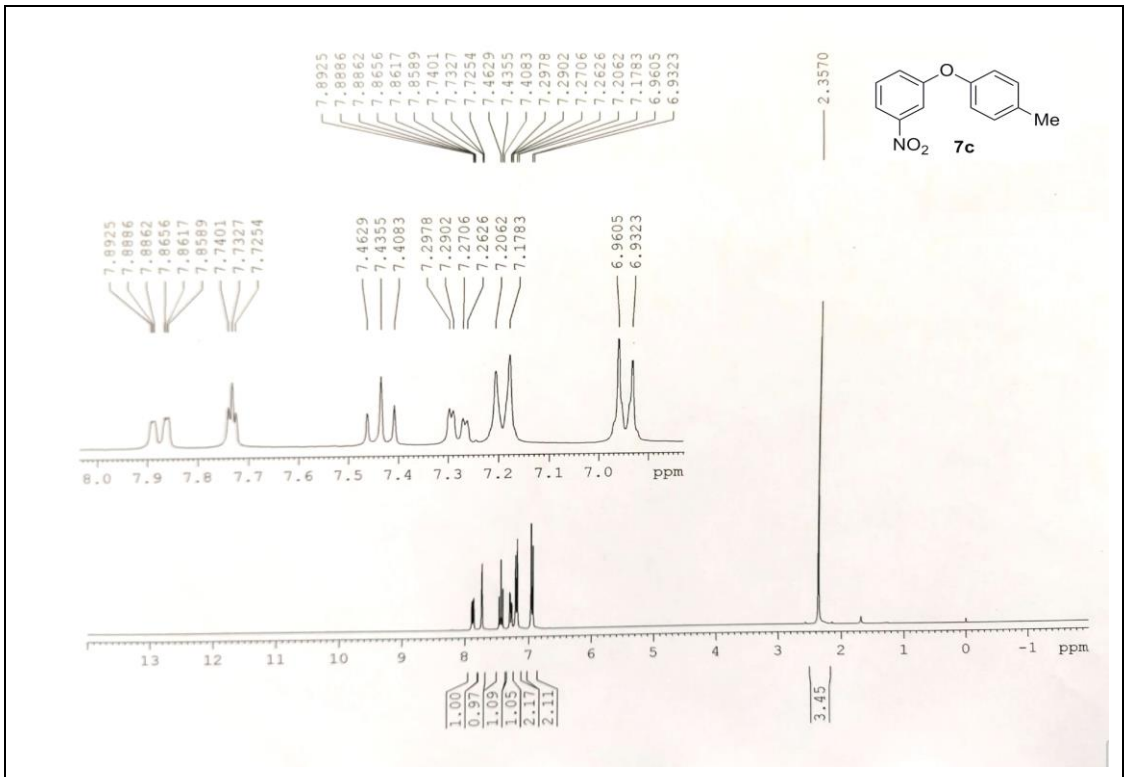

Figure II.C.7 Scanned copy of ^{1}H NMR spectrum of 1-nitro-3-(*p*-tolyloxy)benzene **(7c)**

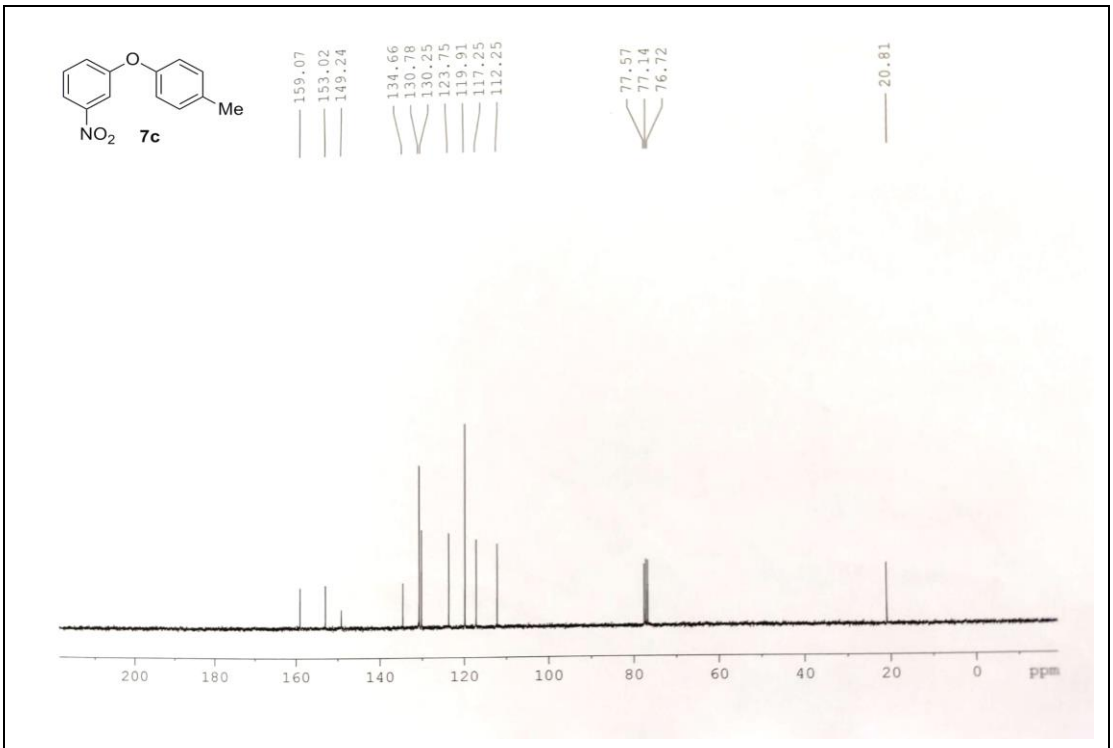

Figure II.C.8 Scanned copy of ^{13}C NMR spectrum of 1-nitro-3-(*p*-tolyloxy)benzene **(7c)**

II.C.6 References

References are given in BIBLIOGRAPHY under Chapter II, Section C.

References (Chapter I, Section A)

1. H. Marsh and F. Rodriguez-Reinonso, Activated Carbon, Elsevier Science & Technology Books, Elsevier, Oxford, 2006.
2. Z. Xu and C. Gao, *Nat. Commun.*, 2011, **2**, 1-9.
3. M. Anafcheh and F. Ektefa, *Struct. Chem.*, 2015, **26**, 1115-1124.
4. H. W. Kroto, J. R. Heath, S. C. O'Brien, R. F. Curl and R. E. Smalley, *Nature*, 1985, **318**, 162-163.
5. M. Coroş, F. Pogăcean, L. Măgeruşan, C. Socaci and S. Pruneanu, *Front. Mater. Sci.*, 2019, **13**, 23-32.
6. D. R. Dreyer, R. S. Ruoff and C. W. Bielawski, *Angew. Chem. Int. Ed.*, 2010, **49**, 9336-9344.
7. K. S. Novoselov, A. K. Geim, S. V. Morozov, D. Jiang, Y. Zhang, S. V. Dubonos, I. V. Grigorieva and A. A. Firsov, *Science*, 2004, **306**, 666-669.
8. S. Zhang, H. Wang, J. Liu and C. Bao, *Mater. Lett.*, 2020, **261**, 127098.
9. B. Qiu, M. Xing and J. Zhang, *Chem. Soc. Rev.*, 2018, **47**, 2165-2216.
10. P. Brisebois and M. Siaj, *J. Mater. Chem. C*, 2020, **8**, 1517-1547.
11. R. Tarcan, O. Todor-Boer, I. Petrovai, C. Leordean, S. Astilean and I. Botiz, *J. Mater. Chem. C*, 2020, **8**, 1198-1224.
12. V. Dhand, K. Y. Rhee, H. Ju Kim and D. Ho Jung, *J. Nanomater.*, 2013, article ID 763953.
13. S. N. Tripathi, G. S. Rao, A. B. Mathur and R. Jasra, *RSC Adv.*, 2017, **7**, 23615-23632.
14. A. Eatemadi, H. Daraee, H. Karimkhanloo, M. Kouhi, N. Zarghami, A. Akbarzadeh, M. Abasi, Y. Hanifehpour and S. W. Joo, *Nanoscale Res. Lett.*, 2014, **9**, article number 393.
15. K. S. Ibrahim, *Carbon lett.*, 2013, **14**, 131-144.
16. D. Vairavapandian, P. Vichchulada and M. D. Lay, *Anal. Chim. Acta*, 2008, **626**, 119-129.
17. J. Granatier, P. Lazar, R. Prucek, K. r. Šafářová, R. Zbořil, M. Otyepka and P. Hobza, *J. Phys. Chem. C*, 2012, **116**, 14151-14162.
18. A. Sinitskii, A. Dimiev, D. A. Corley, A. A. Fursina, D. V. Kosynkin and J. M. Tour, *ACS Nano*, 2010, **4**, 1949-1954.
19. S. Niyogi, E. Bekyarova, M. E. Itkis, H. Zhang, K. Shepperd, J. Hicks, M. Sprinkle, C. Berger, C. N. Lau and W. A. Deheer, *Nano Lett.*, 2010, **10**, 4061-4066.

20. V. Georgakilas, A. B. Bourlinos, R. Zboril, T. A. Steriotis, P. Dallas, A. K. Stubos and C. Trapalis, *Chem. Commun.*, 2010, **46**, 1766-1768.
21. D. Yu, Y. Yang, M. Durstock, J.-B. Baek and L. Dai, *ACS Nano*, 2010, **4**, 5633-5640.
22. X. Zhang, Y. Huang, Y. Wang, Y. Ma, Z. Liu and Y. Chen, *Carbon* 2008, **47**, 313.
23. T. Szabó, E. Tombácz, E. Illés and I. Dékány, *Carbon*, 2006, **44**, 537-545.
24. B. Konkena and S. Vasudevan, *J. Phys. Chem. Lett*., 2012, **3**, 867-872.
25. J. Zhao, G. Chen, W. Zhang, P. Li, L. Wang, Q. Yue, H. Wang, R. Dong, X. Yan and J. Liu, *Anal. Chem.*, 2011, **83**, 9100-9106.
26. D. R. Dreyer, S. Park, C. W. Bielawski and R. S. Ruoff, *Chem. Soc. Rev.*, 2010, **39**, 228-240.
27. L. Peng, Z. Xu, Z. Liu, Y. Wei, H. Sun, Z. Li, X. Zhao and C. Gao, *Nat. Commun.*, 2015, **6**, 5716-5725.
28. J. Shen, Y. Hu, M. Shi, X. Lu, C. Qin, C. Li and M. Ye, *Chem. Mater.*, 2009, **21**, 3514-3520.
29. B. C. Brodie, *Philos. Trans. R. Soc. London*, 1859, **149**, 249-259.
30. L. Staudenmaier, *Ber. Dtsch. Chem. Ges*., 1898, **31**, 1481-1487.
31. V. L. Hofmann and E. Konig, *Z. Anorg. Allg. Chem*., 1937, **31**, 311-336.
32. W. S. Hummers and R. E. Offeman, *J. Am. Chem. Soc*., 1958, **80**, 1339.
33. D. C. Marcano, D. V. Kosynkin, J. M. Berlin, A. Sinitskii, Z. Sun, A. Slesarev, L. B. Alemany, W. Lu and J. M. Tour, *ACS Nano*, 2010, **4**, 4806-4814.
34. M. Wojtoniszak and E. Mijowska, *J. Nanopart. Res.*, 2012, **14**, 1248.
35. C. Yu, C.-F. Wang and S. Chen, *Sci. Rep.*, 2016, **6**, 17071.
36. Y. Shin, J. Park, D. Hyun, J. Yang, J.-H. Lee, J.-H. Kim and H. Lee, *Nanoscale*, 2015, **7**, 5633-5637.
37. P. Yu, Z. Tian, S. E. Lowe, J. Song, Z. Ma, X. Wang, Z. J. Han, Q. Bao, G. P. Simon and D. Li, *Chem. Mater.*, 2016, **28**, 8429-8438.
38. S. Pei, Q. Wei, K. Huang, H.-M. Cheng and W. Ren, *Nat. Commun.*, 2018, **9**, 1-9.
39. J. Chen, Y. Zhang, M. Zhang, B. Yao, Y. Li, L. Huang, C. Li and G. Shi, *Chem. Sci.*, 2016, **7**, 1874-1881.
40. A. Lerf, H. He, M. Forster and J. Klinowski, *J. Phys. Chem. B*, 1998, **102**, 4477-4482.
41. A. Lerf, H. He, T. Riedl, M. Forster and J. Klinowski, *Solid State Ionics*, 1997, **101**, 857-862.
42. H. He, J. Klinowski, M. Forster and A. Lerf, *Chem. Phys. Lett.*, 1998, **287**, 53-56.
43. H. He, T. Riedl, A. Lerf and J. Klinowski, *J. Phys. Chem.*, 1996, **100**, 19954-19958.

44. D. R. Dreyer, H. P. Jia and C. W. Bielawski, *Angew. Chem. Int. Ed.*, 2010, **49**, 6813-6816.
45. H.-P. Jia, D. R. Dreyer and C. W. Bielawski, *Tetrahedron*, 2011, **67**, 4431-4434.
46. D. R. Dreyer, H.-P. Jia, A. D. Todd, J. Geng and C. W. Bielawski, *Org. Biomol. Chem.*, 2011, **9**, 7292-7295.
47. M. Saha and A. R. Das, *ChemistrySelect*, 2017, **2**, 10249-10260.
48. B. Roy, D. Sengupta and B. Basu, *Tetrahedron Lett.*, 2014, **55**, 6596-6600.
49. X. Shuai, Z. Bo, J. Kong, J. Yan and K. Cen, *RSC Adv.*, 2017, **7**, 2667-2675.
50. D. Zhan, Z. Ni, W. Chen, L. Sun, Z. Luo, L. Lai, T. Yu, A. T. S. Wee and Z. Shen, *Carbon*, 2011, **49**, 1362-1366.
51. S. Pei and H.-M. Cheng, *Carbon*, 2012, **50**, 3210-3228.
52. S. J. An, Y. Zhu, S. H. Lee, M. D. Stoller, T. Emilsson, S. Park, A. Velamakanni, J. An and R. S. Ruoff, *J. Phys. Chem. Lett.*, 2010, **1**, 1259-1263.
53. F. Iskandar, U. Hikmah, E. Stavila and A. H. Aimon, *RSC Adv.*, 2017, **7**, 52391-52397.
54. Y. Zhang, L. Guo, S. Wei, Y. He, H. Xia, Q. Chen, H.-B. Sun and F.-S. Xiao, *Nano Today*, 2010, **5**, 15-20.
55. S. Stankovich, D. A. Dikin, G. H. B. Dommett, K. M. Kohlhaas, E. J. Zimney, E. A. Stach, R. D. Piner, S. T. Nguyen and R. S. Ruoff, *Nature*, 2006, **442**, 282-286.
56. H.-J. Shin, K. K. Kim, A. Benayad, S.-M. Yoon, H. K. Park, I.-S. Jung, M. H. Jin, H.-K. Jeong, J. M. Kim, J.-Y. Choi and Y. H. Lee, *Adv. Funct. Mater.*, 2009, **19**, 1987-1992.
57. W. Gao, L. B. Alemany, L. Ci and P. M. Ajayan, *Nat. Chem.*, 2009, **1**, 403-408.
58. I. K. Moon, J. Lee, R. S. Ruoff and H. Lee, *Nat. Commun.*, 2010, 1, 73.
59. M. J. Fernandez-Merino, L. Guardia, J. I. Paredes, S. Villar- Rodil, P. Solis-Fernandez, A. Martinez-Alonso and J. M. D. Tascon, *J. Phys. Chem. C*, 2010, **114**, 6426-6432.
60. B. Roy, Y. Jing and B. Basu, *Curr. Graphene Sci.*, 2017, **1**, 71-79.
61. S. Moussa, A. R. Siamaki, B. F. Gupton and M. S. El-Shall, *ACS Catal.*, 2012, **2**, 145-154.
62. J. O. Sofo, A. S. Chaudhari and G. D. Barber, *Phys. Rev. B*, 2007, **75**, 153401.
63. S. Ryu, M. Y. Han, J. Maultzsch, T. F. Heinz, P. Kim, M. L. Steigerwald and L. E. Brus, *Nano Lett.*, 2008, **8**, 4597-4602.
64. D. C. Elias, R. R. Nair, T. Mohiuddin, S. Morozov, P. Blake, M. Halsall, A. C. Ferrari, D. Boukhvalov, M. Katsnelson, A. Geim and K. S. Novoselov, *Science*, 2009, **323**, 610-613.

65. J. T. Robinson, J. S. Burgess, C. E. Junkermeier, S. C. Badescu, T. L. Reinecke, F. K. Perkins, M. K. Zalalutdniov, J. W. Baldwin, J. C. Culbertson and P. E. Sheehan, *Nano Lett.*, 2010, **10**, 3001-3005.
66. S.-H. Cheng, K. Zou, F. Okino, H. R. Gutierrez, A. Gupta, N. Shen, P. Eklund, J. O. Sofo and J. Zhu, *Phys. Rev. B*, 2010, **81**, 205435.
67. B. Fang, D. Chang, Z. Xu and C. Gao, *Adv. Mater.*, 2020, **32**, 1902664.
68. Z. Xu and C. Gao, *Nat. Commun.*, 2011, **2**, 1-9.
69. V. Georgakilas, M. Otyepka, A. B. Bourlinos, V. Chandra, N. Kim, K. C. Kemp, P. Hobza, R. Zboril and K. S. Kim, *Chem. Rev.*, 2012, **112**, 6156-6214.

References (Chapter I, Section B)

1. C.-J. Li, *Acc. Chem. Res.*, 2009, **42**, 335-344.
2. L. Su, J. Dong, L. Liu, M. Sun, R. Qiu, Y. Zhou and S.-F. Yin, *J. Am. Chem. Soc.*, 2016, **138**, 12348-12351.
3. Z. Li and C.-J. Li, *J. Am. Chem. Soc.*, 2004, **126**, 11810-11811.
4. N. Kambe, T. Iwasaki and J. Terao, *Chem. Soc. Rev.*, 2011, **40**, 4937-4947.
5. S. Monfette and D. E. Fogg, *Chem. Rev.*, 2009, **109**, 3783-3816.
6. C. J. Scheuermann, *Chem. Asian J.*, 2010, **5**, 436-451.
7. S. A. Girard, T. Knauber and C.-J. Li, *Angew. Chem. Int. Ed.*, 2014, **53**, 74-100.
8. B. V. Varun, J. Dhineshkumar, K. R. Bettadapur, Y. Siddaraju, K. Alagiri and K. R. Prabhu, *Tetrahedron Lett.*, 2017, **58**, 803-824.
9. R. Singha, M. Ghosh, Y. Nuree and J. K. Ray, *Tetrahedron Lett.*, 2016, **57**, 1325-1327.
10. Y. Nuree, R. Singha, M. Ghosh, P. Roy and J. K. Ray, *Tetrahedron Lett.*, 2016, **57**, 1479-1482.
11. K. Mishra, A. K. Pandey, J. B. Singh and R. M. Singh, *Org. Biomol. Chem.*, 2016, **14**, 6328-6336.
12. Q. Yang, P. Y. Choy, Y. Wu, B. Fan and F. Y. Kwong, *Org. Biomol. Chem.*, 2016, **14**, 2608-2612.
13. Z. Xie, X. Liu and L. Liu, *Org. Lett.*, 2016, **18**, 2982-2985.
14. X. Huang, Y. Chen, S. Zhen, L. Song, M. Gao, P. Zhang, H. Li, B. Yuan and G. Yang, *J. Org. Chem.*, 2018, **83**, 7331-7340.
15. P. T. Parvatkar, R. Manetsch and B. K. Banik, *Chem. Asian J.*, 2019, **14**, 6-30.
16. L. Yang, D. Zhang-Negrerie, K. Zhao and Y. Du, *J. Org. Chem.*, 2016, **81**, 3372-3379.

17. S.-T. Mei, H.-W. Liang, B. Teng, N.-J. Wang, L. Shuai, Y. Yuan, Y.-C. Chen and Y. Wei, *Org. Lett.*, 2016, **18**, 1088-1091.
18. P. M. Wang, F. Pu, K. Y. Liu, C. J. Li, Z. W. Liu, X. Y. Shi, J. Fan, M. Y. Yang and J. F. Wei, *Chem. Eur. J.*, 2016, **22**, 6262-6267.
19. M. Adib, R. Pashazadeh, S. Rajai-Daryasarei, R. Kabiri and S. J. A. Gohari, *Synlett*, 2016, **27**, 2241-2245.
20. A. M. Faisca Phillips and A. J. Pombeiro, *ChemCatChem*, 2018, **10**, 3354-3383.
21. S. Yamada, K. Murakami and K. Itami, *Org. Lett.*, 2016, **18**, 2415-2418.
22. F. Bartoccini, D. M. Cannas, F. Fini and G. Piersanti, *Org. Lett.*, 2016, **18**, 2762-2765.
23. G. Pandey, R. Laha and D. Singh, *J. Org. Chem.*, 2016, **81**, 7161-7171.
24. M. Belal and A. T. Khan, *RSC Adv.*, 2016, **6**, 18891-18894.
25. Y. Wei, J. He, Y. Liu, L. Xu, L. Vaccaro, P. Liu and Y. Gu, *ACS omega*, 2020, **5**, 18515-18526.
26. L. S. Huang, D. Y. Han and D. Z. Xu, *Adv. Synth. Catal.*, 2019, **361**, 4016-4021.
27. J. Rafique, S. Saba, M. S. Franco, L. Bettanin, A. R. Schneider, L. T. Silva and A. L. Braga, *Chem. Eur. J.*, 2018, **24**, 4173-4180.
28. Z. Li and C.-J. Li, *Org. Lett.*, 2004, **6**, 4997-4999.
29. Z. Li, P. D. MacLeod and C.-J. Li, *Tetrahedron Asymmetry*, 2006, **17**, 590-597.
30. W. Su, J. Yu, Z. Li and Z. Jiang, *J. Org. Chem.*, 2011, **76**, 9144-9150.
31. R. J. Cremlyn, *An Introduction to Organosulfur Chemistry*, Wiley New York, 1996.
32. R. Ragno, A. Coluccia, G. La Regina, G. De Martino, F. Piscitelli, A. Lavecchia, E. Novellino, A. Bergamini, C. Ciaprini and A. Sinistro, *J. Med. Chem.*, 2006, **49**, 3172-3184.
33. A. J. Kochanowska-Karamyan and M. T. Hamann, *Chem. Rev.*, 2010, **110**, 4489-4497.
34. D. Crich and A. Banerjee, *Acc. Chem. Res.*, 2007, **40**, 151-161.
35. C. Viglianisi, E. Marcantoni, V. Carapacchi, S. Menichetti and L. Marsili, *Eur. J. Org. Chem.*, 2014, 6405-6410.
36. C. D. Prasad, S. Kumar, M. Sattar, A. Adhikary and S. Kumar, *Org. Biomol. Chem.*, 2013, **11**, 8036-8040.
37. P. Katrun, S. Hongthong, S. Hlekhlai, M. Pohmakotr, V. Reutrakul, D. Soorukram, T. Jaipetch and C. Kuhakarn, *RSC Adv.*, 2014, **4**, 18933-18938.
38. S. S. Khandekar, D. R. Gentry, G. S. Van Aller, P. Warren, H. Xiang, C. Silverman, M. L. Doyle, P. A. Chambers, A. K. Konstantinidis and M. Brandt, *J. Biol. Chem.*, 2001, **276**, 30024-30030.

39. G. La Regina, A. Coluccia, A. Brancale, F. Piscitelli, V. Gatti, G. Maga, A. Samuele, C. Pannecouque, D. Schols and J. Balzarini, *J. Med. Chem.*, 2011, **54**, 1587-1598.
40. G. De Martino, M. C. Edler, G. La Regina, A. Coluccia, M. C. Barbera, D. Barrow, R. I. Nicholson, G. Chiosis, A. Brancale and E. Hamel, *J. Med. Chem.*, 2006, **49**, 947-954.
41. J. A. Campbell, C. A. Broka, L. Gong, K. A. Walker and J.-H. Wang, *Tetrahedron Lett.*, 2004, **45**, 4073-4075.
42. Y. J. Guo, R. Y. Tang, J. H. Li, P. Zhong and X. G. Zhang, *Adv. Synth. Catal.*, 2009, **351**, 2615-2618.
43. Z. Li, L. Hong, R. Liu, J. Shen and X. Zhou, *Tetrahedron Lett.*, 2011, **52**, 1343-1347.
44. Y. Chen, C.-H. Cho and R. C. Larock, *Org. Lett.*, 2009, **11**,173-176.
45. Y. Chen, C.-H. Cho, F. Shi and R. C. Larock, *J. Org. Chem.*, 2009, **74**, 6802-6811.
46. H. Zhang, X. Bao, Y. Song, J. Qu and B. Wang, *Tetrahedron*, 2015, **71**, 8885-8891.
47. Y. He, S. Liu, P. Wen, W. Tian, X. Ren, Q. Zhou, H. Ma and G. Huang, *ChemistrySelect*, 2016, **1**, 1567-1570.
48. S. Yi, M. Li, W. Mo, X. Hu, B. Hu, N. Sun, L. Jin and Z. Shen, *Tetrahedron Lett.*, 2016, **57**, 1912-1916.
49. Y. Siddaraju and K. R. Prabhu, *Org. Lett.*, 2016, **18**, 6090-6093.
50. Y. Siddaraju and K. R. Prabhu, *J. Org. Chem.*, 2016, **81**, 7838-7846.
51. Y. Siddaraju and K. R. Prabhu, *J. Org. Chem.*, 2017, **82**, 3084-3093.
52. W. Ge and Y. Wei, *Green Chem.*, 2012, **14**, 2066-2070.
53. J. B. Azeredo, M. Godoi, G. M. Martins, C. C. Silveira and A. L. Braga, *J. Org. Chem.*, 2014, **79**, 4125-4130.
54. P. Hamel, *J. Org. Chem.*, 2002, **67**, 2854-2858.
55. F. Xiao, H. Xie, S. Liu and G. J. Deng, *Adv. Synth. Catal.*, 2014, **356**, 364-368.
56. F. L. Yang and S. K. Tian, *Angew. Chem. Int. Ed.*, 2013, **52**, 4929-4932.
57. G. Kumaraswamy, R. Raju and V. Narayanarao, *RSC Adv.*, 2015, **5**, 22718-22723.
58. Z. Wu, Y.-C. Li, W.-Z. Ding, T. Zhu, S.-Z. Liu, X. Ren and L.-H. Zou, *Asian J. Org. Chem.*, 2016, **5**, 625-628.
59. C. C. Silveira, S. R. Mendes, L. Wolf and G. M. Martins, *Tetrahedron Lett.*, 2010, **51**, 2014-2016.
60. J. Li, C. Li, S. Yang, Y. An, W. Wu and H. Jiang, *J. Org. Chem.*, 2016, **81**, 7771-7783.
61. D. R. Dreyer, H. P. Jia and C. W. Bielawski, *Angew. Chem. Int. Ed.*, 2010, **49**, 6813-6816.

62. S. Navalon, A. Dhakshinamoorthy, M. Alvaro and H. Garcia, *Chem. Rev.*, 2014, **114**, 6179-6212.
63. M. Chen, Z.-T. Huang and Q.-Y. Zheng, *Chem. Commun.*, 2012, **48**, 11686-11688.
64. Y. Maeda, M. Koyabu, T. Nishimura and S. Uemura, *J. Org. Chem.*, 2004, **69**, 7688-7693.
65. J. S. Yadav, B. V. S. Reddy, Y. J. Reddy and K. Praneeth, *Synthesis*, 2009, 1520-1524.
66. M. Tudge, M. Tamiya, C. Savarin and G. R. Humphrey, *Org. Lett.*, 2006, **8**, 565-568.
67. X.-L. Fang, R.-Y. Tang, P. Zhong and J.-H. Li, *Synthesis*, 2009, 4183-4189.
68. B. V. Varun and K. R. Prabhu, *J. Org. Chem.*, 2014, **79**, 9655-9668.
69. M. Iwasaki, W. Kaneshika, Y. Tsuchiya, K. Nakajima and Y. Nishihara, *J. Org. Chem.*, 2014, **79**, 11330-11338.
70. G. Zhang, C. Liu, H. Yi, Q. Meng, C. Bian, H. Chen, J.-X. Jian, L.-Z. Wu and A. Lei, *J. Am. Chem. Soc.*, 2015, **137**, 9273-9280.
71. M. Iwasaki and Y. Nishihara, *Dalton Trans.*, 2016, **45**, 15278-15284.
72. D. Equbal, A. G. Lavekar and A. K. Sinha, *Org. Biomol. Chem.*, 2016, **14**, 6111-6118.
73. Y. Liu, Y. Zhang, C. Hu, J.-P. Wan and C. Wen, *RSC Adv.*, 2014, **4**, 35528-35530.
74. X. Zhang, X. Zhou, H. Xiao and X. Li, *RSC Adv.*, 2013, **3**, 22280-22284.
75. C.-R. Liu and L.-H. Ding, *Org. Biomol. Chem.*, 2015, **13**, 2251-2254.
76. D. C. Marcano, D. V. Kosynkin, J. M. Berlin, A. Sinitskii, Z. Sun, A. Slesarev, L. B. Alemany, W. Lu and J. M. Tour, *ACS Nano*, 2010, **4**, 4806-4814.
77. T. Szabo, E. Tombacz, E. Illes and I. Dekany, *Carbon* 2006, **44**, 537-545.
78. F. Xiao, J. Tian, Q. Xing, H. Huang, G. J. Deng and Y. Liu, *ChemistrySelect*, 2017, **2**, 428-431.
79. D. Yang, K. Yan, W. Wei, J. Zhao, M. Zhang, X. Sheng, G. Li, S. Lu and H. Wang, *J. Org. Chem.*, 2015, **80**, 6083-6092.
80. Y.-D. Wu, J.-R. Ma, W.-M. Shu, K.-L. Zheng and A.-X. Wu, *Tetrahedron*, 2016, **72**, 4821-4826.
81. G. La Regina, V. Gatti, V. Famiglini, F. Piscitelli and R. Silvestri, *ACS Comb. Sci.*, 2012, **14**, 258-262.
82. S. K. R. Parumala and R. K. Peddinti, *Green Chem.*, 2015, **17**, 4068-4072.
83. F. Xiao, S. Chen, C. Li, H. Huang and G. J. Deng, *Adv. Synth. Catal*., 2016, **358**, 3881-3886.
84. X. Kang, R. Yan, G. Yu, X, Pang, X. Liu, X. Li, L. Xiang and G. Huang, *J. Org. Chem*., 2014, **79**, 10605-10610.

References (Chapter I, Section C)

1. M. Baumann and I. R. Baxendale, *Beilstein J. Org. Chem.*, 2013, **9**, 2265-2319.
2. R. Mannhold, B. Jablonka, W. Voigt, K. Schönafinger and E. Schraven, *Eur. J. Med. Chem.*, 1992, **27**, 229-235.
3. R. Bansal, G. Narang, C. Calle, R. Carron, K. Pemberton and A. L. Harvey, *Drug Dev. Res.*, 2013, **74**, 50-61.
4. S. A. Agudoawu and E. E. Knaus, *J. Heterocycl. Chem.*, 2000, **37**, 303-306.
5. C. K. Chu, V. S. Bhadti, K. J. Doshi, J. T. Etse, J. M. Gallo, F. D. Boudinot and R. F. Schinazi, *J. Med. Chem.*, 1990, **33**, 2188-2192.
6. A. T. Manvar and R. R. S. Pissurlenkar, *Mol. Divers.*, 2010, **14**, 285-305.
7. R. Boer and R. Gekeler, *Drugs Future*, 1995, **20**, 499-509.
8. . A. Janis and D. J. Triggle, *Drug Dev. Res.*, 1984, **4**, 257-274.
9. B. Loev, M. M. Goodman, K. M. Snader, R. Tedeschi and E. Macko, *J. Med. Chem.*, 1974, **17**, 956-965.
10. F. Bossert, H. Meyer and E. Wehinger, *Angew. Chem. Int. Ed.*, 1981, **20**, 762-769.
11. B. J. Epstein, K. Vogel and B. F. Palmer, *Drugs*, 2007, **67**, 1309-1327.
12. A. F. E. Rump, M. Boller, R. Berkels, R. Rosen, U. Fricke and W. Klaus, *Gen. Pharmacol.*, 1994, **25**, 447-450.
13. E. Fasani, M. Fagnoni, D. Dondi and A. Albini, *J. Org. Chem.*, 2006, **71**, 2037-2045.
14. V. Klusa, *Drugs Future*, 1995, **20**, 135-138.
15. I. O. Donkor, X. Zhou, J. Schmidt, K. C. Agrawal and V. Kishore, *Bioorg. Med. Chem.*, 1998, **6**, 563-568.
16. T. Straub, C. Boesenberg, V. Gekeler and F. Boege, *Biochemistry*, 1997, **36**, 10777-10783.
17. A. Hilgeroth and H. Lilie, Eur. *J. Med. Chem.*, 2003, **38**, 495-499.
18. R. G. Bretzel, C. C. Bollen, E. Maeser and K. F. Federlin, *Drugs Future*, 1992, **17**, 465-468.
19. W. Huang and X. Cheng, *Synlett*, 2017, **28**, 148-158.
20. S. G. Ouellet, A. M. Walji and D. W. MacMillan, *Acc. Chem. Res.*, 2007, **40**, 1327-1339.
21. K. Xie, Y.-C. Liu, Y. Cui, J.-G. Wang, Y. Fu and T. C. Mak, *Molecules*, 2007, **12**, 415-422.
22. D. L. Comins and S. O'Connor, in *Adv. Heterocycl. Chem.*, Elsevier, 1988, vol. 44, pp. 199-267.
23. D. Wang and D. Astruc, *Chem. Rev.*, 2015, **115**, 6621-6686.

24. A. Hantzsch, *Justus Liebigs Ann. Chem.*, 1882, **215**, 1-82.
25. H. G. O. Alvim, E. N. da Silva Junior and B. A. D. Neto, *RSC Adv.*, 2014, **4**, 54282-54299.
26. B. Qiu, M. Xing and J. Zhang, *Chem. Soc. Rev.*, 2018, **47**, 2165-2216.
27. S. Navalon, A. Dhakshinamoorthy, M. Alvaro and H. Garcia, *Chem. Rev.*, 2014, **114**, 6179-6212.
28. J.-P. Wan and Y. Liu, *RSC Adv.*, 2012, **2**, 9763-9777.
29. V. K. Sharma and S. K. Singh, *RSC Adv.*, 2017, **7**, 2682-2732.
30. A. Amoozadeh, S. Rahmani, M. Bitaraf, F. B. Abadi and E. Tabrizian, *New J. Chem.*, 2016, **40**, 770-780.
31. Y. L. N. Murthy, A. Rajack, M. T. Ramji, J. J. Babu, C. Praveen and K. A. Lakshmi, *Bioorg. Med. Chem. Lett.*, 2012, **22**, 6016-6023.
32. B. Sadeghi, A. Namakkoubi and A. Hassanabadi, *J. Chem. Res.*, 2013, **37**, 11-13.
33. P. Sharma and M. Gupta, *Green Chem.*, 2015, **17**, 1100-1106.
34. G. Brahmachari, S. Begam and K. Nurjamal, *ChemistrySelect*, 2017, **2**, 3311-3316.
35. M. Pramanik and A. Bhaumik, *J. Mater. Chem. A*, 2013, **1**, 11210-11220.
36. T. Demirci, B. Celik, Y. Yldz, S. Eris, M. Arslan, F. Sen and B. Kilbas, *RSC Adv.*, 2016, **6**, 76948-76956.
37. M. Nasr-Esfahani, S. J. Hoseini, M. Montazerozohori, R. Mehrabi and H. Nasrabadi, *J. Mol. Catal. A: Chem.*, 2014, **382**, 99-105.
38. N. Koukabi, E. Kolvari, A. Khazaei, M. A. Zolfigol, B. Shirmardi-Shaghasemi and H. R. Khavasi, *Chem. Commun.*, 2011, **47**, 9230-9232.
39. A. Kumar and R. A. Maurya, *Synlett*, 2008, 883-885.
40. D. D. Pham, N. T. Le and G. Vo-Thanh, *ChemistrySelect*, 2017, **2**, 12041-12045.
41. D. S. Rekunge, C. K. Khatri and G. U. Chaturbhuj, *Tetrahedron Lett.*, 2017, **58**, 1240-1244.
42. B. Das, B. Ravikanth, R. Ramu and B. Vittal Rao, *Chem. Pharm. Bull.*, 2006, **54**, 1044-1045.
43. A. Maleki, M. Kamalzare and M. Aghaei, *J. Nanostruct. Chem.*, 2015, **5**, 95-105.
44. X. Wang, H. Gong, Z. Quan, L. Li and H. Ye, *Synth. Commun.*, 2011, **41**, 3251-3258.
45. A. Debache, W. Ghalem, R. Boulcina, A. Belfaitah, S. Rhouati and B. Carboni, *Tetrahedron Lett.*, 2009, **50**, 5248-5250.
46. A. Zhu, R. Liu, C. Du and L. Li, *RSC Adv.*, 2017, **7**, 6679-6684.
47. S. Zolfagharinia, E. Kolvari and N. Koukabi, *Catal. Lett.*, 2017, **147**, 1551-1566.

48. S. Karhale, C. Bhenki, G. Rashinkar and V. Helavi, *New J. Chem.*, 2017, **41**, 5133-5141.
49. M. Adharvana Chari and K. Syamasundar, *Catal. Commun.*, 2005, **6**, 624-626.
50. E. Rafiee, S. Eavani, S. Rashidzadeh and M. Joshaghani, *Inorg. Chim. Acta*, 2009, **362**, 3555-3562.
51. M. Mirza-Aghayan, F. Asadi and R. Boukherroub, *Monatsh. Chem.*, 2014, **145**, 1919-1924.
52. R. P. Kagne, G. H. Nikam, V. G. Kalalawe, S. N. Niwadange and D. R. Munde, *J. Chem. & Cheml. Sci.*, 2017, **7**, 1064-1070.
53. F. Zhang, H. Jiang, X. Li, X. Wu and H. Li, *ACS Catal.*, 2014, **4**, 394-401.
54. F. Zhang, H. Jiang, X. Wu, Z. Mao and H. Li, *ACS Appl. Mater. Interfaces*, 2015, **7**, 1669-1677.
55. D. C. Marcano, D. V. Kosynkin, J. M. Berlin, A. Sinitskii, Z. Sun, A. Slesarev, L. B. Alemany, W. Lu and J. M. Tour, *ACS Nano*, 2010, **4**, 4806-4814.
56. R. M. Pasternack, S. Rivillon Amy and Y. J. Chabal, *Langmuir*, 2008, **24**, 12963-12971.
57. W. L. Zhang and H. J. Choi, *Langmuir*, 2012, **28**, 7055-7062.
58. Z.-J. Fan, W. Kai, J. Yan, T. Wei, L.-J. Zhi, J. Feng, Y.-m. Ren, L.-P. Song and F. Wei, *ACS Nano*, 2010, **5**, 191-198.
59. H. N. Tien, J. S. Chung and S. H. Hur, *Sens. Actuators B Chem.*, 2013, **185**, 701-705.
60. L. Qiu, H. Zhang, W. Wang, Y. Chen and R. Wang, *Appl. Surf. Sci.*, 2014, **319**, 339-343.
61. A. Kumar, S. Sharma, V. D. Tripathi, R. A. Maurya, S. P. Srivastava, G. Bhatia, A. Tamrakar and A. K. Srivastava, *Bioorg. Med. Chem.*, 2010, **18**, 4138-4148.
62. C. A. Antonyraj and S. Kannan, *Appl. Catal., A*, 2008, **338**, 121-129.
63. R. Kumar, N. H. Andhare, A. Shard and A. K. Sinha, *RSC Adv.*, 2014, **4**, 19111-19121.
64. G. Jones, in *Organic Reactions*, John Wiley & Sons, Inc., 2004, ch. 2, pp. 204-273.
65. M. Maheswara, V. Siddaiah, Y. K. Rao, Y.-M. Tzeng and C. Sridhar, *J. Mol. Catal. A: Chem.*, 2006, **260**, 179-180.
66. A. Nakhaei, N. Hosseininasab and S. Yadegarian, *Heterocycl. Lett.*, 2017, **7**, 81-90.
67. M. G. Dekamin, S. Ilkhanizadeh, Z. Latifidoost, H. Daemi, Z. Karimi and M. Barikani, *RSC Adv.*, 2014, **4**, 56658-56664.
68. J. Safari, F. Azizi and M. Sadeghi, *New J. Chem.*, 2015, **39**, 1905-1909.
69. G. Sabitha, K. Arundhathi, K. Sudhakar, B. S. Sastry and J. S. Yadav, *Synth. Commun.*, 2009, **39**, 2843-2851.
70. R. F. Affeldt, E. V. Benvenutti and D. Russowsky, *New J. Chem.*, 2012, **36**, 1502-1511.
71. M. Kiani and M. Mohammadipour, *RSC Adv.*, 2017, **7**, 997-1007.

72. N. Madankumar and K. Pitchumani, *ChemistrySelect*, 2018, **3**, 10886-10891.
73. W. Su, J. Li and J. Li, *Aust. J. Chem.*, 2008, **61**, 860-863.

References (Chapter I, Section D)

1. M. B. Plutschack, B. u. Pieber, K. Gilmore and P. H. Seeberger, *Chem. Rev.*, 2017, **117**, 11796-11893.
2. M. Trojanowicz, *Molecules*, 2020, **25**, 1434.
3. R. Gérardy, N. Emmanuel, T. Toupy, V. E. Kassin, N. N. Tshibalonza, M. Schmitz and J. C. M. Monbaliu, *Eur. J. Org. Chem.*, 2018, **2018**, 2301-2351.
4. S. R. Gobert, S. Kuhn, L. Braeken and L. C. Thomassen, *Org. Process Res. Dev.*, 2017, **21**, 531-542.
5. J. Britton and C. L. Raston, *Chem. Soc. Rev.*, 2017, **46**, 1250-1271.
6. J. Wegner, S. Ceylan and A. Kirschning, *Chem. Commun.*, 2011, **47**, 4583-4592.
7. H. R. Sahoo, J. G. Kralj and K. F. Jensen, *Angew. Chem. Int. Ed.*, 2007, **46**, 5704-5708.
8. F. M. Akwi and P. Watts, *Chem. Commun.*, 2018, **54**, 13894-13928.
9. I. R. Baxendale and M. R. Pitts, *Chim. Oggi*, 2006, **24**, 41.
10. J. West, B. Karamata, B. Lillis, J. P. Gleeson, J. Alderman, J. K. Collins, W. Lane, A. Mathewson and H. Berney, *Lab. Chip.*, 2002, **2**, 224-230.
11. N. Nikbin and P. Watts, *Org. Process Res. Dev.*, 2004, **8**, 942-944.
12. P. Bayley and M. Anson, *Biochem. Biophys. Res. Commun.*, 1975, **62**, 717-722.
13. M. L. Reback, C. W. Roske, T. E. Bitterwolf, P. R. Griffiths and C. J. Manning, *Appl. Spectrosc.*, 2010, **64**, 907-911.
14. M. D. Christianson, E. H. Tan and C. R. Landis, *J. Am. Chem. Soc.*, 2010, **132**, 11461-11463.
15. J. Britton and T. F. Jamison, *Nat. Protoc.*, 2017, **12**, 2423.
16. R. L. Hartman, J. P. McMullen and K. F. Jensen, *Angew. Chem. Int. Ed.*, 2011, **50**, 7502-7519.
17. B. Gutmann, D. Cantillo and C. O. Kappe, *Angew. Chem. Int. Ed.*, 2015, **54**, 6688-6728.
18. A. Adamo, R. L. Beingessner, M. Behnam, J. Chen, T. F. Jamison, K. F. Jensen, J. C. M. Monbaliu, A. S. Myerson, E. M. Revalor and D. R. Snead, *Science*, 2016, **352**, 61-67.
19. P. Zhang, N. Weeranoppanant, D. A. Thomas, K. Tahara, T. Stelzer, M. G. Russell, M. O'Mahony, A. S. Myerson, H. Lin and L. P. Kelly, *Chem. Eur. J.*, 2018, **24**, 2776-2784.

20. K. P. Cole, J. M. Groh, M. D. Johnson, C. L. Burcham, B. M. Campbell, W. D. Diseroad, M. R. Heller, J. R. Howell, N. J. Kallman and T. M. Koenig, *Science*, 2017, **356**, 1144-1150.
21. B. Gutmann and C. O. Kappe, *J. Flow Chem.*, 2017, **7**, 65-71.
22. M. Movsisyan, E. I. P. Delbeke, J. K. E. T. Berton, C. Battilocchio, S. V. Ley and C. V. Stevens, *Chem. Soc. Rev.*, 2016, **45**, 4892-4928.
23. L. Vaccaro, D. Lanari, A. Marrocchi and G. Strappaveccia, *Green Chem.*, 2014, **16**, 3680-3704.
24. J. C. Serrano-Ruiz, R. Luque, J. M. Campelo and A. A. Romero, *Challenges*, 2012, **3**, 114-132.
25. D. Sun, Y. Yamada, S. Sato, W. Ueda, *Green Chem.*, 2017, **19**, 3186-3213.
26. D. Cambié, C. Bottecchia, N. J. Straathof, V. Hessel and T. Noel, *Chem. Rev.*, 2016, **116**, 10276-10341.
27. A. Petrella, D. Spasiano, P. Cosma, V. Rizzi and M. Race, *Chem. Eng. Commun.*, 2019, **206**, 1286-1296.
28. V. Naddeo, D. Ricco, D. Scannapieco and V. Belgiorno, *Int. J. Photoenergy*, 2012, 624270.
29. L. Xu, X. Ma, J. Niu, J. Chen and C. Zhou, *J. Hazard. Mater.*, 2019, **379**, 120692.
30. J. Kočí, V. Klimešová, K. Waisser, J. Kaustová, H.-M. Dahse and U. Möllmann, *Bioorg. Med. Chem. Lett.*, 2002, **12**, 3275-3278.
31. L. Zhang, J. Fan, K. Vu, K. Hong, J.-Y. Le Brazidec, J. Shi, M. Biamonte, D. J. Busch, R. E. Lough and R. Grecko, *J. Med. Chem.*, 2006, **49**, 5352-5362.
32. W. Huang and G.-F. Yang, *Bioorg. Med. Chem.*, 2006, **14**, 8280-8285.
33. S. F. Nielsen, E. Ø. Nielsen, G. M. Olsen, T. Liljefors and D. Peters, *J. Med. Chem.*, 2000, **43**, 2217-2226.
34. Y. Wang, S. Chackalamannil, Z. Hu, J. W. Clader, W. Greenlee, W. Billard, H. Binch III, G. Crosby, V. Ruperto and R. A. Duffy, *Bioorg. Med. Chem. Lett.*, 2000, **10**, 2247-2250.
35. S. Parveen, M. O. Khan, S. E. Austin, S. L. Croft, V. Yardley, P. Rock and K. T. Douglas, *J. Med. Chem.*, 2005, **48**, 8087-8097.
36. M. C. Bagley, T. Davis, M. C. Dix, V. Fusillo, M. Pigeaux, M. J. Rokicki and D. Kipling, *J. Org. Chem.*, 2009, **74**, 8336-8342.
37. M. Tiecco, *Synthesis*, 1988, 749.
38. R. J. Hickman, B. Christie, R. Guy and T. White, *Aust. J. Chem.*, 1985, **38**, 899-904.

39. M. B. Gawande, A. Goswami, F.-X. Felpin, T. Asefa, X. Huang, R. Silva, X. Zou, R. Zboril and R. S. Varma, *Chem. Rev.*, 2016, **116**, 3722-3811.
40. C. F. Lee, Y. C. Liu and S. S. Badsara, *Chem. Asian J.*, 2014, **9**, 706-722.
41. O. Stadler, *Ber. Dtsch. Chem. Ges.*, 1884, **17**, 2075-2081.
42. J. Ziegler, *Ber. Dtsch. Chem. Ges.*, 1890, **23**, 2469-2472.
43. L. He, G. Qiu, Y. Gao and J. Wu, *Org. Biomol. Chem.*, 2014, **12**, 6965-6971.
44. F. Mo, G. Dong, Y. Zhang and J. Wang, *Org. Biomol. Chem.*, 2013, **11**, 1582-1593.
45. A. Roglans, A. Pla-Quintana and M. Moreno-Manas, *Chem. Rev.*, 2006, **106**, 4622-4643.
46. Y.-C. Shieh, K. Du, R. S. Basha, Y.-J. Xue, B.-H. Shih, L. Li and C.-F. Lee, *J. Org. Chem.*, 2019, **84**, 6223-6231.
47. B. Hong, J. Lee and A. Lee, *Tetrahedron Lett.*, 2017, **58**, 2809-2812.
48. X. Wang, G. D. Cuny and T. Noël, *Angew. Chem. Int. Ed.*, 2013, **52**, 7860-7864.
49. C. Bottecchia, M. Rubens, S. B. Gunnoo, V. Hessel, A. Madder and T. Noël, *Angew. Chem. Int. Ed.*, 2017, **56**, 12702-12707.
50. D. Koziakov, M. Majek and A. J. von Wangelin, *Org. Biomol. Chem.*, 2016, **14**, 11347-11352.
51. N. Mukherjee, T. Chatterjee and B. C. Ranu, *J. Org. Chem.*, 2013, **78**, 11110-11114.
52. D. Kundu, S. Ahammed and B. C. Ranu, *Green Chem.*, 2012, **14**, 2024-2030.
53. M. Barbero, I. Degani, N. Diulgheroff, S. Dughera, R. Fochi and M. Migliaccio, *J. Org. Chem.*, 2000, **65**, 5600-5608.
54. D. R. Dreyer, H. P. Jia and C. W. Bielawski, *Angew. Chem. Int. Ed.*, 2010, **49**, 6813-6816.
55. D. R. Dreyer, S. Park, C. W. Bielawski and R. S. Ruoff, *Chem. Soc. Rev.*, 2010, **39**, 228-240.
56. S. Navalon, A. Dhakshinamoorthy, M. Alvaro and H. Garcia, *Chem. Rev.*, 2014, **114**, 6179-6212.
57. D. R. Dreyer, A. D. Todd and C. W. Bielawski, *Chem. Soc. Rev.*, 2014, **43**, 5288-5301.
58. O. Mohammadi, M. Golestanzadeh and M. Abdouss, *New J. Chem.*, 2017, **41**, 11471-11497.
59. E. Bayer, G. Jung, I. Halasz and I. Sebestian, *Tetrahedron Lett.*, 1970, **11**, 4503-4505.
60. X. Wang, T. Cardwell, R. Cattrall and G. Jenkins, *Anal. Commun.*, 1998, **35**, 97-101.
61. F. Karnatz and F. C. Whitmore, *J. Am. Chem. Soc.*, 1932, **54**, 3461-3461.
62. I. R. Baxendale, J. Deeley, C. M. Griffiths-Jones, S. V. Ley, S. Saaby and G. K. Tranmer, *Chem. Commun.*, 2006, 2566-2568.

63. M.-j. Bu, G.-p. Lu and C. Cai, *Synlett*, 2015, **26**, 1841-1846.
64. Y. Li, J. Pu and X. Jiang, *Org. Lett.*, 2014, **16**, 2692-2695.
65. B. Roy, S. Ghosh, P. Ghosh and B. Basu, *Tetrahedron Lett.*, 2015, **56**, 6762-6767.
66. M. D. Bochare and M. S. Degani, *ACS Sustainable Chem. Eng.*, 2017, **5**, 3716-3720.
67. D. P. Hari, P. Schroll and B. König, *J. Am. Chem. Soc.*, 2012, **134**, 2958-2961.
68. D. Voylov, T. Saito, B. Lokitz, D. Uhrig, Y. Wang, A. Agapov, A. Holt, V. Bocharova, A. Kisliuk and A. P. Sokolov, *ACS Macro Lett.*, 2016, **5**, 199-202.
69. Y. Qiu, Z. Wang, A. C. Owens, I. Kulaots, Y. Chen, A. B. Kane and R. H. Hurt, *Nanoscale*, 2014, **6**, 11744-11755.
70. D. R. Dreyer, H.-P. Jia, A. D. Todd, J. Geng and C. W. Bielawski, *Org. Biomol. Chem.*, 2011, **9**, 7292-7295.
71. D. C. Marcano, D. V. Kosynkin, J. M. Berlin, A. Sinitskii, Z. Sun, A. Slesarev, L. B. Alemany, W. Lu and J. M. Tour, *ACS Nano*, 2010, **4**, 4806-4814.
72. V. Saini and B. Khungar, *New J. Chem.*, 2018, **42**, 12796-12801.
73. D. Sengupta, K. Bhowmik, G. De and B. Basu, *Beilstein J. Org. Chem.*, 2017, **13**, 1796-1806.
74. C. Zong, J. Liu, S. Chen, R. Zeng and J. Zou, *Chin. J. Chem.*, 2014, **32**, 212-218.
75. D. Moser, Y. Duan, F. Wang, Y. Ma, M. J. O'Neill and J. Cornella, *Angew. Chem. Int. Ed.*, 2018, **57**, 11035-11039.

References (Chapter II, Section A)

1. M. Hu, Z. Yao and X. Wang, *Ind. Eng. Chem. Res.*, 2017, **56**, 3477-3502.
2. V. Georgakilas, M. Otyepka, A. B. Bourlinos, V. Chandra, N. Kim, K. C. Kemp, P. Hobza, R. Zboril and K. S. Kim, *Chem. Rev.*, 2012, **112**, 6156-6214.
3. J. Wang, Z. Chen and B. Chen, *Environ. Sci. Technol.*, 2014, **48**, 4817-4825.
4. K. Yang, B. Chen and L. Zhu, *Sci. Rep.*, 2015, **5**, 11641.
5. C. J. Heard, J. Čejka, M. Opanasenko, P. Nachtigall, G. Centi and S. Perathoner, *Adv. Mater.*, 2019, **31**, 1801712.
6. N. Zhang, H. Qiu, Y. Liu, W. Wang, Y. Li, X. Wang and J. Gao, *J. Mater. Chem.*, 2011, **21**, 11080-11083.
7. K.-J. Jeon and Z. Lee, *Chem. Commun.*, 2011, **47**, 3610-3612.
8. S. Zhang, Y. Shao, H.-g. Liao, J. Liu, I. A. Aksay, G. Yin and Y. Lin, *Chem. Mater.*, 2011, **23**, 1079-1081.
9. G. Williams, B. Seger and P. V. Kamat, *ACS Nano*, 2008, **2**, 1487-1491.

10. K. Zhou, Y. Zhu, X. Yang and C. Li, *New J. Chem.*, 2010, **34**, 2950-2955.
11. M. Jahan, Q. Bao, J.-X. Yang and K. P. Loh, *J. Am. Chem. Soc.*, 2010, **132**, 14487-14495.
12. C. Petit and T. J. Bandosz, *Adv. Funct. Mater.*, 2010, **20**, 111-118.
13. D. Cai and M. Song, *J. Mater. Chem.*, 2010, **20**, 7906-7915.
14. T. Kuilla, S. Bhadra, D. Yao, N. H. Kim, S. Bose and J. H. Lee, *Prog. Polym. Sci.*, 2010, **35**, 1350-1375.
15. C.-H. Lu, H.-H. Yang, C.-L. Zhu, X. Chen and G.-N. Chen, *Angew. Chem. Int. Ed.*, 2009, **48**, 4785-4787.
16. Y. Wang, Z. Li, D. Hu, C.-T. Lin, J. Li and Y. Lin, *J. Am. Chem. Soc.*, 2010, **132**, 9274-9276.
17. S. Wang, B. M. Goh, K. K. Manga, Q. Bao, P. Yang and K. P. Loh, *ACS Nano*, 2010, **4**, 6180-6186.
18. T. H. Han, W. J. Lee, D. H. Lee, J. E. Kim, E. Y. Choi and S. O. Kim, *Adv. Mater.*, 2010, **22**, 2060-2064.
19. V. C. Tung, L.-M. Chen, M. J. Allen, J. K. Wassei, K. Nelson, R. B. Kaner and Y. Yang, *Nano Lett.*, 2009, **9**, 1949-1955.
20. E. Yoo, J. Kim, E. Hosono, H.-s. Zhou, T. Kudo and I. Honma, *Nano Lett.*, 2008, **8**, 2277-2282.
21. I. Ali and T. A. Saleh, *Appl. Catal., A*, 2020, 117542.
22. W. L. Zhang and H. J. Choi, *Langmuir*, 2012, **28**, 7055-7062.
23. M. B. Gawande, A. Goswami, F.-X. Felpin, T. Asefa, X. Huang, R. Silva, X. Zou, R. Zboril and R. S. Varma, *Chem. Rev.*, 2016**, 116**, 3722-3811.
24. D. Li, L. Qiu, K. Wang, Y. Zeng, T. Williams, Y. Huang, M. Tsapatsis and H. Wang, *Chem. Commun.*, 2012, **48**, 2249-2251.
25. T. F. Degnan, *Top. Catal.*, 2000, **13**, 349-356.
26. E. Heracleous, E. F. Iliopoulou and A. A. Lappas, *Ind. Eng. Chem. Res.*, 2013, **52**, 14567-14573.
27. J. Zhu, Y. Wang, J. Liu and Y. Zhang, *Ind. Eng. Chem. Res.*, 2014, **53**, 13711-13717.
28. M. Khatamian, N. Khodakarampoor and M. Saket-Oskoui, *J. Colloid Interface Sci.*, 2017, **498**, 433-441.
29. A. Modi, S. K. Verma and J. Bellare, *Mater. Sci. Eng. C*, 2018, **91**, 524-540.
30. J. Wang, Y. Wang, Y. Zhang, A. Uliana, J. Zhu, J. Liu and B. Van der Bruggen, *ACS Appl. Mater. Interfaces*, 2016, **8**, 25508-25519.

31. M. Sarfraz and M. Ba-Shammakh, *J. Membr. Sci.*, 2016, **514**, 35-43.
32. X. Li, Y. Liu, L. Fu, L. Cao, D. Wei and Y. Wang, *Adv. Funct. Mater.*, 2006, **16**, 2431-2437.
33. Y. Zhang, Y. Shen, D. Han, Z. Wang, J. Song and L. Niu, *J. Mater. Chem.*, 2006, **16**, 4592-4597.
34. X. Zhou and T. Shi, *Appl. Surf. Sci.*, 2012, **259**, 566-573.
35. V. Chandra, J. Park, Y. Chun, J. W. Lee, I.-C. Hwang and K. S. Kim, *ACS Nano*, 2010, **4**, 3979-3986.
36. C. Xu, X. Wang, J. Zhu, X. Yang and L. Lu, *J. Mater. Chem.*, 2008, **18**, 5625-5629.
37. M. Bottini, L. Tautz, H. Huynh, E. Monosov, N. Bottini, M. I. Dawson, S. Bellucci and T. Mustelin, *Chem. Commun.*, 2005, 758-760.
38. R. Kumar, M. Barakat, M. Taleb and M. K. Seliem, *J. Clean. Prod.*, 2020, 122290.
39. L. Hao, H. Song, L. Zhang, X. Wan, Y. Tang and Y. Lv, *J. Colloid Interface Sci.*, 2012, **369**, 381-387.
40. X. Zhou and T. Shi, *Appl. Surf. Sci.*, 2012, **259**, 566-573.
41. W. Lu, Y. Luo, G. Chang and X. Sun, *Biosens. Bioelectron.*, 2011, **26**, 4791-4797.
42. F. Liu, Z. Wu, D. Wang, J. Yu, X. Jiang and X. Chen, *Colloids Surf. A Physicochem. Eng. Asp.*, 2016, **490**, 207-214.
43. R. L. Oliveira, C. S. Oliveira, R. Landers and C. R. D. Correia, *ChemistrySelect*, 2018, **3**, 535-543.
44. L. Peng, J. Zhang, S. Yang, B. Han, X. Sang, C. Liu, X. Ma and G. Yang, *Chem. Commun.*, 2015, *51*, 4398-4401.
45. K. Jasuja and V. Berry, *ACS Nano*, 2009, **3**, 2358-2366.
46. S. Zhang, Y. Shao, H.-g. Liao, J. Liu, I. A. Aksay, G. Yin and Y. Lin, *Chem. Mater.*, 2011, **23**, 1079-1081.
47. J. Shen, M. Shi, N. Li, B. Yan, H. Ma, Y. Hu and M. Ye, *Nano Res.*, 2010, **3**, 339-349.
48. A. R. Siamaki, S. K. Abd El Rahman, V. Abdelsayed, M. S. El-Shall and B. F. Gupton, *J. Catal.*, 2011, **279**, 1-11.
49. H. M. Hassan, V. Abdelsayed, S. K. Abd El Rahman, K. M. AbouZeid, J. Terner, M. S. El-Shall, S. I. Al-Resayes and A. A. El-Azhary, *J. Mater. Chem.*, 2009, **19**, 3832-3837.
50. M. Bayati, J. M. Abad, R. J. Nichols and D. J. Schiffrin, *J. Phys. Chem. C*, 2010, **114**, 18439-18448.
51. G. Ren and Y. Xing, *Nanotechnology*, 2006, **17**, 5596.
52. I. V. Lightcap, T. H. Kosel and P. V. Kamat, *Nano Lett.*, 2010, **10**, 577-583.

53. Y. Lin, K. A. Watson, M. J. Fallbach, S. Ghose, J. G. Smith Jr, D. M. Delozier, W. Cao, R. E. Crooks and J. W. Connell, *ACS Nano*, 2009, **3**, 871-884.
54. N. Zhang, H. Qiu, Y. Liu, W. Wang, Y. Li, X. Wang and J. Gao, *J. Mater. Chem.*, 2011, **21**, 11080-11083.
55. H. He and C. Gao, *Sci. China: Chem.*, 2011, **54**, 397-404.
56. R. Pasricha, S. Gupta and A. K. Srivastava, *Small*, 2009, **5**, 2253-2259.
57. M. Stein, J. Wieland, P. Steurer, F. Tölle, R. Mülhaupt and B. Breit, *Adv. Synth. Catal.*, 2011, **353**, 523-527.
58. H. M. A. Hassan, V. Abdelsayed, A. E. R. S. Khder, K. M. AbouZeid, J. Terner, M. S. El-Shall, S. I. Al-Resayes and A. A. El-Azhary, *J. Mater. Chem.*, 2009, **19**, 3832-3837.
59. K. Zhang, Q. Yue, G. Chen, Y. Zhai, L. Wang, H. Wang, J. Zhao, J. Liu, J. Jia and H. Li, *J. Phys. Chem. C*, 2010, **115**, 379-389.
60. H. Paul and D. Mohanta, *Appl. Phys. A: Mater. Sci. Process.*, 2011, **103**, 395-402.
61. G. M. Scheuermann, L. Rumi, P. Steurer, W. Bannwarth and R. Mülhaupt, *J. Am. Chem. Soc.*, 2009, **131**, 8262-8270.
62. C. Nethravathi, E. A. Anumol, M. Rajamathi and N. Ravishankar, *Nanoscale*, 2011, **3**, 569-571.
63. Z. Tang, S. Shen, J. Zhuang and X. Wang, *Angew. Chem. Int. Ed.*, 2010, **49**, 4603-4607.
64. A. Dandia, S. L. Gupta, A. Indora, P. Saini, V. Parewa and K. S. Rathore, *Tetrahedron Lett.*, 2017, **58**, 1170-1175.
65. D. Liu, C. Zhang, F. Wang, Z. Huang, N. Zhang, H. Zhou and Y. Kuang, *J. Mater. Chem. A*, 2015, **3**, 16583-16589.
66. S. Rostamnia, B. Zeynizadeh, E. Doustkhah and H. G. Hosseini, *J. Colloid Interface Sci.*, 2015, **451**, 46-52.
67. H. Naeimi and M. Farahnak Zarabi, *Appl. Organometal. Chem.*, 2018, **32**, e4225.
68. X. Xiong, H. Chen and R. Zhu, *Catal. Commun.*, 2014, **54**, 94-99.
69. G. Williams, B. Seger and P. V. Kamat, *ACS Nano*, 2008, **2**, 1487-1491.
70. S. Chen, J. Zhu, X. Wu, Q. Han and X. Wang, *ACS Nano*, 2010, **4**, 2822-2830.
71. J. Zhang, Z. Xiong and X. Zhao, *J. Mater. Chem.*, 2011, **21**, 3634-3640.
72. K. Zhou, Y. Zhu, X. Yang and C. Li, *New J. Chem.*, 2010, **34**, 2950-2955.
73. S. Wu, Z. Yin, Q. He, X. Huang, X. Zhou and H. Zhang, *J. Phys. Chem. C*, 2010, **114**, 11816-11821.
74. E. S. Orth, J. E. S. Fonsaca, S. H. Domingues, H. Mehl, M. M. Oliveira and A. J. G. Zarbin, *Carbon*, 2013, **61**, 543-550.

75. M. Pirveysian and M. Ghiaci, *Appl. Surf. Sci.*, 2018, **428**, 98-109.
76. V. H. Reddy, Y. R. Reddy, B. Sridhar and B. S. Reddy, *Adv. Synth. Catal.*, 2016, **358**, 1088-1092.
77. M. Zhang, P. Liu, Y.-H. Liu, Z.-R. Shang, H.-C. Hu and Z.-H. Zhang, *RSC Adv.*, 2016, **6**, 106160-106170.
78. A. Nakhaei, *Heterocycl. Lett*., 2017, **7**, 967-973.

References (Chapter II, Section B)

1. H. Wamhoff, in *Comprehensive Heterocyclic Chemistry*, ed. A. R. Katritzky and C. W. Rees, Pergamon Press, Oxford, 1984, vol. 5, pp. 669-732.
2. D. Dheer, V. Singh and R. Shankar, *Bioorg. Chem.*, 2017, **71**, 30-54.
3. A. Lauria, R. Delisi, F. Mingoia, A. Terenzi, A. Martorana, G. Barone and A. M. Almerico, *Eur. J. Org. Chem.*, 2014, 3289-3306.
4. M. J. Genin, D. A. Allwine, D. J. Anderson, M. R. Barbachyn, D. E. Emmert, S. A. Garmon, D. R. Graber, K. C. Grega, J. B. Hester and D. K. Hutchinson, *J. Med. Chem.*, 2000, **43**, 953-970.
5. R. Alvarez, S. Velazquez, A. San-Felix, S. Aquaro, E. D. Clercq, C.-F. Perno, A. Karlsson, J. Balzarini and M. J. Camarasa, *J. Med. Chem.*, 1994, **37**, 4185-4194.
6. S. G. Agalave, S. R. Maujan and V. S. Pore, *Chem. Asian J.*, 2011, **6**, 2696-2718.
7. R.M.C. Dawson, D.C. Elliot, W.H. Elliot and K.M. Jones, in *Data for Biochemical Research* ed. E.J. Wood, Oxford University Press, Oxford, 1986, vol. 15, pp. 302–303.
8. N. K. Allam, *Appl. Surf. Sci.*, 2007, **253**, 4570-4577.
9. R. Subbaraman, H. Ghassemi and T. A. Zawodzinski, *J. Am. Chem. Soc.*, 2007, **129**, 2238-2239.
10. D. Astruc, L. Liang, A. Rapakousiou and J. Ruiz, *Acc. Chem. Res.*, 2012, **45**, 630-640.
11. R. Huisgen, G. Szeimis and L. Moebius, *Chem. Ber*., 1967, **100**, 2494-2507.
12. R. Huisgen, in *1,3-Dipolar Cycloadditional Chemistry*, ed. A. Padwa, Wiley, New York, 1984, pp. 1-176.
13. R. Huisgen, *Pure Appl. Chem*., 1989, **61**, 613-628.
14. V. V. Rostovtsev, L. G. Green, V. V. Fokin and K. B. Sharpless, *Angew. Chem. Int. Ed.*, 2002**, 41**, 2596-2599.
15. C. W. Tornøe, C. Christensen and M. Meldal, *J. Org. Chem.*, 2002, **67**, 3057-3064.
16. S. Bräse, C. Gil, K. Knepper and V. Zimmermann, *Angew. Chem. Int. Ed.*, 2005, **44**, 5188-5240.

17. Z. Chen, Z. Liu, G. Cao, H. Li and H. Ren, *Adv. Synth. Catal.*, 2017, **359**, 202-224.
18. J. E. Hein and V. V. Fokin, *Chem. Soc. Rev.*, 2010, **39**, 1302-1315.
19. M. Meldal and C. W. Tornøe, *Chem. Rev.*, 2008, **108**, 2952-3015.
20. E. Haldon, M. C. Nicasio and P. J. Perez, *Org. Biomol. Chem.*, 2015, **13**, 9528-9550.
21. B. Dervaux and F. E. Du Prez, *Chem. Sci.*, 2012, **3**, 959-966.
22. F. M. Moghaddam, S. E. Ayati, H. R. Firouzi and F. Ghorbani, *Appl. Organometal. Chem.*, 2016, **30**, 488-493.
23. J. Lu, E.-Q. Ma, Y.-H. Liu, Y.-M. Li, L.-P. Mo and Z.-H. Zhang, *RSC Adv.*, 2015, **5**, 59167-59185.
24. D. Wang, L. Etienne, M. Echeverria, S. Moya and D. Astruc, *Chem. Eur. J.*, 2014, **20**, 4047-4054.
25. S. Mohammed, A. K. Padala, B. A. Dar, B. Singh, B. Sreedhar, R. A. Vishwakarma and S. B. Bharate, *Tetrahedron*, 2012, **68**, 8156-8162.
26. B. J. Borah, D. Dutta, P. P. Saikia, N. C. Barua and D. K. Dutta, *Green Chem.*, 2011, **13**, 3453-3460.
27. S. P. Prakash and K. R. Gopidas, *ChemistrySelect*, 2016, **1**, 4803-4813.
28. A. Pourjavadi, M. Tajbakhsh, M. Farhang and S. H. Hosseini, *New J. Chem.*, 2015, **39**, 4591-4600.
29. S. Roy, T. Chatterjee, M. Pramanik, A. S. Roy, A. Bhaumik and S. M. Islam, *J. Mol. Catal. A: Chem.*, 2014, **386**, 78-85.
30. M. Nasr-Esfahani, I. Mohammadpoor-Baltork, A. R. Khosropour, M. Moghadam, V. Mirkhani, S. Tangestaninejad and H. Amiri Rudbari, *J. Org. Chem.*, 2014, **79**, 1437-1443.
31. M. Nasrollahzadeh, S. M. Sajadi, A. Rostami-Vartooni and M. Khalaj, *J. Colloid Interface Sci.*, 2015, **453**, 237-243.
32. S. Chassaing, A. Sani Souna Sido, A. Alix, M. Kumarraja, P. Pale and J. Sommer, *Chem. Eur. J.*, 2008, **14**, 6713-6721.
33. Y. Wang, J. Liu and C. Xia, *Adv. Synth. Catal.*, 2011, **353**, 1534-1542.
34. A. Megia-Fernandez, M. Ortega-Munoz, J. Lopez-Jaramillo, F. Hernandez-Mateo and F. Santoyo-Gonzalez, *Adv. Synth. Catal.*, 2010, **352**, 3306-3320.
35. J. C. Park, A. Y. Kim, J. Y. Kim, S. Park, K. H. Park and H. Song, *Chem. Commun.*, 2012, **48**, 8484-8486.
36. S. Kovács, K. Zih-Perényi, Á. Révész and Z. Novák, *Synthesis*, 2012, **44**, 3722-3730.
37. V. Reddy, Y. Reddy, B. Sridhar and B. Reddy, *Adv. Synth. Catal.*, 2016, **358**, 1088-1092.

38. A. Pourjavadi, N. Safaie, S. H. Hosseini and C. Bennett, *Appl. Organometal. Chem.*, 2015, **29**, 601-607.
39. X. Xiong, H. Chen, Z. Tang and Y. Jiang, *RSC Adv.*, 2014, **4**, 9830-9837.
40. A. S. Nia, S. Rana, D. Döhler, X. Noirfalise, A. Belfiore and W. H. Binder, *Chem. Commun.*, 2014, **50**, 15374-15377.
41. I. Roy, A. Bhattacharyya, G. Sarkar, N. R. Saha, D. Rana, P. P. Ghosh, M. Palit, A. R. Das and D. Chattopadhyay, *RSC Adv.*, 2014, **4**, 52044-52052.
42. S. Dadashi-Silab, B. Kiskan, M. Antonietti and Y. Yagci, *RSC Adv.*, 2014, **4**, 52170-52173.
43. F. Alonso, Y. Moglie, G. Radivoy and M. Yus, *Org. Biomol. Chem.*, 2011, **9**, 6385-6395.
44. B. H. Lipshutz and B. R. Taft, *Angew. Chem. Int. Ed.*, 2006, **45**, 8235-8238.
45. C. Zhou, J. Zhang, P. Liu, J. Xie and B. Dai, *RSC Adv.*, 2015, **5**, 6661-6665.
46. C. Wang, D. Wang, S. Yu, T. Cornilleau, J. Ruiz, L. Salmon and D. Astruc, *ACS Catal.*, 2016, **6**, 5424-5431.
47. A. Nunes, L. Djakovitch, L. Khrouz, F.-X. Felpin and V. Dufaud, *J. Mol. Catal. A: Chem.*, 2017, **437**, 150-157.
48. A. Khojastehnezhad, M. Bakavoli, A. Javid, M. M. K. Siuki and M. Shahidzadeh, *Res. Chem. Intermed.*, 2019, **45**, 4473-4485.
49. B. R. Buckley, M. M. Figueres, A. N. Khan and H. Heaney, *Synlett*, 2016, **27**, 51-56.
50. A. A. Ali, M. Konwar, M. Chetia and D. Sarma, *Tetrahedron Lett.*, 2016, **57**, 5661-5665.
51. A. Mishra, P. Rai, M. Srivastava, B. P. Tripathi, S. Yadav, J. Singh and J. Singh, *Catal. Lett.*, 2017, **147**, 2600-2611.
52. W. Qian, D. Wang, H. Wang, P. Yu, S. Liu and S. Chen, *Tetrahedron Lett.*, 2018, **59**, 2167-2169.
53. Z. Qureshi, J. Y. Kim, T. Bruun, H. Lam and M. Lautens, *ACS Catal.*, 2016, **6**, 4946-4952.
54. C. Wang, D. Ikhlef, S. Kahlal, J.-Y. Saillard and D. Astruc, *Coord. Chem. Rev.*, 2016, **316**, 1-20.
55. M. A. Morozova, M. S. Yusubov, B. Kratochvil, V. Eigner, A. A. Bondarev, A. Yoshimura, A. Saito, V. V. Zhdankin, M. E. Trusova and P. S. Postnikov, *Org. Chem. Front.*, 2017, **4**, 978-985.
56. A. Gupta, R. Jamatia, M. Mahato and A. K. Pal, *Ind. Eng. Chem. Res.*, 2017, **56**, 2375-2382.

57. B. C. Boren, S. Narayan, L. K. Rasmussen, L. Zhang, H. Zhao, Z. Lin, G. Jia and V. V. Fokin, *J. Am. Chem. Soc.*, 2008, **130**, 8923-8930.
58. L. Zhang, X. Chen, P. Xue, H. H. Sun, I. D. Williams, K. B. Sharpless, V. V. Fokin and G. Jia, *J. Am. Chem. Soc.*, 2005, **127**, 15998-15999.
59. J. R. Johansson, P. Lincoln, B. Nordén and N. Kann, *J. Org. Chem.*, 2011, **76**, 2355-2359.
60. H. S. P. Rao and G. Chakibanda, *RSC Adv.*, 2014, **4**, 46040-46048.
61. W. G. Kim, M. E. Kang, J. B. Lee, M. H. Jeon, S. Lee, J. Lee, B. Choi, P. M. Cal, S. Kang and J.-M. Kee, *J. Am. Chem. Soc.*, 2017, **139**, 12121-12124.
62. W. G. Kim, S.-y. Baek, S. Y. Jeong, D. Nam, J. H. Jeon, W. Choe, M.-H. Baik and S. Y. Hong, *Org. Biomol. Chem.*, 2020, **18**, 3374-3381.
63. D. Yadav, N. Singh, T. W. Kim, J. Y. Kim, N.-J. Park and J.-O. Baeg, *Green Chem.*, 2019, **21**, 2677-2685.
64. H. Jiang, S. Lu, X. Zhang, W. Dai and J. Qiao, *Molecules*, 2016, **21**, 833-843.
65. M. B. Gawande, A. Goswami, F.-X. Felpin, T. Asefa, X. Huang, R. Silva, X. Zou, R. Zboril and R. S. Varma, *Chem. Rev.*, 2016**, 116**, 3722-3811.
66. D. Sengupta, K. Bhowmik, G. De and B. Basu, *Beilstein J. Org. Chem.*, 2017**, 13**, 1796-1806.
67. C. J. Heard, J. Čejka, M. Opanasenko, P. Nachtigall, G. Centi and S. Perathoner, *Adv. Mater.*, 2019, **31**, 1801712.
68. D. C. Marcano, D. V. Kosynkin, J. M. Berlin, A. Sinitskii, Z. Sun, A. Slesarev, L. B. Alemany, W. Lu and J. M. Tour, *ACS Nano*, 2010, **4**, 4806-4814.
69. P. He, W. Wang, L. Du, F. Dong, Y. Deng and T. Zhang, *Anal. Chim. Acta*, 2012, **739**, 25-30.
70. M. Khatamian, B. Divband and F. Farahmand-Zahed, *Mater. Sci. Eng. C*, 2016, **66**, 251-258.
71. W. L. Zhang and H. J. Choi, *Langmuir*, 2012, **28**, 7055-7062.
72. W. Ruan, J. Hu, J. Qi, Y. Hou, R. Cao and X. Wei, *Materials*, 2018, **11**, 865.
73. J. Zhang, Y. Xu, Z. Liu, W. Yang and J. Liu, *RSC Adv.*, 2015**, 5**, 54275-54282.
74. S. L. Hailu, B. U. Nair, M. Redi-Abshiro, R. Aravindhan, I. Diaz and M. Tessema, *RSC Adv.*, 2015, **5**, 88636-88645.
75. K. K. Bania, D. Bharali, B. Viswanathan and R. C. Deka, *Inorg. Chem.*, 2012, **51**, 1657-1674.

76. S. C. Mohan, R. V. Solomon, P. Venuvanalingam and K. Jothivenkatachalam, *New J. Chem.*, 2017, **41**, 9505-9512.
77. Y.-L. Huang, H.-W. Tien, C.-C. M. Ma, S.-Y. Yang, S.-Y. Wu, H.-Y. Liu and Y.-W. Mai, *J. Mater. Chem.*, 2011, **21**, 18236-18241.
78. S. Chattopadhyay, S. Maiti, I. Das, S. Mahanty and G. De, *Adv. Mater. Interfaces*, 2016, **3**, 1600761.
79. C. Zhou, J. A. Szpunar and X. Cui, *ACS Appl. Mater. Interfaces*, 2016, **8**, 15232-15241.
80. P. Gebhardt, S. W. Pattinson, Z. Ren, D. J. Cooke, J. A. Elliott and D. Eder, *Nanoscale*, 2014, **6**, 7319-7324.
81. D. Li, L. Qiu, K. Wang, Y. Zeng, T. Williams, Y. Huang, M. Tsapatsis and H. Wang, *Chem. Commun.*, 2012, **48**, 2249-2251.
82. A. K. Feldman, B. Colasson, K. B. Sharpless and V. V. Fokin, *J. Am. Chem. Soc.*, 2005, **127**, 13444-13445.
83. R. Salvio, S. Krabbenborg, W. J. Naber, A. H. Velders, D. N. Reinhoudt and W. G. van der Wiel, *Chem. Eur. J.*, 2009, **15**, 8235-8240.
84. K. Guo, Y. Zhang, Q. Shi and Z. Yu, *Energy Fuels*, 2017, **31**, 6045-6055.
85. K. Bhowmik, D. Sengupta and B. Basu, G. De, *RSC Adv.*, 2014, **4**, 35442-35448.
86. S. S. E. Ghodsinia, B. Akhlaghinia and R. Jahanshahi, *RSC Adv.*, 2016, **6**, 63613-63623.
87. N. Touj, I. Ozdemir, S. Yasar and N. Hamdi, *Inorganica Chim. Acta*, 2017, **467**, 21-32.
88. C. Shao, X. Wang, Q. Zhang, S. Luo and J. Zhao, Y. Hu, *J. Org. Chem.*, 2011, **76**, 6832-6836.
89. A. Coelho, P. Diz, O. Caamano and E. Sotelo, *Adv. Synth. Catal.*, 2010, **352**, 1179-1192.
90. M. d'Halluin, T. Mabit, N. Fairley, V. Fernandez, M. B. Gawande, E. Le Grognec and F.-X. Felpin, *Carbon*, 2015, **93**, 974-983.
91. S. Ghosh, S. Saha, D. Sengupta, S. Chattopadhyay, G. De and B. Basu, *Ind. Eng. Chem. Res.*, 2017, **66**, 11726-11733.
92. P. S. Reddy and B. Sreedhar, *Synthesis*, 2009, 4203-4207.
93. A. Pourjavadi, N. Safaie, S. H. Hosseini and C. Bennett, *Appl. Organometal. Chem.*, 2015, **29**, 601-607.

References (Chapter II, Section C)

1. L.-C. Campeau and N. Hazari, *Organometallics*, 2018, **38**, 3-35.
2. A. Biffis, P. Centomo, A. Del Zotto and M. Zecca, *Chem. Rev.*, 2018, **118**, 2249-2295.

3. M. B. Gawande, A. Goswami, F.-X. Felpin, T. Asefa, X. Huang, R. Silva, X. Zou, R. Zboril and R. S. Varma, *Chem. Rev.*, 2016, **116**, 3722-3811.
4. L. González-Sebastián and D. Morales-Morales, *J. Organomet. Chem.*, 2019, **893**, 39-51.
5. K. Loza, M. Heggen and M. Epple, *Adv. Funct. Mater.*, 2020, **30**, 1909260.
6. D. Sengupta, J. Saha, G. De and B. Basu, *J. Mater. Chem. A*, 2014, **2**, 3986-3992.
7. L. Liu and A. Corma, *Chem. Rev.*, 2018, **118**, 4981-5079.
8. A. Taher, D. Nandi, M. Choudhary and K. Mallick, *New J. Chem.*, 2015, **39**, 5589-5596.
9. H. Targhan, A. Hassanpour, S. Sohrabnezhad and K. Bahrami, *Catal. Lett.*, 2020, **150**, 660-673.
10. R. L. Oliveira, C. S. Oliveira, R. Landers and C. R. D. Correia, *ChemistrySelect*, 2018, **3**, 535-543.
11. R. L. Oliveira, P. K. Kiyohara and L. M. Rossi, *Green Chem.*, 2010, **12**, 144-149.
12. X. Zhang, H. Yin, J. Wang, L. Chang, Y. Gao, W. Liu and Z. Tang, *Nanoscale*, 2013, **5**, 8392-8397.
13. M. Guerrero, N. J. S. Costa, L. L. R. Vono, L. M. Rossi, E. V. Gusevskaya and K. Philippot, *J. Mater. Chem. A*, 2013, **1**, 1441-1449.
14. Y. Liu, X. Meng, Z. Liu, M. Meng, F. Jiang, M. Luo, L. Ni, J. Qiu, F. Liu and G. Zhong, *Langmuir*, 2015, **31**, 8841-8851.
15. A. Gupta, R. Jamatia, R. A. Patil, Y.-R. Ma and A. K. Pal, *ACS Omega*, 2018, **3**, 7288-7299.
16. A. Suzuki, *Angew. Chem. Int. Ed.*, 2011, **50**, 6722-6737.
17. N. Miyaura, K. Yamada and A. Suzuki, *Tetrahedron Lett.*, 1979, **20**, 3437-3440.
18. N. Miyaura and A. Suzuki, *J. Chem. Soc., Chem. Commun.*, 1979, 866-867.
19. I. P. Beletskaya, F. Alonso and V. Tyurin, *Coord. Chem. Rev.*, 2019, **385**, 137-173.
20. S. E. Hooshmand, B. Heidari, R. Sedghi and R. S. Varma, *Green Chem.*, 2019, **21**, 381-405.
21. P. Ruiz-Castillo and S. L. Buchwald, *Chem. Rev.*, 2016, **116**, 12564-12649.
22. I. P. Beletskaya and V. P. Ananikov, *Chem. Rev.*, 2011, **111**, 1596-1636.
23. H. Zhang, P. Ruiz-Castillo and S. L. Buchwald, *Org. Lett.*, 2018, **20**, 1580-1583.
24. K. Didehban, E. Vessally, A. Hosseinian, L. Edjlali and E. S. Khosroshahi, *RSC Adv.*, 2018, **8**, 291-301.
25. Z. Tang, S. Shen, J. Zhuang and X. Wang, *Angew. Chem. Int. Ed.*, 2010, **49**, 4603-4607.
26. C. Premi and N. Jain, *RSC Adv.*, 2016, **6**, 74961-74967.

27. Q. Yang, Z. Quan, S. Wu, B. Du, M. Wang, P. Li, Y. Zhang and X. Wang, *Tetrahedron*, 2015, **71**, 6124-6134.
28. D. Sengupta, K. Bhowmik, G. De and B. Basu, *Beilstein J. Org. Chem.*, 2017, **13**, 1796-1806.
29. H. Li, C. Li, J. Bai, C. Zhang and W. Sun, *RSC Adv.*, 2014, **4**, 48362-48367.
30. V. P. Reddy, A. V. Kumar, K. Swapna and K. R. Rao, *Org. Lett.*, 2009, **11**, 951-953.
31. W. L. Zhang and H. J. Choi, *Langmuir*, 2012, **28**, 7055-7062.
32. D. C. Marcano, D. V. Kosynkin, J. M. Berlin, A. Sinitskii, Z. Sun, A. Slesarev, L. B. Alemany, W. Lu and J. M. Tour, *ACS Nano*, 2010, **4**, 4806-4814.
33. K. G. Lee, R. Wi, M. Imran, T. J. Park, J. Lee, S. Y. Lee and D. H. Kim, *ACS Nano*, 2010, **4**, 3933-3342.
34. A. Khan, A. Rashid, R. Younas and R. Chong, *Int. Nano Lett.*, 2016, **6**, 21-26.
35. P. Innocenzi, L. Malfatti, B. Lasio, A. Pinna, D. Loche, M. F. Casula, V. Alzari and A. Mariani, *New J. Chem.*, 2014, **38**, 3777-3782.
36. Y. Song, D. Cho, S. Venkateswarlu and M. Yoon, *RSC Adv.*, 2017, **7**, 10592-10600.

INDEX

REPRINT

OF

PAPERS

ACES Asian Chemical Editorial Society

DOI: 10.1002/ajoc.201700275

ASIAN JOURNAL OF ORGANIC CHEMISTRY Communication

Sulfenylation

Sustainable and Site-Selective C–H Sulfenylation of Aromatic Compounds with Thiol using Catalytic Graphene Oxide and NaI

Prasun Choudhury, Babli Roy, and Basudeb Basu*[a]

Abstract: Graphene oxide (GO) in combination with NaI is used as the catalytic system for site-selective C–H sulfenylation of 1*H*-indole, 2-naphthol, resorcinol and 2-naphthylamines with thiols. The reaction is usually achieved in the presence of metal catalysts as well as under metal-free conditions using iodine and a strong oxidizing agent. The present protocol avoids the use of any metal catalysts, strong oxidizing agents and the use of thiols instead of other sulfur-based reagents making it atom-economic and environmentally benign. Broader tolerance to functional groups has been tested and a plausible mechanism is proposed. The recovered GO can be recycled without significant loss in catalytic activity up to four runs.

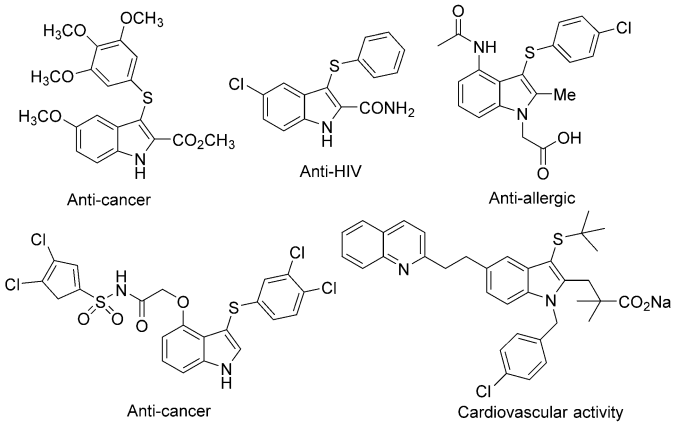

Figure 1. Biologically active poly-functionalized 3-sulfenylindoles.

Introduction

Organosulfur compounds are ubiquitous in nature.[1] Organosulfanes play an important role in both chemical and biological processes like total synthesis, medicinal chemistry and material sciences.[2] Moreover, aryl sulfides are essential building blocks for various pharmaceutically important compounds.[3] The incorporation of sulfenyl groups into heterocyclic moieties like indole has garnered much attention because of their wide uses. Among the various indole derivatives, 3-sulfenylindoles are significant owing to their potential uses as drugs for the treatment of cancer,[3] heart diseases,[3] allergies,[4] HIV[5] and Alzheimer's disease (Figure 1).[3] Because of their synthetic importance and diverse pharmacological activities, synthesis of aryl sulfanes represents an important chemical reaction in organic chemistry. Although a metal-catalyzed C–S bond formation between an aryl halide and thiol is well known,[6] metal-free C–S bond formation by a C(sp^2)–H bond activation is less common and has attracted much attention primarily because the metal-free procedures are greener and cost-effective.[7]

Transition-metal-catalyzed regioselective sulfenylation of indoles has been reported with various metals like Cu, Fe, Mg, Ce, V, Ru, etc., using both thiol and other sulfur-based reagents like sulfonyl chloride, *N*-(arylthio)phthalimide and disulfide.[8] Direct C–H sulfenylations of aromatic compounds have been reported either using peroxides or transition-metal catalysts in combination with DMSO,[9a–d] and C–H thiocyanation using GO-H_2O_2.[9e] Considering the toxicity as well as a high cost of various transition-metal-based catalysts, metal-free approaches have also been developed. The most common is to use iodine in the presence of thiol,[10] or other sulfur-based reagents like disulfide,[11] sulfinate,[5,12] sulfonyl chloride,[13] sulfonyl hydrazide.[14] However, most of these conditions using thiols require the presence of an oxidant, such as *tert*-butyl hydroperoxide (TBHP),[10a] hydrogen peroxide (H_2O_2),[10b] or DMSO.[10c–f] Moreover, the use of different sulfur-based reagents other than thiol generate by-products resulting in lower atom economy of the reaction as well as difficulty in separation.[11–14] Although the use of aromatic thiols in the regioselective sulfenylation appears to be atom-economic, the presence of strong oxidants limits for their versatile applications.[10] The reaction has been reported to be successful also without using any metal catalysts or iodine but requires a strong base like NaOH.[15] There is also a report of using biocatalyst (bovine serum albumin) in combination with iodine for the regioselective sulfenylation of aromatic C(sp^2)–H using thiol.[16] A schematic presentation regarding recent developments in catalytic systems towards site-specific C–H activation and sulfenylation of 1*H*-indole is shown in Scheme 1. In this context, new catalytic systems with the

[a] *P. Choudhury, Dr. B. Roy, Prof. Dr. B. Basu*
Department of Chemistry
North Bengal University
Darjeeling 734013 (India)
E-mail: basu_nbu@hotmail.com

Supporting information and the ORCID identification number(s) for the author(s) of this article can be found under https://doi.org/10.1002/ajoc.201700275.

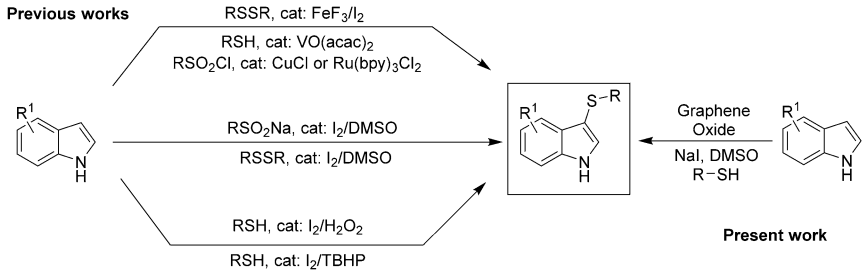

Scheme 1. Recent developments in the catalytic systems for the 3-sulfenylation of indoles.

avoidance of metal and toxic oxidizing agents as well as greener and atom-economic conditions are of great interest.

Graphene oxide (GO), obtained easily from graphite powder by oxidation and subsequent exfoliation, has been used as a potential "carbocatalyst" for promoting various organic transformations.[17] Its mild acidic nature (pH 4.5 at 0.1 mg mL^{-1}),[18] and oxidizing properties have been exploited in various organic transformations since its first application in 2010.[19] We report herein a new metal-free method for the regioselective sulfenylation of indole using thiols (both aromatic and aliphatic thiols) in the presence of graphene oxide (GO) and NaI as the additive. The reaction conditions are facile and versatile to diverse functional groups present with the indole moiety as well as with thiols and the catalyst (GO) is recyclable.

Results and Discussion

We began our preliminary investigations by using 1*H*-indole and 4-chlorothiophenol as model substrates for the reaction using GO and NaI under different conditions (see Table 1). In our first reaction, we used GO (50 mg per mmol of the substrate indole) and NaI (10 mol%) in toluene at 80 °C for 24 h. The reaction proceeded with isolation of the desired product 3-(4-chlorophenylthio)-1*H*-indole in 68% yield (entry 1). Reducing the amount of GO (25 mg) did result in similar conversion (entry 2). Whereas changing the solvent to polar aprotic (CH_3CN) or protic (MeOH) resulted in lower yield of the sulfenylated product (entries 4 and 5), the reaction in DMSO gave excellent conversion (entry 6, 97%), indicating significant role of the solvent. Absence of any of the components like GO, NaI or DMSO did exhibit considerable effect in the course of the reaction and in terms of yield of the product. For example, a neat mixture of reactants, GO and NaI afforded the product in lower yield (entry 7, 55%), whereas there was meagre conversion without using GO or NaI (entries 8 and 9). However, in the absence of GO and NaI, we did not notice any conversion on TLC plate (entry 10). Changing NaI with KI, KBr or NaCl did not result in excellent conversions. We obtained the desired products in 20–72% yields (entries 11–13). Use of I_2 also afforded the product but in lower yield (entry 14, 64%). Scaling up the reaction at the optimized conditions (entry 6) also gave excellent conversion to the desired product (entry 15, 94%).

To explore the scope of the reaction, we employed the optimized reaction conditions with various 1*H*-indoles and thiols, as listed in Table 2. Arylthiols containing chloro, methyl, amino group or 2-naphthylthiol worked efficiently affording exclusive formation of corresponding 3-sulfenylated products (Table 2, entries 1–4). No specific effect of any functional group was noticed in these reactions. Further attempt with aliphatic thiols like cyclohexylthiol, *n*-pentylthiol or *n*-heptylthiol also worked fairly efficiently affording the desired products in 81–89% yields (entries 5–7). On the part of the indole moiety, we tried with an electron withdrawing group at C-6 position of indole and that too gave excellent conversions, exhibiting similar reactivity, selectivity and yield of products and establishing no significant influence of the substituents in either of the reaction partner (entries 8–10). We then checked the presence of substituents in the *N*-containing five-membered ring of the indole moiety. Whereas 3-substituted indole underwent sulfenylation selectively at C-2 position (entry 11), the 2-substituted indole gave the corresponding 3-sulfenylated product in 95% yield (entry 12). Substrate scope has been further extended using heterocyclic thiols like 2-thiazoline-2-thiol and pyridine-2-thiol. In both cases, the reaction worked efficiently giving the desired product in 81 and 89% yield, respectively (entries 13

Table 1. Optimization of reaction conditions.[a]

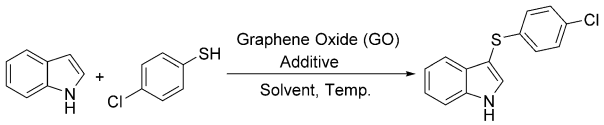

Entry	GO [mg]	Additive [10 mol%]	Solvent	T [°C]/t [h]	Yield [%][b]
1	50	NaI	toluene	80/ 24	68
2	25	NaI	toluene	80/ 24	70
3	10	NaI	toluene	100/ 24	43
4	25	NaI	CH_3CN	80/ 24	10
5	25	NaI	MeOH	80/ 24	12
6	**25**	**NaI**	**DMSO**	**80/ 12**	**97**
7	25	NaI	–	80/ 24	55
8	25	–	DMSO	80/ 24	trace[c]
9	–	NaI	DMSO	80/ 24	trace[c]
10	–	–	DMSO	80/ 24	no product[d]
11	25	KI	DMSO	80/ 12	72
12	25	KBr	DMSO	80/ 12	20
13	25	NaCl	DMSO	80/ 12	24
14	25	I_2	DMSO	80/ 12	64
15	60	NaI	DMSO	80/ 12	94[e]

[a] Reaction conditions: 1*H*-indole (1 mmol), 4-chloro thiophenol (1.5 mmol), solvent (2 mL). [b] Isolated yield. [c] Not isolable but faint spot on TLC. [d] No spot on TLC. [e] Reaction was performed on 5 mmol scale.

Table 2. Sulfenylation of various indoles.[a]

Entry	1*H*-Indole	Thiol	Product	*t* [h]	Yield [%][b]
1		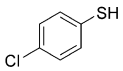	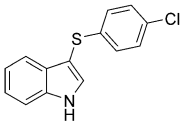	12	97
2		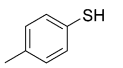	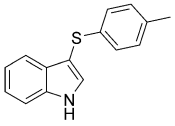	12	94
3		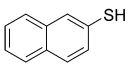	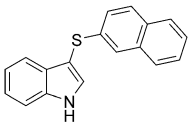	12	81
4			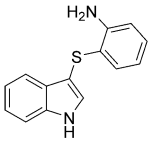	12	85
5			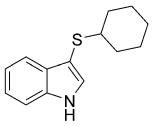	18	81
6		n-C_5H_{11}–SH	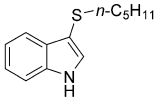	14	89
7		n-C_7H_{15}–SH	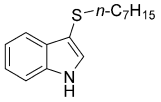	14	86
8	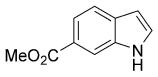	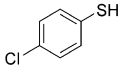	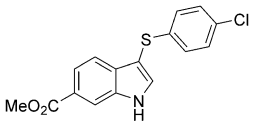	12	91
9	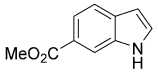	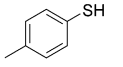	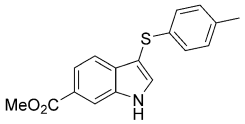	12	90
10	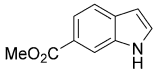	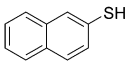	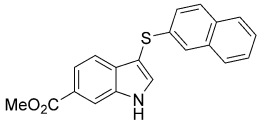	18	81
11		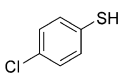	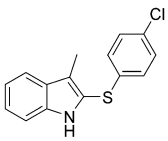	12	85
12	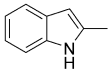	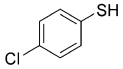	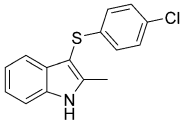	12	95

and 14). Thus the reaction conditions are apparently robust, clean, highly site-selective and performed at 80 °C affording high conversions (81–97%).

In order to broaden the efficacy of the catalytic system (GO/NaI), we then examined with other aryl alcohols or amines like 2-naphthol, resorcinol and 2-naphthylamine.[20] Gratifyingly, in all cases, the reaction worked successfully as well as selectively affording the desired sulfenylated products in good to excellent yields. The results are presented in Table 3, Table 4 and Table 5. While 2-naphthol and 2-naphthylamine afforded exclusive formation of C-1 sulfenylated products, sulfenylation of resorcinol occurred selectively at C-4 position. Aromatic thiols with different substations and aliphatic thiol reacted in the same manner without any significant variations in terms of reactivity.

The reusability of the catalyst (GO) was also checked in the sulfenylation reaction of indole system. The recovery of the graphene oxide (GO) was as follows: after the first run conducted in 2 mmol scale using GO (50 mg), the reaction mixture was partitioned between ethyl acetate and water. The aqueous part was separated out and centrifuged at 5000 rpm. Decantation of the supernatant aqueous part and repeating the process two times more, the remaining solid material was dried under vacuum to obtain free flowing GO powder. The recovery was however ≈10% less than the used quantity. The recovered catalyst was then used for second run (1 mmol scale) using GO (25 mg) with almost equal efficiency. From the third run, there was a decreasing trend in its performance and in the fourth run, the isolated yield was significantly low. The reactions were performed (0.75 and 0.5 mmol scale) using GO (18 and 12 mg, respectively) and the catalyst is found to be active with some decrease in yields (Figure 2). The FT-IR spectrum of the recovered GO after first, second and fourth run was recorded. The IR absorption after fourth run indicated partial loss of oxygenated functional groups which might be due to the repeated use of the recovered catalyst under the reaction condition (see Supporting Information).

Proposed mechanism for the reaction

Similar reactions with thiol mediated by molecular iodine (I_2) are believed to occur via disulfide formation, which subsequently produces an electrophilic species **1** (Scheme 2).[11a] Trying our reaction conditions using a disulfide instead of thiol [1*H*-indole and bis(4-chlorophenyl) disul-

Table 2. (Continued)

Entry	1*H*-Indole	Thiol	Product	*t* [h]	Yield [%][b]
13			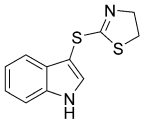	18	81
14	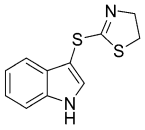		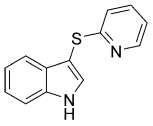	12	89

[a] Reaction conditions: 1*H*-indole (1 mmol), thiol (1.5 mmol), GO (25 mg), NaI (10 mol%) and DMSO (2 mL) were stirred at 80 °C. [b] Isolated yield after purification through column chromatography on silica gel.

though we do not have a clear explanation but our observation leads to suppose that the freshly generated I_2 from the oxidation of NaI in the presence of GO is likely to be more reactive towards thiol to form the electrophilic species (**1**), which then reacts with 1*H*-indole to produce (**2**) and finally HI is liberated to give the desired product (**3**). HI is further oxidized in the presence of GO in DMSO to form I_2 for the next catalytic cycle. Recycling of GO results in partial conversion to reduced graphene oxide (RGO), which causes the lower yield of the product as well as the presence of RGO was clearly indicated after the fourth run by FT-IR spectral data (see the Supporting Information). Further comparative X-ray powder diffraction patterns of

Table 3. Sulfenylation of 2-naphthol.[a]

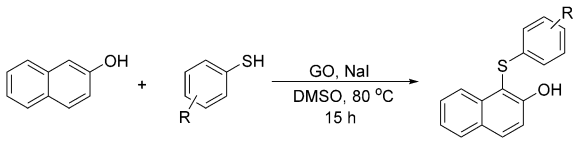

Entry	Thiophenol	Product	Yield [%][b]
1		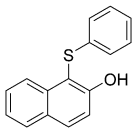	85
2	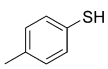	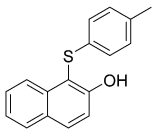	87
3	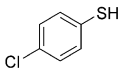	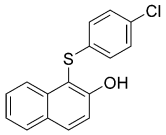	89
4	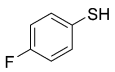	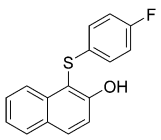	90
5	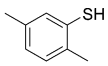	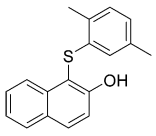	84

[a] Reaction conditions: 2-Naphthol (1 mmol), thiophenol (1.5 mmol), GO (25 mg), NaI (10 mol%) and DMSO (2 mL) were stirred at 80 °C. [b] Isolated yield after purification through column chromatography on silica gel.

Table 4. Sulfenylation of resorcinol.[a]

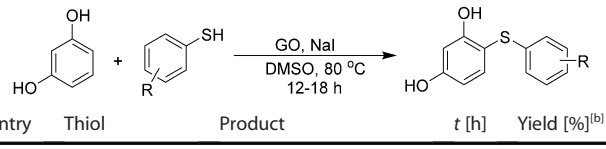

Entry	Thiol	Product	*t* [h]	Yield [%][b]
1	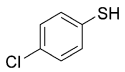	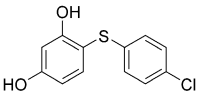	12	93
2	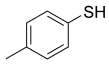	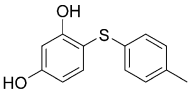	12	92
3	n-$C_5H_{11}SH$	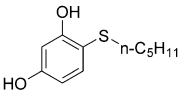	16	89
4	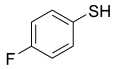	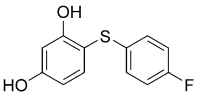	12	91
5		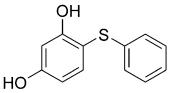	18	84

[a] Reaction conditions: Resorcinol (1 mmol), thiol (1.5 mmol), GO (25 mg), NaI (10 mol%) and DMSO (2 mL) were stirred at 80 °C for the time indicated above. [b] Isolated yield after purification through column chromatography on silica gel.

fide] did not afford any desired product. This means a strong oxidizing agent is required for the reaction. Moreover, GO-catalyzed reaction in the presence of molecular iodine (I_2) did not give good conversion to the product (Table 1, entry 14). Although the fresh GO and recovered catalyst (after the first run) indicated such trends of formation of RGO (see the experimental section as well as the Supporting Information).

Conclusions

In summary, we have described a metal-free, facile and atom-economic protocol for the site-selective C–H sulfenylation of various aromatic compounds leading to the synthesis of corresponding thioethers in good to excellent yields. The reaction

Table 5. Sulfenylation of 2-naphthylamine.[a]

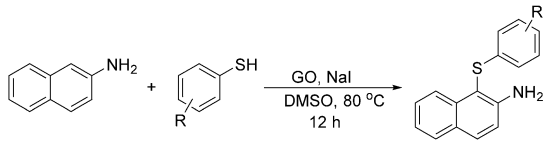

Entry	Thiophenol	Product	Yield[b]
1	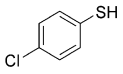	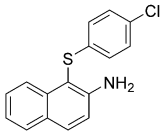	85
2	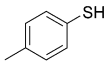	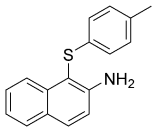	82
3		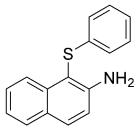	79
4	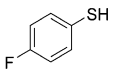	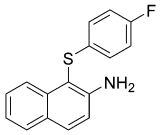	85
5	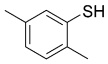	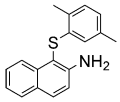	91

[a] Reaction conditions: 2-Naphthylamine (1 mmol), thiophenol (1.5 mmol), GO (25 mg), NaI (10 mol%) and DMSO (2 mL). [b] Isolated yield after purification through column chromatography on silica gel.

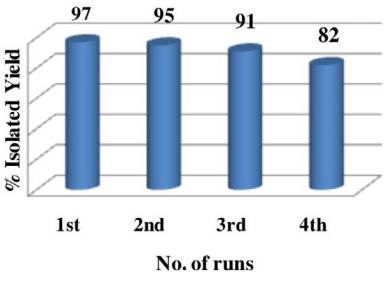

Figure 2. Reusability of GO for the sulfenylation of 1*H*-indole with 4-chlorothiophenol.

shows good tolerance towards several substituted aromatic systems. Harnessing the catalytic role of sustainable carbon materials like graphene oxide (GO) is an emerging area of research and has been demonstrated herein in new reactions eliminating the need of metal catalysts, strong oxidizing agents and different sulfur-based reagents. GO-catalyzed incipient iodine could be highly reactive towards forming the electrophilic species (**1**) that adds to an indole to afford finally the desired thioether. The present protocol is likely to attract the

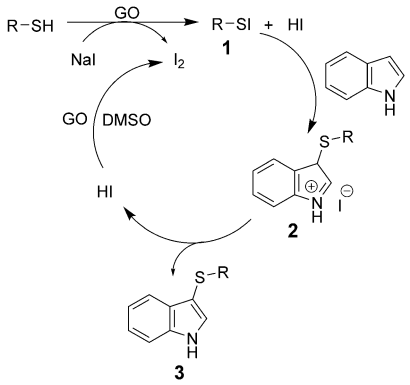

Scheme 2. Proposed reaction mechanism for the 3-sulfenylation of 1*H*-indole.

interest of synthetic chemists because of simple and greener aspects, reusability and broader applicability.

Experimental Section

General procedure for the preparation of graphene oxide (GO)

Graphene oxide was prepared by following Tour's method.[21] In this method a 9:1 ($v\,v^{-1}$) mixture of H_2SO_4/ H_3PO_4 (180:20 mL) was added to a mixture of graphite powder (1.5 g) and $KMnO_4$ (9.0 g). The mixture was then stirred at 50 °C for 12 h. After cooling the mixture to room temperature, it was gradually poured into crushed ice (200 g) followed by the slow addition of H_2O_2 (30%, 1.5 mL). The solution was then centrifuged (5000 rpm) and the supernatant was discarded. The residual solid material was successively washed with deionized water (100 mL) and then with 30% HCl (100 mL). The solid material was then repeatedly washed with water and centrifuged. Finally, the solid brown material was collected and dried at 60 °C under vacuum to obtain solid graphene oxide.

Some characterization data of GO (fresh and after the first run)

The Raman and X-ray powder diffraction patterns (XRD) of the as-prepared GO and the recovered GO were compared and given in the Supporting Information. Whereas in the Raman spectra the D- and G-bands are fairly similar, the XRD peak of the fresh GO was observed at $2\theta = 9.5°$ and the recovered GO consisted of additional peak at $2\theta = 24.9°$, indicating partial removal of oxygenated functional groups.[17,21] The pH potentiometric acid–base titration of the fresh GO (50 mg) with 0.1 M NaOH aqueous solution using 50 mL of 0.5 M NaCl aqueous solution as back electrolyte was performed and calculated an approximate value of 1.68 mmol g^{-1} for the presence of carboxylic and hydroxyl groups. In the case of using recovered GO (after the first run), the calculated value was 1.60 mmol g^{-1}.[18] Further characterization data of GO in aqueous suspension as regard to particle size and surface area measurements are previously studied and reported.[19e,22]

General procedure for the sulfenylation of 1*H*-indole

In a screw-capped sealed tube equipped with a magnetic stir bar, 1*H*-indole (1 mmol), thiol (1.5 mmol), NaI (10 mol%) and GO

(25 mg) were added to 2 mL of freshly distilled DMSO. The resulting reaction mixture was stirred at 80 °C for 12–18 h. After completion of the reaction (monitored by TLC), the reaction mixture was cooled to room temperature. The catalyst GO was then recovered through simple filtration. The reaction mixture was diluted with water and extracted by ethyl acetate (3×5 mL). Finally, the combined organic layer was dried over anhydrous Na_2SO_4 and concentrated. The residue was then further purified by column chromatography on silica gel using the light petroleum ether/ ethyl acetate as eluent to afford the desired product. All products were characterized by ^1H, ^{13}C NMR data and compared with the reported melting points for known solid compounds.

Acknowledgements

Financial support from SERB, New Delhi, India is gratefully acknowledged (Grant No. EMR/2015/000549). PC and BR thank UGC, New Delhi, for award of fellowship under UGC-NET and UGC-FDP respectively.

Conflict of interest

The authors declare no conflict of interest.

Keywords: graphene oxide · indoles · naphthols · naphthylamines · resorcinol

[1] R. J. Cremlyn, *An Introduction to Organosulfur Chemistry*, Wiley, New York, **1996**.
[2] T. Nakazawa, J. Xu, T. Nishikawa, T. Oda, A. Fujita, K. Ukai, R. E. P. Mangindaan, H. Rotinsulu, H. Kobayashi, M. Namikoshi, *J. Nat. Prod.* **2007**, *70*, 439 – 442.
[3] C. Viglianisi, E. Marcantoni, V. Carapacchi, S. Menichetti, L. Marsili, *Eur. J. Org. Chem.* **2014**, 6405 – 6410.
[4] C. D. Prasad, S. Kumar, M. Sattar, A. Adhikary, S. Kumar, *Org. Biomol. Chem.* **2013**, *11*, 8036 – 8040.
[5] P. Katrun, S. Hongthong, S. Hlekhlai, M. Pohmakotr, V. Reutrakul, D. Soorukram, T. Jaipetch, C. Kuhakarn, *RSC Adv.* **2014**, *4*, 18933 – 18938.
[6] C. F. Lee, Y. C. Liu, S. S. Badsara, *Chem. Asian J.* **2014**, *9*, 706 – 722.
[7] S. K. R. Parumala, R. K. Peddinti, *Green Chem.* **2015**, *17*, 4068 – 4072.
[8] a) Z. Wu, Y. C. Li, W. Z. Ding, T. Zhu, S. Z. Liu, X. Ren, L. H. Zou, *Asian J. Org. Chem.* **2016**, *5*, 625 – 628; b) M. Chen, Z. T. Huang, Q. Y. Zheng, *Chem. Commun.* **2012**, *48*, 11686 – 11688; c) Y. Maeda, M. Koyabu, T. Nishimura, S. Uemura, *J. Org. Chem.* **2004**, *69*, 7688 – 7693; d) J. S. Yadav, B. V. S. Reddy, Y. J. Reddy, K. Praneeth, *Synthesis* **2009**, 1520 – 1524; e) C. C. Silveira, S. R. Mendes, L. Wolf, G. M. Martins, *Tetrahedron Lett.* **2010**, *51*, 2014 – 2016; f) M. Tudge, M. Tamiya, C. Savarin, G. R. Humphrey, *Org. Lett.* **2006**, *8*, 565 – 568; g) X. L. Fang, R. Y. Tang, P. Zhong, J. H. Li, *Synthesis* **2009**, 4183 – 4189.
[9] a) B. V. Varun, K. R. Prabhu, *J. Org. Chem.* **2014**, *79*, 9655 – 9668; b) M. Iwasaki, W. Kaneshika, Y. Tsuchiya, K. Nakajima, Y. Nishihara, *J. Org. Chem.* **2014**, *79*, 11330 – 11338; c) G. Zhang, C. Liu, H. Yi, Q. Meng, C. Bian, H. Chen, J. X. Jian, L. Z. Wu, A. Lei, *J. Am. Chem. Soc.* **2015**, *137*, 9273 – 9280; d) M. Iwasaki, Y. Nishihara, *Dalton Trans.* **2016**, *45*, 15278 – 15284; e) D. Khalili, *New J. Chem.* **2016**, *40*, 2547 – 2553.
[10] a) H. Zhang, X. Bao, Y. Song, J. Qu, B. Wang, *Tetrahedron* **2015**, *71*, 8885 – 8891; b) Y. He, S. Liu, P. Wen, W. Tian, X. Ren, Q. Zhou, H. Ma, G. Huang, *ChemistrySelect* **2016**, *1*, 1567 – 1570; c) S. Yi, M. Li, W. Mo, X. Hu, B. Hu, N. Sun, L. Jin, Z. Shen, *Tetrahedron Lett.* **2016**, *57*, 1912 – 1916; d) Y. Siddaraju, K. R. Prabhu, *Org. Lett.* **2016**, *18*, 6090 – 6093; e) Y. Siddaraju, K. R. Prabhu, *J. Org. Chem.* **2016**, *81*, 7838 – 7846; f) Y. Siddaraju, K. R. Prabhu, *J. Org. Chem.* **2017**, *82*, 3084 – 3093.
[11] a) W. Ge, Y. Wei, *Green Chem.* **2012**, *14*, 2066 – 2070; b) J. B. Azeredo, M. Godoi, G. M. Martins, C. C. Silveira, A. L. Braga, *J. Org. Chem.* **2014**, *79*, 4125 – 4130.
[12] F. Xiao, H. Xie, S. Liu, G. J. Deng, *Adv. Synth. Catal.* **2014**, *356*, 364 – 368.
[13] G. Kumaraswamy, R. Raju, V. Narayanarao, *RSC Adv.* **2015**, *5*, 22718 – 22723.
[14] F. L. Yang, S. K. Tian, *Angew. Chem. Int. Ed.* **2013**, *52*, 4929 – 4932; *Angew. Chem.* **2013**, *125*, 5029 – 5032.
[15] a) Y. Liu, Y. Zhang, C. Hu, J. P. Wan, C. Wen, *RSC. Adv.* **2014**, *4*, 35528 – 35530; b) X. Zhang, X. Zhou, H. Xiao, X. Li, *RSC Adv.* **2013**, *3*, 22280 – 22284.
[16] Saima, D. Equbal, A. G. Lavekar, A. K. Sinha, *Org. Biomol. Chem.* **2016**, *14*, 6111 – 6118.
[17] S. Navalon, A. Dhakshinamoorthy, M. Alvaro, H. Garcia, *Chem. Rev.* **2014**, *114*, 6179 – 6212.
[18] T. Szabó, E. Tombacz, E. Illes, I. Dekany, *Carbon* **2006**, *44*, 537 – 545.
[19] a) D. R. Dreyer, H. P. Jia, C. W. Bielawski, *Angew. Chem. Int. Ed.* **2010**, *49*, 6813 – 6816; *Angew. Chem.* **2010**, *122*, 6965 – 6968; b) B. Basu, S. Kundu, D. Sengupta, *RSC Adv.* **2013**, *3*, 22130 – 22134; c) B. Roy, D. Sengupta, B. Basu, *Tetrahedron Lett.* **2014**, *55*, 6596 – 6600; d) S. Kundu, B. Basu, *RSC Adv.* **2015**, *5*, 50178 – 50185; e) B. Roy, S. Ghosh, P. Ghosh, B. Basu, *Tetrahedron Lett.* **2015**, *56*, 6762 – 6767; f) S. Bhattacharya, P. Ghosh, B. Basu, *Tetrahedron Lett.* **2017**, *58*, 926 – 931.
[20] a) F. Xiao, J. Tian, Q. Xing, H. Huang, G. J. Deng, Y. Liu, *ChemistrySelect* **2017**, *2*, 428 – 431; b) D. Yang, K. Yan, W. Wei, J. Zhao, M. Zhang, X. Sheng, G. Li, S. Lu, H. Wang, *J. Org. Chem.* **2015**, *80*, 6083 – 6092.
[21] D. C. Marcano, D. V. Kosynkin, J. M. Berlin, A. Sinitskii, Z. Sun, A. Slesarev, L. B. Alemany, W. Lu, J. M. Tour, *ACS Nano* **2010**, *4*, 4806 – 4814.
[22] P. Montes Navajas, N. G. Asenjo, R. Santamaria, R. Menendez, A. Corma, H. Garcia, *Langmuir* **2013**, *29*, 13443 – 13448.

Manuscript received: May 11, 2017
Revised manuscript received: June 24, 2017
Accepted manuscript online: July 9, 2017
Version of record online: August 29, 2017

Molecular Diversity (2020) 24:283–294
https://doi.org/10.1007/s11030-019-09949-0

SHORT COMMUNICATION

Amine-functionalized graphene oxide nanosheets (AFGONs): an efficient bifunctional catalyst for selective formation of 1,4-dihydropyridines, acridinediones and polyhydroquinolines

Prasun Choudhury[1] · Pranab Ghosh[1] · Basudeb Basu[1,2]

Received: 12 February 2019 / Accepted: 27 March 2019 / Published online: 6 April 2019

Abstract

We report here selective formation of functionalized 1,4-dihydropyridines (DHP), acridinediones and polyhydroquinolines in high yields using amine-functionalized graphene oxide nanosheets (AFGONs) as the bifunctional catalyst. The method overcomes the limitations of previous protocols affording a mixture of DHP and pyridine derivatives using graphene oxide as the catalyst. The mild reaction conditions are found compatible with a wide range of functional groups. It is presumed that a cooperative effect between the acidic and basic functionalities present in AFGONs may have exerted high catalytic efficiency as well as prevented further oxidation to pyridine derivatives. A plausible mechanism is proposed on the basis of some control experiments. The reactions can be scaled up conveniently, and the catalyst can be recycled for five consecutive runs without loss of its activity.

Graphical abstract

Amine-functionalized graphene oxide nanosheets (AFGONs): an efficient bifunctional catalyst for selective formation of 1,4–dihydropyridines, acridinediones and polyhydroquinolines
Prasun Choudhury, Pranab Ghosh and Basudeb Basu*

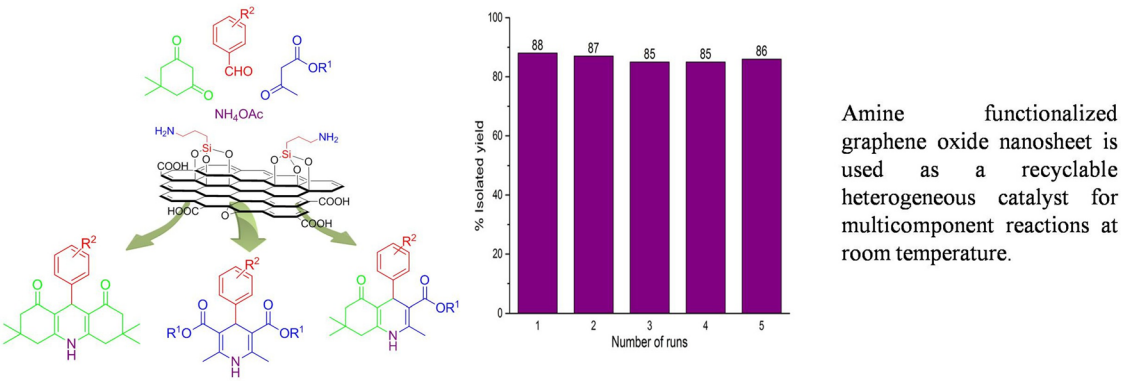

Amine functionalized graphene oxide nanosheet is used as a recyclable heterogeneous catalyst for multicomponent reactions at room temperature.

Keywords Amine-functionalized graphene oxide · Bifunctional catalyst · 1,4-Dihydropyridine · Hantzsch reaction · Multi-component reaction (MCR)

Introduction

1,4-Dihydropyridines (1,4-DHPs) are ubiquitous in the field of medicinal chemistry and represent a privileged class of pharmacophore for multifarious marketed drugs

Electronic supplementary material The online version of this article (https://doi.org/10.1007/s11030-019-09949-0) contains supplementary material, which is available to authorized users.

✉ Basudeb Basu
basu_nbu@hotmail.com

Extended author information available on the last page of the article

[1]. Functionalized 1,4-DHPs exhibit diverse pharmacological activities such as bronchodilators, vasodilators, antihypertensive, antitumor and antidiabetic agents [2–4]. For example, nifedipine, amlodipine and nitrendipine bearing 1,4-DHP scaffolds are important class of drugs for calcium-channel blockers in the treatment of cardiovascular diseases [5–8]. Certain 1,4-DHPs due to their close resemblance with NADH coenzyme are considered as biomimetic agents in biological redox processes [9–11] and are also used in the preparation of several alkaloids [12]. 1,4-DHPs are often used as sacrificial H-source for the transfer hydrogenation of organic functional groups like C=O, C=N and C=C [13].

The preparation of 1,4-DHPs by Arthur Hantzsch dates back to 1882 [14]. The classical method involves a one-pot three-component reaction of an aldehyde, ethyl acetoacetate and ammonia in either acetic acid or refluxing ethanol. This multi-component approach has certain limitations, and as a result, numerous reports are available to improve the Hantzsch reaction [15]. A vast array of homogeneous and heterogeneous catalysts have been used for the synthesis of functionalized 1,4-DHPs [16]. Various metal salts and metal nanoparticles [17–26], magnetic nanocatalysts [27–30], strong acids [31–35], silica-based catalysts [36–42], *p*-TSA [43, 44], zeolite [45], montmorillonite clay [46–48], chitosan nanoparticles [49, 50], PPh_3 [51], sulfated polyborate [52], polyethylene glycol [53], heteropoly acids [54–56], ionic liquids [57–59] and organocatalysts [60–65] are noteworthy to mention. Nevertheless, many protocols still require harsh reaction conditions and tedious purification and generate toxic by-products/wastes. Thus, there is a need for new methods addressing improved reaction control and green chemistry.

Presently, carbonaceous nanomaterials like graphene and other chemically modified or functionalized graphenes have received remarkable attention as heterogeneous catalysts and support due to their easy access, high surface area and diverse functionalities [66, 67]. As a part of our continuing interest using graphene oxide (GO) as the "carbocatalyst" for diverse organic transformations [68–71], we were interested to explore the three-component Hantzsch synthesis of 1,4-dihydropyridine. Literature survey reveals that GO-catalyzed Hantzsch synthesis has been studied previously [72, 73]. However, these protocols result in the formation of both 1,4-DHP and further oxidized pyridine derivatives in various ratios. Moreover, the processes require high temperature (refluxing conditions) and no recycling experiment has been reported in details. We reasoned that GO possessed high oxidizing properties and, when used in excess, could undergo further oxidation resulting in pyridine derivatives. We therefore thought further functionalization of GO could prevent it from being reduced and selectively form the 1,4-DHP as the sole product. Amine-functionalized graphene oxide nanosheets (AFGONs) have been previously prepared, designated as NH_2-GO [74], and AP-GO (GO-supported primary amine) [75], and used as the catalyst in Knoevenagel reaction and Henry–Michael reaction, respectively. We report herein AFGONs as an excellent catalyst for a facile one-pot selective synthesis of dihydropyridines (DHPs), polyhydroacridines (PHAs) and polyhydroquinolines (PHQs) under ambient conditions (Scheme 1). We synthesised AFGONs in our laboratory from GO, characterized it by various spectroscopic and other techniques and finally used it as an efficient and recyclable catalyst. The reaction conditions are mild producing 1,4-DHPs in good to excellent yield and formation of no trace of the oxidized pyridine derivative is observed. High and selective catalytic activity of AFGONs are presumably due to the unique cooperative effect between amines on the basal plane of GO and the adjacent carboxylic acid functionalities on its edges. Furthermore, the AFGONs can be easily recovered from the reaction mixture and reused for at least five consecutive runs without any loss of catalytic performance.

Results and discussion

AFGONs were prepared by following a reported procedure [75]. At first, GO was prepared by the Tour's method [76]. It was then exfoliated in an ultrasonic bath for 2 h, and then the amine groups were grafted onto the basal surface of GO

Scheme 1 AFGONs-catalyzed one-pot synthesis of 1,4-DHPs

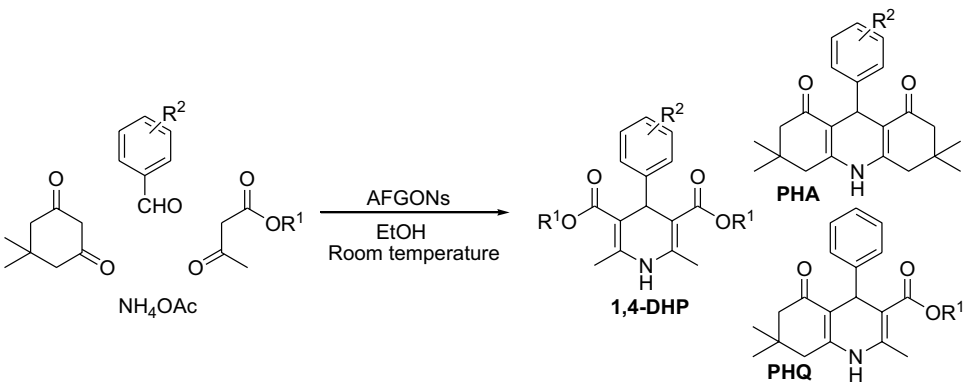

through a facile amine-coupling reaction using (3-aminopropyl)triethoxysilane (Scheme 2).

After the preparation of the catalyst, it was characterized by FT-IR, Raman spectra, powder X-ray diffraction (PXRD) and scanning electron microscopy (SEM). In the case of AFGONs, the peaks at 2963 and 2924 cm^{-1} were due to the asymmetric and symmetric stretching modes pertaining to C–H bonds of aminopropyl groups [74, 77]. The additional peak at 1593 cm^{-1} was due to the terminal NH_2 scissor vibration, and the less intense band at 1198 cm^{-1} was due to the rocking mode of SiO–C [77]. The disappearance of carbonyl band at 1734 cm^{-1} might indicate the removal of oxygenated functional groups to form partially reduced graphene oxide (RGO) as well as due to the formation of Si–O–C bond [78]. The Raman spectra of both GO and AFGONs showed characteristic D (arising from A_{1g} vibrations of sp^2 carbon rings) and G (arising from first-order scattering of E_{2g} mode of sp^2 C atoms) bands at 1345 and 1592 cm^{-1}, respectively [79]. The intensity ratios of D to G bands (I_D/I_G) of GO and AFGONs were found to be 0.83 and 0.92, respectively. The higher intensity ratio (I_D/I_G) of AFGONs led to suggest restoration of C=C bonds during the grafting process resulting in partial formation of RGO, as also observed previously by others [80, 81]. The XRD patterns of AFGONs showed a broad peak at $2\theta = 22.1°$ in addition to 11.9° (for pristine GO $2\theta = 9.5°$). We suggest that the new broad peak in the XRD patterns of AFGONs at $2\theta = 22.1°$ is due to the effect of silica with GO, as also observed by Zhang et al. [78]. However, partial formation of RGO cannot be ruled out as the peak for RGO appears closely ($2\theta = 25°$) [72, 73]. The interlayer distance (d) of AFGONs was calculated to be 7.4 Å ($2\theta = 11.9°$) and that of pristine GO was 9.2 Å ($2\theta = 9.5°$) which could be attributed to the surface occupancy of aminopropyl-silica groups [78]. In order to get the morphology of AFGONs, we performed scanning electron microscopy (SEM) analysis. The SEM images and XRD patterns clearly indicated the amorphous and fibrous nature of the catalyst. Furthermore, the elemental composition of the catalyst as determined by energy-dispersive X-ray spectroscopy (EDS) showed C (71.26 wt%), O (21.07 wt%), Si (3.96 wt%) and N (3.71 wt%), which confirmed the deposition of silica groups on the surface of GO (see Supplementary Material, Figure 5). A comparison of SEM images and elemental data (by EDS analyses) for GO and AFGONs (fresh and after catalytic uses in the third run) is presented in the Supplementary Material (S4.IV, S4.V and Figures 9 and 10).

In order to optimize the reaction conditions, we began our investigation using ethyl acetoacetate (**1a**), 4-chlorobenzaldehyde (**2a**) and ammonium acetate as model substrates in the presence of AFGONs as catalyst. Initially, the reactants were screened with regard to different solvents and then the other parameters like temperature, catalyst loading and duration of reaction were varied (Table 1). At first, the reaction was carried out with the catalyst AFGONs (50 mg) in ethanol under refluxing conditions and continued for 8 h. While monitoring the reaction, the TLC showed one major spot along with some other spots. After work up of the reaction mixture and purification by column chromatography afforded the compound **4a** in 69% yield (entry 1). We, however, did not make any attempt to isolate or identify compounds corresponding to other spots observed on TLC. Changing the solvent from EtOH to CH_3CN, H_2O and DMF and carrying out the reaction at 80–90 °C also gave the desired product **4a** in the range of 42–68% isolated yields (entries 2–5). Since the TLC in each case showed some other spots, which might be originated from one or more reasons like higher catalyst loading, higher temperature or longer reaction time, we performed another experiment in EtOH at 50 °C with the catalyst loading (25 mg) for 4 h (entry 6). In this case, we obtained the product **4a** in 72% yield indicating that low temperature and catalyst loading are important. We then carried out the reaction at room temperature (r.t.) for 2 h which furnished **4a** in 88% isolated yield (entry 7). In this experiment (entry 7), we observed no other spots on TLC except the desired one (**4a**) indicating that the competitive side reactions could be avoided at lower temperature and lower loading of the catalyst. A neat mixture of the reactants without any solvent afforded the product in 52% yield suggesting that the use of solvent is also essential for better conversion to the product (entry 8). The reaction when conducted without any catalyst resulted in poor conversion even after prolonged reaction time which indicated the imperative role of the catalyst (entry 9, 21%).

With the optimized reaction conditions in hand, we have examined the scope and generality of this MCR and

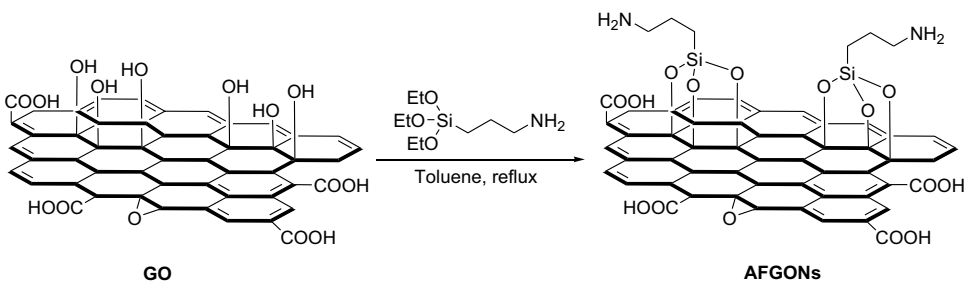

Scheme 2 Schematic presentation of preparation of AFGONs

Table 1 Optimization of reaction conditions

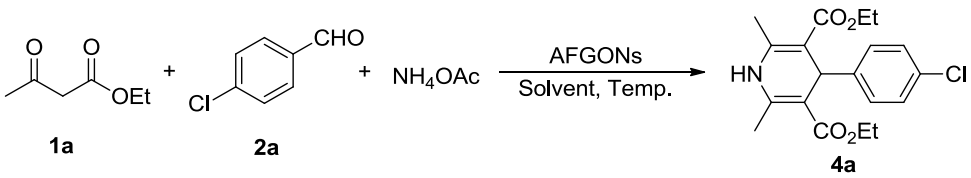

Entry	AFGONs (mg)	Solvent	Temp. (°C)/time (h)	Yield (%)[a]
1	50	EtOH	78/8	69
2	50	CH_3CN	80/8	58
3	50	H_2O	90/8	42
4	50	H_2O	90/8	65[b]
5	50	DMF	80/8	68
6	25	EtOH	50/4	72
7	25	EtOH	r.t./2	88
8	25	–	r.t./2	52
9	–	EtOH	r.t./20	21

Reaction conditions: **1a** (2 mmol), **2a** (1 mmol), NH_4OAc (2 mmol) and solvent (4 mL)

[a]Isolated yield

[b]TBAB (10 mol%) was used

the results are summarized in Table 2. It can be seen that a series of different aldehydes reacted under the standard reaction conditions and in all cases the desired product has been isolated in good to excellent yields. Aromatic aldehydes substituted with both electron-donating (–Cl, –Br, $–CH_3$, $–OCH_3$, –OH and $–NMe_2$) as well as electron-withdrawing (–F and $–NO_2$) groups reacted efficiently to afford the corresponding products (**4a**–**k**). The substitution pattern on the aromatic moiety did not have any significant influence in the course of the reaction. We then checked the reaction with 2-naphthaldehyde and cinnamaldehyde, which furnished the desired products in 84% and 83% yield, respectively (**4l** and **4m**). Further investigation with aliphatic aldehydes also worked efficiently affording the desired products (**4n** and **4o**). Fascinatingly, heterocyclic aldehydes like furfural and 5-bromo-2-thiophenecarboxaldehyde were found to be equally effective affording the anticipated products in 87% and 89% isolated yield, respectively (**4p** and **4q**).

Functionalized acridinediones possess potential biological properties as well as find applications as laser dyes and photo initiators [58]. The 1,8-dioxodecahydroacridine exhibits a wide range of pharmacological properties such as antimalarial, antitumour, anticancer, antimicrobial activities and β-channel opener in cardiovascular diseases [17, 61]. The multi-component reaction was done with benzaldehydes bearing both electron-withdrawing (–F, $–NO_2$) and electron-donating (–Cl, –Br, –OH, –OMe) groups. It is evident from the facile conversion (yields 86–92%) that the substitution patterns on the benzaldehyde partner do not affect the course of the reaction. Replacing dimedone with cyclohexan-1,3-dione also gave the desired product in 88% yield (**5g**) establishing the scope of product diversity (Table 3).

Polyhydroquinolines (PHQs), the unsymmetrical derivatives of 1,4-DHPs, display prominent biological activities associated with cardiovascular diseases and hypertension [30]. Certain 2,4-disubstituted PHQs are active glycogen phosphorylase inhibitors and also exhibit antihyperglycemic activity [82]. We explored the synthesis of PHQs through the four-component catalytic reaction of β-ketoester, aldehyde, dimedone/cyclohexan-1,3-dione and ammonium acetate. Gratifyingly, the reaction worked efficiently affording the desired PHQs in good to excellent yields (Table 4). Like in the synthesis of functionalized acridinediones, the synthesis of PHQs from benzaldehydes with diverse functional groups, electron-donating (–Me, $–CHMe_2$, –Br, –OH) or electron-withdrawing groups (–F, $–NO_2$), was achieved without any difficulty. It is important to mention that this four-component reaction did result in the formation of unsymmetrical PHQs only and no symmetrical derivative of 1,4-DHP was formed. The selective formation of unsymmetrical PHQs is indeed encouraging, though we do not suggest any specific reason at the moment.

While scaling up the reaction, we used different quantities of the catalyst (AFGONs). It is observed that in the reaction of ethyl acetoacetate (2.6 g, 20 mmol), 4-chlorobenzaldehyde (1.4 g, 10 mmol) and ammonium acetate

Table 2 Synthesis of 1,4-DHPs by one-pot three-component reaction

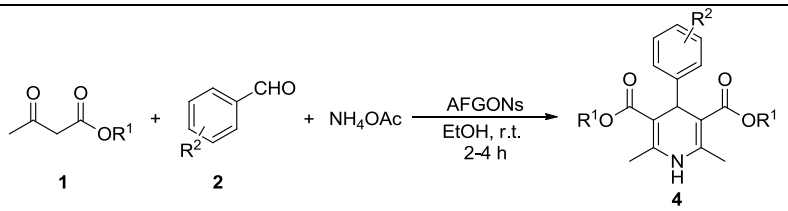

1 **2** **4**

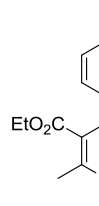

4a, 88%, 2 h

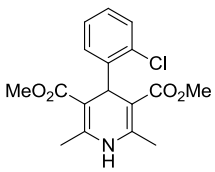

4b, 84%, 4 h

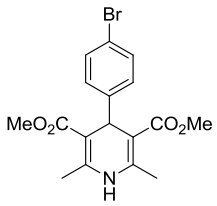

4c, 87%, 2 h

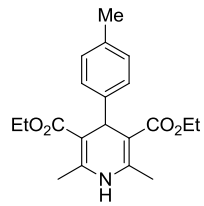

4d, 85%, 3h

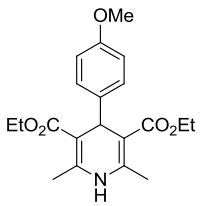

4e, 86%, 3 h

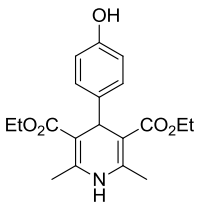

4f, 89%, 2 h

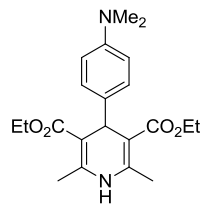

4g, 87%, 3 h

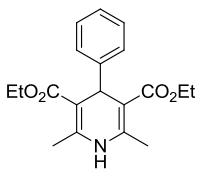

4h, 90%, 2h

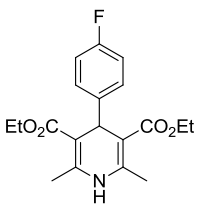

4i, 91%, 2 h

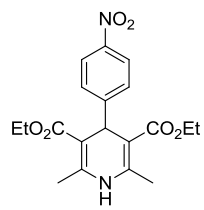

4j, 90%, 2 h

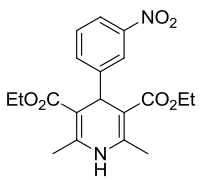

4k, 93%, 2 h

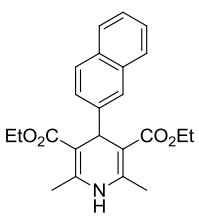

4l, 84%, 4 h

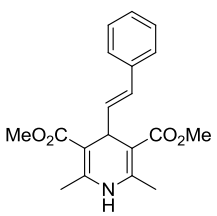

4m, 83%, 4 h

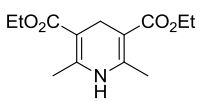

4n, 90%, 3 h

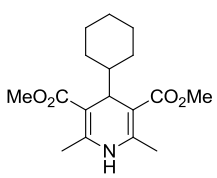

4o, 83%, 4 h

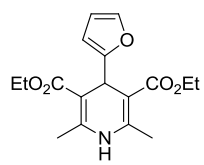

4p, 87%, 3 h

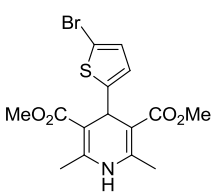

4q, 89%, 4 h

Table 2 (continued)

Reaction conditions: **1** (2 mmol), **2** (1 mmol), NH_4OAc (2 mmol) and AFGONs (25 mg) in EtOH (4 mL) were stirred at r.t. for 2–4 h

Table 3 Synthesis of 1,8-dioxodecahydroacridine by AFGONs

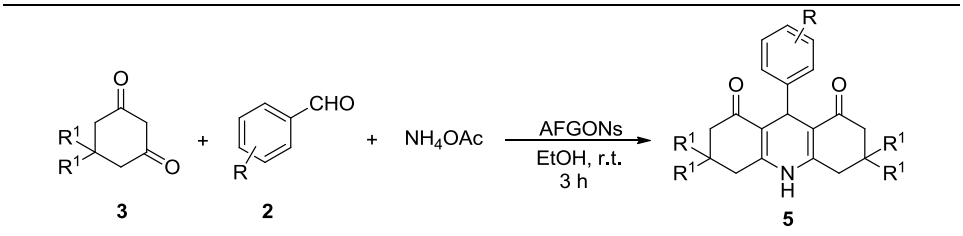

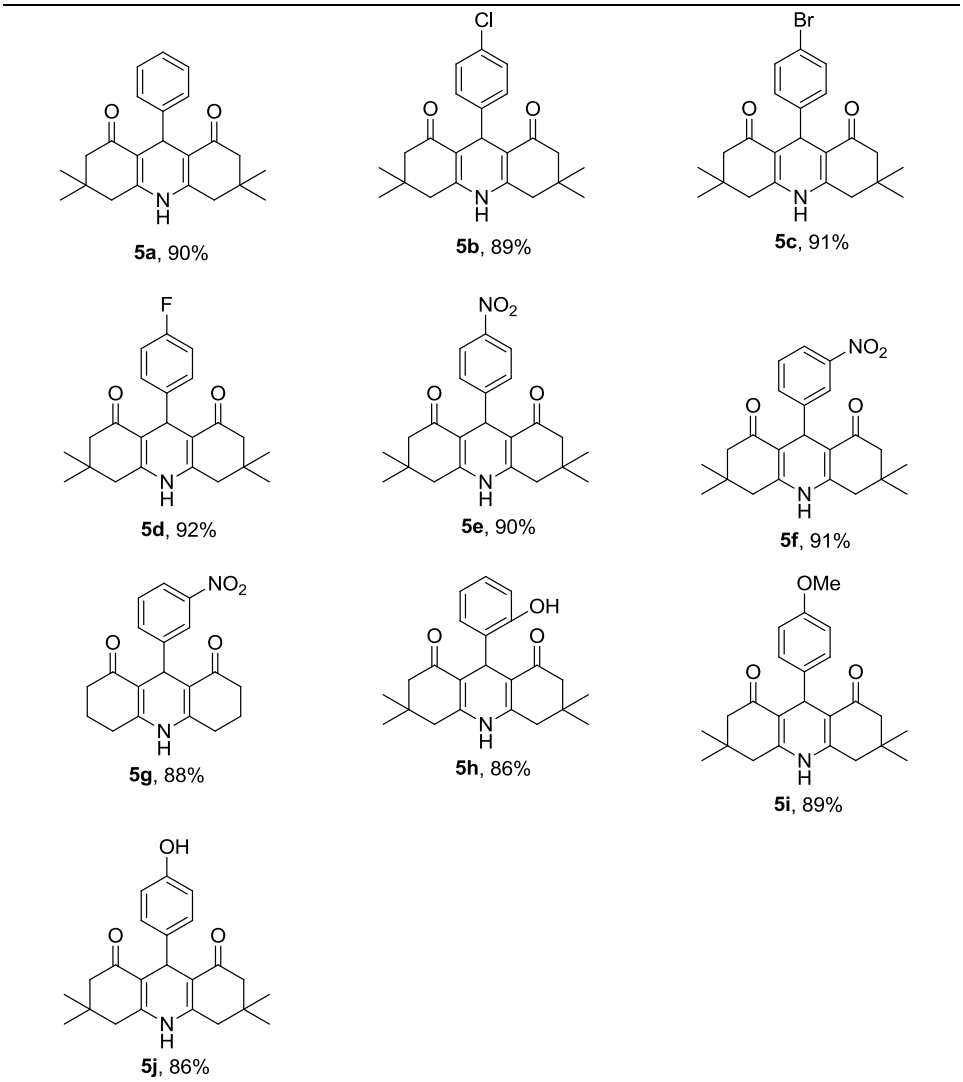

Reaction conditions: **3a** (2 mmol), **2** (1 mmol), NH_4OAc (2 mmol), AFGONs (25 mg) and EtOH (4 mL) were stirred at r.t. for 3 h

(1.5 g, 20 mmol) in ethanol (40 mL), only 100 mg of the catalyst (AFGONs) is enough to catalyze the reaction yielding the desired product (**4a**) in satisfactory yield (Scheme 3). Table 5 shows the results of using AFGONs in varying quantities keeping the starting three components fixed. This suggests that proportionate increase in the catalyst is not required for gram-scale synthesis.

Mechanistically, the multi-component synthesis of the Hantzsch 1,4-dihyropyridine is believed to proceed via different plausible pathways based on the catalysts and reaction

Table 4 AFGONs-catalyzed synthesis of polyhydroquinoline

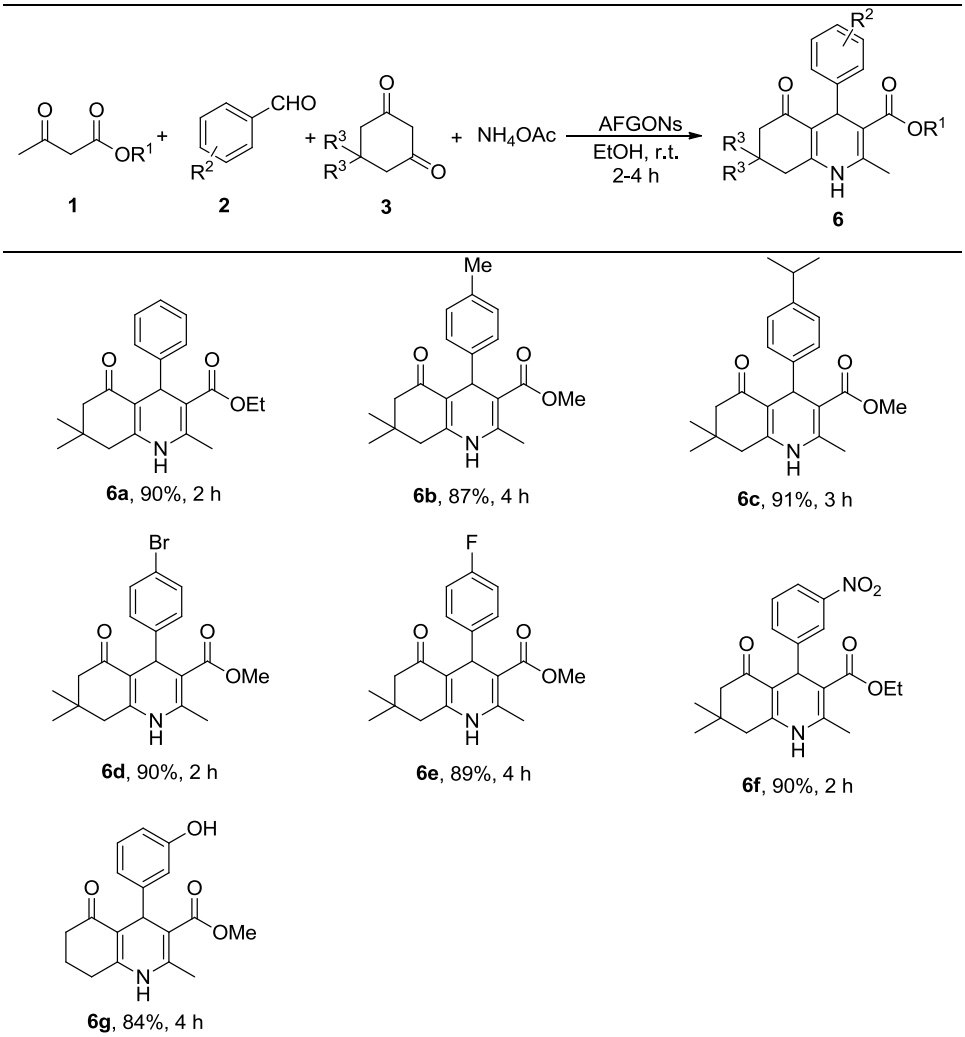

Reaction conditions: **1** (1 mmol), **2** (1 mmol), **3** (1 mmol), NH_4OAc (2 mmol), AFGONs (25 mg) and EtOH (4 mL)

Scheme 3 1,4-Dihydropyridine synthesis on gram scale

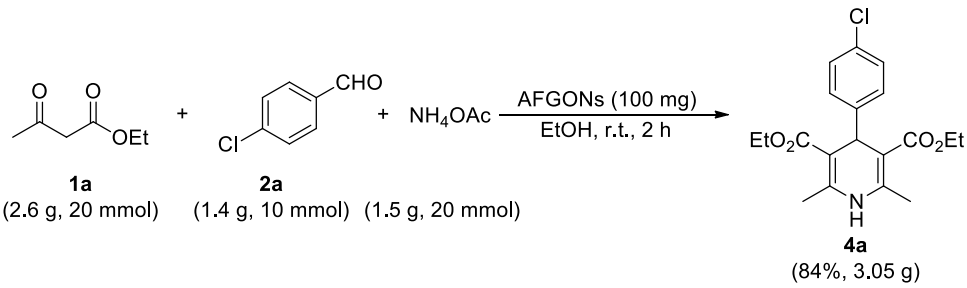

conditions. We set up several control experiments to propose a plausible mechanism for our protocol as outlined in Scheme 3: (i) The reaction of **1a** and **2a** under the optimal condition did not produce compound **7**, (ii) again, there was no product formed in a reaction of **2a** with NH_4OAc and (iii) treatment of **1a** with NH_4OAc did show two spots on TLC after 1 h in addition to the spot corresponding to **1a**. Analyzing the reaction mixture by HPLC and drawing analogy with the previous report [83, 84], we presumed that these two peaks are due to compounds enamine (**8**) and dienamine (**9**). While trying to isolate the intermediates by passing through a short column of silica, we ended up isolating the starting **1a** only. Although this could be possible because of reversibility of the step, it restricted us trying further control experiments involving **7** + **8** + NH_4OAc or **7** + **9** + NH_4OAc, and (iv) however, the addition of the reacting partner **2a** to

Table 5 Catalyst optimization in gram-scale synthesis of 1,4-dihydropyridine (**4a**)

AFGONs (mg)	250	150	100	75
Isolated yield (%)	87	84	84	64

the partial reaction mixture of **1a** and NH_4OAc led to the formation of the desired compound **4a** under the optimal conditions (Scheme 4). On the other hand, similar addition of **7**, prepared in a different method [85], did not produce **4a**. All these experiments led us to propose a plausible mechanism involving the intermediates **8** and/or **9**, as outlined in Scheme 5. The acidic moiety present in the catalyst is involved in the activation of carbonyl groups of both ethyl acetoacetate and the aldehyde. Initially, the dienamine intermediate (**9**) is presumably formed by the reaction of two equivalents of ethyl acetoacetate with ammonia generated from ammonium acetate. This is followed by the addition of aldehyde with dienamine (**9**) to form **10**. The basic moiety of the catalyst then abstracts a proton from **10** aiding in the cyclization to intermediate **11** with the elimination of one molecule of H_2O. Finally, the abstraction of another proton from **11** results in the formation of 1,4-dihydropyridine.

One of the most important aspects of a heterogeneous catalyst is its ability to be recycled. We evaluated the reusability of AFGONs in the synthesis of **4a** under the optimized reaction condition (Fig. 1). The catalyst was easily recovered from the reaction mixture by simple filtration. It was washed with ethyl acetate (3 × 5 mL) followed by water (5 mL) and was dried under vacuum for 6 h before being used for the next run. The catalyst could be used for five consecutive runs without significant loss in its catalytic activity and decrease in the yield of products. Moreover, we have characterized the catalyst after the third run by FT-IR, Raman spectroscopy, X-ray powder diffraction, and SEM–EDS analysis did not show any significant change in the spectral data and diffraction patterns of the catalyst before and after catalytic uses (see Supplementary Material).

Conclusion

In conclusion, we presented here an eco-friendly route for the selective preparation of Hantzsch esters and related heterocyclic biomolecules via a one-pot multi-component reaction using amine-functionalized graphene oxide nanosheets (AFGONs). We have demonstrated that suitable tuning of GO

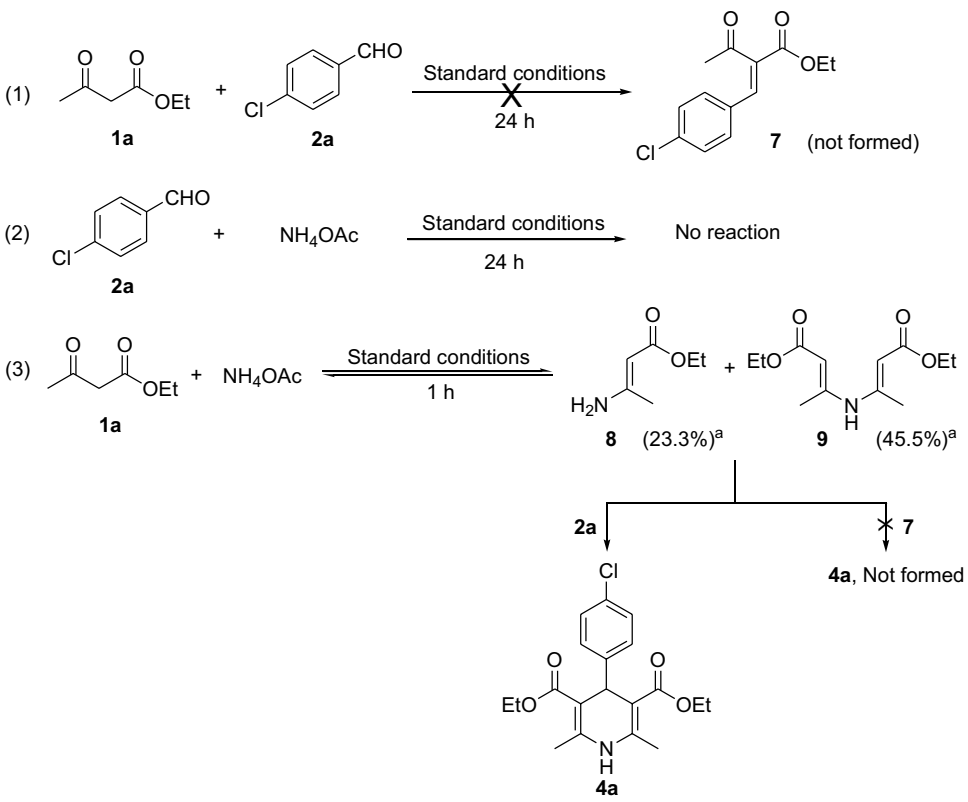

Scheme 4 Control experiments. [a]Conversion percentages analyzed in HPLC, not isolated and characterized

Scheme 5 Plausible mechanism for the synthesis of 1,4-DHP using AFGONs

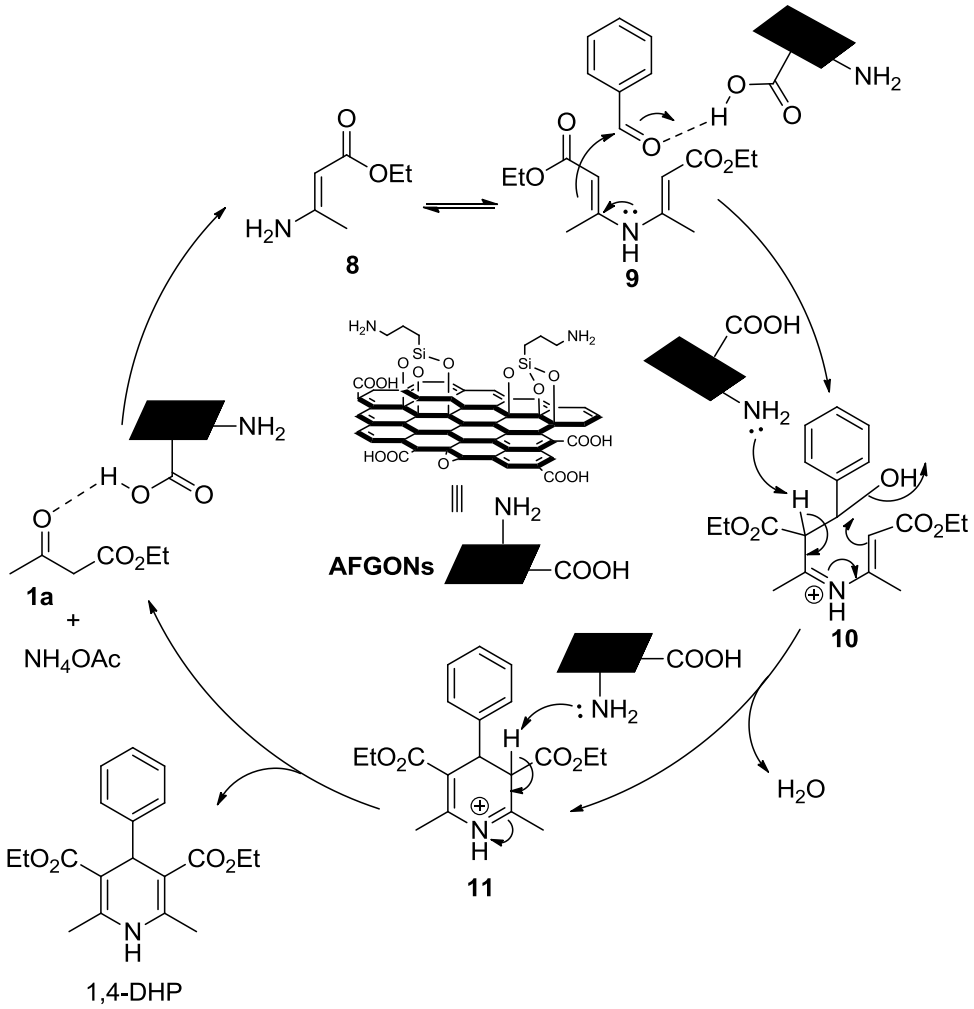

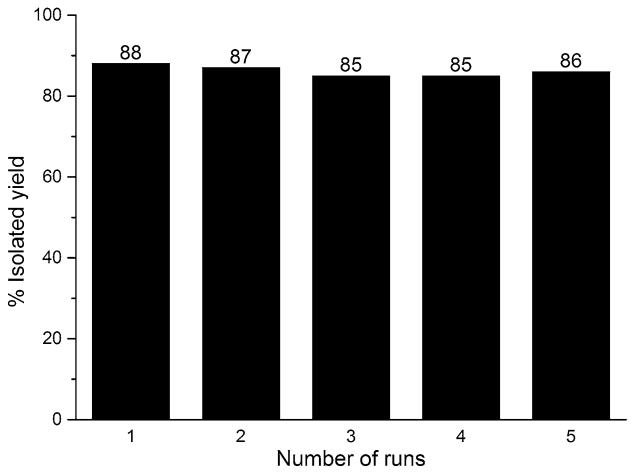

Fig. 1 Recyclability of AFGONs in the synthesis of 1,4-dihydropyridine

prevented further oxidation of the product (1,4-DHP). Short reaction time, ambient reaction temperature, tolerance to a wide range of functional groups, reusability of the catalyst and the ease of product isolation without column purifications are a few important features of the method reported here.

Supplementary material

The Supplementary Material for this article contains the experimental section including synthetic procedure along with analytical and spectral data of all the synthesized compounds and scanned copies of HRMS (selected compounds), ^{1}H-NMR and ^{13}C-NMR spectra.

Acknowledgements Financial support from Science and Engineering Research Board, New Delhi (Grant No EMR/2015/000549), is gratefully acknowledged. PC thanks UGC, New Delhi, for Senior Research Fellowship under UGC–NET. Authors express their sincere thanks to Dr. Sukanta Bhattacharyya, Supra Sciences Inc, San Francisco, CA, USA, for his keen interest in this work. The authors would like to acknowledge University Science and Instrumentation Centre for scanning electron microscopy (SEM) facility.

Compliance with ethical standards

Conflict of interest The authors declare that they have no conflict of interest.

References

1. Baumann M, Baxendale IR (2013) An overview of the synthetic routes to the best selling drugs containing 6-membered heterocycles. Beilstein J Org Chem 9:2265
2. Mannhold R, Jablonka B, Voigt W, Schönafinger K, Schraven E (1992) Calcium- and calmodulin-antagonism of elnadipine derivatives: comparative SAR. Eur J Med Chem 27:229–235
3. Bansal R, Narang G, Calle C, Carron R, Pemberton K, Harvey AL (2013) Synthesis of 4-(carbonyloxyphenyl)-1, 4-dihydropyridines as potential antihypertensive agents. Drug Dev Res 74:50–61
4. Boer R, Gekeler R (1995) Chemosensitizer in tumor therapy: new compounds promise better efficacy. Drugs Future 20:499–509
5. Janis RA, Triggle DJ (1984) 1,4-Dihydropyridine Ca^{2+} channel antagonists and activators: a comparison of binding characteristics with pharmacology. Drug Dev Res 4:257–274
6. Loev B, Goodman MM, Snader KM, Tedeschi R, Macko E (1974) Hantzsch-type dihydropyridine hypotensive agents. J Med Chem 17:956–965. https://doi.org/10.1021/jm00255a010
7. Bossert F, Meyer H, Wehinger E (1981) 4-Aryldihydropyridines, a new class of highly active calcium antagonists. Angew Chem Int Ed 20:762–769. https://doi.org/10.1002/anie.198107621
8. Epstein BJ, Vogel K, Palmer BF (2007) Dihydropyridine calcium channel antagonists in the management of hypertension. Drugs 67:1309–1327. https://doi.org/10.2165/00003495-200767090-00005
9. Huang W, Cheng X (2017) Hantzsch esters as multifunctional reagents in visible-light photoredox catalysis. Synlett 28:148–158. https://doi.org/10.1055/s-0036-1588129
10. Ouellet SG, Walji AM, MacMillan DW (2007) Enantioselective organocatalytic transfer hydrogenation reactions using Hantzsch esters. Acc Chem Res 40:1327–1339
11. Xie K, Liu Y-C, Cui Y, Wang J-G, Fu Y, Mak TC (2007) N-methyl-(R)-3-(tert-butyl)-sulfinyl-1, 4-dihydropyridine: a novel NADH model compound. Molecules 12:415–422
12. Comins DL, O'Connor S (1988) Regioselective substitution in aromatic six-membered nitrogen heterocycles. In: Katritzky AR (ed) Advances in heterocyclic chemistry. Elsevier, London, pp 199–267
13. Wang D, Astruc D (2015) The golden age of transfer hydrogenation. Chem Rev 115:6621–6686. https://doi.org/10.1021/acs.chemrev.5b00203
14. Hantzsch A (1882) Ueber die synthese pyridinartiger verbindungen aus acetessigäther und aldehydammoniak. Justus Liebigs Ann Chem 215:1–82. https://doi.org/10.1002/jlac.18822150102
15. Wan J-P, Liu Y (2012) Recent advances in new multicomponent synthesis of structurally diversified 1, 4-dihydropyridines. RSC Adv 2:9763–9777
16. Sharma VK, Singh SK (2017) Synthesis, utility and medicinal importance of 1, 2- and 1, 4-dihydropyridines. RSC Adv 7:2682–2732
17. Brahmachari G, Begam S, Nurjamal K (2017) Bismuth nitrate catalyzed one-pot multicomponent synthesis of a novel series of diversely substituted 1,8-dioxodecahydroacridines at room temperature#. ChemistrySelect 2:3311–3316. https://doi.org/10.1002/slct.201700265
18. Reddy CS, Raghu M (2008) Cerium (IV) ammonium nitrate catalysed facile and efficient synthesis of polyhydroquinoline derivatives through Hantzsch multicomponent condensation. Chin Chem Lett 19:775–779
19. Rameshwar N, Ramchander J, Parthasarathi T, Reddy AR (2012) Yttrium triflate catalyzed synthesis of 1,4-dihydropyridines under solvent free conditions. Heterocycl Lett 2:455–459
20. Izadkhah V, Mahmoodi J (2016) Ag-TiO_2 nano composite as an efficient and recyclable catalyst for the Hantzsch synthesis of polyhydroquinolines. Heterocycl Lett 6:623–630
21. Goel S, Goel V, Bajwan A (2016) Efficient procedure for synthesis of 1, 4-dihydropyridines under green chemistry conditions. Heterocycl Lett 6:709–715
22. Sapkal SB, Shelke KF, Shingate BB, Shingare MS (2009) Nickel nanoparticle-catalyzed facile and efficient one-pot synthesis of polyhydroquinoline derivatives via Hantzsch condensation under solvent-free conditions. Tetrahedron Lett 50:1754–1756
23. Pramanik M, Bhaumik A (2013) Self-assembled hybrid tinphosphonate nanoparticles with bimodal porosity: an insight towards the efficient and selective catalytic process for the synthesis of bioactive 1,4-dihydropyridines under solvent-free conditions. J Mater Chem A 1:11210–11220. https://doi.org/10.1039/C3TA12476B
24. Paplal B, Nagaraju S, Veerabhadraiah P, Sujatha K, Kanvah S, Vijaya Kumar B, Kashinath D (2014) Recyclable Bi_2WO_6-nanoparticle mediated one-pot multicomponent reactions in aqueous medium at room temperature. RSC Adv 4:54168–54174. https://doi.org/10.1039/C4RA07708C
25. Demirci T, Celik B, Yldz Y, Eris S, Arslan M, Sen F, Kilbas B (2016) One-pot synthesis of Hantzsch dihydropyridines using a highly efficient and stable PdRuNi@GO catalyst. RSC Adv 6:76948–76956. https://doi.org/10.1039/C6RA13142E
26. Sabitha G, Arundhathi K, Sudhakar K, Sastry BS, Yadav JS (2009) $CeCl_3{\cdot}7H_2O$-catalyzed one-pot synthesis of Hantzsch 1,4-dihydropyridines at room temperature. Synth Commun 39:2843–2851. https://doi.org/10.1080/00397910802656091
27. Koukabi N, Kolvari E, Khazaei A, Zolfigol MA, Shirmardi-Shaghasemi B, Khavasi HR (2011) Hantzsch reaction on free nano-Fe_2O_3 catalyst: excellent reactivity combined with facile catalyst recovery and recyclability. Chem Commun 47:9230–9232
28. Safari J, Zarnegar Z (2013) A magnetic nanoparticle supported Ni^{2+}-containing ionic liquid as an efficient nanocatalyst for the synthesis of Hantzsch 1,4-dihydropyridines in a solvent-free dry-system. RSC Adv 3:26094–26101. https://doi.org/10.1039/C3RA43601B
29. Kiani M, Mohammadipour M (2017) Fe_3O_4@SiO_2-MoO_3H nanoparticles: a magnetically recyclable nanocatalyst system for the synthesis of 1,8-dioxo-decahydroacridine derivatives. RSC Adv 7:997–1007. https://doi.org/10.1039/C6RA25571J
30. Nasr-Esfahani M, Hoseini SJ, Montazerozohori M, Mehrabi R, Nasrabadi H (2014) Magnetic Fe_3O_4 nanoparticles: efficient and recoverable nanocatalyst for the synthesis of polyhydroquinolines and Hantzsch 1,4-dihydropyridines under solvent-free conditions. J Mol Catal A Chem 382:99–105
31. Murthy YLN, Rajack A, Taraka Ramji M, Jeson Babu J, Praveen C, Aruna Lakshmi K (2012) Design, solvent free synthesis, and antimicrobial evaluation of 1,4 dihydropyridines. Bioorg Med Chem Lett 22:6016–6023
32. Nakhaei A, Hosseininasab N, Yadegarian S (2017) Synthesis of 1, 4-dihydropyridine derivatives using nano-zirconia sulfuric acid as highly efficient recyclable catalyst. Heterocycl Lett 7:81–90
33. Evans CG, Gestwicki JE (2009) Enantioselective organocatalytic Hantzsch synthesis of polyhydroquinolines. Org Lett 11:2957–2959. https://doi.org/10.1021/ol901114f
34. Mohammadipour M, Amoozadeh A (2017) The synthesis of polyhydroacridines by covalent 5-sulfobenzoic acid-functionalized graphene oxide as a novel, green, efficient, and heterogeneous

catalyst. Monatsh Chem 148:1075–1084. https://doi.org/10.1007/s00706-016-1876-6
35. Amoozadeh A, Rahmani S, Bitaraf M, Abadi FB, Tabrizian E (2016) Nano-zirconia as an excellent nano support for immobilization of sulfonic acid: a new, efficient and highly recyclable heterogeneous solid acid nanocatalyst for multicomponent reactions. New J Chem 40:770–780. https://doi.org/10.1039/C5NJ02430G
36. Adharvana Chari M, Syamasundar K (2005) Silica gel/$NaHSO_4$ catalyzed one-pot synthesis of Hantzsch 1,4-dihydropyridines at ambient temperature. Catal Commun 6:624–626
37. Rafiee E, Eavani S, Rashidzadeh S, Joshaghani M (2009) Silica supported 12-tungstophosphoric acid catalysts for synthesis of 1,4-dihydropyridines under solvent-free conditions. Inorg Chim Acta 362:3555–3562
38. Datta B, Pasha MA (2011) Silica sulfuric acid: an efficient heterogeneous catalyst for the one-pot synthesis of 1,4-dihydropyridines under mild and solvent-free conditions. Chin J Catal 32:1180–1184
39. Sadeghi B, Namakkoubi A, Hassanabadi A (2013) $BF_3.SiO_2$ nanoparticles: a solid phase acidic catalyst for efficient one-pot Hantzsch synthesis of 1,4-dihydropyridines. J Chem Res 37:11–13. https://doi.org/10.3184/174751912X13542975429543
40. Maheswara M, Siddaiah V, Rao YK, Tzeng Y-M, Sridhar C (2006) A simple and efficient one-pot synthesis of 1,4-dihydropyridines using heterogeneous catalyst under solvent-free conditions. J Mol Catal A Chem 260:179–180
41. Affeldt RF, Benvenutti EV, Russowsky D (2012) A new in-SiO_2 composite catalyst in the solvent-free multicomponent synthesis of Ca^{2+} channel blockers nifedipine and nemadipine B. New J Chem 36:1502–1511. https://doi.org/10.1039/C2NJ40060J
42. Sharma P, Gupta M (2015) Silica functionalized sulphonic acid coated with ionic liquid: an efficient and recyclable heterogeneous catalyst for the one-pot synthesis of 1,4-dihydropyridines under solvent-free conditions. Green Chem 17:1100–1106. https://doi.org/10.1039/C4GC00923A
43. Cherkupally SR, Mekala R (2008) *P*-TSA catalyzed facile and efficient synthesis of polyhydroquinoline derivatives through Hantzsch multi-component condensation. Chem Pharm Bull 56:1002–1004. https://doi.org/10.1248/cpb.56.1002
44. Kumar A, Maurya RA (2008) Efficient synthesis of hantzsch esters and polyhydroquinoline derivatives in aqueous micelles. Synlett. https://doi.org/10.1055/s-2008-1042908
45. Das B, Ravikanth B, Ramu R, Vittal Rao B (2006) An efficient one-pot synthesis of polyhydroquinolines at room temperature using HY-zeolite. Chem Pharm Bull 54:1044–1045. https://doi.org/10.1248/cpb.54.1044
46. Saikia L, Dutta D, Dutta DK (2012) Efficient clay supported Ni^0 nanoparticles as heterogeneous catalyst for solvent-free synthesis of Hantzsch polyhydroquinoline. Catal Commun 19:1–4
47. Song G, Wang B, Wu X, Kang Y, Yang L (2005) Montmorillonite K10 clay: an effective solid catalyst for one-pot synthesis of polyhydroquinoline derivatives. Synth Commun 35:2875–2880. https://doi.org/10.1080/00397910500297255
48. Pham DD, Le NT, Vo-Thanh G (2017) Fast and efficient Hantzsch synthesis using acid-activated and cation-exchanged montmorillonite catalysts under solvent-free microwave irradiation conditions. ChemistrySelect 2:12041–12045. https://doi.org/10.1002/slct.201702681
49. Maleki A, Kamalzare M, Aghaei M (2015) Efficient one-pot four-component synthesis of 1,4-dihydropyridines promoted by magnetite/chitosan as a magnetically recyclable heterogeneous nanocatalyst. J Nanostruct Chem 5:95–105. https://doi.org/10.1007/s40097-014-0140-z
50. Safari J, Azizi F, Sadeghi M (2015) Chitosan nanoparticles as a green and renewable catalyst in the synthesis of 1,4-dihydropyridine under solvent-free conditions. New J Chem 39:1905–1909. https://doi.org/10.1039/C4NJ01730G
51. Debache A, Ghalem W, Boulcina R, Belfaitah A, Rhouati S, Carboni B (2009) An efficient one-step synthesis of 1,4-dihydropyridines via a triphenylphosphine-catalyzed three-component Hantzsch reaction under mild conditions. Tetrahedron Lett 50:5248–5250
52. Rekunge DS, Khatri CK, Chaturbhuj GU (2017) Sulfated polyborate: An efficient and reusable catalyst for one pot synthesis of Hantzsch 1,4-dihydropyridines derivatives using ammonium carbonate under solvent free conditions. Tetrahedron Lett 58:1240–1244
53. Wang X, Gong H, Quan Z, Li L, Ye H (2011) One-pot, three-component synthesis of 1,4-dihydropyridines in PEG-400. Synth Commun 41:3251–3258. https://doi.org/10.1080/00397911.2010.517888
54. Nakhaei A, Yadegarian S, Davoodnia A (2016) Efficient and rapid Hantzsch synthesis of 1,4-dihydropyridines using a nano isopolyoxomolybdate as a reusable catalyst under solvent-free condition. Heterocycl Lett 6:329–339
55. Zolfagharinia S, Kolvari E, Koukabi N (2017) A new type of magnetically-recoverable heteropolyacid nanocatalyst supported on zirconia-encapsulated Fe_3O_4 nanoparticles as a stable and strong solid acid for multicomponent reactions. Catal Lett 147:1551–1566. https://doi.org/10.1007/s10562-017-2015-7
56. Ghattali SN, Saidi K, Khabazzadeh H (2014) $(NH_4)_{2.5}H_{0.5}PW_{12}O_{40}$-catalyzed rapid and efficient one-pot synthesis of dihydropyridines via the Hantzsch reaction under solvent-free conditions. Res Chem Intermed 40:281–291. https://doi.org/10.1007/s11164-012-0962-6
57. Han L, Zhang Y, Zhou Z (2016) Solvent-free synthesis of 1, 8-dioxo-octahydroxanthenes and 1, 8-dioxo-decahydroacridines using $[BPY]HSO_4$ as an efficient reusable catalyst. Heterocycl Lett 6:23–30
58. Zhu A, Liu R, Du C, Li L (2017) Betainium-based ionic liquids catalyzed multicomponent Hantzsch reactions for the efficient synthesis of acridinediones. RSC Adv 7:6679–6684. https://doi.org/10.1039/C6RA25709G
59. Kumar R, Andhare NH, Shard A, Sinha AK (2014) Multicomponent diversity-oriented synthesis of symmetrical and unsymmetrical 1, 4-dihydropyridines in recyclable glycine nitrate ($GlyNO_3$) ionic liquid: a mechanistic insight using Q-TOF, ESI-MS/MS. RSC Adv 4:19111–19121
60. Yarhosseini M, Javanshir S, Dekamin MG, Farhadnia M (2016) Tetraethylammonium 2-(carbamoyl)benzoate as a bifunctional organocatalyst for one-pot synthesis of Hantzsch 1,4-dihydropyridine and polyhydroquinoline derivatives. Monatsh Chem 147:1779–1787. https://doi.org/10.1007/s00706-016-1666-1
61. Karhale S, Bhenki C, Rashinkar G, Helavi V (2017) Covalently anchored sulfamic acid on cellulose as heterogeneous solid acid catalyst for the synthesis of structurally symmetrical and unsymmetrical 1,4-dihydropyridine derivatives. New J Chem 41:5133–5141. https://doi.org/10.1039/C7NJ00685C
62. Baghbanian SM, Khaksar S, Vahdat SM, Farhang M, Tajbakhsh M (2010) One-step, synthesis of Hantzsch esters and polyhydroquinoline derivatives using new organocatalyst. Chin Chem Lett 21:563–567
63. Dekamin MG, Ilkhanizadeh S, Latifidoost Z, Daemi H, Karimi Z, Barikani M (2014) Alginic acid: a highly efficient renewable and heterogeneous biopolymeric catalyst for one-pot synthesis of the Hantzsch 1,4-dihydropyridines. RSC Adv 4:56658–56664. https://doi.org/10.1039/C4RA11801D

64. Khodja IA, Ghalem W, Dehimat ZI, Boulcina R, Carboni B, Debache A (2014) Solvent-free synthesis of dihydropyridines and acridinediones via a salicylic acid-catalyzed Hantzsch multicomponent reaction. Synth Commun 44:959–967. https://doi.org/10.1080/00397911.2013.838791
65. Sehout I, Boulcina R, Boumoud B, Boumoud T, Debache A (2017) Solvent-free synthesis of polyhydroquinoline and 1,8-dioxodecahydroacridine derivatives through the Hantzsch reaction catalyzed by a natural organic acid: a green method. Synth Commun 47:1185–1191. https://doi.org/10.1080/00397911.2017.1316406
66. Qiu B, Xing M, Zhang J (2018) Recent advances in three-dimensional graphene based materials for catalysis applications. Chem Soc Rev 47:2165–2216. https://doi.org/10.1039/C7CS00904F
67. Navalon S, Dhakshinamoorthy A, Alvaro M, Garcia H (2014) Carbocatalysis by graphene-based materials. Chem Rev 114:6179–6212. https://doi.org/10.1021/cr4007347
68. Choudhury P, Roy B, Basu B (2017) Sustainable and site-selective C−H sulfenylation of aromatic compounds with thiol using catalytic graphene oxide and NaI. Asian J Org Chem 6:1569–1574. https://doi.org/10.1002/ajoc.201700275
69. Bhattacharya S, Ghosh P, Basu B (2017) Graphene oxide (GO): an efficient carbocatalyst for the benign synthesis of functionalized 1, 4-benzothiazines. Tetrahedron Lett 58:926–931. https://doi.org/10.1016/j.tetlet.2017.01.068
70. Bhattacharya S, Ghosh P, Basu B (2018) Graphene oxide (GO) catalyzed transamidation of aliphatic amides: an efficient metal-free procedure. Tetrahedron Lett 59:899–903. https://doi.org/10.1016/j.tetlet.2018.01.060
71. Roy B, Ghosh S, Ghosh P, Basu B (2015) Graphene oxide (GO) or reduced graphene oxide (rGO): efficient catalysts for one-pot metal-free synthesis of quinoxalines from 2-nitroaniline. Tetrahedron Lett 56:6762–6767. https://doi.org/10.1016/j.tetlet.2015.10.065
72. Mirza-Aghayan M, Asadi F, Boukherroub R (2014) Graphite oxide-promoted one-pot synthesis and oxidative aromatization of Hantzsch 1, 4-dihydropyridines. Monatsh Chem 145:1919–1924. https://doi.org/10.1007/s00706-014-1259-9
73. Kagne RP, Nikam GH, Kalalawe VG, Niwadange SN, Munde DR (2017) An efficient protocol for synthesis of 1,4-dihydropyridine derivatives by using graphene oxide nanoparticles as a catalyst. J Chem Chem Sci 7:1064–1070
74. Zhang F, Jiang H, Li X, Wu X, Li H (2014) Amine-functionalized GO as an active and reusable acid-base bifunctional catalyst for one-pot cascade reactions. ACS Catal 4:394–401. https://doi.org/10.1021/cs400761r
75. Zhang F, Jiang H, Wu X, Mao Z, Li H (2015) Organoamine-functionalized graphene oxide as a bifunctional carbocatalyst with remarkable acceleration in a one-pot multistep reaction. ACS Appl Mater Interfaces 7:1669–1677. https://doi.org/10.1021/am507221a
76. Marcano DC, Kosynkin DV, Berlin JM, Sinitskii A, Sun Z, Slesarev A, Alemany LB, Lu W, Tour JM (2010) Improved synthesis of graphene oxide. ACS Nano 4:4806–4814. https://doi.org/10.1021/nn1006368
77. Pasternack RM, Rivillon Amy S, Chabal YJ (2008) Attachment of 3-(aminopropyl) triethoxysilane on silicon oxide surfaces: dependence on solution temperature. Langmuir 24:12963–12971. https://doi.org/10.1021/la8024827
78. Zhang WL, Choi HJ (2012) Silica-graphene oxide hybrid composite particles and their electroresponsive characteristics. Langmuir 28:7055–7062. https://doi.org/10.1021/la3009283
79. Fan Z-J, Kai W, Yan J, Wei T, Zhi L-J, Feng J, Y-M Ren, Song L-P, Wei F (2010) Facile synthesis of graphene nanosheets via Fe reduction of exfoliated graphite oxide. ACS Nano 5:191–198. https://doi.org/10.1021/nn102339t
80. Tien HN, Chung JS, Hur SH (2013) Fabrication of a novel 2D-graphene/2D-NiO nanosheet-based hybrid nanostructure and its use in highly sensitive NO_2 sensors. Sens Actuators B Chem 185:701–705. https://doi.org/10.1016/j.snb.2013.05.050
81. Qiu L, Zhang H, Wang W, Chen Y, Wang R (2014) Effects of hydrazine hydrate treatment on the performance of reduced graphene oxide film as counter electrode in dye-sensitized solar cells. Appl Surf Sci 319:339–343. https://doi.org/10.1016/j.apsusc.2014.07.133
82. Kumar A, Sharma S, Tripathi VD, Maurya RA, Srivastava SP, Bhatia G, Tamrakar A, Srivastava AK (2010) Design and synthesis of 2,4-disubstituted polyhydroquinolines as prospective antihyperglycemic and lipid modulating agents. Bioorg Med Chem 18:4138–4148. https://doi.org/10.1016/j.bmc.2009.11.061
83. Antonyraj CA, Kannan S (2008) Hantzsch pyridine synthesis using hydrotalcites or hydrotalcite-like materials as solid base catalysts. Appl Catal A 338:121–129. https://doi.org/10.1016/j.apcata.2007.12.028
84. Alvim HGO, da Silva Junior EN, Neto BAD (2014) What do we know about multicomponent reactions? Mechanisms and trends for the Biginelli, Hantzsch, Mannich, Passerini and Ugi MCRs. RSC Adv 4:54282–54299. https://doi.org/10.1039/C4RA10651B
85. Jones G (2004) The Knoevenagel condensation. In: Andrew Evans P, Weinreb S, Press J (eds) Organic reactions. Wiley, New York, pp 204–273

Affiliations

Prasun Choudhury[1] · Pranab Ghosh[1] · Basudeb Basu[1,2]

[1] Department of Chemistry, North Bengal University, Darjeeling 734013, India

[2] Department of Chemistry, Raiganj University, University Road, Raiganj 733134, India

Journal of Flow Chemistry (2020) 10:389–396
https://doi.org/10.1007/s41981-019-00048-7

FULL PAPER

Graphene oxide-catalyzed two-step continuous-flow conversion of aryl amine to unsymmetrical thioether

Prasun Choudhury [1] · Basudeb Basu [1,2]

Received: 24 July 2019 / Accepted: 4 September 2019 / Published online: 22 November 2019

Abstract

A sustainable continuous-flow protocol for the conversion of aryl amine to unsymmetrical thioether is described. This technique is a two-step process involving graphene oxide (GO) catalyzed diazotization followed by the reaction with aryl/alkyl thiols. The continuous-flow conditions afford the desired thioethers in very good yields, effectively suppressing formation of possible disulfide, a common by-product in conventional process. The flow reaction is carried out under ambient conditions, applied to a variety of aryl amines and aryl/alkyl thiols and found to be scalable. The catalytic activity of the GO bed under continuous-flow conditions is found within standard time range and recyclable for ten consecutive runs without any loss of its performance.

Keywords Arylamine · Catalysis · Continuous-flow reaction · Diazotization · Graphene oxide · Green chemistry · Thioether

Introduction

The 'flow chemistry' refers to a continuous-flow reaction process performing in a tube or pipe and constitutes a new paradigm for molecular assembly [1]. The flow reactor is a new technology using pressure and heating apparatus and mixing the reactants under controlled manner [2, 3]. Flow chemistry has become a popular sustainable technique because of rapid and safer operation in an integrated synthetic process to afford cleaner products [4–7].

On the other hand, harnessing the nanocarbon materials like graphene oxide as the carbocatalysts in diverse organic reactions has been well studied since the first seminal paper by Bielawaski in 2010 [8]. The sustainable 2D honeycomb structure of carbonaceous graphene on oxidation and subsequent exfoliation provides an easy access to graphene oxide (GO), which bears several oxygenated functional groups, particularly –COOH on its peripheral sides and –OH, epoxy groups on its basal plane [9]. Both oxidative and acidic properties of GO have been exploited in several catalytic organic transformations [10–15]. However, this carbocatalyst (GO) has not been used in a flow reaction to the best of our knowledge. We report herein the application of GO as the catalyst in the Stadler–Ziegler reaction using flow chemistry technique.

While metal–catalyzed C–S cross coupling of aryl halides (or boronic acids) and thiols are known to produce diaryl sulfides, several impediments like strong base, precious and toxic metals, and lack of compatibility with diverse functional group attract for other alternative and benign protocols [16, 17]. Diazonium compounds serves as an important intermediate in diverse organic transformations owing to their versatile reactivity [18–20]. Traditional Stadler–Ziegler reaction involves the reaction between in situ aniline derived aryl diazonium salt (using an acid) and thiolate anion (using a base) [21, 22]. Further developments in this direction have been made with the aid of photoredox catalysts [23], or transition metal catalysts [24–26]. For instance, a visible light mediated arylation of cysteine via diazotization has been accomplished by using eosin Y as photocatalyst under continuous-flow conditions [27]. While, the Stadler–Ziegler reaction offers access to the preparation of unsymmetrical thioethers, the use of strong acids, bases for making the thiolate anion and the use

Article Highlights
- Graphene oxide (GO) catalysis in flow reaction.
- A metal-free continuous-flow synthesis of thioethers.
- The catalytic bed of GO is recyclable for ten cycles.

Electronic supplementary material The online version of this article (https://doi.org/10.1007/s41981-019-00048-7) contains supplementary material, which is available to authorized users.

✉ Basudeb Basu
basu_nbu@hotmail.com

[1] Department of Chemistry, North Bengal University, Darjeeling 734013, India

[2] Department of Chemistry, Raiganj University, Raiganj 733134, India

of metal catalysts restrict its wide applicability [28–31]. As the graphene oxide (GO) often exhibits dual properties i.e. both acidic and oxidative properties, we examined whether the Stadler–Ziegler reaction can be performed in the presence of GO as the catalyst under flow conditions. The particle size of GO was measured previously by DLS studies and found to be 544 ± 37 nm for 82% of the GO particles [32]. We report herein our successful efforts to establish the GO–catalyzed flow reaction as a sustainable protocol for making unsymmetrical diaryl sulfides in good yields along with recyclability of the catalyst (Scheme 1). Organyl nitrites [18], and supported nitrites [33], have been shown to be efficient and better diazotizing agents than inorganic nitrites in terms of safer handling, cost effectiveness and by-product formation, and we used in our studies *tert*–butylnitrite (*t*-BuONO) as the cheaper and commonly available nitrosation agent.

Results and discussions

The flow reaction bed of graphene oxide was prepared in a chromatographic column, the base of which was plugged with a thick cotton bed followed by packing with GO. The glass column had provisions for wrapping with ice jacket that could maintain low temperature (0–5 °C). Firstly, a solution of aromatic amine in CH_3CN was placed on GO bed followed by the addition of the nitrosation reagent in CH_3CN. The reaction bed was then kept at 0–5 °C for 30 min using the ice jacket. Then the ice jacket was removed and a solution of thiol in CH_3CN was added at room temperature (r.t.) to the reactor column drop wise at different flow rates (mL/min) and the reaction mixture was allowed to pass through the flow reaction column to afford the desired diaryl sulfide (Fig. 1).

In the optimization process, we used 4–methoxyaniline (**1a**) (1 mmol) and thiophenol (**2a**) (1 mmol) as model substrates, *tert*–butylnitrite (*t*-BuONO) (1.2 mmol) as the nitrosation reagent, and the catalyst bed of 2 mm height was prepared with GO (300 mg). The reaction protocol involves primarily two steps: (i) a solution of aryl amine and *tert*–butylnitrite in solvent was soaked on to the GO bed and kept at 0–5 °C for 30 min (step A), (ii) the thiol in the same solvent was added at different flow rates to the resulting diazonium species on GO (step B). After the addition was complete, the desired product was eluted with the solvent. Use of CH_3OH at a flow rate of 0.050 mL/min (6 mL solution during 2 h) gave the desired thioether (**3a**) in 60% yield along with diphenyl disulfane (23%) (Table 1, Entry 1). Changing the solvent from CH_3OH to CH_3CN resulted in increase of the product yield to 77% (Entry 2). The reaction carried out in H_2O afforded the desired diaryl sulfide in 21% yield only (Entry 3). This might be due to the poor solubility of aryl amine in H_2O. Next, the effect of other nitrosation agents on the course of the reaction was studied. The use of butylnitrite (BuONO) instead of *t*-BuONO did not show any pronounced effect in the course of the reaction (Entry 4, 76%). Since the CH_3CN solvent was found to be better, we now examined addition of solution of thiol in CH_3CN (step B) at different flow rates. These experiments resulted in further developments in terms of higher yield of the desired diaryl sulfide as well as suppression of conversion to disulfides via oxidative dimerization. Thus, addition of the thiol solution at a flow rate of 0.025 mL/min yielded the desired diaryl disulfide (**3a**) in 82% (Entry 5) and further decreasing the flow rate to 0.016 mL/min increased the product yield to 86% along with the diaryl disulfide in 8% (Entry 6). However, the flow rate at 0.012 mL/min resulted in a lower yield of the desired product (75%) (Entry 7), presumably due to the fact that the diazonium intermediate is decomposed under longer exposure on to the surface of GO catalyst. We conducted an experiment under the optimized reaction condition by conventional method under stirring. A one–pot two–step strategy was employed, where **1a** (1 mmol), GO (25 mg), *t*-BuONO (1.2 equiv) and CH_3CN (2 mL) were stirred at 0 °C for 30 min and then the thiol (1 mmol) was added to this diazotization mixture and the reaction was continued for 6 h at room temperature. The desired thioether (**3a**) in this conventional method was formed in 72% isolated yield along with the disulfane (17%, Entry 8). Furthermore, the reaction did not occur when carried out in the absence of nitrosation reagent (Entry 9). In order to examine the scalability of the flow reaction, we performed the reaction in 5 mmol scale taking 4-methoxyaniline, GO (1.0 g) and keeping the flow over a period of 10 h that gave the unsymmetrical thioether **3a** in 81% yield. This indicates that large scale flow reactions can be performed within standard time limit.

After optimization of the continuous-flow reaction conditions, the protocol was extended towards the synthesis of diverse unsymmetrical thiothers from different aromatic amines and aryl/alkyl thiols. The results are presented in Table 2.

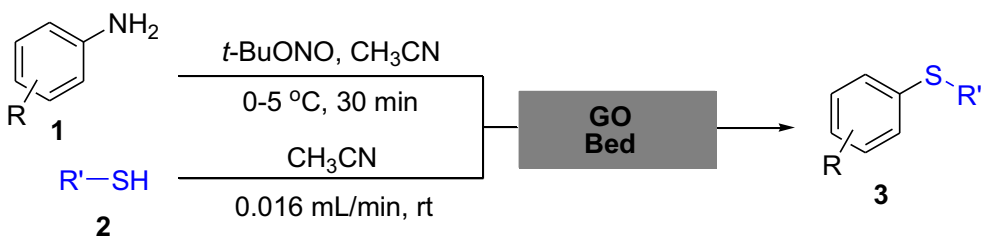

Scheme 1 Continuous-flow GO-catalyzed two-step synthesis of thioether from arylamine

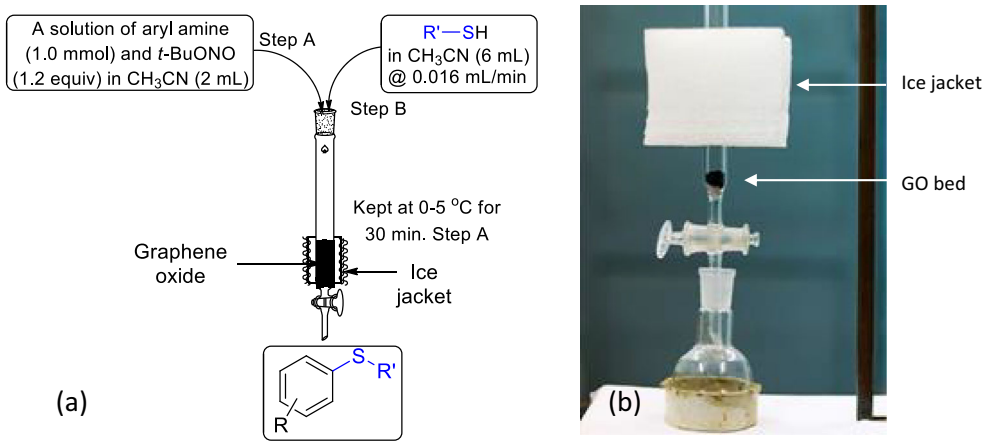

Fig. 1 Experimental setup for continuous flow two-step synthesis of thioether; (**a**): Schematic, (**b**): Digital image

Aromatic amines containing both electron donating groups (–OCH_3, –CH_3, –Br and –Cl) as well as electron withdrawing groups (–NO_2 and –$COCH_3$) were tolerated under the reaction conditions. In the case of aromatic thiols, substitution pattern comprising of electron donating and electron withdrawing groups also did not affect the course of the reaction affording significant conversion to the desired product (Entries 1–8). The reaction was also successful with aliphatic thiols. For example, long chain aliphatic thiols like heptanethiol and pentanethiol gave the corresponding thioethers (**3g**–**3i**) in 82–87% yield (Entries 9–11). We also explored the reactions involving heterocyclic substrates (both heterocyclic amines

Table 1 Optimization of the continuous-flow reaction conditions

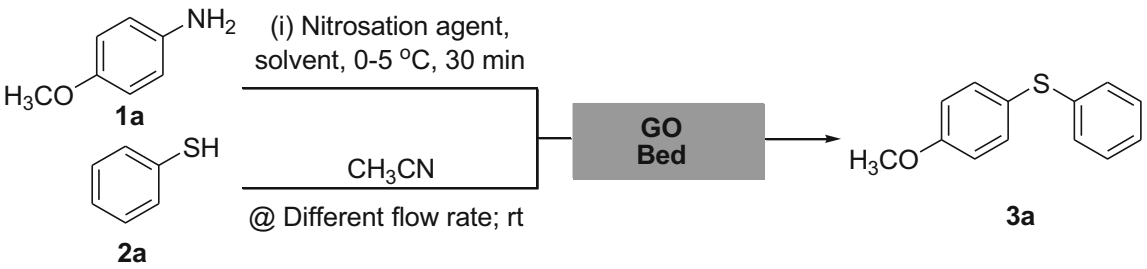

Entry	Solvent	Nitrosation reagent	Flow rate (mL/min)[a]	Yield (%)[b]
1	CH_3OH	*t*-BuONO	0.050	60
2	CH_3CN	*t*-BuONO	0.050	77
3	H_2O	*t*-BuONO	0.050	21
4	CH_3CN	BuONO	0.050	76
5	CH_3CN	*t*-BuONO	0.025	82
6	**CH_3CN**	***t*-BuONO**	**0.016**	**86**[c]
7	CH_3CN	*t*-BuONO	0.012	75
8	CH_3CN	*t*-BuONO	–	72[d]
9	CH_3CN	–	0.016	No reaction
10	CH_3CN	*t*-BuONO	0.016	81[e]

Reaction conditions: (i) **1a** (1 mmol), nitrosation reagent (1.2 equiv), solvent (2 mL); (ii) **2a** (1 mmol), solvent (6 mL)

[a] The rate at which thiol solution was added to the flow reactor column

[b] Isolated yield

[c] Diphenyl disulfane was formed in 8% yield

[d] Reaction conducted by conventional method under stirring. Diphenyl disulfane was formed in 17% yield

[e] Reaction performed with **1a** (5 mmol), GO (1.0 g), **2a** (5 mmol) in solvent (10 mL) and flow time 10 h

Table 2 GO catalyzed synthesis of thioethers under continuous-flow reaction

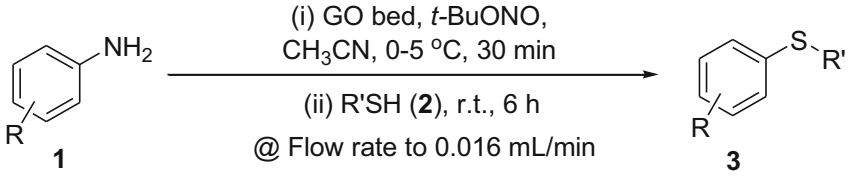

Entry	Aromatic amine	Thiol	Product	Yield (%)[a]
1	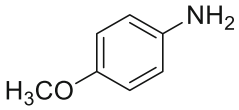	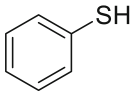	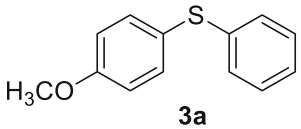 **3a**	86
2	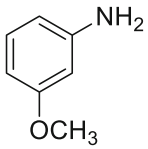	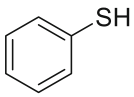	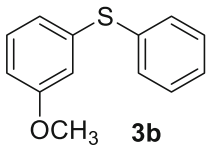 **3b**	83
3	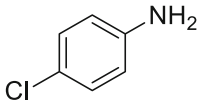	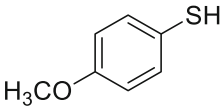	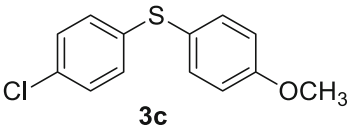 **3c**	84
4	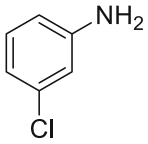	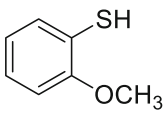	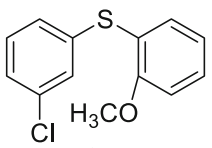 **3d**	81
5	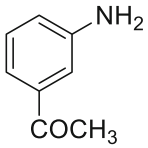	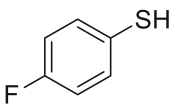	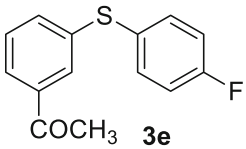 **3e**	88

and heterocyclic thiols). The reaction between 4–aminopyridine and 4–methylbenzenethiol or 4–methoxyaniline and pyridine–2–thiol went smoothly to afford the corresponding unsymmetrical diayl sulfides in 79–84% yield (Entries 12 and 13). Thus, GO appears to be innocuous to heterocyclic moiety in comparison to other acids normally used in the diazotization process. Again, the reaction between 2–naphthylamine with 4-tolylthiol or between 4-toluidine and naphthalene–2–thiol worked efficiently affording the same product (**3l**) in nearly similar yields (79–82%) (Entries 14 and 15). It is evident from this study that the reaction conditions i.e. the diazotization of aryl amine followed by continuous-flow of thiols over the catalyst bed (GO) do not affect much or have any significant effect in the course of the reaction.

To get some insights into the mechanistic pathway for the reaction, we conducted some control experiments (Scheme 2). The Stadler–Ziegler reaction is believed to proceed via radical intermediates [34]. Firstly, we set up one reaction under the optimized conditions using 4–methoxyaniline (**1a**) and thiophenol (**2a**) in presence of a radical scavenger, TEMPO. In this case, the desired product (**3a**) was isolated in 17% yield only, suggesting clear evidence that the reaction may proceed through aryl radical intermediate. Since we observed partial formation of diaryl disulfide, which could originate via oxidative dimerization of aryl thiol, we performed one reaction between **1a** (1 mmol) and 1,2–diphenyldisulfane **4** (0.5 mmol) under the standard continuous-flow conditions. This reaction afforded **3a** in 85% yield suggesting that the disulfide could be other intermediate in the reaction. Based on these observations

Table 2 (continued)

6	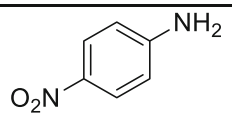	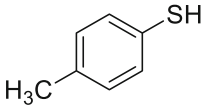	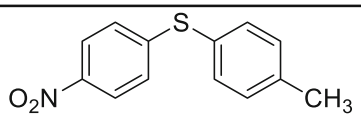 **3f**	84
7	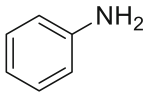	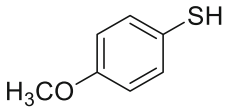	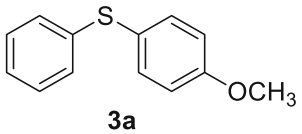 **3a**	87
8	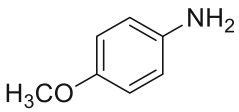	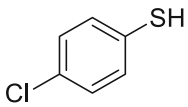	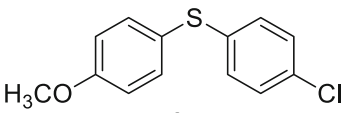 **3c**	83
9	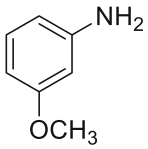	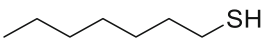	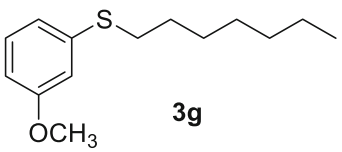 **3g**	82
10	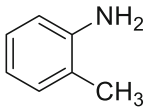	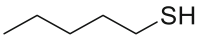	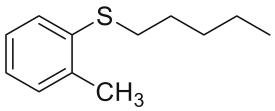 **3h**	87
11	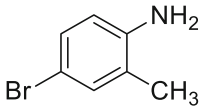	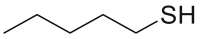	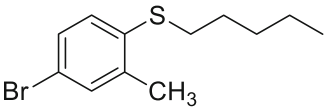 **3i**	87
12	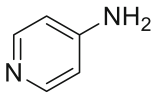	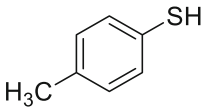	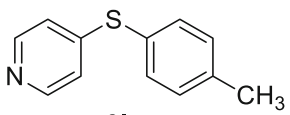 **3j**	79
13	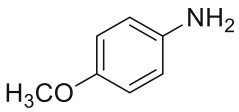	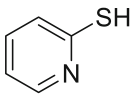	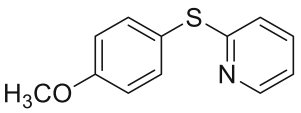 **3k**	84
14	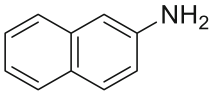	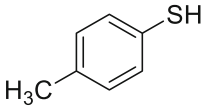	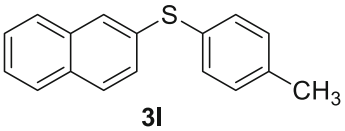 **3l**	79
15	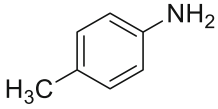	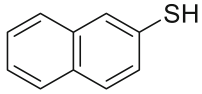	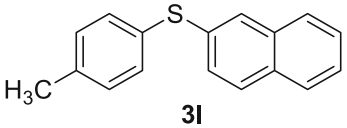 **3l**	82

Reaction conditions: (i) **1** (1 mmol), *t*-BuONO (1.2 equiv), CH_3CN (2 mL); (ii) **2** (1 mmol), CH_3CN (6 mL)

[b] Isolated yield after purification through column chromatography

Scheme 2 Control experiments

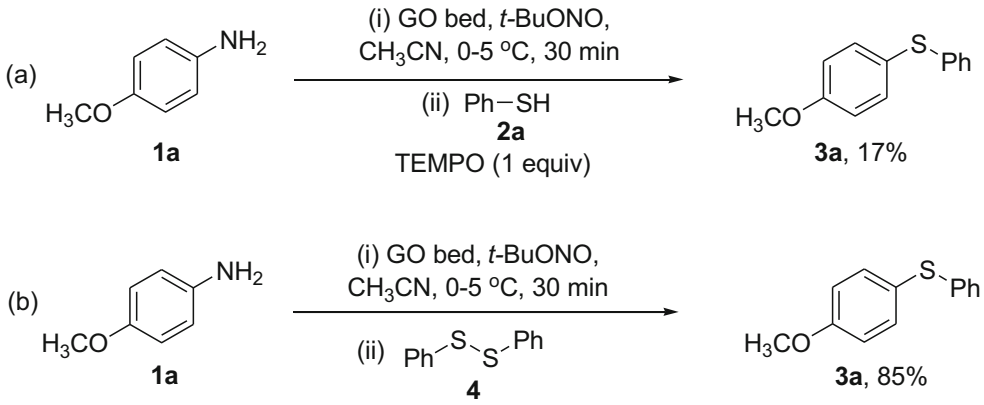

and keeping analogy with literature reports [34, 35], we proposed a plausible mechanism (Scheme 3). The diazotization of aromatic amine **1a** using *t*-BuONO in presence of GO gives rise to the formation of the diazonium salt **6**, which underwent homolytic dediazotization to provide the aryl radical **7**. It is believed that the formation of the aryl radical **7** is facilitated by graphene oxide [36, 37]. On the other hand, the thiol (**2a**) undergoes GO–catalyzed oxidative dimerization to generate the disulfide intermediate **4** [38], which subsequently form the thiyl radical **5**. Finally, the reaction between aryl radical **7** and thiyl radical **5** result in the formation of the product **3a**.

One of the fundamental principles of green chemistry says about recyclability of the catalyst. We have reused the flow reactor catalyst bed (GO) for ten consecutive runs without any appreciable loss in the yield of the products (Fig. 2). After completion of the reaction, the reaction mixture was eluted with ethyl acetate from the flow reactor column. For use in recycling experiments, the GO bed in the column was washed with ethyl acetate (3 × 5 mL) followed by acetone (1 × 5 mL) and dried with an external hot air blower. We compared the FT-IR spectra of the fresh GO with the recovered GO (after fifth run) and given in the Supplementary material (see S3). Practically, no significant changes in absorptions of different functionalities associated with GO are observed.

Conclusion

In summary, we have demonstrated GO–catalyzed Stadler–Ziegler synthesis of thioethers from aryl amine via diazotization with a safer nitrosation agent (alkyl nitrite) followed by metal–free *S*–transfer under continuous-flow technique. The technique offers the advantages of affording the final thioether under an ambient condition (overall 0 °C to r.t.), suppresses the formation of common by product (disulfides), and is applicable to variety of aryl amines and thiols providing a facile access to various unsymmetrical diaryl/aryl–alkyl sulfanes in very good yields. Moreover, the catalytic bed (GO) can be reused for ten consecutive runs without any loss in its catalytic performance. Graphene oxide has been used as a sustainable

Scheme 3 Plausible reaction mechanism pathway

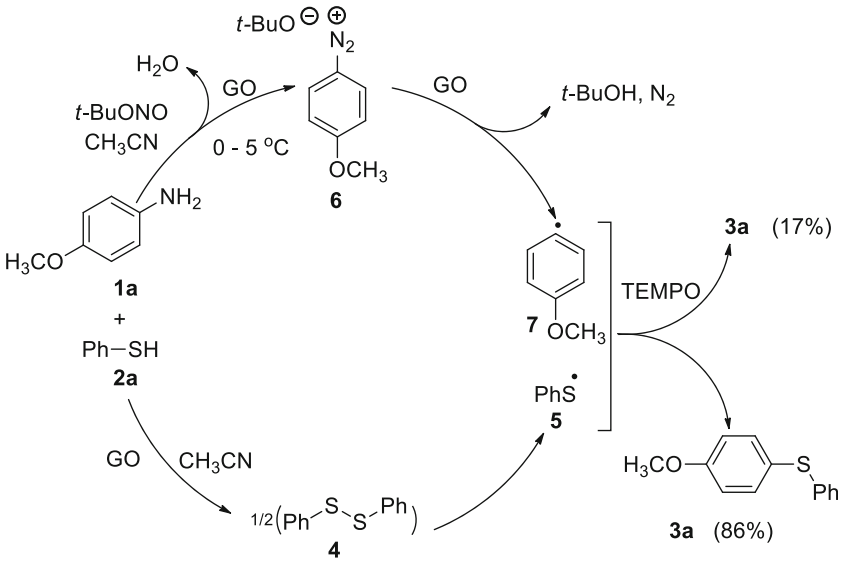

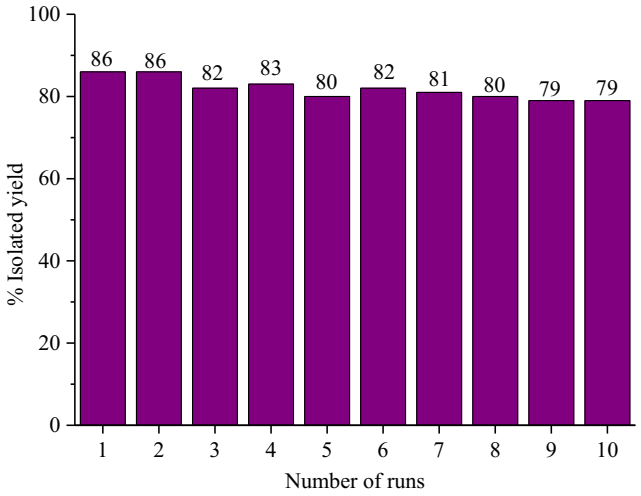

Fig. 2 Recyclability of GO flow reactor bed in Stadler–Ziegler reaction

carbocatalyst in various organic reactions; however, to the best of our knowledge, this example of continuous-flow reaction technique of GO catalyst is reported for the first time. The results are expected to encourage further applications of GO–catalyzed reactions in flow reactor designed in common laboratory.

Experimental section

Preparation of graphene oxide (GO)

Graphene oxide (GO) was prepared according to the Tour's method [39]. In this method a 9:1 (*v*/*v*) mixture of H_2SO_4 / H_3PO_4 (180:20 mL) was added to a mixture of graphite powder (1.5 g) and $KMnO_4$ (9.0 g). The mixture was then stirred at 50 °C for 12 h. After cooling the mixture to room temperature, it was gradually poured into crushed ice (200 g), which was followed by slow addition H_2O_2 (30%, 1.5 mL). The solution was then centrifuged (5000 rpm) and the supernatant aqueous parts were discarded. The residual solid material was successively washed with de–ionized water (100 mL) and then with 30% HCl (100 mL). The solid material was then repeatedly washed with water and centrifuged. Finally, the solid brown material was collected and dried at 60 °C under vacuum to obtain solid graphene oxide. It was characterized and compared with the characterization data of the same prepared in this laboratory [13, 14].

General procedure for the synthesis of thioethers under continuous-flow

The flow reaction set up was made in a chromatographic column, the base of which was plugged with a layer of cotton. It was then supported with graphene oxide catalyst (300 mg) and the height of the catalyst bed was 2 mm. A solution of the aromatic amine (1 mmol) and *t*-BuONO (1.2 equiv., 0.14 mL) in CH_3CN (2 mL) was added to the reactor column. The temperature of the reactor column was maintained at 0–5 °C for 30 min. After that a solution of thiol (1 mmol) in CH_3CN (6 mL) was added to the reaction bed drop wise at a flow rate of 0.016 mL/min. Once the addition is complete, the reactor bed was eluted with ethyl acetate (3 × 5 mL) and all organic parts were collected in a flask. Evaporation of the solvents under vacuum afforded the residue, which was again passed through a short column of silica gel using light petroleum ether and ethyl acetate as eluent to afford the desired unsymmetrical thioether. All products were characterized by ^1H and ^{13}C NMR spectroscopy and compared with the reported melting points for known solid compounds (See Supplementary material (S4–S19)).

Acknowledgements Financial support from Science and Engineering Research Board (Grant No EMR/2015/000549), New Delhi, is gratefully acknowledged. PC thanks UGC, New Delhi, for Senior Research Fellowship under UGC–NET.

References

1. Plutschack MB, Pieber B, Gilmore K, Seeberger PH (2017) The hitchhiker's guide to flow chemistry. Chem Rev 117:11796–11893
2. Akwi FM, Watts P (2018) Continuous flow chemistry: where are we now? Recent applications, challenges and limitations. Chem Commun 54:13894–13928
3. Noël T, Su Y, Hessel V (2015) In: Noël T (ed) Organometallic flow chemistry. Germany, Springer
4. Oger N, Le Grognec E, Felpin F-X (2015) Handling diazonium salts in flow for organic and material chemistry. Org Chem Front 2:590–614
5. Sahoo HR, Kralj JG, Jensen KF (2007) Multistep continuous-flow microchemical synthesis involving multiple reactions and separations. Angew Chem Int Ed 46:5704–5708
6. Yoshida J-I, Nagaki A, Yamada D (2013) Continuous-flow synthesis. Drug Discov Today Technol 10:e53–e59
7. Kockmann N, Thenée P, Fleischer-Trebes C, Laudadio G, Noël T (2017) Safety assessment in development and operation of modular continuous-flow processes. React Chem Eng 2:258–280
8. Dreyer DR, Jia HP, Bielawski CW (2010) Graphene oxide: a convenient carbocatalyst for facilitating oxidation and hydration reactions. Angew Chem Int Ed 49:6813–6816
9. Dreyer DR, Park S, Bielawski CW, Ruoff RS (2010) The chemistry of graphene oxide. Chem Soc Rev 39:228–240
10. Mohammadi O, Golestanzadeh M, Abdouss M (2017) Recent advances in organic reactions catalyzed by graphene oxide and sulfonated graphene as heterogeneous nanocatalysts: a review. New J Chem 41:11471–11497
11. Navalon S, Dhakshinamoorthy A, Alvaro M, Garcia H (2014) Carbocatalysis by graphene-based materials. Chem Rev 114: 6179–6212
12. Dreyer DR, Todd AD, Bielawski CW (2014) Harnessing the chemistry of graphene oxide. Chem Soc Rev 43:5288–5301

13. Bhattacharya S, Ghosh P, Basu B (2018) Graphene oxide (GO) catalyzed transamidation of aliphatic amides: an efficient metal-free procedure. Tetrahedron Lett 59:899–903
14. Choudhury P, Roy B, Basu B (2017) Sustainable and site-selective C−H Sulfenylation of aromatic compounds with thiol using catalytic graphene oxide and NaI. Asian J Org Chem 6:1569–1574
15. Jia HP, Dreyer DR, Bielawski CW (2011) Graphite oxide as an auto-tandem oxidation–hydration–aldol coupling catalyst. Adv Synth Catal 353:528–532
16. Gawande MB, Goswami A, Felpin F-X, Asefa T, Huang X, Silva R, Zou X, Zboril R, Varma RS (2016) Cu and cu-based nanoparticles: synthesis and applications in catalysis. Chem Rev 116:3722–3811
17. Lee CF, Liu YC, Badsara SS (2014) Transition-metal-catalyzed C–S bond coupling reaction. Chem Asian J 9:706–722
18. He L, Qiu G, Gao Y, Wu J (2014) Removal of amino groups from anilines through diazonium salt-based reactions. Org Biomol Chem 12:6965–6971
19. Mo F, Dong G, Zhang Y, Wang J (2013) Recent applications of arene diazonium salts in organic synthesis. Org Biomol Chem 11: 1582–1593
20. Roglans A, Pla-Quintana A, Moreno-Manas M (2006) Diazonium salts as substrates in palladium-catalyzed cross-coupling reactions. Chem Rev 106:4622–4643
21. Stadler O (1884) Zur Kenntniss der Merkaptane. Ber Dtsch Chem Ges 17:2075–2081
22. Ziegler J (1890) Ueber eine Methode zur Darstellung aromatischer Sulfide von bestimmter Constitution und das Thioxanthon. Ber Dtsch Chem Ges 23:2469–2472
23. Wang X, Cuny GD, Noël T (2013) A mild, one-pot Stadler–Ziegler synthesis of arylsulfides facilitated by photoredox catalysis in batch and continuous-flow. Angew Chem Int Ed 52:7860–7864
24. Shieh Y-C, Du K, Basha RS, Xue Y-J, Shih B-H, Li L, Lee C-F (2019) Syntheses of Thioethers and selenide ethers from anilines. J Org Chem 84:6223–6231
25. Hong B, Lee J, Lee A (2017) Visible-light-promoted synthesis of diaryl sulfides under air. Tetrahedron Lett 58:2809–2812
26. Li Y, Pu J, Jiang X (2014) A highly efficient cu-catalyzed S-transfer reaction: from amine to sulfide. Org Lett 16:2692–2695
27. Bottecchia C, Rubens M, Gunnoo SB, Hessel V, Madder A, Noël T (2017) Visible-light-mediated selective Arylation of cysteine in batch and flow. Angew Chem Int Ed 56:12702–12707
28. Koziakov D, Majek M, von Wangelin AJ (2016) Metal-free radical thiolations mediated by very weak bases. Org Biomol Chem 14: 11347–11352
29. Mukherjee N, Chatterjee T, Ranu BC (2013) Reaction under ball-milling: solvent-, ligand-, and metal-free synthesis of unsymmetrical diaryl chalcogenides. J Org Chem 78:11110–11114
30. Kundu D, Ahammed S, Ranu BC (2012) Microwave-assisted reaction of aryl diazonium fluoroborate and diaryl dichalcogenides in dimethyl carbonate: a general procedure for the synthesis of unsymmetrical diaryl chalcogenides. Green Chem 14:2024–2030
31. Barbero M, Degani I, Diulgheroff N, Dughera S, Fochi R, Migliaccio M (2000) Alkyl-and arylthiodediazoniations of dry arenediazonium *o*-benzenedisulfonimides. Efficient and safe modifications of the Stadler and Ziegler reactions to prepare alkyl aryl and diaryl sulfides. J Org Chem 65:5600–5608
32. Roy B, Ghosh S, Ghosh P, Basu B (2015) Graphene oxide (GO) or reduced graphene oxide (rGO): efficient catalysts for one-pot metal-free synthesis of quinoxalines from 2-nitroaniline. Tetrahedron Lett 56:6762–6767
33. Bochare MD, Degani MS (2017) Polyethylene glycol nitrite (PEG-ONO) as a novel diazotizing agent. ACS Sustain Chem Eng 5: 3716–3720
34. M-j B, G-p L, Cai C (2015) Ascorbic acid promoted metal-free synthesis of aryl sulfides with anilines Nitrosated in situ by *tert*-butyl nitrite. Synlett 26:1841–1846
35. Hari DP, Schroll P, König B (2012) Metal-free, visible-light-mediated direct C–H arylation of heteroarenes with aryl diazonium salts. J Am Chem Soc 134:2958–2961
36. Voylov D, Saito T, Lokitz B, Uhrig D, Wang Y, Agapov A, Holt A, Bocharova V, Kisliuk A, Sokolov AP (2016) Graphene oxide as a radical initiator: free radical and controlled radical polymerization of sodium 4-vinylbenzenesulfonate with graphene oxide. ACS Macro Lett 5:199–202
37. Qiu Y, Wang Z, Owens AC, Kulaots I, Chen Y, Kane AB, Hurt RH (2014) Antioxidant chemistry of graphene-based materials and its role in oxidation protection technology. Nanoscale 6:11744–11755
38. Dreyer DR, Jia H-P, Todd AD, Geng J, Bielawski CW (2011) Graphite oxide: a selective and highly efficient oxidant of thiols and sulfides. Org Biomol Chem 9:7292–7295
39. Marcano DC, Kosynkin DV, Berlin JM, Sinitskii A, Sun Z, Slesarev A, Alemany LB, Lu W, Tour JM (2010) Improved synthesis of graphene oxide. ACS Nano 4:4806–4814